

Exploring bacterial metalloproteases as promising drug targets

Dissertation

zur Erlangung des akademischen Grades

des Doktors der Naturwissenschaften

der Naturwissenschaftlich-Technischen Fakultät

der Universität des Saarlandes

von

Alaa Akram Alhayek

Saarbrücken

2022

Tag des Kolloquiums:

18. Juli 2022

Dekan:

Prof. Dr. Jörn Eric Walter

Berichterstatter:

Prof. Dr. Anna K.H. Hirsch
Prof. Dr. Silja Wessler
Prof. Dr. Alexandra K. Kiemer

Akad. Mitarbeiter:

Dr. Muhammad Nasim

Vorsitz:

Prof. Dr. Karin Römisch

Die vorliegende Arbeit wurde von Oktober 2018 bis März 2022 unter Anleitung von Frau Prof. Dr. Anna K. H. Hirsch in der Fachrichtung Pharmazie der Naturwissenschaftlich-Technischen Fakultät der Universität des Saarlandes sowie am Helmholtz-Institut für Pharmazeutische Forschung Saarland (HIPS) – Abteilung Wirkstoffdesign und Optimierung – angefertigt.

”مازلتُ حيّاً
وأؤمن بأنّي سأجدُ الطريق
يوماً ما،
إلى ذاتي، إلى حلمي،
إلى ما أريد.“
محمود درويش

“I am still alive, and I believe that one day I will find my way to myself, to my dream to what I always wanted.”

Mahmoud Darwish

Table of Contents

Table of Contents	V
Abstract	VII
Zusammenfassung	VIII
1 Introduction	1
1.1 Antibiotic resistance.....	1
1.2 Proposed strategies to tackle resistance development	2
1.2.1 Antivirulence strategies	3
1.2.2 Viral phage therapy	4
1.2.3 Immunotherapy	5
1.3 Bacterial metalloproteases as virulence factors.....	5
1.3.1 Elastase B of <i>Pseudomonas aeruginosa</i>	7
1.3.2 Collagenases of <i>Clostridium histolyticum</i>	9
1.3.3 Collagenases of <i>Bacillus cereus</i>	12
1.4 Substrates of bacterial metalloproteases	14
1.4.1 LasB substrates.....	14
1.4.2 Substrate of bacterial collagenases	15
1.5 Antivirulence agent development between concern and hope	16
1.6 Aim of the Thesis	17
1.7 References.....	19
2 Results	28
2.1 Chapter A: N-Aryl-3-mercaptosuccinimides as Antivirulence Agents Targeting <i>Pseudomonas aeruginosa</i> Elastase and <i>Clostridium</i> Collagenases	28
2.1.1 Supporting Information	39
2.2 Chapter B: Inhibition of collagenase Q1 of <i>Bacillus cereus</i> as a novel antivirulence strategy for the treatment of skin wound infections	42
2.2.1 Supporting information	55
2.3 Chapter C: Cocktail therapy approach to treat wound infections induced by collagenase-producing bacteria	66
2.3.1 Supporting information	84
2.4 Chapter D: Discovery and Characterization of Novel, Potent Inhibitors of Clostridial and Bacillary Collagenases.....	88
2.4.1 Supporting information	122
3 Final Discussion	148
4 Perspectives	157
5 Appendix	158

Additional Results, Chapter E: Structure-based Design of α -Substituted Mercaptoacetamides as Inhibitors of the Virulence Factor LasB from <i>Pseudomonas aeruginosa</i>	158
Abbreviations	200
Publications of the Author Included in This Thesis and Contribution Declaration	202
Publications of the Author not Included in This Thesis and Contribution Declaration	203
Manuscripts of the Author Submitted or in Preparation and Contribution Declaration	205
Conference Contributions.....	207
Curriculum Vita.....	209
Acknowledgment.....	210

Abstract

Microbial infection and the rise of antibiotic resistance pose a serious threat to public health. To tackle bacterial infection and resistance, new bacterial targets and non-antibiotic treatment options need to be identified. Virulence factors are gaining attention these days as they play crucial roles in bacterial pathogenicity. As their inhibition does not kill the bacteria, the selection pressure for emerging new resistant mutants is reduced, while also assisting the host immune system in eliminating the disarmed bacteria. Extracellular bacterial collagenases are the etiologic features of many bacterial infections. They are metalloproteases characterized by their ability to digest the main scaffolds of the extracellular matrix, exposing deep tissue to bacteria and other toxins. As the inhibition of virulence factors is considered one powerful non-antibiotic strategy, full characterization of these targets is essential to understand their role during infection. Furthermore, pre-clinical models imitating the infection need to be developed to decipher the role of virulence targets and their inhibitors in pathophysiological settings.

This study addresses the characterization and validation of three bacterial collagenases and their inhibitors: collagenase Q1 (ColQ1) of *Bacillus cereus*, Collagenase H (ColH) of *Clostridium histolyticum*, and elastase B (LasB) of *Pseudomonas aeruginosa*. To promote our understanding of the pathological contribution of bacterial collagenases and to characterize the activity of small-molecule collagenase inhibitors as therapeutic agents, we developed pre-clinical systems modeling the infection settings and validating the collagenases and their inhibitors. These systems include *in vitro* cell-based, *ex vivo* pig skin, and *in vivo* *Galleria mellonella* larvae models. Furthermore, advanced microscopic techniques as well as *in vitro* biological and bioanalytical assays were used to evaluate the effects shown in these models. The newly discovered inhibitors investigated in this study are characterized with their potency, selectivity, and chemical stability, which many previously reported inhibitors lack. The findings of this work shed light on the roles of bacterial collagenases during bacterial infection – in particular in disease progression – and the effect of their inhibition with small-molecule antivirulence agents, which could represent an effective therapeutic strategy.

Zusammenfassung

Mikrobielle Infektionen und die Zunahme der Antibiotikaresistenz stellen eine ernste Bedrohung für die öffentliche Gesundheit dar. Um bakterielle Infektionen und Resistenzen zu bekämpfen, müssen neue bakterielle Angriffspunkte und nicht-antibiotische Behandlungen gefunden werden. Virulenzfaktoren gewinnen in diesen Tagen an Aufmerksamkeit, da sie eine entscheidende Rolle bei der bakteriellen Pathogenität spielen. Ihre Hemmung durch sogenannte "Antivirulenzwirkstoffe" tötet die Bakterien nicht ab. Dadurch wird der Selektionsdruck für die Entstehung neuer resistenter Mutanten verringert und gleichzeitig das Immunsystem des Wirts bei der Beseitigung der deaktivierten Bakterien unterstützt. Extrazelluläre bakterielle Kollagenasen sind die ätiologischen Merkmale vieler bakterieller Infektionen. Es handelt sich dabei um Metalloproteasen, die sich durch ihre Fähigkeit auszeichnen, die Hauptgerüste der extrazellulären Matrix zu verdauen und so tiefes Gewebe für Bakterien und andere Toxine freizulegen. Da Virulenzfaktoren und ihre Inhibitoren als eine vielversprechende nicht-antibiotische Strategie angesehen werden, ist ihre vollständige Charakterisierung unerlässlich, um ihre Rolle während der Infektion zu verstehen und neu entdeckte Faktoren als potenzielle Ziele und Inhibitoren zu validieren. Darüber hinaus müssen präklinische Modelle entwickelt werden, die die Infektion imitieren, um die Rolle der Virulenz-Targets und ihrer Inhibitoren in pathophysiologischen Situationen zu entschlüsseln.

Diese Studie befasst sich mit der Charakterisierung und Validierung drei bakterieller Kollagenasen und ihrer Inhibitoren: der Kollagenase Q1 (ColQ1) von *Bacillus cereus*, der Kollagenase H (ColH) von *Clostridium histolyticum* und der Elastase B (LasB) von *Pseudomonas aeruginosa*. Um unser Verständnis des pathologischen Beitrags bakterieller Kollagenasen zu fördern und die Aktivität von niedermolekularen Kollagenase-Inhibitoren als therapeutische Wirkstoffe zu charakterisieren, haben wir präklinische Systeme entwickelt, die die Infektionsbedingungen nachbilden und die Kollagenasen und ihre Inhibitoren validieren. Zu diesen Systemen gehören *In-vitro*-Zellsysteme, *Ex-vivo*-Schweinehaut und *In-vivo*-Modelle basierend auf *Galleria mellonella* Larven. Darüber hinaus wurden moderne mikroskopische Techniken, sowie biologische und bioanalytische *In-vitro*-Tests eingesetzt, um die in den zuvor genannten Modellen gezeigten Wirkungen zu bewerten. Die neu entdeckten Inhibitoren, die in dieser Studie untersucht werden, zeichnen sich durch ihre Potenz, Selektivität und chemische Stabilität aus, die bei vielen bisher bekannten Inhibitoren fehlen. Die Ergebnisse dieser Arbeit werfen ein Licht auf die Rolle bakterieller Kollagenasen während bakterieller Infektionen, insbesondere bei der Förderung von Krankheiten, und auf die Wirkung ihrer Hemmung durch

niedermolekulare Antivirulenzmittel, die eine wirksame therapeutische Strategie darstellen könnten.

1 Introduction

1.1 Antibiotic resistance

Antibiotics are drugs that prevent bacteria from growing and multiplying.^[1] They function by inhibiting the catalytic activity of enzymes that are involved in bacterial physiology.^[2] For instance, they block certain metabolic processes or reduce bacterial cell-wall construction, or protein, deoxyribonucleic acid (DNA), and ribonucleic acid (RNA) production, or disrupt the cell membrane.^[2] After a lack of antibiotics to treat even minor infections that were likely to kill people, Alexander Fleming discovered the first antibiotic (penicillin),^[3] which transformed medicine and improved human life expectancy. Since then, the antibiotic discovery has grown dramatically.^[4,5] Simultaneously, the irrational use of these medicines has caused their efficacy to deteriorate with time as a consequence of increased selection pressure on bacteria, which favors the emergence of resistance.^[4,5] Fleming already cautioned in his Nobel Prize speech against the possibility of penicillin resistance, as this would accelerate the evolution of antibiotic resistance in bacteria.^[3,6,7]

Today, we are all on the verge of a post-antibiotic era. Scientists and governments across the world are warning that the global antibiotic resistance crisis is rapidly worsening.^[8] There are many reasons contributing to the rapid development of antibiotics inefficacy. Their widespread and inappropriate use has aided the emergence of antibiotic-resistant bacteria.^[9,10] This resistance is further exacerbated by excessive use in animals and agriculture,^[11,12] as well as their misuse for non-bacterial diseases and poor patient compliance.^[10] The most critical contributors in the development of resistance can be found in developing nations where nearly all antibiotics are accessible without a prescription.^[13] **Figure 1** summarizes the main causes of antibiotic resistance development.

Rising antibiotic resistance has prompted scientists to modify the structure of existing natural antibiotics and to create active synthetic equivalents.^[14] Unfortunately, as resistance developed faster than the discovery of new antibiotics, this strategy did not endure.^[14] The discovery of novel synthetic antibiotics proved difficult, especially in regard to their potential to permeate the bacterial cell wall of Gram-negative bacteria to reach their targets.^[15] Another factor complicating the search for synthetic antibiotics is that most synthetic compounds do not comply with Lipinski's rule of five, which increases the probability of their failure.^[16] Furthermore, clinical studies, which must be undertaken prior to the introduction of antimicrobials to the market to ensure drug safety and efficacy are particularly challenging to execute.^[16] This is because placebos are not permitted to be used in infected patients owing to

ethical concerns.^[16] There are also commercial obstacles. For example, the discovery of drugs with a short duration of administration (*e.g.*, antibiotics) has lowered profits of pharmaceutical companies, leading them to focus on producing drugs that can be taken daily and for an extended period of time (*e.g.*, cholesterol-lowering drugs).^[17] In addition, new antibiotics would be reserved for patients suffering from infections by multi-drug resistant and extensively drug-resistant bacteria incompatible with a short patient life time.

To tackle this crisis, a number of measures must be taken, above all prevention of infectious diseases and patient education.^[18] In addition, pathogens that are resistant to antibiotics must be tracked and studied thoroughly, alternative treatment strategies, and classical antibiotics with new modes of action must be developed to manage the infections.^[18–21]

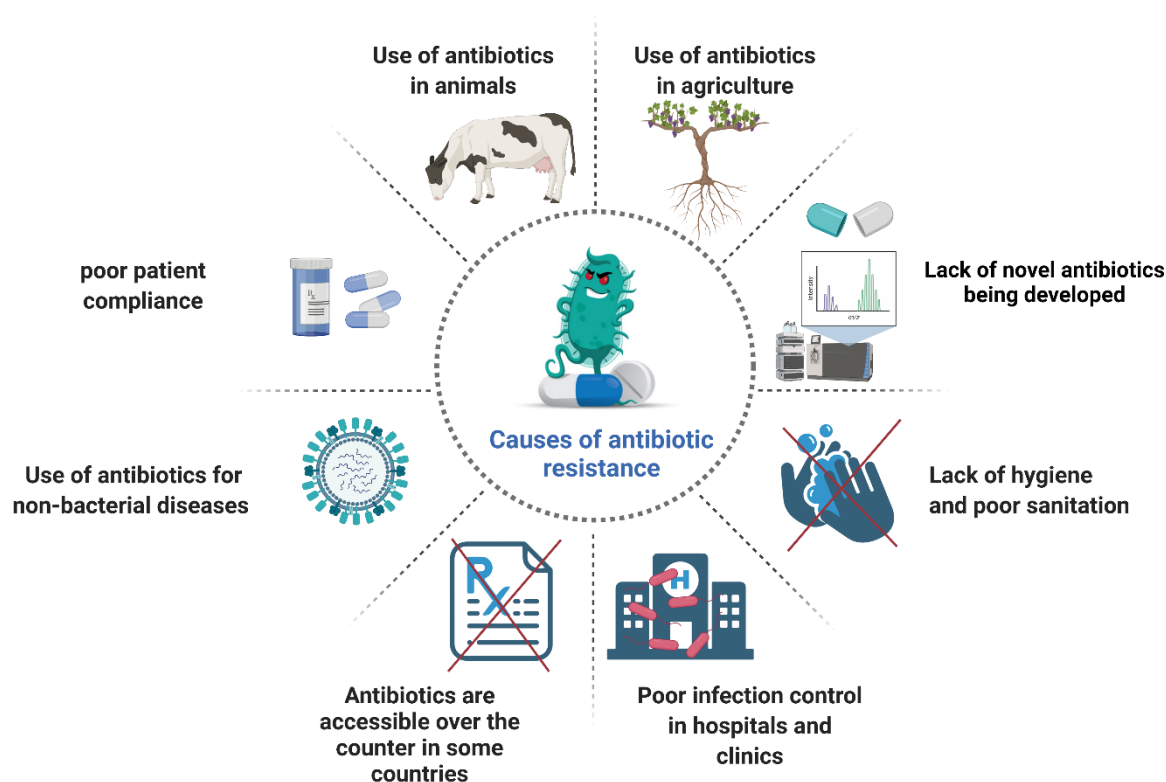


Figure 1. Overview of the main causes of antibiotic resistance development. Adapted from www.euro.who.int.

1.2 Proposed strategies to tackle resistance development

To address the problems posed by this serious health threat, the public and research institutions will need to collaborate to modify behaviors in antibiotic usage and to develop alternative therapeutic options. There are some potential strategies that are now being implemented to manage the resistance development crisis.^[14,18,19,22] These strategies have three key aspects: **1)** development of novel antimicrobial agents that inhibit already known targets preferably in an unprecedented way (*i.e.*, with a new binding mode). **2)** Identification of new essential bacterial targets and using them for the discovery of anti-infectives with a new mode of action (*e.g.*,

enzymes of methylerythritol 4-phosphate pathway).^[23] **3)** looking for non-antibiotic strategies to minimize the emergence of resistance and to restore the efficacy of existing antimicrobials.^[14,18,22,24] The latter is the most promising approach, because the other strategies will inevitably, again, lead to resistance development and narrow the therapeutic options. Several non-antibiotic methods are being explored for the management and prevention of bacterial infections.^[19] Among these methods are:

1.2.1 Antivirulence strategies

Targeting bacterial virulence factors. Pathogenic bacteria produce virulence factors, which enable them to overcome the host's defense mechanisms, invade the tissue, and gain access to deeper locations to spread the infection.^[25] Therefore, it is thought that inhibiting the activity of these virulence factors will reduce the bacterial pathogenicity rather than kill them.^[22,25] This keeps the selection pressure low and delays the emergence of resistant mutants.^[25] To target the virulence mechanism of pathogenic bacteria, the secreted virulence factors can be directly inhibited. In addition, their release occurs through needle-like-secretion systems, which inject the virulence factors and toxins directly into human cells; these secretion systems are also attractive drug targets.^[22] To date, there are no synthetic small-molecules antivirulence or antisecretion agents on the market, although many are in the early or latter phase of clinical trials (**Figure 2**).^[22] The question of whether virulence factor inhibitors will ever be of therapeutic value against pathogenic bacteria is still being investigated.

Targeting biofilm formation and adherence. Biofilm forms when microorganisms adhere and proliferate on a surface, producing extracellular polysaccharides that assist adhesion and matrix development.^[26,27] As a result, the organism's phenotype properties (*e.g.*, growth rate and gene transcription) change.^[26,27] Biofilm-forming bacteria can survive antibiotics that would normally eradicate planktonic-growing bacteria, making their removal difficult.^[26,27] Furthermore, the biofilm's extracellular matrix also impedes antibiotic entry into the biofilm.^[26,27] To avoid the formation of biofilms, new techniques are being developed. However, these techniques are still under clinical investigation.^[28] Biofilm formation often occurs on medical equipment like heart valves and teeth, thus preventing adhesion is one approach to combat biofilm formation.^[22,28] This can be accomplished by coating the devices' outer surface with antiadhesive substances that prevent bacteria from adhering to them.^[29] The biofilm attaches to human epithelial cells *via* lectin-like fimbriae, which bind sugar moieties on cell surfaces.^[30] By inhibiting these lectins, biofilm formation can be prevented (**Figure 2**).^[22,30] Other targets were directly related to biofilm development including quorum sensing (QS) or

small signaling molecule c-di-GMP, which regulates the switch that allows planktonic cells to form a biofilm. Their suppression is suitable to prevent biofilm formation.^[22,31]

Targeting signaling molecules. QS is a communication system that controls gene expression with regard to variations in cell numbers.^[31,32] It generates and releases chemical signals termed auto-inducers, which get more concentrated as cell density rises.^[31,32] Acylated homoserine lactones and processed oligopeptides are used in Gram-negative and -positive bacteria, respectively, as auto-inducers for bacteria to communicate.^[22,31,32] In both Gram-positive and -negative bacteria, QS communication circuits control a wide variety of physiological functions.^[22,31,32] These include biofilm formation, competence, virulence, motility, sporulation, conjugation, and others.^[31,32] Two basic techniques for discovering new drugs that inhibit this type of signal transmission are known. First, by inhibiting the production of QS signaling molecules or suppressing their interactions with their receptors (**Figure 2**).^[22,31,32]

Alternative approaches to limit virulence. Other non-antibiotic methods to target bacterial pathogenicity are being researched.^[19] Liposome-based cytotoxin inhibitors are one of them.^[33] They protect epithelial and endothelial cells as well as the immune system from harm by sequestering a variety of bacterial cytotoxins.^[33] These inhibitors have so far shown promise *in vitro* and *in vivo* against Gram-positive infections with *Staphylococcus aureus* and *Streptococcus pneumoniae*.^[33] Liposomes that target exotoxin-producing Gram-negative bacteria are still being studied.^[33]

1.2.2 Viral phage therapy

Bacteriophages are viruses that attach themselves to particular bacteria and inject their genome into them.^[34] The viral genome replaces the bacterial genome, which prevents the bacteria from multiplying.^[34] In Eastern Europe, phages were used before the discovery of antibiotics, and today owing to the substantial increase in resistance development, an interest has risen to return to this approach.^[34] Phage therapy provides a number of advantages, including high selectivity in targeting bacteria and a high therapeutic index, which reduce side effects in humans.^[19,22,34] This will also limit the ability of bacteria to evolve resistance.^[19,22] In addition, these phages are also non-pathogenic to the gut microbiome, lowering the risk of opportunistic infections.^[19,22] Due to their ability to penetrate biofilms, they have an additional advantage over conventional antibiotics.^[19,22,34] Despite all of these advantages, their ability to match with a single strain makes their discovery challenging and limits their application.^[22] To overcome this obstacle, it is proposed to develop a cocktail of phage mixtures to treat the same infection, because the bacterial components of the same infection might vary from patient to patient.^[35] These cocktails can be also used to lyse most strains from the same species (**Figure 2**).^[35]

1.2.3 Immunotherapy

Immunotherapies protect against infection by targeting or altering immune components to eliminate pathogens and damaged host cells.^[36,37] Vaccines are the most well-known and most effective type of immunotherapy. This includes the Bacillus Calmette-Guérin (BCG) vaccination, which protects children from infection with *Mycobacterium tuberculosis*.^[38] Immunotherapies are classified into two types, passive and active.^[36,37] *Ex vivo* components such as immune cells or recombinant antibodies are delivered to the patients as a form of passive immunotherapy.^[36,37] Active immunotherapies, on the other hand, employ virulence factors to trigger components of the host immune memory, such as T-cell or humoral response.^[36,37] Passive immunotherapies such as monoclonal and polyclonal antibodies, as well as active immunotherapies such as multi-epitope bacterial vaccines, are both being developed to treat bacterial infections.^[36,37] These antibodies might be used alone or in conjugation with conventional antibiotics to boost their efficacy or assure their targeted delivery and activity (Figure 2).^[36,37]

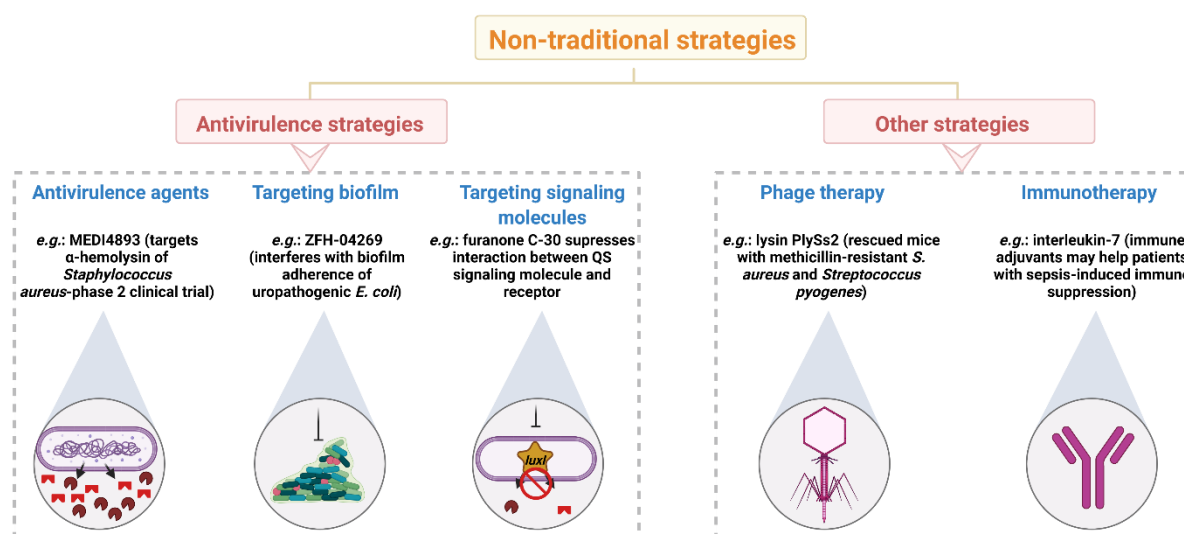


Figure 2. Representation of some indirect-acting strategies that can be used to tackle bacterial infections.

1.3 Bacterial metalloproteases as virulence factors

Proteases are hydrolytic enzymes that catalyze the breakage of peptide bonds in proteins and peptides.^[39,40] They are divided into exoproteases and endoproteases based on their catalytic mechanisms.^[39,40] The N- or C-termini of proteins are where exoproteases operate. Metalloproteases, cysteine proteases, serine proteases, threonine proteases, and aspartic proteases are all endoproteases that hydrolyze internal peptide bonds.^[39,40] Metalloproteases have one or two catalytic metals at their active site, which is usually a Zn^{2+} cation but can also be Mg^{2+} , Ni^{2+} , or Cu^{2+} .^[39,40] They are generated by all living organisms, including plants,

humans, and microbes.^[39,40] They are secreted either inside the cell or outside the cells, the latter being referred to extracellular metalloproteases.^[39,40] Extracellular metalloproteases in humans (*i.e.*, matrix metalloproteases: MMPs) have been widely investigated due to their contribution to numerous illnesses such as cancer, arthritis, and heart diseases.^[41] Several of their inhibitors are in medical use such as antihypertensive drugs (*e.g.*, enalapril and aliskiren)^[42], cancer treatment drugs (*e.g.*, depsipeptide)^[43], and anticoagulant medication (*e.g.*, argatroban).^[44] Bacterial extracellular metalloproteases, on the other hand, received less attention prior to the antibiotic resistance crisis.^[45] Over the past years, substantial progress has been made in identifying and characterizing a variety of bacterial metalloproteases as potential drug target candidates for antivirulence drug development.^[45] These bacterial metalloproteases are produced in an inactive state inside the cell and then go through certain processes to become active.^[39] The active enzyme is released outside the bacterial cell to initiate and maintain the infection.^[39,40,46] For nourishment, the extracellular metalloproteases degrade host proteins into oligopeptides and amino acids (use them as a source of carbon) leading to support the dissemination of bacteria and their toxins (**Figure 3**).^[39,40,46] They also attack the host immune response by destroying certain immunological components.^[39,40,46] All of these actions result in the host's immune system being unable to clear the infection, allowing the bacteria to spread to deeper and more vulnerable sites in the host's body.^[39,40,46]

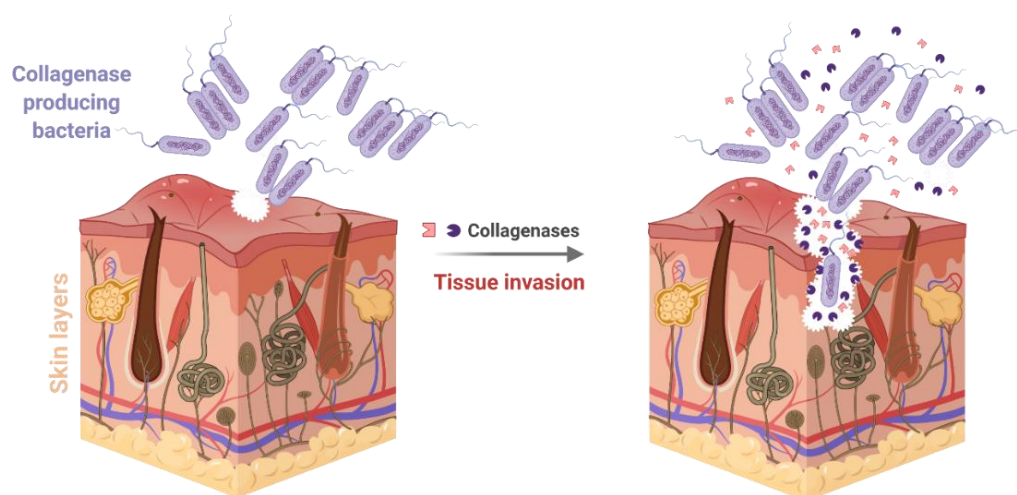


Figure 3. Illustration of tissue invasion induced by bacterial metalloproteases (collagenases). Bacterial collagenases digest the collagen of the extracellular matrix leaving gaps that assist bacteria to spread and reach deep locations.

Many of the extracellular metalloproteases secreted by pathogenic bacteria such as fragilysin from *Bacteroides fragilis*, elastase B (LasB) from *Pseudomonas aeruginosa*, various types of collagenases from *Clostridium* and *Vibrio* have been thoroughly studied. However, none of their inhibitors have been tested in humans yet.^[46,47]

Three of these metalloproteases, which are related to opportunistic infections will be discussed here in detail:

1.3.1 Elastase B of *Pseudomonas aeruginosa*

P. aeruginosa is a Gram-negative bacterium that can cause life-threatening infections, especially in immune-suppressed and cystic fibrosis (CF) patients.^[48] This bacterium is classified by the World Health Organization (WHO) as one of three pathogens that necessitate a quick discovery of anti-infectives (*Acinetobacter baumannii*, *P. aeruginosa*, and *Enterobacter* species).^[49] This is owing to its capacity to evade the effects of antibiotics and develop resistance against a wide range of treatments.^[50] Therefore, a lot of work has been put into understanding the pathogenicity and virulence of this bacterium in order to develop innovative strategies to intervene in the course of its infections.

Serval proteases are released by the opportunistic *P. aeruginosa*. These include elastase A (LasA), elastase B (LasB), pseudomonas small protease, protease IV, alkaline protease, large protease A, large exoprotease A, and aminopeptidase.^[51] These proteases are crucial for the development and maintenance of the infection.^[51,52] Among these proteases, LasB is the most common secreted protease, with proteolytic and elastolytic properties that allow it to target a variety of essential host substrates, resulting in *P. aeruginosa* pathogenicity.^[51,53,54] LasB is a Zn²⁺ - and Ca²⁺-dependent metalloprotease with a molecular weight of 33 kDa that belongs to the M4 thermolysin-peptidase family (according to the classification in the MEROPS database).^[51,53,54] The production of LasB is controlled by *lasI* QS and is secreted *via* the type-2 secretion system after activation of its inactive form (*i.e.*, preproelastase) into a mature enzyme (*i.e.*, LasB).^[51,53,54] The mature enzyme is made up of two domains; the N-terminal domain is mostly made up of antiparallel β -strands, whereas the C-terminal domain is made up of α -helices (**Figure 4**).^[55] Between these two domains, the active site is located. The resulting tertiary structure is identical to *Bacillus thermoproteolyticus* thermolysin.^[55] Besides, Zn²⁺ ligands (*i.e.*, His 144, His 140, and Glu 164) and other residues in the active sites (*e.g.*, Glu 141 and Tyr 155) are similar for LasB and thermolysin.^[55] This explains why LasB belongs to the M4 thermolysin-peptidase family.

LasB processes many host-derived substrates, including elastin (most studied substrate), and other extracellular matrix (ECM) proteins such as collagen, as well as immunological components such as immunoglobulins, cytokines, chemokines, surfactants, and antimicrobial peptides.^[56]

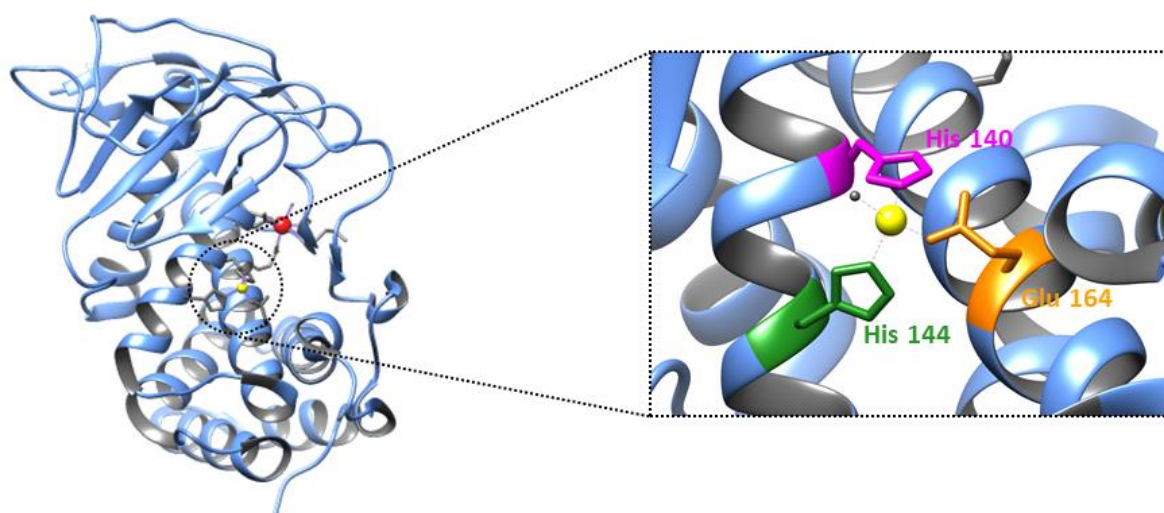


Figure 4. Crystal structure of *apo* LasB (PDB code: 1EZM). The N-terminal part consists of antiparallel β -sheets as illustrated at the top, and the C-terminal has mostly α -helices as shown at the bottom; zoom into Zn^{2+} (yellow) and ligands: His: histidine 144, histidine 140, and Glu: glutamine 164. Ca^{2+} and Zn^{2+} cations are depicted in red and yellow, respectively.

Due to its broad-spectrum proteolytic activity, LasB has various roles during *P. aeruginosa* infections. These include the disruption of the epithelial barriers by damaging intracellular tight junctions, which has been shown by several studies.^[51,57] In addition, its influence on many immunological components that interfere with the host's normal innate and adaptive immune responses allows the infection to reach anaerobic sites and become a chronic infection.^[51,53,54] According to a study in a mouse lung infection model, *lasB* knockout mutant strain RP45 (its wild-type is a clinical isolate from a CF patient, and obtained in the early stage of persistence) did not influence the survival rate of infected mice.^[58] Instead, it resulted in a decreased frequency of chronic lung infections. This displays LasB's significance in *P. aeruginosa*'s early adaptability to chronic colonization.^[58]

On the other hand, Bastaert *et al.* found that mice infected with a *lasB* deletion strain administered intranasally had a greater life expectancy than mice infected with a wild-type strain, implying that this was due to alveolar macrophages' lower capacity to remove LasB+ infections.^[59] According to the same study, they found that recombinant LasB reduced the alveolar macrophages' capacity to eliminate other unrelated pathogens.^[59] Furthermore, Yu *et al.* discovered that LasB plays a role during the biofilm formation, while the *lasB* mutant decreases the biofilm formation through the inhibition of rhamnolipid production.^[60] Other studies were performed on simpler models such as *Galleria mellonella* larvae, showing that injection of recombinant LasB caused a significant reduction in the survival of the larvae.^[61,62] They found that LasB induced a toxic effect *via* activating the prophenoloxidase-activating cascade, which is an important defensive mechanism used by the larvae for entrapping

microorganisms.^[61,62] This activation eventually led to melanization and death. This effect initiated by LasB is comparable to the toxic effect of other M4 peptidases (*i.e.*, thermolysin).^[62–64] These and other studies suggest that LasB is a validated druggable target for pathoblocker development.^[51,53,54,57,65,66] As previously stated (**Section 1.2**), targeting virulence factors is a promising approach due to their important roles *e.g.*, concerning tissue damage and immune response disruption.^[51,53,54,65] In addition, their extracellular localization eliminates the difficulty of penetration, which is the main obstacle to the development of conventional antibiotics against Gram-negatives.^[56]

Inhibition of LasB activity can be accomplished in a number of ways, including direct and indirect inhibition.^[56] These strategies include: **1)** targeting QS-mediated induction to inhibit LasB expression; this method is desirable since it will also lead to the suppression of the expression of other virulence factors.^[67,68] **2)** Sequestering of metal ions necessary for LasB activity (*i.e.*, Zn²⁺ and Ca²⁺); this method is not recommended since it could also inhibit host MMPs.^[69] **3)** Inhibition of the hydrolytic activity of LasB, directly and specifically; this strategy will minimize the influence on host MMPs, which may be essential to re-establish the immune response.^[70–74] **Figure 5.** shows structures of some LasB inhibitors.

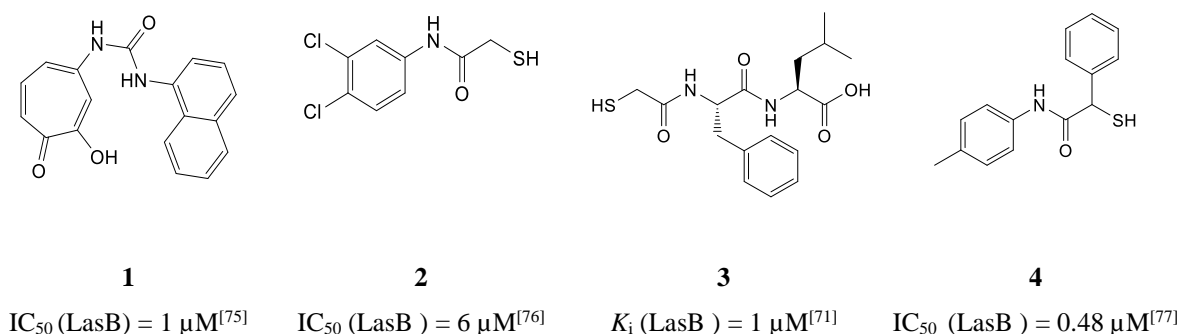


Figure 5. Chemical structure of selected LasB inhibitors with their *in vitro* activity calculated as IC_{50} or K_i . An IC_{50} shows how much compound concentration is required to stop target activity by half. K_i indicates potency of compounds in a biochemical assay with certain substrate concentration.

1.3.2 Collagenases of *Clostridium histolyticum*

Clostridia are anaerobic, sporulating Gram-positive bacteria that include more than 120 species. Well-known species include *C. tetani*, *C. botulinum*, *C. sordellii*, *C. perfringens*, *C. septicum*, *C. novyi*, and *C. histolyticum*.^[45] Many of them pose a public health risk and some even have been used as bioweapons.^[78–80] The clostridial collagenases belong to the M9 peptidase family, which is divided into two classes of well-recognized collagenases.^[81] Class I includes ColG, which is characterized by its high activity on collagen and moderate activity on FALGPA (synthetic peptide used for collagenase kinetic studies).^[81] While class II includes ColH, which

has a moderate activity on collagen and a high activity on FALGPA.^[81] Clostridial collagenases have the ability to cleave collagen (their natural substrate) into a mixture of small peptides by attacking it at multiple sites. Human MMPs, on the other hand, break collagen at a single site.^[45] This high specificity of bacterial collagen-degrading enzymes is ascribed to their active site, which is highly selective for the GPX sequence (a hallmark motif of the collagen triple helix).^[82] *C. histolyticum* (also known as *Hathewayia histolytica*) is one of the most pathogenic bacteria among the clostridial species. It causes gas gangrene, which is a life-threatening infection and could lead to organ amputation.^[78] The histotoxic effect of *C. histolyticum* is largely mediated by its toxins and released hydrolytic enzymes such as protease and collagenase.^[81,83] *C. histolyticum* produces six collagenases.^[83] These have been extensively studied and used as a useful tool for industry^[84] and for clinical use^[85-87] (e.g., to treat some collagen overproduction-related disorders).^[85-87] But their role during bacterial pathogenicity has received less attention.^[45] A few studies^[88] showed the direct role of bacterial collagenase during infection. One of these was performed by Rippon and Peck, who showed that infecting mice with a collagenase-deficient *Actinomadura madura* strain – which causes actinomycosis – resulted in a delayed onset of symptoms and increased their survival rate.^[89] In contrast, infection with a mutant strain that releases excess collagenase resulted in an earlier onset of symptoms and showed high toxicity.^[89] Another study was performed with *Vibrio vulnificus* and showed the significant contribution of the released collagenase in bacterial invasion into human tissue.^[90] The clostridial collagenases have been hypothesized to have similar roles, highlighting the relevance of bacterial collagenases in bacterial infections.^[91,92] This toxicity of collagenases is related to their damaging effect on the main scaffold of the connective tissue (i.e., collagen) and some immunological components.^[93] More studies are needed to characterize the function, kinetics, and specific mechanism of each bacterial collagenase.

The production of clostridial collagenases is regulated by QS. The QS system in *C. perfringens* is the best studied. Studies have shown that two regulatory genes are involved in the expression of the extracellular toxin and collagenase genes namely virR (response regulator) and virS (sensor histidine kinase).^[94,95]

Among the *C. histolyticum* collagenases, ColH and ColG with a molecular weight of ~115 kDa^[45] are the most characterized ones.^[92,96-98] They are Zn²⁺- and Ca²⁺-dependent metalloproteases^[45] and considered as true collagenases (able to cleave the helical region of native folded collagen under physiological conditions).^[45,99] Similar to other bacterial collagenases, ColH and ColG contain a collagenase unit of ~78 kDa. This unit has two domains, the activator and peptidase domains, which are located close to the N-terminus (**Figure**

5).^[96,97,100–102] The Zn^{2+} ion in the active site is coordinated by two histidine residues of the HEXXH motif and a downstream glutamate.^[96,97,100–102] A calcium-binding site was identified near the zinc, which is required for high collagenase activity.^[102,103] The collagenase unit is followed by three accessory domains, which are found at the C-terminus, two polycystic-kidney disease-like domains and one collagen-binding domain for ColH. But there is only one polycystic-kidney disease-like domain and two collagen-binding domains in ColG (**Figure 6**).^[102,104,105]

The first natural product clostridial collagenase inhibitors with nanomolar activities isolated from *Viola yedoensis* were discovered^[106] after that the crystal structure of both proteins (*i.e.*, ColH and ColG) was solved.^[100,102] Then, other inhibitors were found, with a backbone similar to the collagenase substrate. These compounds do have a Zn^{2+} -binding group (ZBG) (such as hydroxamate^[107,108], phosphonic amide^[109,110], and thiol^[111]) that chelates the catalytic Zn^{2+} ion. These inhibitors showed effects at low micromolar to nanomolar concentrations, but their activities on other off-targets (mainly human MMPs) prevented them from progressing to the next stage of drug development.^[107–111]

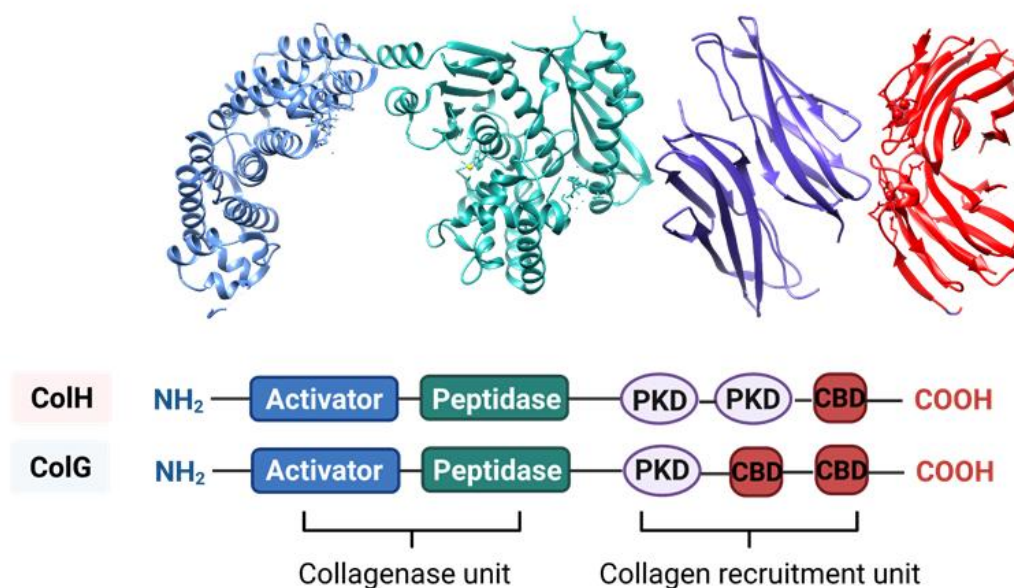


Figure 6. Crystal structures of ColH and ColG domains. Collagenase unit of ColG (PDB: 4ARE), PKD: polycystic kidney disease like-domain (PDB: 4JRW), CBD: collagen-binding domain (PDB: 2O8O). Adapted from Eckhard *et al.*^[105]

In addition, their poor pharmacokinetic profiles, high cytotoxicity, and chemical instability made it difficult for them to be employed for further testing.^[112,113] Therefore, the inhibitor design strategy has been changed in the last several years, shifting the focus to novel ZBGs or non-zinc chelating inhibitors.^[114] In recent years, the Hartmann and Hirsch groups have identified classes of selective inhibitors with unique ZBGs that are active against a wide range

of clostridial collagenases.^[74,115,116] Those inhibitors were shown to have minimal toxicity and some of them proved to be chemically stable (**Figure 7**).

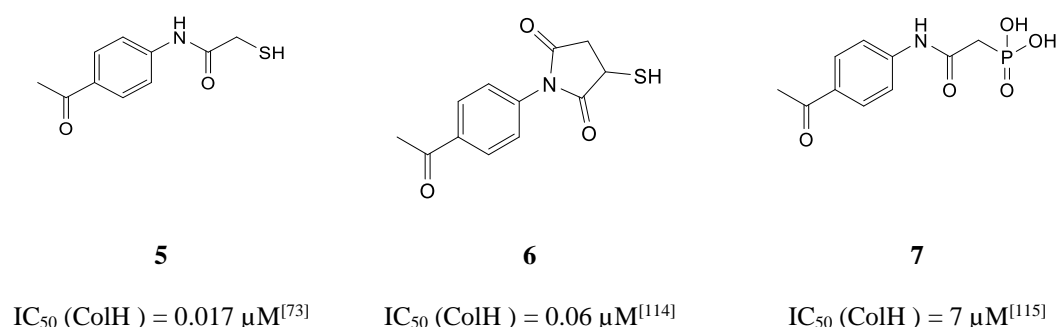


Figure 7. Chemical structure of selected ColH inhibitors with high activity on target and low activity on human off-targets.

1.3.3 Collagenases of *Bacillus cereus*

Bacillus cereus is one of a clinical *Bacillus* isolate; others isolates include *B. megaterium*, *B. mycoides*, *B. cytotoxicus*, *B. thuringiensis*, *B. anthracis*, and *B. pseudomycooides*.^[117] These bacteria are Gram-positive spore-forming motile rod-shaped bacteria that are aerobic or facultatively anaerobic.¹¹⁷ These bacteria can endure harsh ecological circumstances and grow in extremely cold or warm environments because of their capacity to produce spores.^[118] *B. cereus* shares genetic similarities with the human pathogen *B. anthracis* (which causes a fatal disease called anthrax) and the insect pathogen *B. thuringiensis*.^[119] Many studies have been published during this century to record the rise in *B. cereus* infections, indicating that this bacterium causes severe infections that can be fatal.^[117] There are six distinct categories of *B. cereus* infections: **1)** local infections such as burns, post-surgical wounds, and eye infections, **2)** blood infections such as septicemia and bacteremia, **3)** central-nervous-system infections such as meningitis and abscesses, **4)** infections of the respiratory tract, **5)** cardiac infections, and **6)** food poisoning.^[117,118] This opportunistic bacterium generates a range of well-studied toxins and is characterized by the production of extracellular proteases and collagenases.^[119–124] Some of these collagenases are well-characterized.^[119–126] Their significance in *B. cereus* pathogenicity and their direct functions during infection, however, remain not fully understood. Cereolysin, collagenase, hemolysin II, phospholipase C, emetic toxins, proteases, and beta-lactamases are some of the toxins and virulence factors produced by *B. cereus*.^[119] Their synthesis is modulated by QS with the help of a transcription factor named pleiotropic regulon phospholipase C regulator (PlcR).^[127,128]

Bacillary collagenases, like clostridial collagenases, are members of the M9 peptidase family and they target the collagen at multiple locations.^[122,123] They also digest synthetic peptides

such as PZ-PLGPA and FALGPA, which are employed in enzyme-activity assays.^[93] Some collagenases have been shown to play a key role in bacillary infections. For instance, cutaneous anthrax caused by *B. anthracis* is characterized by necrotic skin lesions. As previously reported, this bacterium has the ability to destroy native collagen, which might explain the necrotic lesions.^[126,93] Another study revealed that *B. thuringiensis* utilizes ColB for insect invasion.^[129] Collagenases have also been found to play a role in *B. cereus*-mediated endophthalmitis^[124] and periodontal diseases.^[130] Despite the extensive knowledge of bacillary collagenases, much remains unknown, including crystal structures, characterization of enzymatic activity, and, most importantly, their direct role in *B. cereus* pathogenicity, especially in some severe infections such as wound and gastrointestinal infections.

ColA and ColQ1 from *B. cereus* ATCC 14579 and Q1 strains, respectively, were recently identified.^[122,123] Their crystal structures have not yet been solved, but homology models based on the structure of ColH and ColG were designed for both.^[122,123] These homology models predicted that the domains are arranged similarly to clostridial collagenases, and the catalytic Zn²⁺ ion in the active site of the bacillary collagenase binds also to two histidine residues of the HEXXH motif and to a downstream glutamic acid.^[122,123] In addition, there is a calcium-binding site found in the peptidase domain. Therefore, the enzyme activity is influenced by both Zn²⁺ and Ca²⁺ ions similar to the clostridial collagenases.^[122,123] This similarity in structure might be related to high sequence identity between clostridial collagenases (*i.e.*, ColH and ColG) and ColQ1 and ColA, which is 45% and 70%, respectively.^[122,123]

Furthermore, investigations have shown that these two bacillary collagenases (*i.e.*, ColQ and ColA) have a higher collagenolytic and peptidolytic efficacy than the clostridial enzymes.^[122,123] As previously stated (**Section 1.3**), clostridial ColG harbors the highest collagenolytic activity among bacterial collagenases and is therefore classified in class I, while ColH has the highest peptidolytic activity and belongs to class II.^[81] Bacillary collagenases belong to both classes since they exhibit activity against collagen and small peptides. This activity on both types of substrates can be explained by a different architecture of the active site. The active site of ColG, for instance, has a low affinity for the catalytic Zn²⁺ cation and is comparatively flexible.^[122,123] On the other hand, ColH has a more rigid and stable catalytic core due to the additional Zn²⁺-coordinating residue (*i.e.*, aspartate 421).^[122,123] Instead of Asp 421, ColQ1 has a glutamate, which is thought to help to stabilize the catalytic Zn²⁺ cation.^[123] However, this glutamate is located distant from the catalytic Zn²⁺ cation as suggested by the homology model.^[123] Therefore, it is assumed that the loop area in which it is located is movable. Depending on the substrate type, this loop may either flip up to allow collagen binding

or flip down to allow small peptide binding to resemble the catalytic center of ColH.^[123] This suggests that bacillary collagenases may degrade not only collagen but also other peptides involved in critical physiological mechanisms, thereby speeding up the bacterial invasion. This highlights the need for additional research into their possible functions during infection, as well as the necessity for more investigations into the characterization of novel bacillary collagenases. In contrast to clostridial collagenases, fewer inhibitors are reported in the literature for bacillary collagenases, which may be due to the lack of crystal structures. Some of these compounds are reported to be active against ColH have a lower activity against ColA or ColQ1.^[74,115,116] Examples of these compounds are shown in **Figure 8**.

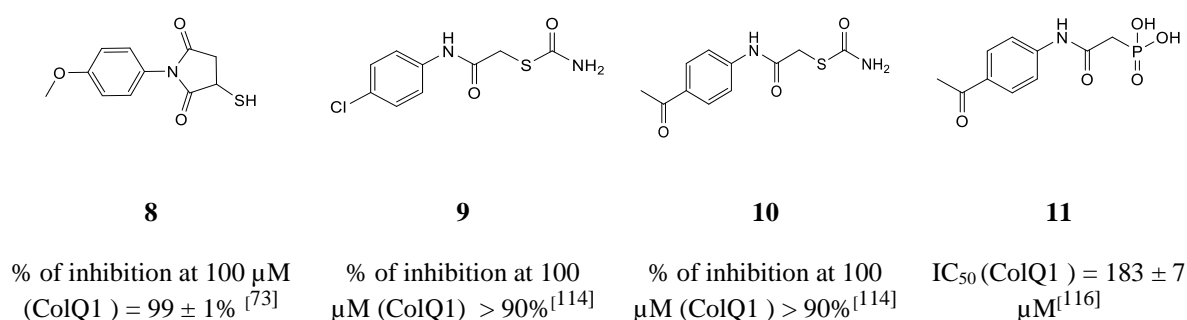


Figure 8. *In vitro* activity and chemical structure of known ColQ1 inhibitors.

1.4 Substrates of bacterial metalloproteases

As indicated in **Section 1.3**, metalloproteases target peptide bonds and may then hydrolyze a wide range of substrates. LasB and bacterial collagenases degrade a variety of substrates, which will be discussed in more detail below.

1.4.1 LasB substrates

Elastin is a crucial protein of the ECM that is found in a wide range of tissues and organs.^[131–133] It gives flexibility to blood vessels, lungs, skin, and breasts and capacity to reshape themselves after being stretched or contracted.^[131–133] Tropoelastin is the primary structural component of elastin fibers (**Figure 9**).^[131–135] It is divided into two domains, one with a hydrophobic and the other with a hydrophilic amino acid sequence.^[131–135] The former contains a lot of hydrophobic amino acids like Gly, Val, and Pro, which help to align the tropoelastin.^[131–135] The hydrophilic domain, on the other hand, is made up of Ala and Lys, which contribute in cross-linking.^[131–135] Due to the substantial cross-linking and durability, elastin resists most proteases and is only susceptible to a few elastases.^[131–139] Elastin does not undergo a considerable turnover in healthy tissue and has a half-life of more than 70 years because of its extensive cross-linking.^[131–139] Elastin degradation is thought to be natural and happens

throughout physiological processes including growth, wound healing, tissue remodeling, and pregnancy.^[131–139] Under some pathogenic circumstances, particularly those that cause breakdown of elastin due to the production of degrading agents, the pace of elastin degradation is accelerated.^[131–139] This deterioration affects not just the equilibrium of ECM components, but also several physiological processes.^[131–140] For instance, when elastin is broken down, it produces elastokines, which stimulate angiogenesis, chemotaxis, proliferation, proteases activation, and apoptosis.^[140] Consequently, it promotes the onset and progression of a variety of diseases, including chronic obstructive pulmonary disease, cancer, metabolic syndrome, and others.^[140] The mechanism of elastin breakdown by LasB starts with LasB approaching the elastin fiber and binding to the hydrophobic domain on the fiber surface.^[137,139,141,142] After that, LasB attacks the sensitive bonds of the hydrophobic and aromatic amino acid residues.^[137,139,141,142] As a result, cavities and holes form on the surface of the fibers. These cavities get larger with time until the fiber is spontaneously broken down into tiny peptides and amino acids.^[137,139,141,142]

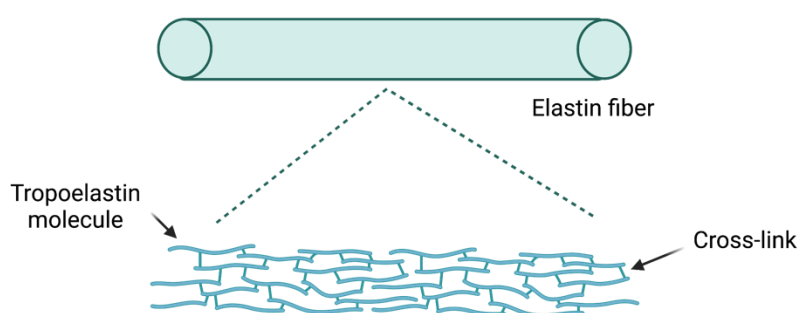


Figure 9. Illustration of an elastin fiber and its composition.

Other structural components that LasB digests include collagen^[143] (see **Section 1.4.2**), laminin,^[144] and peptides involved in the formation of tight junctions, including VE-cadherin and occluding.^[145] It also targets the innate immune components which serve as antimicrobial peptides and antiproteases; LL-37^[145] and elafin,^[145] respectively. LasB hydrolyzes a wide range of host blood components. These include: **1)** lactoferrin and transferrin, causing iron to be released and cytotoxic free radicals to be generated.^[146] **2)** blood clotting proteins such as fibrin, fibrinogen, and thrombin, which causes bleeding.^[147] **3)** hemoglobin, which causes iron-containing heme to be released.^[147] All of these processes induced by LasB will eventually result in bacterial proliferation, tissue injury, and inflammation.

1.4.2 Substrate of bacterial collagenases

The most studied substrate of bacterial collagenases is collagen and its unfolded form (*i.e.*, gelatin).^[98,142,148–150] Collagen is a fibrous protein that provides structure and integrity to tissue

and organs. It is the major component of the ECM, which can be found in skin, bone, blood vessels, and tendons.^[148,151,152] There are 28 subtypes of collagens and their distribution varies among tissues. The most prevalent ones in the ECM are types I, II, and III (80–90%).^[151–153] Fibrillar collagen is made up of three interwoven units, two of which are alpha-1 chains and one of which is an alpha-2 chain (**Figure 10**).^[148,151–153] The chains contain a sequence of repeated amino acids, the most common ones are Gly, Pro, and Hyp.^[154] The high amino acid content and hydrogen bond interactions between the three chains assist to keep the three chains together and stabilize the stiff three-stranded collagen helix.^[148,151–153] Many of these three-stranded collagen molecules clump together side-by-side to form fibrils (**Figure 10**).^[148,151–153] This unique structure of collagen prevents it from being destroyed by most proteolytic enzymes, although it can be destroyed by some MMPs,^[149,150] mammalian cysteine proteases,^[101] and true bacterial collagenases with unique specificities to trigger collagen breakdown.^[82,155] Bacterial collagenases digest collagen by attacking the bond in the repetitive Gly-X-Y motif (ColG and ColH attack distinct sites, thus each has different characteristics for cutting collagen),^[149] resulting in generating a mixture of small peptides and amino acids.^[149] These products can be used by bacteria as a source of carbon and energy.^[82,149,155]

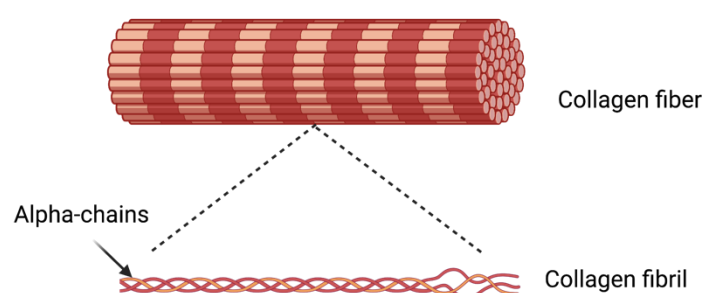


Figure 10. Collagen fiber structure and the alpha-chains of its fibril.

1.5 Antivirulence agent development between concern and hope

As previously indicated (**Section 1.2**), this approach holds a lot of promise, primarily because it does not trigger the evolutionary pressure leading to the development of resistance and preserves the microbiota.^[156] Furthermore, it may enhance antibiotic efficacy and even allow us to use antibiotics that are no longer in use owing to antibiotic resistance.^[25,157,158] Despite these benefits, no small-molecule antivirulence drug has been used in the clinic yet. Most of them are in preclinical or clinical stages.^[25,157,158]

There is a concern about this approach since virulence factors may play a role in bacterial survival *in vivo*, although the *in vitro* data contradict this.^[25,157,158] The main obstacle in determining this *in vivo* is that studying resistance development is challenging. This is due to the complexity of the bacterial transmission and colonization dynamics, which vary between

species and are not well understood.^[159] There are additional practical challenges because compared to antibiotic development, antivirulence agents' development costs more money and time. This is because treating a single germ may require the use of several antivirulence agents.^[159] The limited range of virulence agents may require us to use them in combination with antibiotics. Therefore, the regulatory path of this adjunctive treatment is new. Another obstacle is that the timing of the administration of the antivirulence medicine is very critical because we need to know when the virulence factors are secreted.^[159]

Despite the above-mentioned drawbacks, there is still optimism that these restrictions can be overcome by understanding the specific role of the virulence factors during infection. In addition, a rapid identification of the pathogen would also make it easier to intervene immediately and target the virulence factor once it is released.^[25] An acceleration of clinical trials and a substantial investment would assist scientists to conduct more research and get us more information about these agents and their future.^[25] This hope increased against three pathogens, which are not considered as critical germs, have FDA-approval antivirulence monoclonal antibodies.^[25] These pathogens are *C. botulinum*,^[160] *C. difficile*,^[161] *B. anthracis*,^[162,163] which could cause fatal diseases in some cases. BIG (for *C. botulinum*)^[160], bezlotoxumab (for *C. difficile*)^[161], and raxibacumab (for *B. anthracis*)^[162,163] were authorized for clinical use in 2003, 2016, and 2012, respectively. The clinical trials have demonstrated that inhibition of some of these pathogens' virulence factors and toxins improves patient outcomes.^[160-163] This now calls for showing that also small-molecule antivirulence agents can work in humans.

1.6 Aims of the Thesis

As shown in this chapter, resistance development toward commonly used antibiotics is rapidly evolving, leading to fewer therapeutic options to manage even minor infections. In recent decades, the number of authorized antibiotics has declined, resulting in a substantial gap between the number of available antibiotics and the medical need due to the increasing number of resistant bacteria. The identification of new essential bacterial targets, as well as alternative non-antibiotic approaches, are promising strategies to combat the rise in antibiotic resistance. Extracellular proteases are attractive therapeutic targets for antivirulence agent discovery, as they are pivotal for numerous processes in bacteria, including host colonization, immunological evasion, and exotoxin diffusion. Targeting these proteases will not exert the evolutionary pressure for drug-resistant mutants, offering the host immune system a better chance of eradicating and removing the bacteria. Furthermore, their extracellular localization allows us to

avoid possible permeability and efflux pump concerns, which are currently major issues in the development of antibiotics.

Recently, several monoclonal antibodies – targeting secreted toxins of pathogenic bacteria – have received FDA approval. This implies evidence that small-molecule antivirulence agents represent a promising strategy to confront infections. Several small-molecule inhibitors of bacterial proteases have been discovered, however, due to their poor selectivity toward human MMPs, chemical instability, and cytotoxicity, the majority of them have failed to enter the pre-clinical phase. In addition, the lack of suitable pre-clinical models simulating the infection settings to ensure the biological properties of new targets and efficacy of newly developed antivirulence, lead to the failure to adequately characterize the biological activity of novel compounds. This will subsequently delay their clinical evaluation and application.

This thesis aimed to characterize and validate bacterial collagenases (*i.e.*, LasB of *P. aeruginosa*, ColQ1 of *B. cereus*, and ColH of *C. histolyticum*) by pursuing two approaches:

- I. Establishing pre-clinical models mimicking the infection conditions induced by collagenase-producing bacteria to investigate the activity of the aforementioned collagenases. These models include *in vitro* cell-based, *ex vivo* pig-skin, and *in vivo* *Galleria mellonella* models. The evaluation of the results obtained from these models was conducted using *in vitro* biochemical, bioanalytical, and advanced microscopic techniques. The outcomes of this part are highlighted in **subchapters 2.1, 2.2, and 2.4**.
- II. The second part of this study focuses on the characterization of newly discovered potent, selective, and chemically stable small-molecule collagenase inhibitors. Using the established pre-clinical models, the biological efficacy of the most active inhibitors was evaluated. In addition, selectivity over a panel of human off-targets, cytotoxicity, and *in vitro* efficacy were also assessed using various assays. Two representative bacterial collagenase inhibitors were combined with a collagen inducer molecule, their efficacy as a therapeutic tool for wound infections was explored. The results of this part are outlined in **subchapters 2.1, 2.3, and 2.4**.

1.7 References

1. Varley, A. J., Sule, J. & Absalom, A. R. Principles of antibiotic therapy. *Contin. Educ. Anaesthesia, Crit. Care Pain* **9**, 184–188 (2009).
2. Sahra Kirmusaoğlu, N. G. and B. S. K. Introductory Chapter: The Action Mechanisms of Antibiotics and Antibiotic Resistance, Antimicrobials, Antibiotic Resistance, Antibiofilm Strategies and Activity Methods. in (2019). doi:10.5772/intechopen.78751
3. Fleming, A. On the Antibacterial Action of Cultures of a *Penicillium*, with Special Reference to their Use in the Isolation of *B. influenzae*. *Br. J. Exp. Pathol.* **10(3)**, 226–236 (1929).
4. Zaman, S. Bin *et al.* A Review on Antibiotic Resistance: Alarm Bells are Ringing. *Cureus* **9**, (2017).
5. Levy, S. B. & Bonnie, M. Antibacterial resistance worldwide: Causes, challenges and responses. *Nat. Med.* **10**, S122–S129 (2004).
6. Abraham, E. P. & Chain, E. An Enzyme from Bacteria able to Destroy Penicillin. *Nature* **146**, 837 (1940).
7. Fleming, A. Penicillin (Nobel lecture). (1945).
8. Alanis, A. J. Resistance to antibiotics: Are we in the post-antibiotic era? *Arch. Med. Res.* **36**, 697–705 (2005).
9. Schey, K. L., Luther, J. M. & Rose, K. L. Structure-activity relationship of compounds targeting mycobacterium tuberculosis 1-deoxy-D-xylulose 5-phosphate synthase. **95**, 1–21 (2016).
10. Lee, P. R. (Philip R. & Lin, C. The Antibiotic Paradox: How the Misuse of Antibiotics Destroys Their Curative Powers. *Perspect. Biol. Med.* **46**, 603–604 (2003).
11. Vanderhaeghen, W. & Dewulf, J. Antimicrobial use and resistance in animals. *Lancet Planet. Heal.* **1**, e307–e308 (2017).
12. Witte, W. Medical Consequences of Antibiotic Use in Agriculture. *Science (80-.)*. **279**, 996–997 (1998).
13. De J. Sosa, A. *et al.* Antimicrobial resistance in developing countries. *Antimicrob. Resist. Dev. Ctries.* 1–554 (2010). doi:10.1007/978-0-387-89370-9
14. Coates, A. R. M. & Hu, Y. Novel approaches to developing new antibiotics for bacterial infections. *Br. J. Pharmacol.* **152**, 1147–1154 (2007).
15. Silver, L. L. A Gestalt approach to Gram-negative entry. *Bioorganic Med. Chem.* **24**, 6379–6389 (2016).
16. Lewis, K. Platforms for antibiotic discovery. *Nat. Rev. Drug Discov.* **12**, 371–387 (2013).
17. Årdal, C. *et al.* Antibiotic development — economic, regulatory and societal challenges. *Nat. Rev. Microbiol.* **18**, 267–274 (2020).
18. Bartlett, J. G., Gilbert, D. N. & Spellberg, B. Seven ways to preserve the Miracle of antibiotics. *Clin. Infect. Dis.* **56**, 1445–1450 (2013).
19. Opal, S. M. Non-antibiotic treatments for bacterial diseases in an era of progressive antibiotic resistance. *Crit. Care* **20**, 10–12 (2016).
20. Kealey, C., Creaven, C. A., Murphy, C. D. & Brady, C. B. New approaches to antibiotic discovery. *Biotechnol. Lett.* **39**, 805–817 (2017).
21. Read, A. F. & Woods, R. J. Antibiotic resistance management. *Evol. Med. Public Heal.* **2014**, 147 (2014).
22. Hauser, A. R., Mecsas, J. & Moir, D. T. Beyond antibiotics: New therapeutic approaches for bacterial

- infections. *Clin. Infect. Dis.* **63**, 89–95 (2016).
23. Masini, T. & Hirsch, A. K. H. Development of Inhibitors of the 2 C -Methyl- d -erythritol 4-Phosphate (MEP) Pathway Enzymes as Potential Anti-Infective Agents. *J. Med. Chem.* **57**, 9740–9763 (2014).
 24. Cansizoglu, M. F. & Toprak, E. Fighting against evolution of antibiotic resistance by utilizing evolvable antimicrobial drugs. *Curr. Genet.* **63**, 973–976 (2017).
 25. Dickey, S. W., Cheung, G. Y. C. & Otto, M. Different drugs for bad bugs: Antivirulence strategies in the age of antibiotic resistance. *Nat. Rev. Drug Discov.* **16**, 457–471 (2017).
 26. Dufour, D., Leung, V. & Lévesque, C. M. Bacterial biofilm : structure , function , and antimicrobial resistance. *Endod. Top.* **22**, 2–16 (2010).
 27. Jamal, M., Tasneem, U., Hussain, T. & Andleeb, and S. Bacterial Biofilm: Its Composition, Formation and Role in Human Infections. *Res. Rev. J. Microbiol. Biotechnol.* **4**, 1–14 (2015).
 28. Beloin, C., Renard, S., Ghigo, J. M. & Lebeaux, D. Novel approaches to combat bacterial biofilms. *Curr. Opin. Pharmacol.* **18**, 61–68 (2014).
 29. Chauhan, A. *et al.* Preventing biofilm formation and associated occlusion by biomimetic glycocalyxlike polymer in central venous catheters. *J. Infect. Dis.* **210**, 1347–1356 (2014).
 30. Krachler, A. M. & Orth, K. Targeting the bacteria-host interface strategies in anti-adhesion therapy. *Virulence* **4**, 284–294 (2013).
 31. Rampioni, G., Leoni, L. & Williams, P. The art of antibacterial warfare: Deception through interference with quorum sensing-mediated communication. *Bioorg. Chem.* **55**, 60–68 (2014).
 32. Jiang, Q. *et al.* Quorum Sensing: A Prospective Therapeutic Target for Bacterial Diseases. *Biomed Res. Int.* **2019**, (2019).
 33. Henry, B. D. *et al.* Engineered liposomes sequester bacterial exotoxins and protect from severe invasive infections in mice. *Nat. Biotechnol.* **33**, 81–88 (2015).
 34. Lin, D. M., Koskella, B. & Lin, H. C. Phage therapy: An alternative to antibiotics in the age of multi-drug resistance. *World J. Gastrointest. Pharmacol. Ther.* **8**, 162 (2017).
 35. Liu, N., Lewis, C., Zheng, W. & Fu, Z. Q. Phage Cocktail Therapy: Multiple Ways to Suppress Pathogenicity. *Trends Plant Sci.* **25**, 315–317 (2020).
 36. Hancock, R. E. W., Nijnik, A. & Philpott, D. J. Modulating immunity as a therapy for bacterial infections. *Nat. Rev. Microbiol.* **10**, 243–254 (2012).
 37. Ramamurthy, D. *et al.* Recent advances in immunotherapies against infectious diseases. *Immunother. Adv.* **1**, 1–16 (2021).
 38. WHO. BGC vaccine. Available at: <https://www.who.int/teams/health-product-policy-and-standards/standards-and-specifications/vaccines-quality/bcg>.
 39. Wu, J. W. & Chen, X. L. Extracellular metalloproteases from bacteria. *Appl. Microbiol. Biotechnol.* **92**, 253–262 (2011).
 40. Hase, C. & Finkelstein, R. A. Bacterial extracellular zinc-containing metalloproteases. *Microbiol. Rev.* **57**, 823–837 (1993).
 41. Malemud, C. J. Matrix metalloproteinases (MMPs) in health and disease: an overview. *Front. Biosci.* **11**, 1696–1701 (2006).
 42. Wong, J., Patel, R. A. & Kowey, P. R. The clinical use of angiotensin-converting enzyme inhibitors. *Prog.*

- Cardiovasc. Dis.* **47**, 116–130 (2004).
43. Ververis, K., Hiong, A., Karagiannis, T. C. & Licciardi, P. V. Histone deacetylase inhibitors (HDACIs): multitargeted anticancer agents. *Biol. Targets Ther.* **7**, 47–60 (2013).
 44. Marcello Di Nisio, Saskia Middeldorp, and H. R. B. Direct Thrombin Inhibitors. *N. Engl. J. Med.* (2005). doi:10.1056/NEJMra044440
 45. Brandstetter, H. and Schönauer, E. Inhibition and Activity Regulation of Bacterial Collagenases. in *Zinc Enzyme Inhibitors: Enzymes from Microorganisms* 156 (2017).
 46. Culp, E. & Wright, G. D. Bacterial proteases, untapped antimicrobial drug targets. *J. Antibiot. (Tokyo)*. **70**, 366–377 (2017).
 47. Agbowuro, A. A., Huston, W. M., Gamble, A. B. & Tyndall, J. D. A. Proteases and protease inhibitors in infectious diseases. *Med. Res. Rev.* **38**, 1295–1331 (2018).
 48. Gellatly, S. L. & Hancock, R. E. W. *Pseudomonas aeruginosa*: New insights into pathogenesis and host defenses. *Pathog. Dis.* **67**, 159–173 (2013).
 49. WHO (World Health Organization). WHO publishes list of bacteria for which new antibiotics are urgently needed. (2017). Available at: <https://www.who.int/news/item/27-02-2017-who-publishes-list-of-bacteria-for-which-new-antibiotics-are-urgently-needed>.
 50. Santajit, S. & Indrawattana, N. Mechanisms of Antimicrobial Resistance in ESKAPE Pathogens. *Biomed Res. Int.* **2016**, (2016).
 51. Chakraborti, S. & Dhalla, N. S. *Pseudomonas aeruginosa* and Its Arsenal of Proteases: Weapons to Battle the Host. *Pathophysiol. Asp. Proteases* 1–671 (2017). doi:10.1007/978-981-10-6141-7
 52. Wretling, R. B. & Olgerts, A. *Pseudomonas aeruginosa* Elastase and Its Role in *Pseudomonas* Infections. *Rev Infect Dis.* **5**, S998-1004 (1983).
 53. Kuang, Z. *et al.* *Pseudomonas aeruginosa* Elastase provides an Escape from phagocytosis by degrading the pulmonary surfactant protein-A. *PLoS One* **6**, (2011).
 54. Kessler, E., Safrin, M., Gustin, J. K. & Ohman, D. E. Elastase and the LasA protease of *Pseudomonas aeruginosa* are secreted with their propeptides. *J. Biol. Chem.* **273**, 30225–30231 (1998).
 55. Thayer, M. M., Flaherty, K. M. & McKay, D. B. Three-dimensional structure of the elastase of *Pseudomonas aeruginosa* at 1.5-Å resolution. *J. Biol. Chem.* **266**, 2864–2871 (1991).
 56. Everett, M. J. & Davies, D. T. *Pseudomonas aeruginosa* elastase (LasB) as a therapeutic target. *Drug Discov. Today* **00**, (2021).
 57. van 't Wout, E. F. A. *et al.* Virulence Factors of *Pseudomonas aeruginosa* Induce Both the Unfolded Protein and Integrated Stress Responses in Airway Epithelial Cells. *PLoS Pathog.* **11**, 1–23 (2015).
 58. Cigana, C. *et al.* *Pseudomonas aeruginosa* Elastase Contributes to the Establishment of Chronic Lung Colonization and Modulates the Immune Response in a Murine Model. *Front. Microbiol.* **11**, (2021).
 59. Bastaert, F. *et al.* *Pseudomonas aeruginosa* LasB subverts alveolar macrophage activity by interfering with bacterial killing through downregulation of innate immune defense, reactive oxygen species generation, and complement activation. *Front. Immunol.* **9**, 1–18 (2018).
 60. Hua Yu, Xiaomei He, Wei Xie, Junzhi Xiong, Haili Sheng, Shaodong Guo, Chunji Huang, Di Zhang, and K. Z. Elastase LasB of *Pseudomonas aeruginosa* promotes biofilm formation partly through rhamnolipid-mediated regulation. *Can. J. Microbiol.* (2014).
 61. Andrejko, M. & Mizerska-Dudka, M. Effect of *pseudomonas aeruginosa* elastase B on level and activity

- of immune proteins/peptides of *Galleria mellonella* hemolymph. *J. Insect Sci.* **12**, 1–14 (2012).
62. Andrejko, M. & Mizerska-Dudka, M. Elastase B of *Pseudomonas aeruginosa* stimulates the humoral immune response in the greater wax moth, *Galleria mellonella*. *J. Invertebr. Pathol.* **107**, 16–26 (2011).
 63. Kay, S., Edwards, J., Brown, J. & Dixon, R. *Galleria mellonella* infection model identifies both high and low lethality of clostridium perfringens toxigenic strains and their response to antimicrobials. *Front. Microbiol.* **10**, 1–11 (2019).
 64. Wedde, M., Weise, C., Kopacek, P., Franke, P. & Vilcinskas, A. Purification and characterization of an inducible metalloprotease inhibitor from the hemolymph of greater wax moth larvae, *Galleria mellonella*. *Eur. J. Biochem.* **255**, 535–543 (1998).
 65. Anna Clara M. Galdino, Matheus P. de Oliveira, Teodorico C. Ramalho, Alexandre A. de Castro, Marta H. Branquinha, A. L. S. S. Anti-Virulence Strategy against the Multidrug-Resistant Bacterial Pathogen *Pseudomonas aeruginosa*: Pseudolysin (Elastase B) as a Potential Druggable Target. *Curr. Protein Pept. Sci.* **20**, (2019).
 66. De Bentzmann, S. *et al.* *Pseudomonas aeruginosa* virulence factors delay airway epithelial wound repair by altering the actin cytoskeleton and inducing overactivation of epithelial matrix metalloproteinase-2. *Lab. Investig.* **80**, 209–219 (2000).
 67. Hemmati, F. *et al.* Quorum quenching: A potential target for antipseudomonal therapy. *Infect. Drug Resist.* **13**, 2989–3005 (2020).
 68. Pattnaik, S. S. *et al.* Attenuation of quorum sensing regulated virulence and biofilm development in *Pseudomonas aeruginosa* PAO1 by *Diaporthe phaseolorum* SSP12. *Microb. Pathog.* **118**, 177–189 (2018).
 69. Gi, M. *et al.* A drug-repositioning screening identifies pentetic acid as a potential therapeutic agent for suppressing the elastase-mediated virulence of *Pseudomonas aeruginosa*. *Antimicrob. Agents Chemother.* **58**, 7205–7214 (2014).
 70. Grobelny, D., Poncz, L. & Jj, R. E. G. Inhibition of Human Skin Fibroblast Collagenase, Thermolysin, and *Pseudomonas aeruginosa* elastase by Peptide Hydroxamic Acids. 7152–7154 (1992).
 71. Burns, F. R., Paterson, C. A., Gray, R. D. & Wells, J. T. Inhibition of *Pseudomonas aeruginosa* elastase and *Pseudomonas keratitis* using a thiol-based peptide. *Antimicrob. Agents Chemother.* **34**, 2065–2069 (1990).
 72. Kessler, E. & Spierer, A. Inhibition by phosphoramidon of *pseudomonas aeruginosa* elastase injected intracorneally in rabbit eyes. *Curr. Eye Res.* **3**, 1075–1078 (1984).
 73. Kany, A. M. *et al.* Binding Mode Characterization and Early in Vivo Evaluation of Fragment-Like Thiols as Inhibitors of the Virulence Factor LasB from *Pseudomonas aeruginosa*. *ACS Infect. Dis.* **4**, 988–997 (2018).
 74. Konstantinović, J. *et al.* N-Aryl-3-mercaptosuccinimides as Antivirulence Agents Targeting *Pseudomonas aeruginosa* Elastase and *Clostridium* Collagenases. *J. Med. Chem.* **63**, 8359–8368 (2020).
 75. Jessica L. Fullagar, Amanda L. Garner, Anjali K. Struss, Joshua A. Day, David P. Martin, Jing Yu, Xiaoqing Cai, K. D. J. and S. M. C. Antagonism of a zinc metalloprotease using a unique metal-chelating scaffold: tropolones as inhibitors of *P. aeruginosa* elastase. *Chem. Commun.* (2013). doi:10.1039/C3CC41191E
 76. Kany, A. M. *et al.* Binding Mode Characterization and Early in Vivo Evaluation of Fragment-Like Thiols as Inhibitors of the Virulence Factor LasB from *Pseudomonas aeruginosa*. *ACS Infect. Dis.* **4**, 988–997 (2018).
 77. Kaya, C. *et al.* Substrate-Inspired Fragment Merging and Growing Affords Efficacious LasB Inhibitors. *Angew. Chemie Int. Ed.* (2021). doi:10.1002/anie.202112295

78. Leiblein, M. *et al.* Clostridial Gas Gangrene - A Rare but Deadly Infection: Case series and Comparison to Other Necrotizing Soft Tissue Infections. *Orthop. Surg.* **12**, 1733–1747 (2020).
79. Hatheway, C. L. Toxigenic clostridia. *Clin. Microbiol. Rev.* **3**, 66–98 (1990).
80. Borriello, S. P. Clostridial disease of the Gut. *Clin. Infect. Dis.* **20**, S242–S250 (1995).
81. Duarte, A. S., Correia, A. & Esteves, A. C. Bacterial collagenases - A review. *Crit. Rev. Microbiol.* **42**, 106–126 (2016).
82. Eckhard, U., Huesgen, P. F., Brandstetter, H. & Overall, C. M. Proteomic protease specificity profiling of clostridial collagenases reveals their intrinsic nature as dedicated degraders of collagen. *J. Proteomics* **100**, 102–114 (2014).
83. Bond, M. D. & Van Wart, H. E. Characterization of the Individual Collagenases from *Clostridium histolyticum*. *Biochemistry* **23**, 3085–3091 (1984).
84. Pal, G. K. & Suresh, P. V. Microbial collagenases: Challenges and prospects in production and potential applications in food and nutrition. *RSC Adv.* **6**, 33763–33780 (2016).
85. Hurst LC, Badalamente MA, H. V. Injectable collagenase clostridium histolyticum for Dupuytren's contracture. *N. Engl. J. Med.* (2009). doi:10.1056/nejmoa0810866
86. Dhillon, S. Collagenase *Clostridium Histolyticum*: A Review in Peyronie's Disease. *Drugs* **75**, 1405–1412 (2015).
87. Shi Lei, C. D. Collagenase Santyl ointment. A selective agent for wound debridement. *Wound Ostomy Cont. Nurs.* (2009). doi:10.1097/WON.0b013e3181bfdd1a.
88. Michel R Popoff, P. B. Clostridial toxins. *Futur. Microbiol* (2009). doi:10.2217/fmb.09.72
89. Rippon JW, P. G. Experimental infection with *Streptomyces madurae* as a function of collagenase. *J Invest Dermatol.* (1967). doi:10.1038/jid.1967.151
90. Smith, G. C. & Merkel, J. R. Collagenolytic activity of *Vibrio vulnificus*: Potential contribution to its invasiveness. *Infect. Immun.* **35**, 1155–1156 (1982).
91. Matsushita, O., Yoshihara, K., Katayama, S. I., Minami, J. & Okabe, A. Purification and characterization of a *Clostridium perfringens* 120- kilodalton collagenase and nucleotide sequence of the corresponding gene. *J. Bacteriol.* **176**, 149–156 (1994).
92. Matsushita, O. & Okabe, A. Clostridial hydrolytic enzymes degrading extracellular components. **39**, (2001).
93. Harrington, D. J. Bacterial Collagenases and Collagen-Degrading Enzymes and Their Potential Role in Human Disease. **64**, 1885–1891 (1996).
94. Ba-Thein, W. *et al.* The *virR/virS* locus regulates the transcription of genes encoding extracellular toxin production in *Clostridium perfringens*. *J. Bacteriol.* **178**, 2514–2520 (1996).
95. Ohtani, K. *et al.* Virulence gene regulation by the *agr* system in *Clostridium perfringens*. *J. Bacteriol.* **191**, 3919–3927 (2009).
96. Matsushita, O. *et al.* Gene duplication and multiplicity of collagenases in *Clostridium histolyticum*. *J. Bacteriol.* **181**, 923–933 (1999).
97. Matsushita, O., Koide, T., Kobayashi, R., Nagata, K. & Okabe, A. Substrate Recognition by the Collagen-binding Domain of *Clostridium histolyticum* Class I Collagenase. *J. Biol. Chem.* **276**, 8761–8770 (2001).
98. Shi, L., Ermis, R., Garcia, A., Telgenhoff, D. & Aust, D. Degradation of human collagen isoforms by

- Clostridium collagenase and the effects of degradation products on cell migration. *Int. Wound J.* **7**, 87–95 (2010).
99. Mitchell, W. M. Pseudocollagenase: A protease from *Clostridium histolyticum*. *BBA - Enzymol.* **159**, 554–557 (1968).
100. Eckhard, U., Schönauer, E., Nüss, D. & Brandstetter, H. Structure of collagenase G reveals a chew-and-digest mechanism of bacterial collagenolysis. *Nat. Struct. Mol. Biol.* **18**, 1109–1114 (2010).
101. Zhang, Y. Z., Ran, L. Y., Li, C. Y. & Chen, X. L. Diversity, structures, and collagen-degrading mechanisms of bacterial collagenolytic proteases. *Appl. Environ. Microbiol.* **81**, 6098–6107 (2015).
102. Bauer, R. *et al.* Structural comparison of ColH and ColG collagen-binding domains from *Clostridium histolyticum*. *J. Bacteriol.* **195**, 318–327 (2013).
103. D L Head, J. A. Y. J. The effect of calcium chloride on the activity and inhibition of bacterial collagenase. *Int J Pept Protein Res.* (1976). doi:10.1111/j.1399-3011.1976.tb02491.x
104. Jung C.M., Matsushita O., Katayama S., Minami J., Sakurai J., O. A. Identification of metal ligands in the *Clostridium histolyticum* ColH collagenase. *J. Bacteriol.* (1999). doi:10.1128/JB.181.9.2816-2822
105. Eckhard, U., Schönauer, E. & Brandstetter, H. Structural Basis for Activity Regulation and Substrate Preference of Clostridial Collagenases G , H , and T * □. **288**, 20184–20194 (2013).
106. Oshima, N., Narukawa, Y., Takeda, T. & Kiuchi, F. Collagenase inhibitors from *Viola yedoensis*. *J. Nat. Med.* **67**, 240–245 (2013).
107. Clare, B. W., Scozzafava, A. & Supuran, C. T. Protease inhibitors: Synthesis of a series of bacterial collagenase inhibitors of the sulfonyl amino acyl hydroxamate type. *J. Med. Chem.* **44**, 2253–2258 (2001).
108. A, S. & CT, S. Protease inhibitors: synthesis of clostridium histolyticum collagenase inhibitors incorporating sulfonyl-L-alanine hydroxamate moieties. *Bioorg. Med. Chem. Lett.* (2000). doi:10.1016/s0960-894x(00)00026-3
109. DIVE, V., YIOTAKIS, A., NICOLAOU, A. & TOMA, F. Inhibition of *Clostridium histolyticum* collagenases by phosphonamide peptide inhibitors. *Eur. J. Biochem.* **191**, 685–689 (1990).
110. R E Galaray, D. G. Inhibition of collagenase from *Clostridium histolyticum* by phosphoric and phosphonic amides. *Biochemistry* (1983). doi:10.1021/bi00288a032
111. Biochimie, S. De, Biologie, D. De, Biochimie, S. De & Biologie, D. New thiol inhibitors of *Clostridium histolyticum* collagenase. **766**, 761–766 (1988).
112. Scozzafava, A. & Supuran, C. T. Protease inhibitors: Synthesis of matrix metalloproteinase and bacterial collagenase inhibitors incorporating 5-amino-2-mercapto-1,3,4-thiadiazole zinc binding functions. *Bioorganic Med. Chem. Lett.* **12**, 2667–2672 (2002).
113. Rouffet, M. & Cohen, S. M. Emerging trends in metalloprotein inhibition. *Dalt. Trans.* **40**, 3445–3454 (2011).
114. Jacobsen, J. A., Major Jourden, J. L., Miller, M. T. & Cohen, S. M. To bind zinc or not to bind zinc: An examination of innovative approaches to improved metalloproteinase inhibition. *Biochim. Biophys. Acta - Mol. Cell Res.* **1803**, 72–94 (2010).
115. Voos, K. *et al.* Phosphonate as a Stable Zinc-Binding Group for “Pathoblocker” Inhibitors of Clostridial Collagenase H (ColH). *ChemMedChem* **16**, 1257–1267 (2021).
116. Schönauer, E. *et al.* Discovery of a Potent Inhibitor Class with High Selectivity toward Clostridial Collagenases. *J. Am. Chem. Soc.* **139**, 12696–12703 (2017).

117. Yilmaz, N. *et al.* *Bacillus cereus* and Related Species. **6**, 39–54 (2012).
118. Callegan, M. C., Kane, S. T., Cochran, D. C. & Gilmore, M. S. Epidemiology and pathogenesis of *Bacillus cereus* infections. *DNA Cell Biol.* **21**, 367–373 (2002).
119. Turnbull, P. C. B. *Bacillus cereus* toxins. *Pharmacol. Ther.* **13**, 453–505 (1981).
120. Pequeno, A. C. L. *et al.* Production and characterization of collagenase from a new Amazonian *Bacillus cereus* strain. *Prep. Biochem. Biotechnol.* **49**, 501–509 (2019).
121. Liu, L., Ma, M., Cai, Z., Yang, X. & Wang, W. Purification and properties of a collagenolytic protease produced by *Bacillus cereus* MBL13 strain. *Food Technol. Biotechnol.* **48**, 151–160 (2010).
122. Abfalter, C. M. *et al.* Cloning, Purification and Characterization of the Collagenase ColA Expressed by *Bacillus cereus* ATCC 14579. *PLoS One* **11**, 1–19 (2016).
123. Hoppe, I. J., Brandstetter, H. & Schönauer, E. Biochemical characterisation of a collagenase from *Bacillus cereus* strain Q1. *Sci. Rep.* **11**, 1–15 (2021).
124. Beecher, D. J., Olsen, T. W., Somers, E. B. & Wong, A. C. L. Evidence for contribution of tripartite hemolysin BL, phosphatidylcholine-preferring phospholipase C, and collagenase to virulence of *Bacillus cereus* endophthalmitis. *Infect. Immun.* **68**, 5269–5276 (2000).
125. Zhang, X. X. *et al.* Identification of a collagenase produced by *Bacillus cereus* R75E isolated from human colostrum. *Appl. Biochem. Microbiol.* **51**, 511–521 (2015).
126. EVANS, D. G. & WARDLAW, A. C. Gelatinase and collagenase production by certain species of *Bacillus*. *J. Gen. Microbiol.* **8**, 481–487 (1953).
127. Rutherford, S. T. & Bassler, B. L. Bacterial quorum sensing: Its role in virulence and possibilities for its control. *Cold Spring Harb. Perspect. Med.* **2**, 1–25 (2012).
128. Gohar, M. *et al.* The PlcR virulence regulon of *Bacillus cereus*. *PLoS One* **3**, 1–9 (2008).
129. Peng, D. *et al.* A novel metalloproteinase virulence factor is involved in *Bacillus thuringiensis* pathogenesis in nematodes and insects. *Environ. Microbiol.* **18**, 846–862 (2016).
130. Makinen, K. K. & Makinen, P. L. Purification and properties of an extracellular collagenolytic protease produced by the human oral bacterium *Bacillus cereus* (strain Soc 67). *J. Biol. Chem.* **262**, 12488–12495 (1987).
131. Cay M. Kielty, M. J. S. and C. A. S. Elastic fibre. *Therm. Eng.* **46**, 51–54 (1999).
132. Keeley, F. W., Bellingham, C. M. & Woodhouse, K. A. Elastin as a self-organizing biomaterial: Use of recombinantly expressed human elastin polypeptides as a model for investigations of structure and self-assembly of elastin. *Philos. Trans. R. Soc. B Biol. Sci.* **357**, 185–189 (2002).
133. Debelle, L. & Alix, A. J. P. The structures of elastins and their function. *Biochimie* **81**, 981–994 (1999).
134. Vindin H, Mithieux SM, W. A. Elastin architecture. *Matrix Biol.* (2019). doi:10.1016/j.matbio.2019.07.005
135. MECHAM, R. P. Elastin Synthesis and Fiber Assembly. *Ann. N. Y. Acad. Sci.* (1991). doi:10.1111/j.1749-6632.1991.tb17013.x
136. HALL, D. A. & GARDINER, J. E. The reaction between elastase and elastic tissue. *Biochem. J.* **59**, 465–470 (1955).
137. Nakamura, Y., Okamoto, K., Tanimura, A., Kato, M. & Morimatsu, M. Elastase digestion and biochemical analysis of the elastin from an elastofibroma. *Cancer* **58**, 1070–1075 (1986).

138. Lamy, F., Craig, C. P. & Tauber, S. Studies on Elastase and Elastin. *J. Biol. Chem.* **236**, 86–91 (1961).
139. Werb, Z., Banda, M. J., McKerrow, J. H. & Sandhaus, R. A. Elastases and elastin degradation. *J. Invest. Dermatol.* **79**, 154–159 (1982).
140. Heinz, A. Elastases and elastokines: elastin degradation and its significance in health and disease. *Crit. Rev. Biochem. Mol. Biol.* **55**, 252–273 (2020).
141. Yang, J. *et al.* Mechanistic Insights into Elastin Degradation by Pseudolysin, the Major Virulence Factor of the Opportunistic Pathogen *Pseudomonas aeruginosa*. *Sci. Rep.* **5**, 1–7 (2015).
142. Mindaye, S. T. New Insights in the Degradation of Elastin and Collagens by Matrix Metalloproteinases. (2010).
143. Nagano, T. *et al.* Stimulatory effect of pseudomonal elastase on collagen degradation by cultured keratocytes. *Investig. Ophthalmol. Vis. Sci.* **42**, 1247–1253 (2001).
144. LOUIS W. HECK, KAZUYUKI MORIHARA, A. D. R. A. Degradation of Soluble Laminin and Depletion of Tissue-Associated Basement Membrane Laminin by *Pseudomonas aeruginosa* Elastase and Alkaline Protease. **54**, 149–153 (1986).
145. Beaufort, N., Corvazier, E., Mlanaoindrou, S., de Bentzmann, S. & Pidard, D. Disruption of the Endothelial Barrier by Proteases from the Bacterial Pathogen *Pseudomonas aeruginosa*: Implication of Matrilysin and Receptor Cleavage. *PLoS One* **8**, 1–16 (2013).
146. Wolz, C. *et al.* Iron release from transferrin by pyoverdinin and elastase from *Pseudomonas aeruginosa*. *Infect. Immun.* **62**, 4021–4027 (1994).
147. Komori, Y., Nonogaki, T. & Nikai, T. Hemorrhagic activity and muscle damaging effect of *Pseudomonas aeruginosa* metalloproteinase (elastase). *Toxicon* **39**, 1327–1332 (2001).
148. Charvolin, J. & Sadoc, J. F. About collagen, a tribute to Yves Bouligand. *Interface Focus* **2**, 567–574 (2012).
149. Fields, G. B. Interstitial collagen catabolism. *J. Biol. Chem.* **288**, 8785–8793 (2013).
150. Lauer-Fields JL, Juska D, F. G. Matrix metalloproteinases and collagen catabolism. *Biopolymers*. (2002). doi:10.1002/bip.10201
151. Ricard-Blum, S. The Collagen Family. *Cold Spring Harb. Perspect. Biol.* **3**, 1–19 (2011).
152. Gordon, M. K. & Hahn, R. A. Collagens. *Cell Tissue Res.* **339**, 247–257 (2010).
153. Gelse, K., Pöschl, E. & Aigner, T. Collagens - Structure, function, and biosynthesis. *Adv. Drug Deliv. Rev.* **55**, 1531–1546 (2003).
154. Kadler, K. E., Baldock, C., Bella, J. & Boot-Handford, R. P. Collagens at a glance. *J. Cell Sci.* **120**, 1955–1958 (2007).
155. Lecroisey, A. & Keil, B. Differences in the degradation of native collagen by two microbial collagenases. *Biochem. J.* **179**, 53–58 (1979).
156. Casadevall, A. & Pirofski, L. A. Host-pathogen interactions: Redefining the basic concepts of virulence and pathogenicity. *Infect. Immun.* **67**, 3703–3713 (1999).
157. Koch, G. Disarming pathogens: benefits and challenges of antimicrobials that target bacterial virulence instead of growth and viability. *Future Med. Chem.* **71**, 643 (2017).
158. Totsika, M. Benefits and Challenges of Antivirulence Antimicrobials at the Dawn of the Post-Antibiotic Era. *Drug Deliv. Lett.* **6**, 30–37 (2016).

159. Payne, D. J., Gwynn, M. N., Holmes, D. J. & Pompliano, D. L. Drugs for bad bugs: Confronting the challenges of antibacterial discovery. *Nat. Rev. Drug Discov.* **6**, 29–40 (2007).
160. Jewell, N. P., Ph, D. & Hatheway, C. L. Human Botulism Immune Globulin for the Treatment of Infant Botulism. *NEW Engl. JOURNAL Med.* **354**, 462–471 (2006).
161. Baxter, R. *et al.* Treatment with Monoclonal Antibodies against Clostridium difficile Toxins. 197–205 (2010).
162. Tsai, C. W. & Morris, S. Approval of Raxibacumab for the treatment of inhalation anthrax under the US food and drug administration ‘Animal Rule’. *Front. Microbiol.* **6**, 1–5 (2015).
163. Craik, C. Designing Inhibitors of Anthrax. *Bone* **23**, 1–7 (2008).

2 Results

2.1 Chapter A

***N*-Aryl-3-mercaptosuccinimides as Antivirulence Agents Targeting *Pseudomonas aeruginosa* Elastase and *Clostridium* Collagenases**

Jelena Konstantinović[⊥], *Samir Yahiaoui*[⊥], *Alaa Alhayek*[⊥], *Jörg Haupenthal*, *Esther Schönauer*, *Anastasia Andreas*, *Andreas M. Kany*, *Rolf Müller*, *Jesko Koehnke*, *Fabian K. Berger*, *Markus Bischoff*, *Rolf W. Hartmann*, *Hans Brandstetter*, *Anna K.H. Hirsch*

[⊥] these authors contributed equally

Reprinted with permission from *J. Med. Chem.* **2020**, 63 (15), 8359-8368.

DOI: 10.1021/acs.jmedchem.0c00584

Copyright (2020) American Chemical Society

N-Aryl-3-mercaptosuccinimides as Antivirulence Agents Targeting *Pseudomonas aeruginosa* Elastase and *Clostridium* Collagenases

Jelena Konstantinović,[▽] Samir Yahiaoui,[▽] Alaa Alhayek,[▽] Jörg Haupenthal, Esther Schönauer, Anastasia Andreas, Andreas M. Kany, Rolf Müller, Jesko Koehnke, Fabian K. Berger, Markus Bischoff, Rolf W. Hartmann, Hans Brandstetter, and Anna K. H. Hirsch*

Cite This: *J. Med. Chem.* 2020, 63, 8359–8368

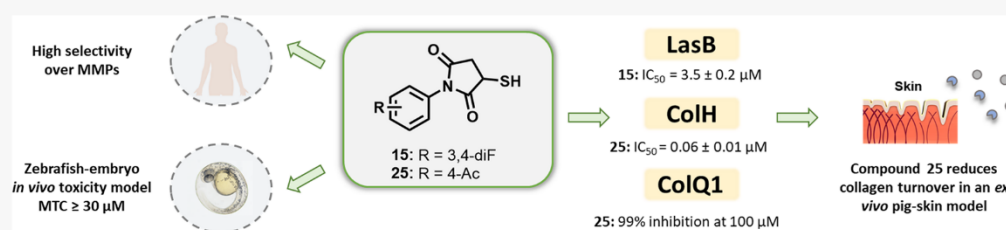
Read Online

ACCESS |

Metrics & More

Article Recommendations

Supporting Information



ABSTRACT: In light of the global antimicrobial-resistance crisis, there is an urgent need for novel bacterial targets and antibiotics with novel modes of action. It has been shown that *Pseudomonas aeruginosa* elastase (LasB) and *Clostridium histolyticum* (*Hathewayia histolytica*) collagenase (ColH) play a significant role in the infection process and thereby represent promising antivirulence targets. Here, we report novel N-aryl-3-mercaptosuccinimide inhibitors that target both LasB and ColH, displaying potent activities *in vitro* and high selectivity for the bacterial over human metalloproteases. Additionally, the inhibitors demonstrate no signs of cytotoxicity against selected human cell lines and in a zebrafish embryo toxicity model. Furthermore, the most active ColH inhibitor shows a significant reduction of collagen degradation in an *ex vivo* pig-skin model.

INTRODUCTION

The growing number of antibiotic-resistant bacteria represents one of the biggest risks to public health, leading to an increasing number of infections that are difficult to treat. Bacterial resistance to antibiotics is natural, yet overuse and misuse of antibiotics accelerate resistance development, bringing the world to the verge of the so-called “post-antibiotic era”. Of special importance are infections caused by multidrug-resistant bacteria on the WHO priority pathogen list,¹ such as carbapenem-resistant variants of the Gram-negative pathogen *Pseudomonas aeruginosa*,² which are responsible for many nosocomial,³ eye and burn infections,^{4,5} as well as fatal lung infections in cystic-fibrosis and bronchiectasis patients.^{6,7} *P. aeruginosa* also affects injured tissue such as skin via surgical or wound infections.⁸ The versatile pathogen is known to produce numerous virulence factors.⁹ One of them is elastase, the metalloenzyme that shows hydrolytic activity toward connective tissue, which significantly contributes to the virulence of these bacteria.¹⁰ Clostridiaceae represent a family of Gram-positive bacteria that are known as causative agents of numerous fatal diseases with high mortality rates worldwide, such as botulism (*Clostridium botulinum*), soft-tissue infections like gas gangrene and wound infections (*Clostridium perfringens*, *Clostridium histolyticum*) and tetanus (*Clostridium tetani*).^{11,12} *Bacillus cereus* is another Gram-positive bacterium

responsible for foodborne illnesses and traumatic wound infections in humans.^{13,14} The high lethality of these bacteria is closely related to the production of collagenases, extracellular enzymes that enable the bacteria to colonize specific niches in the host, to evade the host immune response and to obtain nutrition from infected cells. Moreover, collagenases cause tissue destruction via collagen degradation, which plays a significant role in the infection process by allowing the bacteria to reach anaerobic sites in host tissue and spread the infection.^{15,16} This especially affects the wound infection prognosis and results in a delayed healing process.^{17,18}

Recently, particular emphasis has been put on targeting bacterial virulence as an alternative approach for fighting microbial infections. The pursued “pathblockers” preserve the commensal microbiome and are expected to be less susceptible to the development of resistance than conventional antibiotics. In our work, we focus on two zinc metalloproteases that are secreted virulence factors: elastase (LasB) from *P. aeruginosa*

Received: April 9, 2020

Published: May 29, 2020



and collagenase H (ColH) from *C. histolyticum* (recently renamed as *Hathewayia histolytica*).¹⁹ Both enzymes have a major impact on the infectivity of *P. aeruginosa* and *C. histolyticum*.^{11,20} Moreover, their extracellular localization makes these enzymes particularly attractive targets, considering the difficulties associated with crossing the Gram-negative bacterial cell wall in the former species.

Most LasB and ColH inhibitors found in the literature contain various metal-chelating warheads.^{20–24} Among them, hydroxamates represent the most common structural motif.^{21,25–27} The main problem with such hydroxamate-containing protease inhibitors is their lack of stability under physiological conditions and their lack of selectivity over human matrix metalloproteases (MMPs), which makes them unsuitable candidates for antibacterial treatment *in vivo*.^{26,28} and rationalizes why there is still no drug on the market that could effectively inhibit these virulence factors. A selection of LasB and ColH inhibitors described in the literature is shown in Figure 1.

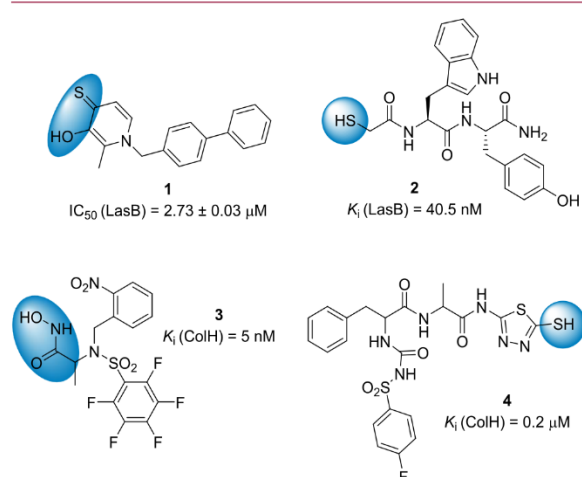


Figure 1. Structural motifs of some LasB and ColH inhibitors described in the literature (Zn-binding groups are highlighted in blue).^{21,22,24,26}

In our previous work, we discovered *N*-aryl mercaptoacetamide inhibitors with low micromolar and nanomolar affinities toward LasB and ColH, respectively.^{29,30} To constrain the flexibility and freeze the active conformation of our previously published thiols, we designed a novel succinimide class (Figure 2). The succinimide core has been reported for inhibitors of various enzyme targets, such as serine proteases,³¹ human leukocyte elastase, cathepsin G and proteinase 3,³² tumor necrosis factor, and phosphodiesterase.³³ It can also be found in several drugs, such as ethosuximide, phensuximide,

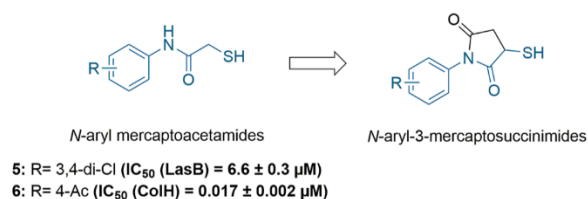


Figure 2. Our previous results and the design of new inhibitors.^{29,30}

methsuximide, and lurasidone, used to treat absence seizures, schizophrenia, and bipolar disorder.³⁴

Here, we report new *N*-aryl-3-mercaptosuccinimides, showing low micromolar potencies against *P. aeruginosa* elastase and nanomolar potencies against *Clostridium* collagenases. The most active compounds were investigated for their cytotoxicity and selectivity for the bacterial over human metalloproteases. To validate collagenases as targets, we have established an *ex vivo* pig-skin model and demonstrated the impact of our most potent inhibitor on this human skin mimic.

RESULTS AND DISCUSSION

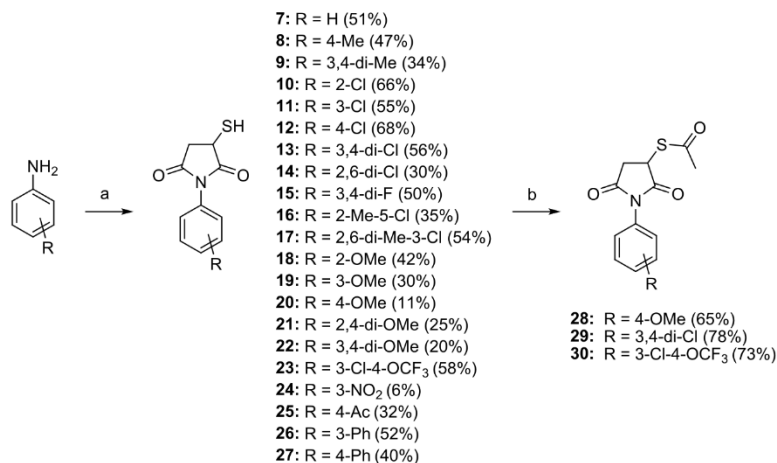
Design of New Compounds. We designed the initial succinimide core based on our previously published *N*-aryl mercaptoacetamide inhibitors.^{29,30} To expand the structure–activity relationships (SARs) further and provide more detailed information on the aromatic moiety's influence on the activity, we designed a series of compounds bearing polar, lipophilic, electron-withdrawing or -donating functional groups. In order to prevent disulfide formation, we protected the free thiol group in the form of thioacetate. Finally, we explored the possibility of growing the structure further by introducing an additional carbon spacer between the succinimide and the free thiol.

Synthesis of New Compounds. Reaction of anilines with mercaptosuccinic acid at 120–160 °C afforded 21 new free thiol-containing succinimides 7–27 in 6–68% yield. Due to the presence of an *ortho*-substituent, compounds 16–18 and 21 were obtained as mixtures of atropisomers. Acetic anhydride in the presence of pyridine and DMAP at room temperature led to protection of the free thiol group to obtain derivatives 28–30 in moderate yield (65–78%). The general synthetic route is presented in Scheme 1.

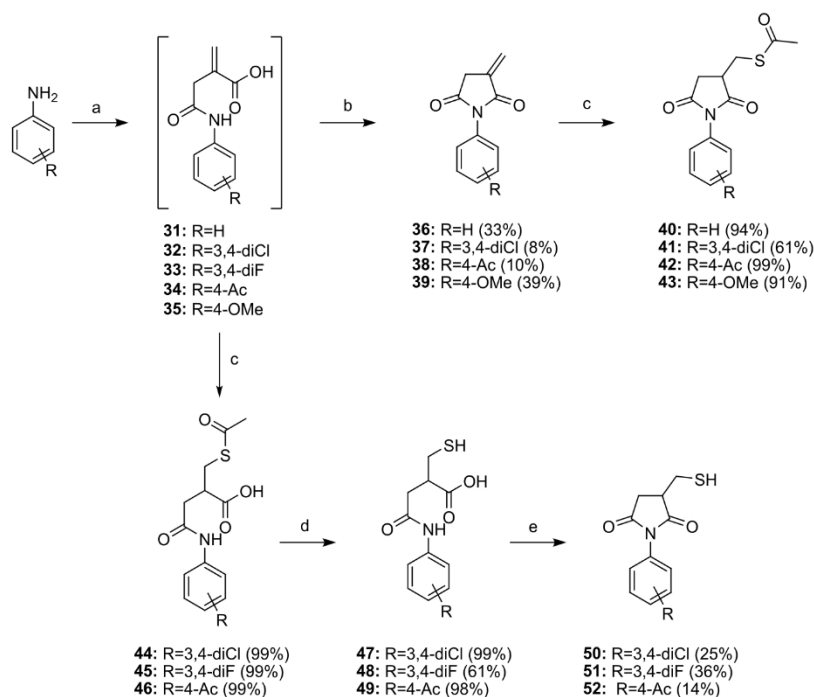
Synthesis of *N*-aryl-3-mercaptomethylsuccinimides started from itaconic anhydride and the corresponding anilines (Scheme 2). Cyclization of intermediate α -itaconamic acids 31, 32, 34, and 35 in the presence of acetic anhydride and sodium acetate at 100 °C³⁵ afforded itaconimides 36–39 in relatively low yield (8–39%). Michael addition of thioacetic acid on obtained itaconimides in the presence of triethylamine in dimethoxyethane or dichloromethane at room temperature led to the final compounds 40–43 in high yield (61–99%). α -Itaconamic acids 32–34 under the same reaction conditions in THF as a solvent provided compounds 44–46 in quantitative yield. Hydrolysis of thioacetate using sodium hydroxide in methanol at room temperature afforded free thiol-containing carboxylic acids 47–49 in moderate to quantitative yield (61–99%). A final neat cyclization step furnished target compounds 50–52 in low yield (14–36%).

Activity against Antivirulence Targets. We evaluated all compounds synthesized in this work for their inhibitory activity against both LasB and ColH. IC_{50} values and percentage of inhibition results were determined from at least two independent experiments performed in duplicate.

SAR of Novel Succinimides on LasB. To expand the SAR, we designed and synthesized 31 succinimide-based derivatives and investigated their inhibitory activity against LasB using a functional FRET-based *in vitro* assay (Table 1).³⁶ Among the first group of compounds 7–27, electronegative substituents such as chlorine or fluorine were found to be favorable for the activity. In particular, compounds 13 and 15, both with a 3,4-dihalo pattern, displayed more potent inhibitory activities when compared to the *ortho*-, *meta*-, or

Scheme 1. Synthesis of Novel Free Thiol Succinimides and Thioacetate Derivatives^a

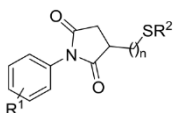
^aReagents and conditions: (a) mercaptosuccinic acid, 120–160 °C, Ar, neat, 3.5 h to overnight; (b) Ac₂O, Pyr, DMAP, DCM, rt, overnight.

Scheme 2. Synthesis of *N*-Aryl-3-Mercaptomethylsuccinimides and Their Acetylthio Analogues^a

^aReagents and conditions: (a) itaconic anhydride, CHCl₃, 2 h, rt; (b) Ac₂O, NaOAc, 1–2 h, 100 °C; (c) AcSH, Et₃N, DME or DCM or THF, rt; (d) 2 M NaOH, MeOH, 1–2 h, rt; (e) 120 °C, Ar, neat, overnight.

para-monosubstituted analogues. Furthermore, several examples indicate that polar groups, particularly electron-donating substituents are detrimental for the activity. In fact, all mono and dimethoxy derivatives were less potent than their chlorine analogues, with 3,4-dimethoxy derivative **22** showing the most dramatic loss in activity (47-fold compared to **13**). This is further supported by the 5-fold difference in activity between 3,4-dimethyl (**9**) and 3,4-dimethoxy analogues (**22**). Among both chlorine and methoxy isomers, *ortho*- (**10** and **18**) and *meta*-derivatives (**11** and **19**) proved to be more potent than the *para*-derivatives (**12** and **20**), most probably due to

electronic effects or disruption of the planar structure caused by the vicinity of the substituents to the succinimide core. Compound **25** with its polar electron-withdrawing *para*-acetyl substituent was 1.7 times more active than its methoxy-analogue, but still much less potent than compounds bearing lipophilic chlorine substituents. The observation that polar, electron-withdrawing substituents are better tolerated than electron-donating ones is illustrated through the example of nitro-compound **24**, being more active than its 3-methoxy analogue **19**. Compounds with an additional phenyl ring in positions 3 (**26**) and 4 (**27**) showed comparable activity to the

Table 1. Structures and LasB Inhibition of a Series of Novel Succinimide Derivatives^a


compd	R ¹	R ²	n	IC ₅₀ (μM)	compd	R ¹	R ²	n	IC ₅₀ (μM)
7	H	H	0	44.2 ± 2.3	23	3-Cl-4-OCF ₃	H	0	55.2 ± 4.4
8	4-Me	H	0	50.6 ± 1.6	24	3-NO ₂	H	0	22.2 ± 0.4
9	3,4-di-Me	H	0	29.4 ± 0.9	25	4-Ac	H	0	64.0 ± 7.5
10	2-Cl	H	0	8.5 ± 0.4	26	3-Ph	H	0	27.6 ± 4.0
11	3-Cl	H	0	8.1 ± 0.5	27	4-Ph	H	0	44.6 ± 1.1
12	4-Cl	H	0	16.5 ± 0.8	28	4-OMe	Ac	0	>200
13	3,4-di-Cl	H	0	3.4 ± 0.2	29	3,4-di-Cl	Ac	0	>200
14	2,6-di-Cl	H	0	16.0 ± 3.7	30	3-Cl-4-OCF ₃	Ac	0	>200
15	3,4-di-F	H	0	3.5 ± 0.2	40	H	Ac	1	>200
16	2-Me-5-Cl	H	0	15.0 ± 0.6	41	3,4-di-Cl	Ac	1	>200
17	2,6-di-Me-3-Cl	H	0	30.5 ± 5.4	42	4-Ac	Ac	1	>200
18	2-OMe	H	0	28.9 ± 1.6	43	4-OMe	Ac	1	>200
19	3-OMe	H	0	40.2 ± 1.4	50	3,4-di-Cl	H	1	5.4 ± 0.7
20	4-OMe	H	0	111.8 ± 8.9	51	3,4-di-F	H	1	10.1 ± 1.4
21	2,4-di-OMe	H	0	45.0 ± 0.8	52	4-Ac	H	1	>200
22	3,4-di-OMe	H	0	160.2 ± 10.1					

^a3,4-Di-halo pattern in **13**, **15**, and **50** proved to be beneficial for the activity. Means and SD of at least two independent experiments.

compound with a naked core, with 3-phenyl derivative even being 1.6-fold more active than compound **7**. Although these derivatives were less potent than compound **13**, the fact that they show inhibition of LasB paves the way for further optimization of this part of the structure. In addition, the fact that compounds **8** (R¹ = 4-Me) and **27** (R¹ = 4-Ph) show no significant difference in the activity suggests that there are no steric limitations in *para*-position. An additional carbon spacer next to the free thiol in compounds **50** and **51** did not improve the activities of the most potent derivatives **13** and **15**, respectively. However, the IC₅₀ values determined for **50** and **51**, being in the range of 5–10 μM, open the possibility to further grow the structure in the direction of the free thiol group. All thioacetate derivatives proved to be inactive, with <50% of inhibition at 200 μM, which confirms that the free thiol is crucial for the activity against LasB.

SAR of Novel Succinimides on ColH. In our previous work, we have shown that there is a structural similarity between the inhibitors of LasB and ColH.^{29,30} It was therefore of interest to investigate the activity of all new compounds against ColH and to compare the SAR with that observed for LasB. Figure 3 represents the inhibition of the peptidase domain of ColH (ColH-PD) in the presence of 1 μM of the selected compounds. Previously, we reported that polar substituents in *para*-position have the most beneficial effect on the activity of *N*-aryl mercaptoacetamides.³⁰ Here, we observed the same trend with the new succinimide class, with compound **25**, bearing a *para*-acetyl substituent, being the most active one with 95% of ColH-PD inhibition. The *para*-methoxy derivative **20** was slightly less active with 74% of inhibition, but still following the trend of polar substituents being more favorable for the activity than nonpolar, lipophilic substituents, such as chlorine. The protection of the free thiol functional group proved to be detrimental for the activity, as in the case of LasB. The two compounds showing >50% of inhibition of ColH-PD were further tested in a dose–response manner in the presence of the reducing agent TCEP. This

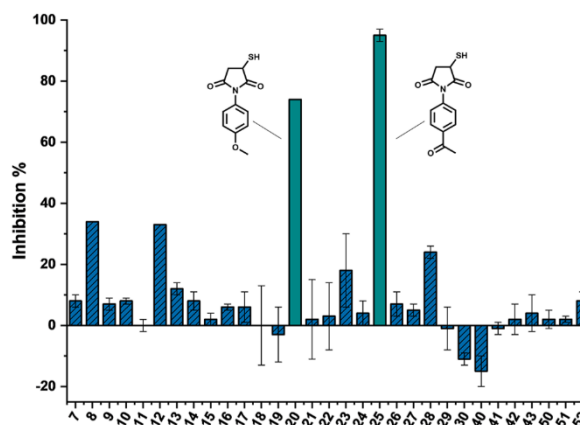


Figure 3. Inhibition of the peptidolytic activity of ColH-PD in the presence of 1 μM of the respective compound in a FRET-based assay: *para*-Acetyl substituent in compound **25** proved to be most favorable for the activity. Data are presented as means and SD of three independent experiments.

experiment revealed nanomolar IC₅₀ values for **25** (0.06 ± 0.01 μM) and **20** (0.32 ± 0.05 μM). Overall, since the inhibitors presented in this work have a similar structure and SAR we described for *N*-aryl mercaptoacetamides, we expect the interactions with LasB and ColH to be similar as those in our previously published co-crystal structures.^{29,30}

We consider the difference observed in SARs between LasB and ColH inhibitors beneficial in terms of their selectivity for each particular target. Each hit can be further developed for the treatment of single infections caused by either *P. aeruginosa* or *C. histolyticum*. However, wound infections, due to their nature, are likely to be colonized with other bacteria.^{37,38} Therefore, having a common structural motif that inhibits both targets is particularly interesting, and if the inhibitors were to be used for *Clostridia* and *P. aeruginosa* co-infections purpose, their

structure could be further optimized and adapted as dual inhibitors of ColH and LasB.

Broad-Spectrum Inhibition of Other Bacterial Collagenases. In addition to ColH from *C. histolyticum*, other *Clostridium* and *Bacillus* species also secrete collagenases that play pivotal roles in the pathogenesis of these bacteria by destroying the connective-tissue components in the infected host.¹⁶ We therefore tested the two most active ColH-PD inhibitors (**20** and **25**) on three additional collagenases, using the collagenase unit of ColG (ColG-CU) from *C. histolyticum*, the peptidase domain of ColT (ColT-PD) from *C. tetani*, and the collagenase unit of ColQ1 (ColQ1-CU) from *B. cereus* strain Q1. As anticipated, the succinimide-based scaffold retained the broad-spectrum inhibitory properties of the mercaptoacetamide-based inhibitors (Table 2).³⁰

Table 2. Inhibition of ColH-PD, ColT-PD, ColG-CU, and ColQ1-CU in the Presence of 100 μM of Compounds 20 and 25^a

compd	% inhibition @ 100 μM			
	ColH-PD	ColG-CU	ColT-PD	ColQ1-CU
20	95 \pm 1	85 \pm 3	89 \pm 4	99 \pm 1
25	96 \pm 2	100 \pm 2	102 \pm 3	99 \pm 2

^aMeans and SD of at least two independent experiments.

Selectivity against MMPs, HDACs, and TACE as Human Off-Targets. Previously, we described *N*-aryl mercaptoacetamides with high selectivity for the bacterial over a broad range of human MMPs.^{29,30} MMPs are calcium-dependent zinc metalloproteases that play a pivotal role in numerous biochemical processes in humans.^{39,40} Based on the depth of their S1' binding pocket, MMPs can be divided into three classes: deep (e.g., MMP-3 and -14), intermediate (e.g., MMP-2 and -8), and shallow (e.g., MMP-1 and -7). With the aim to explore the interactions of our inhibitors with all three pocket types, which could help us to assess potential effects on other not-tested representatives, we chose a panel of six MMPs, comprising two members of each class. In addition, HDAC-3, HDAC-8, and TACE (ADAM-17)—enzymes involved in gene expression and the processing of TNF- α ,^{41,42} respectively—were selected as important additional human off-targets. Our results showed that the most potent inhibitors of LasB and ColH (**13** and **25**, respectively) fortunately possess a high selectivity over most of the off-targets tested. While both compounds did not inhibit MMP-1, -3, and -7 as well as both HDAC enzymes, we observed certain inhibition of MMP-2, -8, and -14 at 100 μM . Inhibition of TACE, which was observed for both compounds, will be considered as high priority in the future optimization of the structures (Tables 3 and 4).

Table 3. Inhibition of Six MMPs in the Presence of 100 μM of Compounds 13 and 25^a

compd	% inhibition @ 100 μM					
	MMP-1	MMP-2	MMP-3	MMP-7	MMP-8	MMP-14
13	n.i.	39 \pm 32	n.i.	n.i.	84 \pm 8	n.i.
25	n.i.	14 \pm 4	n.i.	n.i.	94 \pm 1	84 \pm 8

^aMeans and SD of at least two independent experiments. n.i. = <10% inhibition.

Table 4. Activity of Compounds 13 and 25 against HDAC-3, HDAC-8, and TACE^a

compd	IC ₅₀ (μM)		
	HDAC-3	HDAC-8	TACE
13	>100	>100	5.2 \pm 0.6
25	>100	>100	3.4 \pm 1.2

^aMeans and SD of at least two independent experiments.

Cytotoxicity Assays. Broad-spectrum inhibition of bacterial collagenases and selectivity against a panel of off-targets supported the further evaluation of the compounds' toxicity *in vitro*. In this context, we investigated **13** and **25**, the two most active compounds against both targets, for their cytotoxicity against the three human cell lines: HepG2 (hepatocellular carcinoma), HEK293 (embryonal kidney), and A549 (lung carcinoma). Neither of the compounds showed cytotoxic effects, with IC₅₀ values >100 μM (Table 5), making them

Table 5. Cytotoxicity of Compounds 13, 25, 5, and 6 against HepG2, HEK293, and A549 Cell Lines^a

compd	IC ₅₀ (μM)		
	HepG2	HEK293	A549
13	>100	>100	>100
25	>100	>100	>100
5	>100	>100	>100
6	>100	100	>100

^aMeans and SD of at least two independent experiments.

suitable for further investigation in *in vivo* model systems. Compared to our previous hits, **5** and **6**, they displayed similar or even lower toxicities in most of the cell lines tested. Particularly, compound **25** proved to be even less toxic than **6**, which showed an IC₅₀ of 100 μM in HEK293 cells.

In Vivo Toxicity in Zebrafish-Embryo Model. Due to the promising *in vitro* activities against antivirulence targets LasB and ColH and the lack of cytotoxicity against three human cell lines, we subjected compounds **15** and **25** to a toxicity study based on zebrafish embryos. An advantage of this nonmammalian *in vivo* model is the high genetic homology to humans and that it provides follow-up information on the type of toxicity encountered (e.g., hepatic, cardiovascular, etc.). In addition, this model can also predict mammalian teratogenicity by evaluation of lethality and malformation during the development of embryonic zebrafish.^{43,44} Both compounds tested showed a maximum tolerated concentration (MTC) of ≥ 30 μM , which is higher than for the corresponding mercaptoacetamide-based LasB inhibitor **5** we published previously (MTC = 10 μM) (Table S1).²⁹

Ex Vivo Pig-Skin Model. We established an *ex vivo* model based on pig skin to address the impact of our inhibitors on living mammalian tissue and on the contained collagen as the natural substrate of collagenase. We challenged the skin, prepared from the ear of freshly slaughtered pigs, with pure ColQ1 from *B. cereus* to degrade collagen. We assessed the activity of ColQ1 by quantifying the formation of hydroxyproline as an indicator for collagen turnover (Figure 4). Optimization of the assay conditions for the model consisted of examining different buffer conditions and different protein concentrations (Figures S1 and S2). To evaluate the potential effect of **25** on collagen turnover, we incubated the skin with

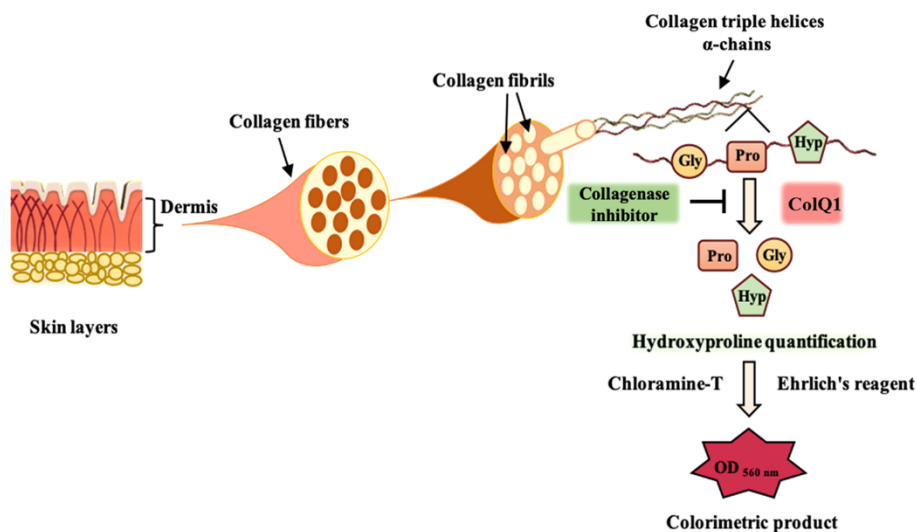


Figure 4. Representation of the pig-skin model: The composition of the skin, the dermal layer, and the amino acids of collagen are illustrated. The concept of the hydroxyproline quantification assay is explained by mixing chloramine-T and Ehrlich's reagent to obtain a product that can be detected with a spectrophotometer.

ColQ1 in the absence and presence of defined concentrations of this compound. The subsequent quantification of hydroxyproline revealed that **25** inhibited the collagenolytic activity of ColQ1, as demonstrated by the significantly reduced amount of hydroxyproline released compared to control (Figure 5).

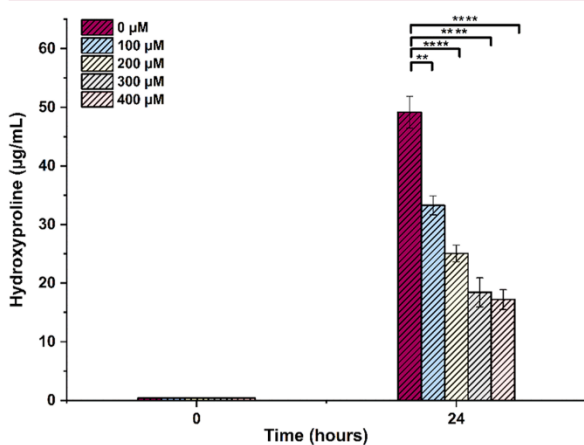


Figure 5. Amount of hydroxyproline at different concentrations of **25**. Data shown represent the means \pm SD from three independent measurements. One-way ANOVA followed by Tukey's HSD test (** = $p < 0.01$, **** = $p < 0.0001$).

These results support our previous finding that **25** is an inhibitor of a broad range of bacterial collagenases. The good performance of our inhibitors in this model is a sound starting point for their subsequent testing under *in vivo* conditions. We expect that our inhibitors will accelerate the *in vivo* healing process, by preventing the distribution of infection. The immune system will clear the bacteria, promoting remodeling of collagen and skin regeneration.

Antibacterial Activity. The aim of this study was to create "pathoblockers" that target bacterial virulence factors without directly affecting bacterial viability. These have the ability to

disarm, rather than to kill pathogens in order to make them less pathogenic. In this context, it was of interest to test the antibacterial activity of the new derivatives against *P. aeruginosa* strain PA14 and *C. histolyticum* strain DSM 1126 to exclude growth inhibition by selected compounds. We therefore selected the four most potent compounds against LasB (**13**, **15**, **50**, and **51**) and the most active succinimide against ColH (**25**). As shown in Table 6, it is clear that compounds **13**, **15**,

Table 6. Antibacterial Activity of Selected Compounds against *P. aeruginosa* and *C. histolyticum*^a

compd	MIC (μ M)	
	<i>P. aeruginosa</i>	<i>C. histolyticum</i>
13	>100	n.d.
15	>100	n.d.
50	>100	n.d.
51	>100	n.d.
25	n.d.	>100

^an.d. = not determined.

50, and **51** did not affect the growth of PA14 and **25** did not affect the growth of DSM 1126, with a minimal inhibitory concentration (MIC) > 100 μ M. This assures that the activity of these compounds is only through targeting the secreted bacterial virulence factors.

CONCLUSIONS

In this study, we aimed to constrain the conformation of previously published *N*-aryl mercaptoacetamide inhibitors,^{29,30} which led to a series of novel succinimide inhibitors of the antivirulence targets LasB and ColH. Among these compounds, we identified **13** and **25** to show the best potency against LasB and ColH, respectively. Compound **13** displays two-fold improved activity against LasB compared to our previous hit **5**, while compound **25** was slightly less potent than **6** against ColH; however, it maintained the activity in the nanomolar range. Both compounds showed sufficient

selectivity for the bacterial metalloproteases over human MMPs and three other off-targets. The two most active compounds against ColH, **25** and **20**, showed in addition broad-spectrum inhibition of homologous bacterial collagenases. These most potent LasB and ColH inhibitors showed no signs of cytotoxicity in three human cell lines. Interestingly, compounds **15** and **25** showed a MTC of $\geq 30 \mu\text{M}$ in our zebrafish model. This is, for **15**, a 3-fold lower toxicity compared to our published LasB hit **5**. Moreover, we have established a pig-skin model to further characterize the most promising collagenase inhibitor. In this *ex vivo* assay, compound **25** showed a promising effect in preventing collagen degradation, which paves the way for this compound's further evaluation under *in vivo* conditions. To investigate the compounds in such *in vivo* models, additional work should be carried out to improve their pharmacokinetic profiles. However, we strongly believe that the new succinimide inhibitors presented in this work have a great potential to be developed further and to be used as therapeutics.

EXPERIMENTAL SECTION

Chemistry. All reagents were used from commercial suppliers without further purification. Procedures were not optimized regarding yield. NMR spectra were recorded on a Bruker AV 500 (500 MHz) spectrometer. Chemical shifts are given in parts per million (ppm) and referenced against the residual proton, ^1H , or carbon, ^{13}C , resonances of the $>99\%$ deuterated solvents as internal reference. Coupling constants (J) are given in Hertz (Hz). Data are reported as follows: chemical shift, multiplicity (s = singlet, d = doublet, t = triplet, q = quartet, m = multiplet, dd = doublet of doublets, dt = doublet of triplets, br = broad and combinations of these) coupling constants, and integration. Liquid chromatography-mass spectrometry (LC-MS) was performed on a LC-MS system, consisting of a Dionex UltiMate 3000 pump, autosampler, column compartment, and detector (Thermo Fisher Scientific, Dreieich, Germany) and ESI quadrupole MS (MSQ Plus or ISQ EC, Thermo Fisher Scientific, Dreieich, Germany). High-resolution mass was determined by LC-MS/MS using Thermo Scientific Q Exactive Focus Orbitrap LC-MS/MS system. Purity of the final compounds was determined by LC-MS using the area percentage method on the UV trace recorded at a wavelength of 254 nm and found to be $>95\%$. Melting points were determined by using a Stuart melting point SMP30 device.

General Procedure A: Synthesis of Succinimides 7–27 and 50–52. Mercaptosuccinic acid (1.0 equiv) and the corresponding aniline (1.0 equiv) were mixed in a crimp vial under Ar atmosphere and heated at 120–160 °C from 3.5 h to overnight. The crude product was purified using column chromatography. In case of *N*-aryl-3-mercaptopomethylsuccinimides, 4-(aminoaryl)-2-(mercaptopomethyl)-4-oxobutanoic acid was heated at 120 °C overnight.

General Procedure B: Synthesis of Thioacetates 28–30 by Acetylation of Free Thiol. Succinimide (1.0 equiv) was dissolved in DCM, and the solution was cooled in an ice bath. Pyridine (2.0 equiv) and DMAP (0.1 equiv) were added, followed by dropwise addition of Ac_2O (2.0 equiv). After 30 min at 0 °C, the reaction mixture was allowed to warm up to room temperature (rt) and stirred overnight. Volatiles were evaporated under reduced pressure, and crude product was purified using column chromatography.

General Procedure C: Synthesis of α -Itaconamic Acids 31–35. α -Itaconamic acids were synthesized following the procedure described in the literature.³⁵ Itaconic anhydride (1.0 equiv) was dissolved in CHCl_3 . The corresponding aniline (1.0 equiv) was added to the vigorously stirring solution. After 2 h, the product was collected by filtration and washed with a small amount of chloroform. The product was used in the next step without further purification.

General Procedure D: Synthesis of Itaconimides 36–39. Itaconimides were synthesized following the procedure described in the literature from intermediate α -itaconamic acids described in general procedure C.³⁵ α -Itaconamic acid (1.0 equiv) was mixed with

NaOAc (0.5 equiv) and Ac_2O (3.5 equiv) and heated at 100 °C for 1–2 h. The dark reaction mixture was cooled to rt, poured into ice-cold water, and extracted 3 times with EtOAc. Combined organic layers were washed with brine and dried over anhydrous Na_2SO_4 , filtered and the solvent removed under reduced pressure. The crude product was purified using column chromatography. In all cases except in the case of the 4-OMe derivative, the corresponding itaconimides were isolated as a side product, and therefore the yield of obtained itaconimides was low to moderate.

General Procedure E: Synthesis of Thioacetates 40–46 Using Michael Addition. Corresponding itaconimide/ α -itaconamic acid (1.0 equiv) was dissolved in DME/DCM/THF under Ar atmosphere. Thioacetic acid (1.1–1.5 equiv) was added, followed by Et_3N (0.01–0.1 equiv). The reaction mixture was stirred at rt overnight. Crude product was purified using column chromatography or used in the next step without further purification.

General Procedure F: Thioacetate Hydrolysis to Obtain Compounds 47–49. Thioacetate (1.0 equiv) was dissolved in methanol under Ar atmosphere, and 2 M aqueous solution of NaOH (2.0–3.0 equiv) was added. The reaction was stirred 1–2 h at rt. After quenching with 1 M HCl, the reaction was extracted three times with EtOAc. Combined organic extracts were washed with brine and dried over anhydrous Na_2SO_4 , filtered and the solvent was removed under reduced pressure. The crude product was purified using column chromatography or used in the next step without further purification.

1-(3,4-Dichlorophenyl)-3-mercaptopyrrolidine-2,5-dione (13). Compound **13** was synthesized according to the general procedure A, using 3,4-dichloroaniline (162 mg, 1 mmol) and mercaptosuccinic acid (150 mg, 1 mmol), at 120 °C overnight. The product was purified using column chromatography (100% DCM). The final product was obtained as white solid (155 mg, 56%, Mp 141 °C). ^1H NMR (500 MHz, $\text{DMSO}-d_6$) δ ppm: 7.81 (d, J = 8.5 Hz, 1H), 7.62 (d, J = 2.0 Hz, 1H), 7.34 (dd, J = 2.0, 8.5 Hz, 1H), 4.10 (dd, J = 4.5, 9.0 Hz, 1H), 3.87 (s, 1H), 3.37 (dd, J = 9.0, 18.0 Hz, 1H), 2.73 (dd, J = 4.5, 18.5 Hz, 1H). ^{13}C NMR (126 MHz, $\text{DMSO}-d_6$) δ ppm: 176.2, 173.8, 132.4, 131.2, 131.1, 131.0, 128.9, 127.5, 39.2, 34.9. HRMS (ESI⁻) m/z calcd for $\text{C}_{10}\text{H}_6\text{Cl}_2\text{NO}_2\text{S}$ [$M - \text{H}$]⁻ 273.94963, found 273.94931.

1-(4-Acetylphenyl)-3-mercaptopyrrolidine-2,5-dione (25). Compound **25** was synthesized according to the general procedure A, using 4-aminoacetophenone (200 mg, 1.48 mmol) and mercaptosuccinic acid (222 mg, 1.48 mmol), at 120 °C overnight. The product was purified using column chromatography (Hex/EtOAc = 7/3). The final product was obtained as pale yellow solid (117.1 mg, 32%, Mp 104 °C). ^1H NMR (500 MHz, CDCl_3) δ ppm: 8.11–8.04 (m, 2H), 7.50–7.44 (m, 2H), 4.14–4.08 (m, 1H), 3.38 (dd, 1H, J = 9.3, 18.8 Hz), 2.77 (dd, 1H, J = 4.3, 18.8 Hz), 2.73 (d, 1H, J = 4.4 Hz), 2.63 (s, 3H). ^{13}C NMR (126 MHz, CDCl_3) δ ppm: 196.9, 175.6, 172.7, 136.9, 135.5, 129.2, 126.2, 37.4, 34.2, 26.7. HRMS (ESI⁻) m/z calcd for $\text{C}_{12}\text{H}_{10}\text{NO}_3\text{S}$ [$M - \text{H}$]⁻ 248.038687, found 248.03867.

Expression and Purification of LasB and ColH-PD. LasB and ColH-PD were expressed and purified as described previously.^{29,45}

In Vitro Inhibition Assays (LasB, ColH, ColT, ColG, ColQ1, MMPs, TACE, and HDACs). All *in vitro* inhibition assays were performed as described previously.^{29,30} TACE and HDAC inhibitor screening kits were purchased from Sigma-Aldrich (Saint Louis, MO). The assays were performed according to the guidelines of the manufacturer. Fluorescence signals were measured using a CLAR-Iostar plate reader (BMG Labtech, Ortenberg, Germany).

Cytotoxicity Assays. Cytotoxicity assays on HepG2, HEK293 and A549 cells were performed as described previously.⁴⁶

Zebrafish Embryo Toxicity. Toxicity testing was performed according to the procedure described in the literature⁴⁷ with minor modifications using zebrafish embryos of the AB wild-type line at 1 day post-fertilization. Embryos were collected and kept in a Petri dish at 28 °C until the next day in 0.3× Danieau's medium (17 mM NaCl, 2 mM KCl, 1.8 mM $\text{Ca}(\text{NO}_3)_2$, 1.5 mM HEPES (pH 7.1–7.3), 0.12 mM MgSO_4 , and 1.2 μM methylene blue). The toxicity assay was performed using a 96-well plate with one embryo per well and 10

embryos per condition. To obtain compound concentrations between 2 μM and 100 μM , solutions of **15** and **25** were prepared freshly using 0.3X Danieau's medium with a final DMSO concentration of 1% (v/v). Single zebrafish embryos were placed in wells and directly incubated in the corresponding compound solutions. Monitoring of developmental defects, heart rate, touch-evoked locomotion response, and survival rate was done daily (up to 120 hpf) via microscopy (Table S1). All of the described experiments were performed with zebrafish embryos <120 h post-fertilization (hpf) and are not classified as animal experiments according to EU Directive 2010/63/EU. Protocols for husbandry and care of adult animals are in accordance with the German Animal Welfare Act (§11 Abs. One TierSchG).

Ex Vivo Pig-Skin Model. Skin explants were obtained from freshly slaughtered pig ears, which were supplied by a local slaughterhouse. The explants were made using sterile medical biopsy punches (pfm medical, Cologne, Germany) with a diameter of 5 mm. The skin was washed once each with 70% isopropanol and sterile water and three times with Dulbecco's modified Eagle medium (DMEM) (Thermo Fisher Scientific, Schwerte, Germany) containing 1% penicillin and streptomycin. The punches were stored in DMEM medium and 15% glycerol at $-80\text{ }^{\circ}\text{C}$ until the time of the experiment. To do the experiment, a mixture of 300 nM of ColQ1, 4 mM CaCl_2 , 10 μM ZnCl_2 , and DMEM medium was prepared. The compound was pre-incubated with the mixture for 1 h at $37\text{ }^{\circ}\text{C}$ and 5% CO_2 . Afterward, one skin explant was added to each well in a 24-well plate and incubated in an incubator at $37\text{ }^{\circ}\text{C}$ and 5% CO_2 while shaking at 300 rpm. Aliquots of DMEM medium were taken at different time points in order to measure the formed hydroxyproline using a hydroxyproline assay kit (Sigma-Aldrich). This assay was performed according to the protocol of the manufacturer. Absorbance was measured using a PHERAstar plate reader (BMG Labtech). The absorbance values were converted into the hydroxyproline concentration ($\mu\text{g}/\text{mL}$) using the calibration curve of hydroxyproline as a reference (Figure S3).

Bacterial Growth Inhibition Assay. Assays regarding the determination of the MIC were performed as described recently for *P. aeruginosa* PA14.⁴⁸ MICs concerning *C. histolyticum* (*Hathewayia histolytica* (Weinberg and Séguin 1916) Lawson and Rainey 2016) DSM 1126 strain were performed in brain heart infusion (BHI) medium. The McFarland standard was adjusted to 2, followed by predilution of 1:100. The dilution series of the substances (100 μM , 50 μM , 25 μM , 12.5 μM , 6.75 μM , and 3.13 μM final concentration) was carried out in a 96-well plate in BHI and mixed with the bacterial suspension. The plates were subsequently incubated at $37\text{ }^{\circ}\text{C}$ for 48 h under anaerobic conditions, followed by growth control and evaluation of MIC values. The given MIC values are means of at least two independent determinations.

Screening of the Compounds for PAINS and Prediction of BBB Penetration. All of the compounds that were tested in biological assays were screened for PAINS and the possibility of BBB penetration using StarDrop software, Optibrium Ltd., Cambridge, UK (Table S2).

■ ASSOCIATED CONTENT

Supporting Information

The Supporting Information is available free of charge at <https://pubs.acs.org/doi/10.1021/acs.jmedchem.0c00584>.

Results of zebrafish embryo toxicity for compounds **15**, **25**, **5**, and **6**, additional figures for pig-skin assay, synthetic procedures for all compounds and results of the screening of the active compounds for PAINS and BBB penetration (PDF)

Molecular formula strings (CSV)

■ AUTHOR INFORMATION

Corresponding Author

Anna K. Hirsch – Department of Drug Design and Optimization, Helmholtz Institute for Pharmaceutical Research Saarland (HIPS) – Helmholtz Centre for Infection Research (HZI), 66123 Saarbrücken, Germany; Department of Pharmacy, Saarland University, 66123 Saarbrücken, Germany; orcid.org/0000-0001-8734-4663; Email: anna.hirsch@helmholtz-hips.de

Authors

Jelena Konstantinović – Department of Drug Design and Optimization, Helmholtz Institute for Pharmaceutical Research Saarland (HIPS) – Helmholtz Centre for Infection Research (HZI), 66123 Saarbrücken, Germany

Samir Yahiaoui – Department of Drug Design and Optimization, Helmholtz Institute for Pharmaceutical Research Saarland (HIPS) – Helmholtz Centre for Infection Research (HZI), 66123 Saarbrücken, Germany; orcid.org/0000-0001-5134-5007

Alaa Alhayek – Department of Drug Design and Optimization, Helmholtz Institute for Pharmaceutical Research Saarland (HIPS) – Helmholtz Centre for Infection Research (HZI), 66123 Saarbrücken, Germany; Department of Pharmacy, Saarland University, 66123 Saarbrücken, Germany

Jörg Haupenthal – Department of Drug Design and Optimization, Helmholtz Institute for Pharmaceutical Research Saarland (HIPS) – Helmholtz Centre for Infection Research (HZI), 66123 Saarbrücken, Germany

Esther Schönauer – Department of Biosciences, University of Salzburg, 5020 Salzburg, Austria; orcid.org/0000-0002-2625-9446

Anastasia Andreas – Department of Microbial Natural Products, Helmholtz Institute for Pharmaceutical Research Saarland (HIPS) – Helmholtz Centre for Infection Research (HZI), 66123 Saarbrücken, Germany

Andreas M. Kany – Department of Drug Design and Optimization, Helmholtz Institute for Pharmaceutical Research Saarland (HIPS) – Helmholtz Centre for Infection Research (HZI), 66123 Saarbrücken, Germany

Rolf Müller – Department of Pharmacy, Saarland University, 66123 Saarbrücken, Germany; Department of Microbial Natural Products, Helmholtz Institute for Pharmaceutical Research Saarland (HIPS) – Helmholtz Centre for Infection Research (HZI), 66123 Saarbrücken, Germany

Jesko Koehnke – Workgroup Structural Biology of Biosynthetic Enzymes, Helmholtz Institute for Pharmaceutical Research Saarland (HIPS), 66123 Saarbrücken, Germany

Fabian K. Berger – Institute of Medical Microbiology and Hygiene, Saarland University, 66421 Homburg, Germany

Markus Bischoff – Institute of Medical Microbiology and Hygiene, Saarland University, 66421 Homburg, Germany

Rolf W. Hartmann – Department of Drug Design and Optimization, Helmholtz Institute for Pharmaceutical Research Saarland (HIPS) – Helmholtz Centre for Infection Research (HZI), 66123 Saarbrücken, Germany; Department of Pharmacy, Saarland University, 66123 Saarbrücken, Germany; orcid.org/0000-0002-5871-5231

Hans Brandstetter – Department of Biosciences, University of Salzburg, 5020 Salzburg, Austria; orcid.org/0000-0002-6089-3045

Complete contact information is available at: <https://pubs.acs.org/doi/10.1021/acs.jmedchem.0c00584>

Author Contributions

^vThese authors contributed equally.

Funding

A.K.H.H. gratefully acknowledges funding from the European Research Council (ERC starting grant 757913) and the Helmholtz-Association's Initiative and Networking Fund. E.S. thankfully acknowledges support by the Austrian Science Fund (FWF): P31843. J.K. acknowledges funding by the Alexander von Humboldt Foundation.

Notes

The authors declare no competing financial interest.

ACKNOWLEDGMENTS

The authors thank J. Jung, D. Jener, A. Nimmegern, and M. Wiesbauer for excellent technical support and A. Sikandar for providing purified LasB. The authors are furthermore grateful to the E. Färber GmbH & Co. KG for providing fresh pig ears and to R. Christmann for help regarding the pig-skin assays.

ABBREVIATIONS USED

LasB, *Pseudomonas aeruginosa* elastase; ColH, *Clostridium histolyticum* (*Hathewayia histolytica*) collagenase; MMPs, human matrix metalloproteases; SAR, structure–activity relationships; DMAP, 4-dimethylaminopyridine; Pyr, pyridine; DCM, dichloromethane; DME, dimethoxyethane; THF, tetrahydrofuran; IC₅₀, the half maximal inhibitory concentration; TCEP, Tris(2-carboxyethyl)phosphine hydrochloride; ColG-CU, collagenase unit of ColG from *C. histolyticum*; ColT-PD, peptidase domain of ColT from *C. tetani*; ColQ1-CU, collagenase unit of ColQ1 from *B. cereus* strain Q1; HepG2, hepatocellular carcinoma cell line; HEK293, embryonal kidney cell line; A549, lung carcinoma cell line; HDAC, histone deacetylase; TACE, tumor necrosis factor- α -converting enzyme; MTC, maximum tolerated concentration; MIC, minimum inhibitory concentration; DMEM, Dulbecco's modified Eagle's medium

REFERENCES

- (1) WHO publishes list of bacteria for which new antibiotics are urgently needed. <https://www.who.int/news-room/detail/27-02-2017-who-publishes-list-of-bacteria-for-which-new-antibiotics-are-urgently-needed> (accessed 2019-09-15).
- (2) Wagner, S.; Sommer, R.; Hinsberger, S.; Lu, C.; Hartmann, R. W.; Empting, M.; Titz, A. Novel Strategies for the Treatment of *Pseudomonas aeruginosa* Infections. *J. Med. Chem.* **2016**, *59*, 5929–5969.
- (3) Obritsch, M. D.; Fish, D. N.; MacLaren, R.; Jung, R. Nosocomial Infections Due to Multidrug-Resistant *Pseudomonas aeruginosa*: Epidemiology and Treatment Options. *Pharmacotherapy* **2005**, *25*, 1353–1364.
- (4) Teweldemedhin, M.; Gebreyesus, H.; Atsbaha, A. H.; Asgedom, S. W.; Saravanan, M. Bacterial Profile of Ocular Infections: a Systematic Review. *BMC Ophthalmol.* **2017**, *17*, 212.
- (5) Lyczak, J. B.; Cannon, C. L.; Pier, G. B. Establishment of *Pseudomonas aeruginosa* Infection: Lessons from a Versatile Opportunist. *Microbes Infect.* **2000**, *2*, 1051–1060.
- (6) Hancock, R. E. W.; Speert, D. P. Antibiotic Resistance in *Pseudomonas aeruginosa*: Mechanisms and Impact on Treatment. *Drug Resist. Updates* **2000**, *3*, 247–255.
- (7) Sordé, R.; Pahissa, A.; Rello, J. Management of Refractory *Pseudomonas aeruginosa* Infection in Cystic Fibrosis. *Infect. Drug Resist.* **2011**, *4*, 31–41.
- (8) Kim, M.; Christley, S.; Khodarev, N.; Fleming, I.; Huang, Y.; Chang, E.; Zaborina, O.; Alverdy, J. *Pseudomonas aeruginosa* Wound

Infection Involves Activation of Its Iron Acquisition System in Response to Fascial Contact. *J. Trauma Acute Care Surg.* **2015**, *78*, 823–829.

(9) Strateva, T.; Mitov, I. Contribution of an Arsenal of Virulence Factors to Pathogenesis of *Pseudomonas aeruginosa* Infections. *Ann. Microbiol.* **2011**, *61*, 717–732.

(10) Wretling, B.; Pavlovskis, O. R. *Pseudomonas aeruginosa* Elastase and Its Role in *Pseudomonas* Infections. *Clin. Infect. Dis.* **1983**, *5*, S998–S1004.

(11) Hatheway, C. L. Toxigenic Clostridia. *Clin. Microbiol. Rev.* **1990**, *3*, 66–98.

(12) Titball, R. W.; Rood, J. I. 89 - Clostridium perfringens: Wound Infections. *Molecular Medical Microbiology* **2002**, *3*, 1875–1903.

(13) Granum, P. E.; Lund, T. *Bacillus cereus* and Its Food Poisoning Toxins. *FEMS Microbiol. Lett.* **1997**, *157*, 223–228.

(14) Drobniowski, F. A. *Bacillus cereus* and Related Species. *Clin. Microbiol. Rev.* **1993**, *6*, 324–338.

(15) Matsushita, O.; Okabe, A. Clostridial Hydrolytic Enzymes Degrading Extracellular Components. *Toxicon* **2001**, *39*, 1769–1780.

(16) Harrington, D. J. Bacterial Collagenases and Collagen-degrading Enzymes and Their Potential Role in Human Disease. *Infect. Immun.* **1996**, *64*, 1885–1891.

(17) Bowler, P. G.; Duerden, B. I.; Armstrong, D. G. Wound Microbiology and Associated Approaches to Wound Management. *Clin. Microbiol. Rev.* **2001**, *14*, 244–269.

(18) Guo, S.; DiPietro, L. A. Factors Affecting Wound Healing. *J. Dent. Res.* **2010**, *89*, 219–229.

(19) Lawson, P. A.; Rainey, F. A. Proposal to Restrict the Genus *Clostridium* Prazmowski to *Clostridium butyricum* and Related Species. *Int. J. Syst. Evol. Microbiol.* **2016**, *66*, 1009–1016.

(20) Zhu, J.; Cai, X.; Harris, T. L.; Gooyit, M.; Wood, M.; Lardy, M.; Janda, K. D. Disarming *Pseudomonas aeruginosa* Virulence Factor LasB by Leveraging a *Caenorhabditis elegans* Infection Model. *Chem. Biol.* **2015**, *22*, 483–491.

(21) Garner, A. L.; Struss, A. K.; Fullagar, J. L.; Agrawal, A.; Moreno, A. Y.; Cohen, S. M.; Janda, K. D. 3-Hydroxy-1-alkyl-2-methylpyridine-4(1H)-thiones: Inhibition of the *Pseudomonas aeruginosa* Virulence Factor LasB. *ACS Med. Chem. Lett.* **2012**, *3*, 668–672.

(22) Cathcart, G. R. A.; Quinn, D.; Greer, B.; Harriott, P.; Lynas, J. F.; Gilmore, B. F.; Walker, B. Novel Inhibitors of the *Pseudomonas aeruginosa* Virulence Factor LasB: a Potential Therapeutic Approach for the Attenuation of Virulence Mechanisms in Pseudomonas Infection. *Antimicrob. Agents Chemother.* **2011**, *55*, 2670–2678.

(23) Yiotakis, A.; Hatgiyannacou, A.; Dive, V.; Toma, F. New Thiol Inhibitors of *Clostridium histolyticum* Collagenase. Importance of the P3' Position. *Eur. J. Biochem.* **1988**, *172*, 761–766.

(24) Scozzafava, A.; Supuran, C. T. Protease Inhibitors: Synthesis of Matrix Metalloproteinase and Bacterial Collagenase Inhibitors Incorporating 5-Amino-2-mercapto-1,3,4-thiadiazole Zinc Binding Functions. *Bioorg. Med. Chem. Lett.* **2002**, *12*, 2667–2672.

(25) Supuran, C. T.; Scozzafava, A. Protease inhibitors. Part 7: Inhibition of *Clostridium histolyticum* Collagenase with Sulfonlated Derivatives of L-valine Hydroxamate. *Eur. J. Pharm. Sci.* **2000**, *10*, 67–76.

(26) Clare, B. W.; Scozzafava, A.; Supuran, C. T. Protease Inhibitors: Synthesis of a Series of Bacterial Collagenase Inhibitors of the Sulfonl Amino Acyl Hydroxamate Type. *J. Med. Chem.* **2001**, *44*, 2253–2258.

(27) Scozzafava, A.; Supuran, C. T. Protease Inhibitors - Part 5. Alkyl/Arylsulfonyl- and Arylsulfonylureido-/Arylureido- Glycine Hydroxamate Inhibitors of *Clostridium histolyticum* Collagenase. *Eur. J. Med. Chem.* **2000**, *35*, 299–307.

(28) Flipo, M.; Charton, J.; Hocine, A.; Dassonneville, S.; Deprez, B.; Deprez-Poulain, R. Hydroxamates: Relationships between Structure and Plasma Stability. *J. Med. Chem.* **2009**, *52*, 6790–6802.

(29) Kany, A. M.; Sikandar, A.; Hauptenthal, J.; Yahiaoui, S.; Maurer, C. K.; Proschak, E.; Köhnke, J.; Hartmann, R. W. Binding Mode Characterization and Early in Vivo Evaluation of Fragment-Like

Thiols as Inhibitors of the Virulence Factor LasB from *Pseudomonas aeruginosa*. *ACS Infect. Dis.* **2018**, *4*, 988–997.

(30) Schönauer, E.; Kany, A. M.; Hauptenthal, J.; Hüsecken, K.; Hoppe, I. J.; Voos, K.; Yahiaoui, S.; Elsässer, B.; Ducho, C.; Brandstetter, H.; Hartmann, R. W. Discovery of a Potent Inhibitor Class with High Selectivity toward Clostridial Collagenases. *J. Am. Chem. Soc.* **2017**, *139*, 12696–12703.

(31) Martyn, D. C.; Moore, M. J.; Abell, A. D. Succinimide and Saccharin-Based Enzyme-Activated Inhibitors of Serine Proteases. *Curr. Pharm. Des.* **1999**, *5*, 405–415.

(32) Groutas, W. C.; Brubaker, M. J.; Chong, L. S.; Venkataraman, R.; Huang, H.; Epp, J. B.; Kuang, R.; Hoidal, J. R. Design, Synthesis and Biological Evaluation of Succinimide Derivatives as Potential Mechanism-Based Inhibitors of Human Leukocyte Elastase, Cathepsin G and Proteinase 3. *Bioorg. Med. Chem.* **1995**, *3*, 375–381.

(33) Muller, G. W.; Shire, M. Succinimide and Maleimide Cytokine Inhibitors. WO1997012859, April 10, 1997.

(34) <https://www.drugbank.ca/drugs/DB00593>; <https://www.drugbank.ca/drugs/DB00832>; <https://www.drugbank.ca/drugs/DB05246>; <https://www.drugbank.ca/drugs/DB08815> (accessed 2019-09-15).

(35) Mortensen, K. T. Development of a UV-Cleavable Protecting Group for Hydroxylamines, Synthesis of a Structurally Wide Variety of Hydroxamic Acids, and Identification of Histone Deacetylase Inhibitors. *Ph.D. Thesis*; Technical University of Denmark, 2017.

(36) Nishino, N.; Powers, J. C. *Pseudomonas aeruginosa* Elastase. Development of a New Substrate, Inhibitors, and an Affinity Ligand. *J. Biol. Chem.* **1980**, *255*, 3482–3486.

(37) Baishya, J.; Wakeman, C. A. Selective Pressures During Chronic Infection Drive Microbial Competition and Cooperation. *npj Biofilms and Microbiomes* **2019**, *5*, 16.

(38) Woods, J.; Boegli, L.; Kirker, K. R.; Agostinho, A. M.; Durch, A. M.; deLancey Pulcini, E.; Stewart, P. S.; James, G. A. Development and Application of a Polymicrobial, In Vitro, Wound Biofilm Model. *J. Appl. Microbiol.* **2012**, *112*, 998–1006.

(39) Van Lint, P.; Libert, C. Chemokine and Cytokine Processing by Matrix Metalloproteinases and Its Effect on Leukocyte Migration and Inflammation. *J. Leukocyte Biol.* **2007**, *82*, 1375–1381.

(40) Sternlicht, M. D.; Werb, Z. How Matrix Metalloproteinases Regulate Cell Behavior. *Annu. Rev. Cell Dev. Biol.* **2001**, *17*, 463–516.

(41) Gooz, M. ADAM-17: The Enzyme That Does It All. *Crit. Rev. Biochem. Mol. Biol.* **2010**, *45*, 146–169.

(42) Ropero, S.; Esteller, M. The Role of Histone Deacetylases (HDACs) in Human Cancer. *Mol. Oncol.* **2007**, *1*, 19–25.

(43) Chakraborty, C.; Sharma, A. R.; Sharma, G.; Lee, S.-S. Zebrafish: A Complete Animal Model to Enumerate the Nanoparticle Toxicity. *J. Nanobiotechnol.* **2016**, *14*, 65.

(44) MacRae, C. A.; Peterson, R. T. Zebrafish as Tools for Drug Discovery. *Nat. Rev. Drug Discovery* **2015**, *14*, 721–731.

(45) Eckhard, U.; Schönauer, E.; Brandstetter, H. Structural Basis for Activity Regulation and Substrate Preference of Clostridial Collagenases G, H, and T. *J. Biol. Chem.* **2013**, *288*, 20184–2019.

(46) Hauptenthal, J.; Baehr, C.; Zeuzem, S.; Piiper, A. RNase A-Like Enzymes in Serum Inhibit the Anti-Neoplastic Activity of siRNA Targeting Polo-Like Kinase 1. *Int. J. Cancer* **2007**, *121*, 206–210.

(47) Maes, J.; Verlooy, L.; Buenafe, O. E.; de Witte, P. A. M.; Esguerra, C. V.; Crawford, A. D. Evaluation of 14 Organic Solvents and Carriers for Screening Applications in Zebrafish Embryos and Larvae. *PLoS One* **2012**, *7*, e43850.

(48) Elgaher, W.; Fruth, M.; Groh, M.; Hauptenthal, J.; Hartmann, R. W. Expanding the Scaffold for Bacterial RNA Polymerase Inhibitors: Design, Synthesis and Structure–Activity Relationships of Ureido-Heterocyclic-Carboxylic Acids. *RSC Adv.* **2014**, *4*, 2177–2194.

2.1.1 Supporting Information

Supplementary Table

Zebrafish embryo toxicity

Table S1. Results of zebrafish embryo toxicity for compounds 15, 25, 5 and 6

Compound	Conc. [μ M]	Observations after 1 day of incubation	Observations after 2 days of incubation	Observations after 3 days of incubation	Observations after 4 days of incubation	Final survival rate [%]
15	100	no pigmentation, cpd precipitation	impaired pigmentation cpd precipitation	impaired pigmentation cpd precipitation	impaired pigmentation cpd precipitation	90
	30	impaired pigmentation	impaired pigmentation	-	-	100
	10	impaired pigmentation	-	-	-	100
	2	-	-	-	-	90
25	100	no pigmentation, cpd precipitation	impaired pigmentation cpd precipitation	impaired pigmentation cpd precipitation	impaired pigmentation cpd precipitation	100
	30	-	-	-	-	100
	10	-	-	-	-	100
	2	-	-	-	malformation: 1 embryo	90
5	100	all embryos dead, cpd precipitation	all embryos dead cpd precipitation	all embryos dead cpd precipitation	all embryos dead cpd precipitation	0
	30	all embryos dead, cpd precipitation	all embryos dead cpd precipitation	all embryos dead cpd precipitation	all embryos dead cpd precipitation	0
	10	no pigmentation	impaired pigmentation	impaired pigmentation	impaired pigmentation	90
	2	-	-	-	-	80
6	100	no pigmentation, cpd precipitation	impaired pigmentation cpd precipitation	impaired pigmentation cpd precipitation	malformation: 5 embryos cpd precipitation	70 (however, malformation in 50% of embryos)
	30	slightly impaired pigmentation	-	-	-	90
	10	-	-	-	-	100
	2	-	-	-	-	100

Precipitation of compound 5 was observed by eye at 30 μ M and 100 μ M, while for compounds 6, 15 and 25 it was observed only at the highest concentration tested (100 μ M)

Supplementary Figures

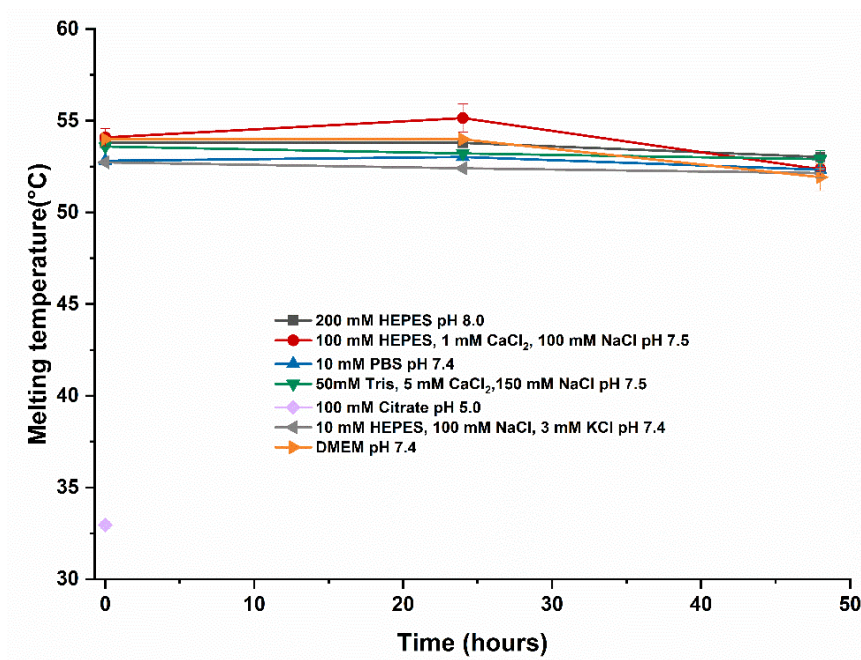
Ex vivo pig skin experiment

Figure S1. Stability of ColQ1 after different time points and under different buffer conditions.

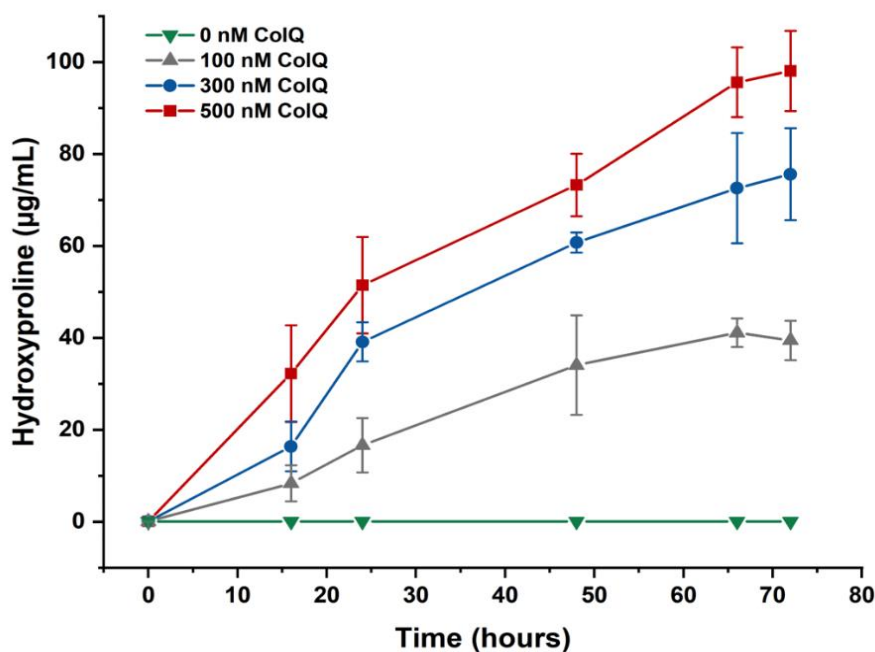


Figure S2. Quantification of hydroxyproline as a product of ColQ1-induced degradation of collagen in small pieces of pig ear skin. Different concentrations (0 – 500 nM) ColQ1 were used; hydroxyproline formation was determined after different time points. Mean \pm SD of three independent measurements are presented.

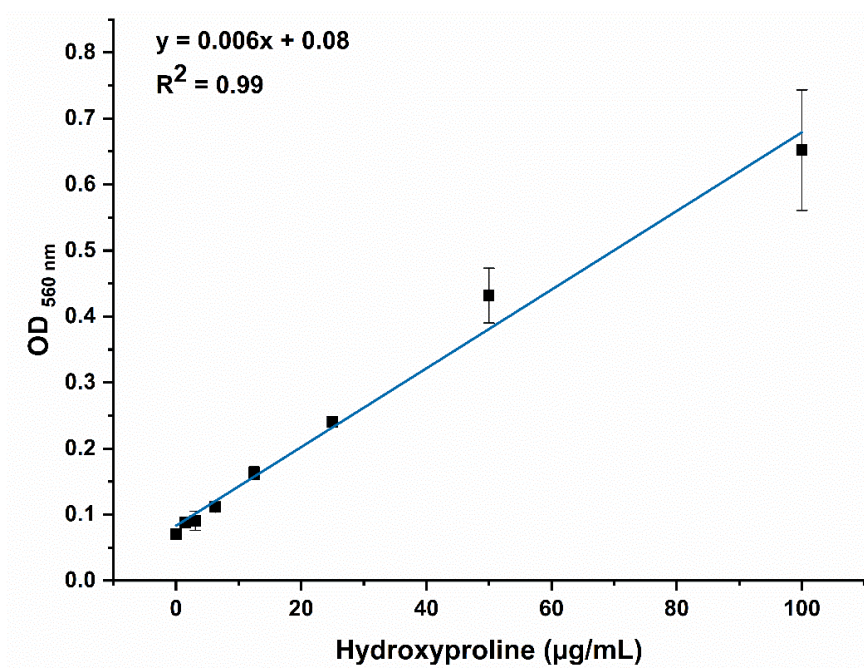


Figure S3. Calibration curve of hydroxyproline. Mean \pm SD of three independent measurements are depicted.

Chemistry

The supplementary information of the chemistry part can be found online under the following link:

https://pubs.acs.org/doi/suppl/10.1021/acs.jmedchem.0c00584/suppl_file/jm0c00584_si_001.pdf

2.2 Chapter B

Inhibition of collagenase Q1 of *Bacillus cereus* as a novel antivirulence strategy for the treatment of skin wound infections

Alaa Alhayek, Essak S. Khan, Esther Schönauer, Tobias Däinghaus, Roya Shafiei, Katrin Voos, Mitchell K. L. Han, Christian Ducho, Gernot Posselt, Silja Wessler, Hans Brandstetter, Jörg Hauptenthal, Aránzazu del Campo, and Anna K. H. Hirsch

Open access article, *Advanced Therapeutics* **2022**.

DOI: 10.1002/adtp.202100222

Copyright (2022) Wiley-VCH GmbH

Inhibition of Collagenase Q1 of *Bacillus cereus* as a Novel Antivirulence Strategy for the Treatment of Skin-Wound Infections

Alaa Alhayek, Essak S. Khan, Esther Schönauer, Tobias Däinghaus, Roya Shafiei, Katrin Voos, Mitchell K. L. Han, Christian Ducho, Gernot Posselt, Silja Wessler, Hans Brandstetter, Jörg Haupenthal, Aránzazu del Campo, and Anna K. H. Hirsch*

Despite the progress in surgical techniques and antibiotic prophylaxis, opportunistic wound infections with *Bacillus cereus* remain a public health problem. Secreted toxins are one of the main factors contributing to *B. cereus* pathogenicity. A promising strategy to treat such infections is to target these toxins and not the bacteria. Although the exoenzymes produced by *B. cereus* are thoroughly investigated, little is known about the role of *B. cereus* collagenases in wound infections.

In this report, the collagenolytic activity of secreted collagenases (Col) is characterized in the *B. cereus* culture supernatant (csn) and its isolated recombinantly produced ColQ1 is characterized. The data reveals that ColQ1 causes damage on dermal collagen (COL). This results in gaps in the tissue, which might facilitate the spread of bacteria. The importance of *B. cereus* collagenases is also demonstrated in disease promotion using two inhibitors. Compound 2 shows high efficacy in peptidolytic, gelatinolytic, and COL degradation assays. It also preserves the fibrillar COLs in skin tissue challenged with ColQ1, as well as the viability of skin cells treated with *B. cereus* csn. A *Galleria mellonella* model highlights the significance of collagenase inhibition in vivo.

diarrheal food poisoning worldwide, but also associated with serious opportunistic non-gastrointestinal-tract infections.^[1,2] Moreover, it is able to cause wound infections.^[1,3,4] Like many pathogenic bacteria, *B. cereus* is currently evolving multi-drug resistance,^[5-7] which narrows the choice of possible treatments and consequently increases economic costs, morbidity, and mortality rates.^[8-10] To overcome this therapeutic crisis, the development of new antibiotics will not produce lasting success, but alternative strategies need to be employed to cope with resistance development.^[11] To combat the emergence of resistance, the development of antivirulence agents targeting the pathogenicity of bacteria rather than their viability, has gained major interest.^[11-13] These agents specifically block the virulence factors involved in bacterial invasion and colonization of the host.^[14] This reduces the selection pressure for drug-resistant mutants

and provides a window of opportunity for the host immune system to eliminate the bacteria.^[7,11,13] The pathogenicity of *B. cereus* arises from the production and dissemination of tissue-destructive exoenzymes such as hemolysins, phospholipases, and proteases.^[1,15,16] It is believed that these exoenzymes assist

1. Introduction

Bacillus cereus (*B. cereus*) is a widely distributed Gram-positive bacterium. This bacterium is the major cause of emetic and

A. Alhayek, R. Shafiei, J. Haupenthal, A. K. H. Hirsch
Helmholtz Institute for Pharmaceutical Research Saarland (HIPS)
Helmholtz Centre for Infection Research (HZI)
38124 Saarbrücken, Germany
E-mail: anna.hirsch@helmholtz-hips.de

A. Alhayek, A. K. H. Hirsch
Department of Pharmacy
Saarland University, Saarbrücken Campus
Campus E8.1, 66123 Saarbrücken, Germany

 The ORCID identification number(s) for the author(s) of this article can be found under <https://doi.org/10.1002/adtp.202100222>

© 2022 The Authors. *Advanced Therapeutics* published by Wiley-VCH GmbH. This is an open access article under the terms of the Creative Commons Attribution License, which permits use, distribution and reproduction in any medium, provided the original work is properly cited.

DOI: 10.1002/adtp.202100222

E. S. Khan, T. Däinghaus, M. K. L. Han, A. del Campo
Leibniz Institute for New Materials (INM)
Saarland University
Campus D2 2, 66123 Saarbrücken, Germany

A. del Campo
Chemistry Department
Saarland University
66123 Saarbrücken, Germany

E. Schönauer, G. Posselt, S. Wessler, H. Brandstetter
Department of Biosciences and Medical Biology
Hellbrunner Str. 34

University of Salzburg
Salzburg 5020, Austria

K. Voos, C. Ducho
Department of Pharmacy
Pharmaceutical and Medicinal Chemistry
Saarland University
Campus C2 3, 66123 Saarbrücken, Germany

in maintaining the infection, allowing the bacteria to reach multiple sites in the body and to evade the immune system. There have been only few studies to support the idea of *Bacillus* exoenzymes contributing to the pathology of wound infections and little evidence to elucidate the direct role of specific toxins during the infection.^[17,18]

The skin is the largest and most exposed of all human organs and, therefore, most prone to injury.^[19] The dermal layer makes up 90% of the skin structure.^[20] The architecture and integrity of the dermis are maintained by COL. COL I, II, and III are predominant in the extracellular matrix (ECM) of the skin.^[21,22] COL fibers are supramolecular structures, COL molecule is made up by regular packing of three supertwisted alpha helices.^[21,22] The individual alpha chains consist of a repeated three amino acid motif (Glycine-X-Y), with X-Y often being proline (28%) and hydroxyproline (Hyp) (38%).^[21,22] Because of its highly intertwined structure and high content of specific amino acids (i.e., Glycine-X-Y),^[23] fibrillar COLs resist most proteases and can be degraded only by certain types of mammalian or bacterial collagenases with unique specificities to degrade COL.^[21,24,25]

Bacterial wound infection is a public health problem occurring when bacteria adhere to an impaired skin.^[26,27] After the initial local colonization, bacteria can potentially invade into deeper tissues with the help of necrotic virulence factors such as collagenases.^[26,28] By degrading the structural COL scaffold of the ECM at multiple sites, bacterial collagenases assist the bacteria in invading the tissue.^[29,30] Bacterial collagenases belong to the zinc metalloprotease family M9.^[29] They harbor a collagenase unit, which is accompanied by accessory domains involved in substrate recognition and COL swelling.^[29] To date, only a few collagenase-secreting bacterial genera (e.g., *Bacillus*, *Clostridium*, and *Vibrio*) have been identified. *Clostridium* collagenases such as ColH and ColG are the best characterized ones.^[29] *Bacillus* collagenases have received less attention. Their contribution to wound infections however is assumed to be a main factor in the wound-invasion stage.

Here, we report on the establishment of a simple pre-clinical ex vivo pig-skin model to evaluate the effect of COL degradation by *B. cereus* in the skin. Our results showed that the model *B. cereus* collagenase ColQ1 degrades the dermal fibrillar COLs and confirmed it as a promising for drug target. Using two small molecules, which we had recently described as inhibitors of the collagenase ColH (produced by *Clostridium histolyticum*)^[31] and the elastase LasB (produced by *Pseudomonas aeruginosa*),^[32] we could substantiate that these inhibitors also inhibit *B. cereus* collagenase activity. Indeed, we found that these compounds were able to protect the integrity of the dermal COL in an ex vivo pig-skin model treated with recombinant ColQ1, confirming their potency as broad-spectrum inhibitors of bacterial collagenases, as suggested earlier by Schönauer et al.^[33] Moreover, these compounds reduced in vitro cytotoxic effects of the *B. cereus* csn, containing various collagenases, toward fibroblast and keratinocyte cell lines, restored their morphology, and improved their adhesion. The toxicity of *B. cereus* csn and ColQ1 was verified in vivo in *Galleria mellonella* larvae. Furthermore, we showed that treatment with collagenase inhibitors significantly improved their survival rate.

2. Results and Discussion

2.1. *B. cereus* csn and Recombinant *B. cereus* ColQ1 Act as Collagenolytic Agents

To study the effect of bacteria-derived collagenase on COL degradation in skin wounds, we used the recombinant collagenase unit of ColQ1 (Uniprot: B9J3S4)^[34] and the csn of *B. cereus* ATCC 14579^[35] to challenge our skin model. ColQ1 was selected as a model *Bacillus* collagenase to study the isolated effect of this virulence factor in a skin wound setting. ColQ1 is a close homologue of ColA of *B. cereus* ATCC 14579 (Uniprot: Q81BJ6) and similarly to ColA, it displays a remarkably high peptido- and collagenolytic activity compared to clostridial collagenases.^[34] Both enzymes share an overall sequence identity of 72% and a similarity of 84%. Sequence conservation is higher within the collagenase unit, i.e., the catalytic core of the enzyme, increasing to 79% and 89%, respectively.^[34,36] Proteolytic activity of ColQ1 and of *B. cereus* csn (which represents a more complex source of COL-degrading factors)^[34,36] were validated in an in vitro peptidolytic assay using a custom-made collagenase-specific quenched fluorescence substrate.^[33] The csn of *B. cereus* showed peptidolytic activity that could be completely abrogated by the addition of 20 mM EDTA and was only marginally affected by serine and cysteine protease inhibitors, consistent with its metalloprotease mechanism (Figure S1, Supporting Information). The peptidolytic activity of the csn determined in the presence of serine and cysteine protease inhibitors was comparable to the activity of $0.9 \pm 0.1 \times 10^{-9}$ M of recombinant collagenase unit of ColQ1. These results were determined based on a standard curve that was generated using recombinant ColQ1 (Figure S2, Supporting Information).

2.2. *B. Cereus*-Induced COL Degradation Quantified in an Ex vivo Pig-Skin Model

To analyze the collagenolytic activity of *B. cereus* csn and ColQ1 during wound infection, an ex vivo pig-skin model of *B. cereus* infection was established.^[38] For this purpose, porcine ear skin biopsy punches were treated with different concentrations of *B. cereus* csn (35%, 65%, and 100% v/v) or ColQ1 (100×10^{-9} , 300×10^{-9} , and 500×10^{-9} M) to simulate COL matrix degradation after infection with *B. cereus*. The release of hydroxyproline (Hyp) was used as a biomarker for COL breakdown.^[39,40] While we did not observe Hyp release in non-treated skin preparations, a significant release was detected in skin treated with various concentrations of *Bacillus* csn and ColQ1 (Figure 1a,b). In detail, incubation with 35% (v/v) of the csn led to an increase of Hyp levels to $22 \pm 6 \mu\text{g mL}^{-1}$ release of Hyp after 24 h, and 100% (v/v) csn, Hyp levels rendered $60 \pm 4 \mu\text{g mL}^{-1}$ (Figure 1a) Hyp in the supernatant. As we showed before,^[38] treatment with 100×10^{-9} or 500×10^{-9} M of the enzyme led to $16 \pm 6 \mu\text{g mL}^{-1}$ and $51 \pm 10 \mu\text{g mL}^{-1}$ Hyp release after 24 h incubation, respectively (Figure 1b). Longer incubation times led to larger Hyp concentrations until a plateau value was reached. These data confirm that ColQ1 exhibited an effect on collagen degradation that was comparable to the csn. To analyze the collagenase-specific effects, we focused on ColQ1 in the following ex vivo studies.

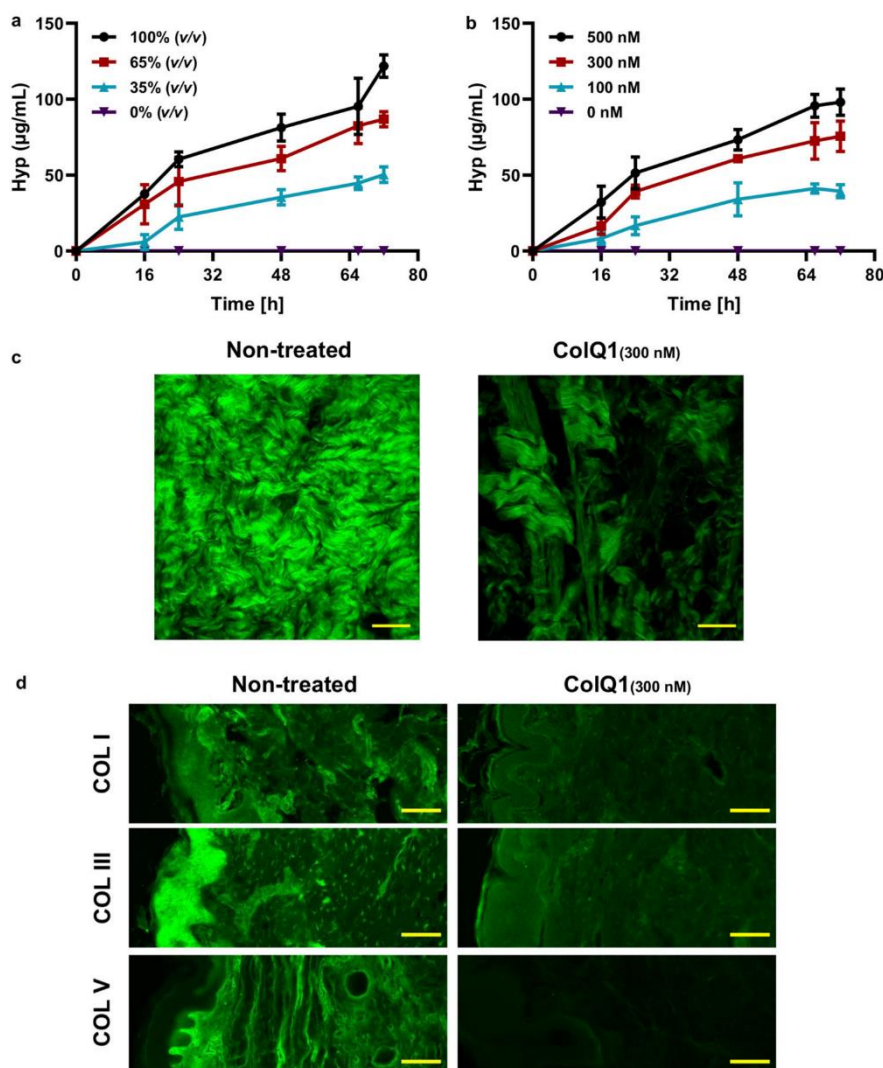


Figure 1. The effect of ColQ1 on dermal COL of pig-skin. **a,b)** Quantification of Hyp release over time after treatment with different concentrations of a) *B. cereus* csn (0–100% v/v) and b) ColQ1 (0 – 500×10^{-9} M). This graph contains data adapted from our previous publication.^[38] **c)** Confocal SHG Z-stack images of the COL structure in skin dermal region that was non-treated or treated with 300×10^{-9} M ColQ1. **d)** *B. cereus* ColQ1 (300×10^{-9} M) degraded the fibrillar COLs, immunostaining of non-treated and ColQ1 treated skin with COL antibodies (COL I, III, and V). COL: collagen, Hyp: hydroxyproline, *B. cereus*: *Bacillus cereus*, csn: culture supernatant, SHG: second harmonic generation. Data point represents mean value \pm standard deviation ($n = 3$). Scale bar: 100 μ m for SHG images and immunostained images. Bright-field and DAPI images of the immunostained non-treated and ColQ1-treated tissue are shown in Figure S4, Supporting Information.

We visualized the loss of matrix COL of the skin tissue challenged with ColQ1 using SHG imaging. This method allows a label-free imaging of the COL fibers.⁴¹ The confocal SHG Z-stack images of non-treated skin showed COL structures with the characteristic wave-like morphology of dermal COL^[42] (Figure 1c). This morphology is essential for elastic integrity and it provides the biomechanical prerequisites necessary to sustain the shape and strength of the skin tissue.^[20,43,44] In contrast, skin treated with 300×10^{-9} M ColQ1 showed a lower SHG signal and large gaps between the COL structures (Figure 1c). Higher ColQ1 concentrations resulted in fragile

tissue samples and lower ColQ1 concentrations did not show a significant collagenolytic effect (data not shown). Therefore, a concentration of 300×10^{-9} M ColQ1 was chosen for further experiments.

Our evaluation of both COL structure and the released Hyp showed that *B. cereus* collagenases have a highly destructive effect on native COL in skin. Based on the disruptive effect of *B. cereus* collagenase on the collagen matrix, we hypothesize, that collagenolytic activities diminish skin tissue integrity and thus aid passage of the bacteria to deeper dermal layers in settings of wound infection.

2.3. ColQ1 Targets Fibrillar COLs in the Dermis

The skin dermis and hypodermis are rich in COL I, which forms heterotypic structures with other COLs such as III and/or V.^[45] To test the ability of ColQ1 to target these fibrillar COLs in skin, immunostaining of skin samples after the treatment was performed with antibodies against COL I, III, and V followed by epifluorescence imaging of the stained tissue. Non-treated samples showed strong signals for COL I in the dermis, COL III in the epidermis, and around cellular components of the dermis, and COL V in the basal and dermal layers (Figure 1d). Upon treatment with ColQ1 a moderate reduction in the signal of all three fibrillar COLs (i.e., Col I, III, and V) was observed (Figure 1d). These data indicate that ColQ1 is targeting fibrillar COL subtypes enriched in the dermal region. The effect of ColQ1 on fibrillar COLs can be explained by the tertiary and primary structure of the substrate. Fibrillar COLs are mainly composed of one large triple-helical domain (e.g., COL I: 96%) with (Gly-X-Y) tripeptide repeats.^[45] The active site sequence specificity of bacterial collagenases is perfectly adapted to this tripeptide motif, as it has been shown for clostridial collagenases.^[46]

2.4. Collagenase Inhibitors Neutralize the Collagen Degradation Effect of *B. cereus* Collagenases In vitro

To study whether we could inhibit ColQ1 with small molecules, we investigated two previously described inhibitors of bacterial metalloproteases. Compound 1 is one of the first reported ColH inhibitors ($IC_{50} = 7 \times 10^{-6}$ M) being stable and selective over several human metalloproteases.^[31] Compound 2 is a moderately active LasB inhibitor ($IC_{50} = 17.3 \times 10^{-6}$ M)^[32] and was a hit in a virtual screening study performed on the active site of ColH.

Using a FRET-based peptidolytic assay with a collagenase-specific substrate as well as a COL cleavage assay with the natural triple-helical substrate of collagenases (i.e., COL I), the impact of these two inhibitors on ColQ1 activity was measured in vitro. The FRET-based assay confirmed that compounds 1 and 2 inhibit ColQ1 with IC_{50} values of $183 \pm 7 \times 10^{-6}$ M^[31] and $95 \pm 4 \times 10^{-6}$ M, respectively (Figure S3, Supporting Information; Figure 2a). In addition, the COL cleavage assay demonstrated a full collagenase inhibition with protection of the structural integrity of COL I at 75×10^{-6} and 6×10^{-6} M with compounds 1 and 2, respectively (Figure 2b).

To further investigate the activity of compounds 1 and 2, we tested them on the *B. cereus* csn, which contains a heterogeneous mixture of ColA isoforms and other collagenase homologs. The *B. cereus* csn was treated with 1.83 mM ($10 \times IC_{50}$) of compound 1. The FRET-based assay revealed that the proteolytic activity furnished by the csn could be reduced by $84 \pm 2\%$ compared to the uninhibited control (Figure S1, Supporting Information). Due to the low solubility of compound 2 under assay conditions, compound 2 could only be tested at a concentration of 95×10^{-6} M ($1 \times IC_{50}$). Remarkably, this concentration led to a decrease in the proteolytic activity of $57 \pm 7\%$ (Figure S1, Supporting Information). The positive control (20 mM EDTA) completely inhibited substrate turnover, while an inhibitor cocktail specific for serine and cysteine proteases reduced the total activity by only $14 \pm 7\%$ (Figure S1, Supporting Information).

We could qualitatively confirm the inhibitory effect of compounds 1 and 2 on the *B. cereus* csn using gelatin zymography (Figure 2c,d). For this, the csn was separated by electrophoresis and then subjected to an in-gel activity assay. Gelatinolytically active species were detected by the degradation of denatured COL I that had been co-polymerized with the polyacrylamide matrix of the SDS-PAGE gel, visible as white bands in the zymogram. Similar to previous reports,^[35,48] it revealed the presence of various gelatinolytically active species in the csn of *B. cereus* most prominently at a molecular weight of approx. 115 kDa and smaller. The zymogram performed in presence of i) serine and cysteine protease inhibitors, ii) compound 1, and iii) compound 2 showed a selective reduction of the gelatinolytic activities in all cases (Figure 2c). In particular, the high molecular weight species corresponding to full-length ColA and C-terminally truncated ColA species in the range of 120–80 kDa, as identified before by Abfalter et al.,^[35] were inhibited by compounds 1 and 2 (Figure 2c).

In all in vitro assays, compound 2 was more active than compound 1. Both compounds not only inhibit ColH, LasB, and ColQ1, as reported previously,^[31,32] but also demonstrated an inhibitory effect on gelatinases of *B. cereus* csn. We have previously reported a similar broad-spectrum inhibition of *Bacillus* and *Clostridium* collagenases in in vitro assays for closely related compounds,^[33,38] which might be beneficial in wound infections colonized by multiple bacterial genera.^[28]

2.5. Docking Studies with Bacterial Collagenases Rationalize Differences in Inhibitory Potency

The observed difference in efficacy between compounds 1 and 2 can be rationalized based on the binding mode of both compounds to bacterial collagenases. For this purpose, molecular docking was performed using the crystal structure of the peptidase domain of ColH as target that had been determined at a resolution of 1.87 Å. The crystal structure of the homologue ColH was chosen, as there are to date no high-resolution crystal structures from a *B. cereus* collagenase available to ensure reliable docking results. The peptidase domain of ColH shares 74% and 73% sequence similarity with the peptidase domains of ColA and ColQ1 from *B. cereus*, respectively, and the sequence and topology of the active sites are highly conserved.^[34,35] Since docking to metalloproteins is non-trivial in drug design, AutoDock Vina v1.2.2^[48] and the Molecular Forecaster suite^[49] were both evaluated for this end and their performance judged by their ability to generate poses that comply with standard atom-to-zinc distances and zinc-binding geometries.^[50] Following this criterion, the Molecular Forecaster suite was used for the final docking of compounds 1 and 2 to ColH.

As expected, we found that the best docking pose for compound 1 showed a similar binding mode as was determined for the *N*-aryl mercaptoacetamide ligand in the complex crystal structure with ColH^[33] (Figure 3a,b). Both compounds share the same *N*-aryl backbone, but differ in their zinc-binding group. Instead of the thiolate sulfur atom of the mercaptoacetamide compound, the phosphonate oxygen atom of compound 1 is predicted to coordinate the catalytic zinc ion (2.1 Å). The amide oxygen and nitrogen atoms form a hydrogen bond with the main-chain amide nitrogen atom of Tyr428 and the carbonyl oxygen of Glu487, re-

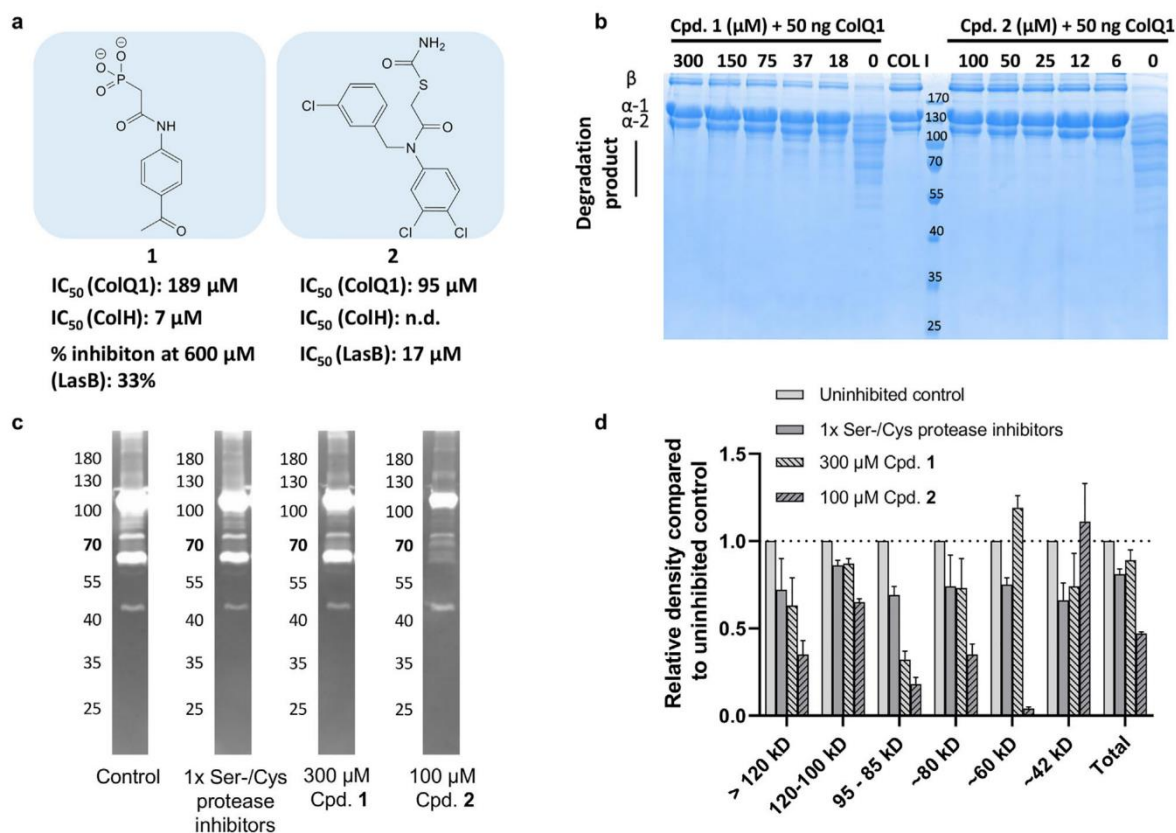


Figure 2. Inhibition of ColQ1 and the collagenase of *B. cereus* csn by compounds **1** and **2** in a collagenase-specific peptidic and a gelatinolytic assay. **a)** Chemical structures of compounds **1** and **2** and the calculated IC_{50} value in the FRET-based ColQ1, ColH,^[31] and LasB^[32] inhibition assay. **b)** Effect of ColQ1 inhibitors on the cleavage of COL I after challenge with 50 ng of ColQ1. **c,d)** Effect of compounds **1** and **2** on *B. cereus* csn monitored by **c)** gelatin zymography. The gelatin-degradation assay was performed in the presence of inhibitors or the buffer control. Due to limited solubility in the reaction buffer, compound **2** could only be tested at 100×10^{-6} M compared to 300×10^{-6} M of compound **1**. **d)** Densitometric analysis of gelatin zymography shown in **(c)**. Image analysis was performed with Image Studio Lite v5.2 software (Li-Cor Biosciences, USA). *B. cereus*: *Bacillus cereus*, csn: culture supernatant, COL: collagen, n.d.: not determined.

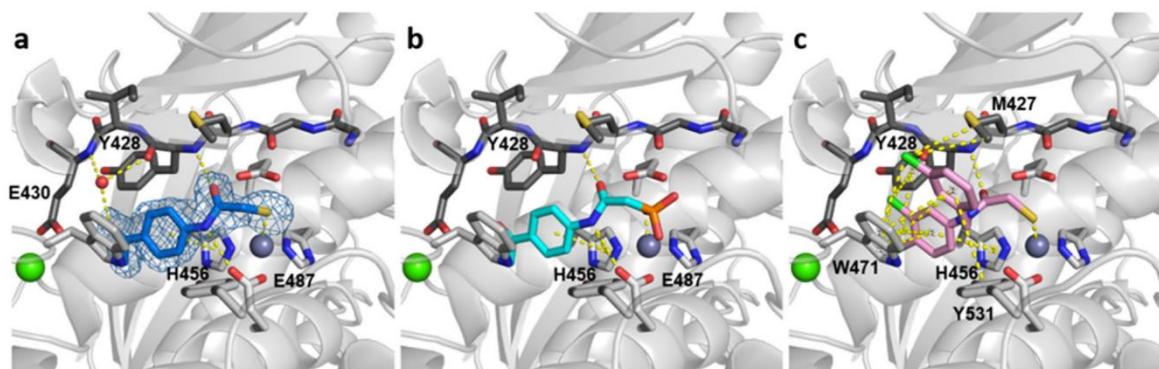


Figure 3. Comparison of the crystallized complex of the *N*-aryl mercaptoacetamide compound with the docking poses of compounds **1** and **2** in the active site of ColH. **a)** Close-up view of the active site in ball-and-stick representation. The co-crystallized inhibitor (blue) is shown in sticks with the maximum likelihood weighted $2F_o - F_c$ electron density map contoured at 1σ . Top docking poses of compounds **1 b)** and of **2 c)** in the active site of ColH. The catalytic zinc ion (dark gray), calcium ion (green), and water molecule (red) are shown as spheres. The edge strand formed by Gly425 to E430 is shown in dark gray sticks. The figures were prepared using the PyMOL Molecular Graphics System.

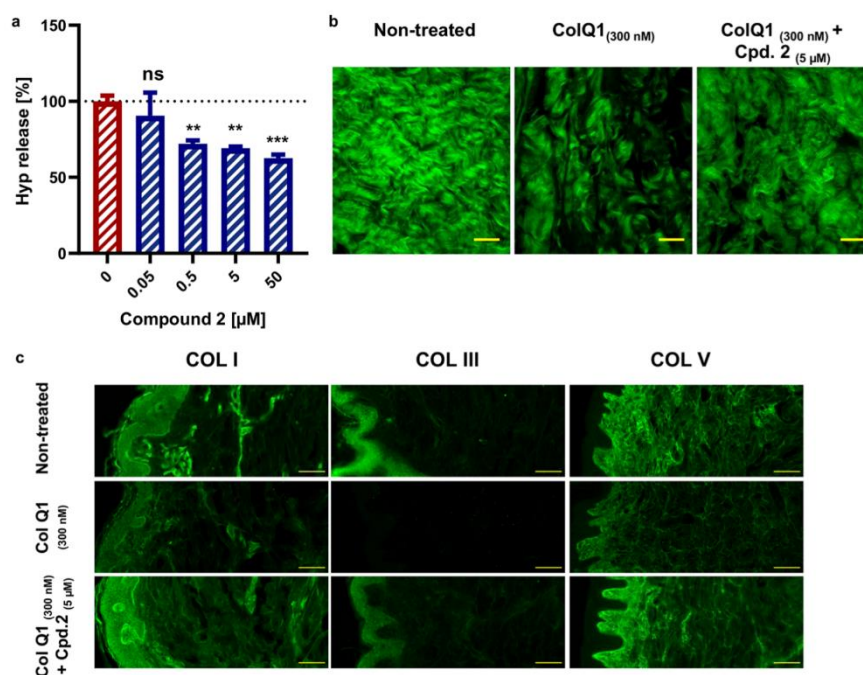


Figure 4. Compound 2 suppressed the collagenolytic effect of ColQ1 ex vivo in skin tissue. **a)** Dose-dependent effect of compound 2 quantified by Hyp release assay. **b)** Confocal SHG images showed an improved COL signal with 5×10^{-6} M of compound 2 (tissue challenged with 300×10^{-9} M ColQ1) compared with 300×10^{-9} M ColQ1 without inhibitor. **c)** Immunostaining of fibrillar COLs of the non-treated skin and treated with ColQ1 with or without compound 2. Statistical analysis was performed with one-way ANOVA and statistical significance was analyzed by Tukey test. Significance was calculated by comparing non-treated versus treated tissue with compound 2 (mean \pm SD, *** $p \leq 0.001$, ** $p \leq 0.01$). Hyp: hydroxyproline, COL: collagen, SHG: second harmonic generation. Scale bar: 100 μ m for SHG images and 100 μ m for the immunostained images.

spectively, while the aryl ring of compound 1 is involved in a π - π -stacking interaction with the imidazole ring of His459 (3.9 Å). In contrast to compound 1, compound 2 has a different, much larger molecular backbone, but shares the same thiol prodrug moiety with the co-crystallized *N*-aryl mercaptoacetamide,^[33] i.e., a thio-carbamate group. Similarly to the *N*-aryl mercaptoacetamide, we found that the deprotonated sulfur atom of compound 2 can coordinate the active-site zinc cation (2.3 Å), while the amide oxygen forms a hydrogen bond with the main-chain nitrogen atom of Tyr428 (Figure 3c). The active site of ColH can accommodate the two aromatic moieties of compound 2 in the non-primed side via a network of π - π -stacking interactions involving His456, Trp471, and Tyr531, which is supported by a parallel network of π -alkyl and π -sigma interactions via the chlorine substituents with Tyr428, Trp471, and Met427. This extensive system of π -interactions found by the docking experiment anchors compound 2 firmly into the active site in-between the upper and lower subdomains of the peptidase domain and it might explain the observed higher efficacy of compound 2 compared to compound 1 that lacks this dense interaction network.

2.6. Compounds 1 and 2 Inhibit the Collagenolytic Activity of ColQ1 in an Ex vivo Pig-Skin Model

As compounds 1 and 2 suppressed ColQ1 activity in vitro, we furthermore tested their effects on collagenase activity in the

skin model. Different concentrations of compounds 1 (50 – 400×10^{-6} M) and 2 (0.05 – 50×10^{-6} M) based on their activity in the different in vitro assays along with 300×10^{-9} M ColQ1 were used. Non-treated and ColQ1-treated samples were used as controls. After one day of incubation, we quantified the release of Hyp and visualized the dermal COL in the skin tissue using SHG and epifluorescence microscopic techniques. Overall, compound 1 resulted in a reduction in Hyp release in a concentration-dependent manner as we had shown previously (Figure S6, Supporting Information).^[31] A concentration of 300×10^{-6} M of compound 1 was selected for further analysis. Addition of compound 2 at concentrations between 5 and 50×10^{-6} M caused a reduction in the release of Hyp by 35% and 48%, respectively (Figure 4a). Based on these data, a concentration of the inhibitory molecule 2 of 5×10^{-6} M was chosen for further analysis.

Next, we performed SHG imaging of samples treated with compounds 1 or 2. The ability of these molecules to reduce the ColQ1-mediated degradation of matrix COL fibers was confirmed compared to the ColQ1-treated control. A higher density of collagen fibers was observed in the presence of both compounds, similar to the morphology of non-treated skin (Figure 4b; Figure S6, Supporting Information). Further experiments were carried out to investigate which COL types (I, III, and V) are protected in presence of compounds 1 and 2. We performed epifluorescence imaging with the tissue treated with 300×10^{-9} M ColQ1 and 300×10^{-6} M compound 1 or 5×10^{-6} M compound 2. Both compounds led to a higher-intensity signal for

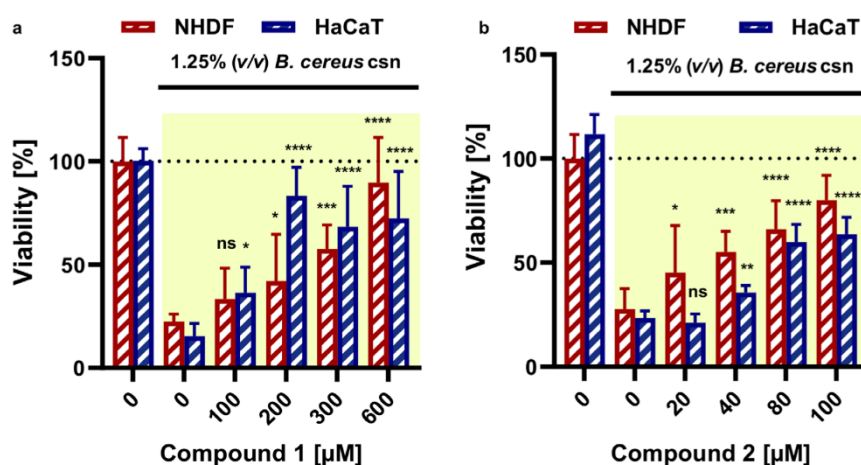


Figure 5. Compounds 1 and 2 maintained the viability of skin cells upon treatment with 1.25% (v/v) of *B. cereus* csn. Cell viability calculated after performance of an MTT assay for the cells challenged with *B. cereus* csn with a) compounds 1 and b) 2. The data in yellow background indicate cells treated with the csn. Statistical analysis was performed with one-way ANOVA and statistical significance was analysed by Tukey test. Significance was calculated by comparing non-treated versus treated cells with compound 1 and 2 (mean \pm SD, **** $p \leq 0.0001$, *** $p \leq 0.001$, ** $p \leq 0.01$, * $p \leq 0.05$, and ns: non-significant). *B. cereus*: *Bacillus cereus*, csn: culture supernatant.

COL I, V, and III when compared to the signal of the ColQ1-treated skin control (Figure 4c; Figure S6, Supporting Information). Overall, the results from the ex vivo skin model support the previous results on Hyp release and confirm that ColQ1 inhibition prevents degradation of fibrillar COL. Moreover, the findings underline the higher efficacy of compound 2 compared to compound 1 that had initially been observed in our in vitro assays.

2.7. Collagenase Inhibitors Reduce the Cytotoxic Effect of *B. cereus* csn on Human Skin Cell Lines

We further investigated whether the *B. cereus* csn has a cytotoxic effect on skin cells and whether this effect could be inhibited with collagenase targeting pathoblockers (i.e., compounds 1 and 2). For this purpose, normal human dermal fibroblasts (NHDF) and human epidermal keratinocytes (HaCaT) were chosen due to their ability to produce fibrillar COLs and their roles during wound healing.^[51]

These cells were exposed to different concentrations of *B. cereus* csn (0–15% v/v). The cytotoxic effect of the csn was evaluated by assessing the viability using a colorimetric MTT assay^[52] and live/dead staining,^[53] followed by visualization with epifluorescence microscopy.

A reduction in the viability of the cells was observed depending on the concentration of the *B. cereus* csn (Figure S7, Supporting Information). This cytotoxic effect increased slightly with incubation time of 24 h to 48 h (Figure S7, Supporting Information). The csn appeared more toxic for HaCaT cells than for NHDF cells (Figure S7, Supporting Information). The difference between the toxicity against HaCaT and NHDF cells might be due to the protective effect of fibroblasts provided by its high collagen contents, which help them to maintain the structure of the dermal layer.^[54] Bright-field images showed a strong detachment of cells, rounding, and shrinkage in both cell lines (example for NHDF

cells is shown in Figure S8, Supporting Information, indicating apoptosis).

To demonstrate the inhibitory effect of compounds 1 and 2 in subsequent experiments, we used 1.25% (v/v) of the *B. cereus* csn, due to the prominent cytotoxic effects observed at this concentration in both NHDF and HaCaT cell lines. Cell viability was dose-dependent, but a significant rescue of viability ($80 \pm 20\%$ and $70 \pm 25\%$) was observed at 600×10^{-6} and 100×10^{-6} M of compounds 1 and 2, respectively, in both NHDF and HaCaT cell lines (Figure 5). The live/dead staining results were consistent with the MTT data and showed an increase in the number of viable relative to dead cells (Figure S9, Supporting Information). Both compounds showed high viability at high concentration, which confirms their activity against the collagenase and its isoforms and maybe against other virulence factors. The property of these compounds to restore the viability of NHDF cells is important for a therapeutic context, since fibroblasts are active depositors of matrix proteins in connective tissues in the processes of wound closure.^[51] Also, keratinocytes play an important role during wound healing, as they fill the gaps in the wound and produce proinflammatory mediators once pathogen invasion starts.^[55,56] The protection of both cell types by collagenase inhibitors is promising, as their cross-talk is fundamental to assure wound healing and hemostasis.^[57] Thus, collagenase inhibitors might serve as promising therapeutic agents in the future not only to stop bacterial dissemination but also to accelerate the immune response and subsequently accelerate the wound-healing process.^[58,59]

2.8. Collagenase Inhibitors Diminish the Virulence Activity Induced by ColQ1 and *B. cereus* csn on *Galleria mellonella* Larvae

To examine the virulence of the *B. cereus* collagenase ColQ1 or csn and their inhibition in a simple in vivo model, *Galleria mellonella* larvae were used. This model is accepted as an

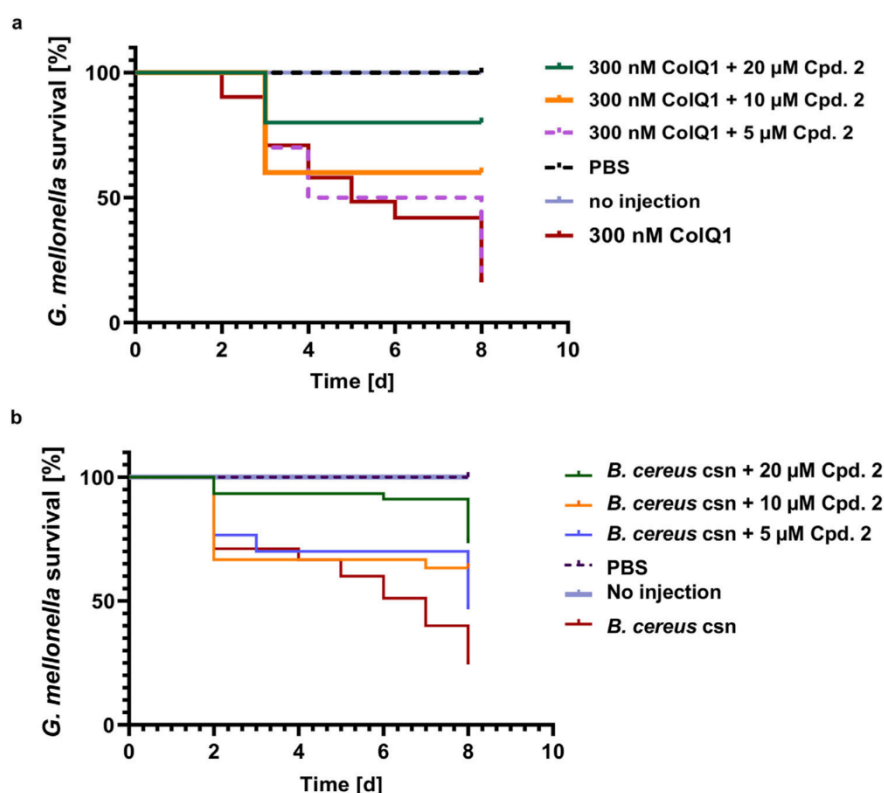


Figure 6. Kaplan–Meier survival analysis of larvae treated with *B. cereus* csn with and without compound 2. **a)** Survival analysis of larvae treated with 300×10^{-9} M ColQ1 and with various concentrations (5×10^{-6} – 20×10^{-6} M) compound 2. **b)** The improvement in the survival of larvae challenged with 100% (v/v) *B. cereus* csn and various concentrations of compound 2 (5×10^{-6} – 20×10^{-6} M). The statistical difference between groups treated with 20, 10, and 5×10^{-6} M of compound 2 and treated with only 300×10^{-9} M ColQ1 is $p < 0.0001$, $p = 0.0042$, and $p = 0.5800$, sequentially (log-rank). The statistical difference between groups treated with 20, 10, and 5×10^{-6} M of compound 2 and treated with only 100% (v/v) *B. cereus* csn is $p < 0.0001$, $p = 0.0052$, and $p = 0.034$, respectively. The survival rate for the larvae treated with compound 2 in PBS was 100%. *B. cereus*: *Bacillus cereus*, csn: culture supernatant.

alternative to murine models in microbial infection research due to its ease to obtain and use without elaborate equipment and ethical considerations.^[60] Moreover, the mechanisms of the innate immune system are closely related to those of the mammals.^[61,62]

To explore the effect of ColQ1 and a catalytically inactive mutant of ColQ1 (i.e., ColQ1 E502A)^[34] on the larvae, we injected them with various enzyme concentrations (100×10^{-9} – 500×10^{-9} M). The survival of the larvae was monitored daily for eight days. Larvae injected with the catalytically inactive mutant enzyme survived (at all concentrations). In contrast, eight days after treatment with active ColQ1, the survival dropped to 0%, 20%, and 50% at concentrations of 500×10^{-9} , 300×10^{-9} , and 100×10^{-9} M enzyme, respectively (Figure S10, Supporting Information). In a next step, we examined the effects of compounds 1 and 2 on the survival of the larvae in presence of 300×10^{-9} M of ColQ1. Co-injection of 300×10^{-6} M of compound 1 increased larvae survival by 60% while 150 and 50×10^{-6} M concentrations showed a lower impact (~30 and 0%, Figure S11, Supporting Information). Compound 2 maintained 60% survival at 20×10^{-6} M until day eight while 10×10^{-6} and 5×10^{-6} M showed a

lower effect (~40% and 0%) compared to the control (i.e., ColQ1) (Figure 6a).

Similar experiments were performed with *B. cereus* derived csn at concentrations of 35–100% (v/v). The survival of the larvae was studied for eight days after injection. After five days, only 15% of larvae injected with 100% (v/v) csn survived. With 65% and 35% (v/v) of the csn, the death of the larvae was delayed (Figure S10, Supporting Information). To investigate the effect of the collagenase inhibitors 1 and 2, we injected the larvae with 100% (v/v) of *B. cereus* csn together with compounds 1 (50×10^{-6} – 300×10^{-6} M) (Figure S11, Supporting Information) or 2 (5×10^{-6} – 20×10^{-6} M) (Figure 6b). Compound 1 at 300×10^{-6} M showed an increase of the survival rate from 20 to 75%, while at 150×10^{-6} M, the survival improved to 45% (Figure S11, Supporting Information). Compound 2 enhanced the survival from 25% to 73% at 20×10^{-6} M (Figure 6b). This difference between survival of larvae injected with ColQ1 and csn might be due to the high quantities of ColQ1 used in the experiment (i.e., 300×10^{-9} M), which is 300-fold the collagenase concentration in csn. This indicates that the action of csn on the larvae might be connected to other virulence factors (such as sphingomyelinase and non-hemolytic

enterotoxins) as well as collagenase, which could work together to kill the larvae.^[63,64] This also suggests that both compounds might target other virulence factors in the csn, therefore further experiments could be performed in the future to confirm this.

The toxic effect exerted by *B. cereus* collagenases might be related to the activation of melanization mechanisms in the larvae since the dead larvae turned black, as suggested for other metalloproteases.^[65–70] In addition, it has been shown that collagenases digest hemolymph proteins of the larvae into small peptides, which trigger an immune response finally leading to their death.^[65–69]

3. Conclusions

Virulence factors and their inhibitors are currently gaining wide attention because of their potential to limit the evolution of antibiotic resistance and to treat infections by reducing bacterial pathogenicity.^[13] Therefore, full characterization of virulence factors is essential to understand their role during infection and to predict whether their inhibition is beneficial for the treatment. In the present work, we characterized the collagenolytic activity of a recently discovered recombinant *B. cereus* ColQ1 virulence factor^[34] and *B. cereus* csn. In addition, we evaluated the biological effects of two small molecules that inhibit collagenases of *B. cereus* and other pathogens. In this context, an ex vivo pig-skin model of *B. cereus* infection was used to investigate *B. cereus* collagenases and the consequences of their inhibition. This model highlights the ability of *B. cereus* collagenase to decompose fibrillar COLs and disrupt their regular alignment. This mechanism might lead to an accelerated bacterial infiltration and penetration into deeper sites of the host. Moreover, as previously reported, this mechanism is one of the main obstacles to the wound-healing process.^[59,73] We demonstrated that *B. cereus* csn collagenases induced cytotoxicity in fibroblasts and keratinocytes, which could be minimized using bacterial collagenase inhibitors. In an in vivo model using *G. mellonella* larvae, we showed that ColQ1 and *B. cereus* csn are toxic and induce the death of the larvae. Treatment with collagenase inhibitors significantly increased their survival rate. These findings provide new insights into the functions of *B. cereus* collagenases in wound infections and the importance of its inhibition by antivirulence, which could represent a promising therapeutic option.

4. Experimental Section

Production of *B. cereus* ColQ1: The collagenase unit of ColQ1 from *B. cereus* strain Q1 (Uniprot: B9J3S4; Tyr94-Gly765) was expressed and purified as previously described.^[34]

***B. cereus* csn Production:** *B. cereus* ATCC 14579 strain was prepared as described before.^[35] *B. cereus* was grown in RPMI medium (+10% FCS, 1% Glutamine) (Gibco) at 30 °C ON with 160 rpm shaking. The next day, csn was harvested by centrifugation at 3000 x g for 10 min at 4 °C. The csn was sterile-filtered with 0.22 µm filter (Greiner) then, it was aliquoted and stored at –80 °C until use.

In vitro FRET-Based Peptidolytic Assay: IC₅₀ measurements were performed as previously reported.^[33] In short, ColQ1 was incubated with compound 2 at RT for 1 h. The reaction was initiated by the addition of 2 × 10^{–6} M of the collagenase-specific peptide substrate Mca-Ala-Gly-Pro-Gly-Pro-Dpa-Gly-Arg-NH₂ (FS1-1; Mca = (7-methoxycoumarin-4-yl)acetyl;

Dpa = *N*-3-(2,4-dinitrophenyl)-L-2,3-diaminopropionyl). The fluorescence was monitored for 2 min (excitation: 328 nm, emission: 392 nm) at 25 °C. The final concentrations were 1 × 10^{–9} M ColQ1, 250 mM HEPES pH 7.5, 400 mM NaCl, 10 mM CaCl₂, 10 × 10^{–6} M ZnCl₂, 2 × 10^{–6} M FS1-1, and 0 to 120 × 10^{–6} M compound 2. Due to poor compound solubility, the DMSO concentration was adjusted to 5%. The percentage of enzyme inhibition was calculated in relation to a blank reference without compound added. All experiments were performed in triplicate. Limited by the solubility of the compound, the IC₅₀ value could not be determined using non-linear regression, but was determined by linear regression using only data within the 40–60% inhibition range. Regression analysis was performed using GraphPad Prism 5 (Graph Pad Software, San Diego, CA, USA). To determine the peptidolytic activity versus FS1-1 of the *B. cereus* csn, a similar assay as described above was performed. Csn samples were freshly thawed and used in the assay in three different concentrations (12%, 16% and 20% v/v). Samples were preincubated with buffer control or inhibitors for 30 min at RT, before the reactions were started upon addition of 2 × 10^{–6} M FS1-1. The final inhibitor concentrations were: 20 mM EDTA, 1x EDTA-free complete protease inhibitor cocktail (Roche, Woerden, The Netherlands) as serine and cysteine protease inhibitors, 1.83 mM compound 1 and 95 × 10^{–6} M compound 2 at a final DMSO concentration of 5%. All results were extrapolated to 100% v/v and inhibition rates were normalized to the uninhibited control. Experiments were performed in triplicate and are presented as means ± standard deviation.

Gelatin Zymography: Aliquots of the *B. cereus* csn were loaded onto 10% SDS-PAGE gels containing 0.2% gelatin (Roth, Karlsruhe, Germany) and separated by electrophoresis at 4 °C. After separation, the gels were sliced into 4 pieces (marker lane plus 2 sample lanes) each and incubated in the respective renaturation buffer (50 mM HEPES pH 7.5, 200 mM NaCl, 10 × 10^{–3} M CaCl₂, 10 × 10^{–6} M ZnCl₂, 2.5% Triton X-100) supplemented with (i) nothing (control), (ii) 1x EDTA-free cComplete protease inhibitor cocktail (Roche, Woerden, The Netherlands), (iii) 300 × 10^{–6} M compound 1 or (iv) 100 × 10^{–6} M compound 2 at RT for 2x30 min with gentle agitation. The gel slices were then equilibrated in the respective developing buffer (50 mM HEPES pH 7.5, 200 mM NaCl, 10 mM CaCl₂, 10 × 10^{–6} M ZnCl₂, 0.02% Brij-35) supplemented with the aforementioned compounds (i–iv) at RT for 2x10 min with gentle agitation, and then incubated on at 37 °C in fresh, supplemented developing buffer. Transparent bands of gelatinolytic activity were visualized by staining with 0.1% Coomassie brilliant blue G-250 dye ON. Gels were scanned using ChemiDoc XRS+ imaging system (Biorad, USA) and image analysis was performed with Image Studio Lite v5.2 software (Li-Cor Biosciences, USA). The integration area of the indicated molecular weight regions was measured, and values were expressed as a ratio of the control area from the same gel (no additional treatment; set to unity). Results were thereby standardized for each gel and expressed in dimensionless units. Results were obtained from two separate experiments for each condition.

COL Cleavage Assay: Acid-soluble type I COL from bovine tail (Thermo Fischer Scientific) at a final concentration of 1 mg mL^{–1} was digested at 25 °C by 50 ng ColQ1 in 250 mM HEPES, 150 mM NaCl, 5 mM CaCl₂, 5 × 10^{–6} M ZnCl₂, pH 7.5. Compounds 1 and 2 were included at different concentrations, and incubated together with COL and ColQ1 for 3 h. The reaction was stopped by the addition of 50 mM EDTA followed by visualization with 12% SDS-PAGE gels. Results were obtained from two independent experiments for each compound.

Synthesis of Compounds 1 and 2: The synthesis was performed according to the synthetic scheme that we published before.^[32,30]

Docking of Compounds 1 and 2: The crystal structure of the peptidase domain of ColH (5o7e) with 1.87 Å resolution was used as target model for the docking. Ligand files were prepared as input for the docking software using OpenBabel (protonation state)⁷¹ In case of compound 2, the thio-late derivative was used as input, as the mercaptoacetamide compound is known to hydrolyze in aqueous solution.^[33] The final docking was performed using the Molecular Forecaster suite.^[49] In short, the protein structure was prepared using the PREPARE and PROCESS modules with a ligand cutoff of 7 Å (particle water option). The ligands were prepared using the SMART module. Docking calculations were performed using FITTED. The docking software was validated via redocking the ligand 9NB, result-

ing in an RMSD of 0.43 Å. The PyMOL Molecular Graphics System, version 2.0.6.0a0, Schrödinger, LLC, was used for generating figures.^[72]

ColQ1 Activity on Ex vivo Pig-Skin Model: The ex vivo pig-skin model was performed as reported earlier.^[38] The skin explants of 15 mm diameter were made from ears of young pigs which were provided by a local slaughterhouse. Once the ears were received, several steps of sterilization were performed. The ears were punched, washed with sterile water followed with 3 x DMEM medium containing 10% FBS, 1% Pen-Strep and 250 ng mL⁻¹ amphotericin B, with a minimum of 15 min incubation time. To assess the sterilization by antibiotics, randomly selected skin punches were incubated in DMEM medium at 37 °C ON. The next day, the exposed DMEM was plated on LB-agar plate without antibiotic to check for bacterial growth. After washing the explants, they were stored at -80 °C for a maximum of one month in DMEM supplemented with 15% (v/v) glycerol. The storage conditions were selected based on the viability of the skin which we evaluated over one month with the MTT assay at 37 °C, -20 °C and -80 °C (Figure S3, Supporting Information). To investigate the activity of collagenase effect ex vivo, the skin samples were thawed and incubated at 37 °C for one hour in DMEM medium containing 10 × 10⁻⁶ M ZnCl₂ and 4 mM CaCl₂. While the epidermal side of the skin was exposed to air, the dermal side was incubated in DMEM medium with ColQ1 or csn for several time periods. The skin was incubated with different concentrations of ColQ1 ranging from 100 × 10⁻⁹–500 × 10⁻⁹ M and of *B. cereus* csn (0–100% v/v) for several days in a total volume of 300 µL containing ColQ1 or csn together with DMEM and tissue explant. To estimate the release of Hyp into the DMEM medium, the medium was collected and stored at -20 °C. Hyp quantification was performed using a Hydroxyproline assay kit (Sigma Aldrich). In short, Hyp was converted into a colorimetric product after adding 100 µL chloramine T/oxidation buffer mixture, 100 µL 4-(dimethylamino)benzaldehyde diluted in perchloric acid/isopropanol to 10 µL of DMEM medium and measured at a wavelength of 560 nm. For further evaluation, the skin tissues that were treated for 24 h were fixed with 4% paraformaldehyde (PFA) and stored at 4 °C. The fixed skin was stored ON with 10% and then 25% sucrose in PBS ON in order to prevent tissue damage before downstream evaluation. The data were plotted with GraphPad Prism 8 for three independent experiments and to calculate the probability value one-way ANOVA was performed and statistical significance was analyzed by Tukey test.

Ex vivo Pig-Skin Model for Evaluating the Effect of ColQ1 Inhibitors: In order to select adequate inhibitor concentrations, the skin was treated with 300 × 10⁻⁹ M ColQ1 (optimal concentration of ColQ1 selected from the previous assay) and gradient concentrations of collagenase inhibitors 1 and 2. A total of 12 skin punches per compound were treated in duplicate for six conditions followed by incubation at 37 °C for 24 h, 5% CO₂ and 300 rpm. Non-treated condition was considered as a healthy state, the other samples were incubated with 300 × 10⁻⁹ M ColQ1 combined with either compound 1 (0–400 × 10⁻⁶ M) or compound 2 (0–50 × 10⁻⁶ M). After 24 h, all samples were fixed in 4% PFA and stored after treating them with 10% and 25% sucrose/PBS as described before and prepared for microscopic and biochemical analysis. To analyze the Hyp content in the DMEM medium for each condition, the DMEM was collected before and after treatment and stored at -20 °C. Finally, the optimal inhibitor concentration was determined by microscopy and biochemical evaluation. Results of three independent experiments were plotted, mean ± standard deviation. To estimate the probability value one-way ANOVA was performed and statistical significance was analyzed to illustrate the significant differences between non-treated versus treated samples. (***) $p \leq 0.001$.

Sample Preparation for SHG and Immunostaining of COL Subtypes: The tissue punches were sliced into half with surgical scissors and placed into a separate holder such that the sliced edge faced inside the cavity of the holder in orthogonal direction. Next, the cryogel (ThermoFisher) was added to the samples and skin were readjusted upright if necessary, and then frozen at -80 °C for at least 30 min. For each condition, a glass slide (Superfrost Plus, Menzel Gläser, ThermoFisher) was used and three circles were drawn using a hydrophobic liquid blocker pen (PAP pen (ab2601), Abcam). Prior to the sectioning, samples were cryo-glued onto steel molds which were then inserted into the cryostat and clamped at the correct angle (the long edge of the sample orthogonal to the blades edge). Subsequently,

the sample was trimmed to form a smooth surface and thereby reduced the risk of artefacts. Depending on the desired microscopy method, the tissue samples were sliced in 20 µm for epifluorescence microscopy or 100 µm for SHG microscopy on poly-L-lysine coated glass slides. The cryogel was washed off with 3 × 100 µL sterile PBS carefully from the corner in order to avoid movement, overlapping or even rinsing off of the specimen. No staining was performed for SHG imaging.

For immunostaining, tissue samples were stained with primary antibodies. (COL I (Rabbit polyclonal anti-type I collagen, (600-401-103-0.1 Rockland); COL III (rabbit anti human collagen III antibody, (Abcam, ab7778)); COL V (rabbit anti human collagen V antibody, (Abcam, ab7046)) (1:200 dilutions in PBS) at RT for 1 h or at 4 °C ON. Next, the solution was removed, and all samples were gently washed with 3 × 100 µL PBS, followed by addition of 50 µL secondary antibody solution ((IgG (H+L) Highly Cross-Adsorbed; conjugated with AF647 (Abcam, A-21245)) in PBS (0.8% goat serum (Sigma-Aldrich, G9023-5ML)) and 1:5000 DAPI (Thermo Fisher)) at RT for 1 h or at 4 °C ON. Samples were washed 3 x with PBS again. For each slide, a 0.17 µm thick 24 mm x 60 mm cover glass (ThermoFisher) was placed on top of a layer of Parafilm and prepared with three evenly distributed drops of in total 60 µL FluoroMountG (ThermoFisher, 00-4958-02, refractive index: 1.4). The slides were placed at one edge of the cover glass and slowly lowered towards it in a decreasing angle, from one side to the other. Even distribution of the mounting medium required some time and a sense of applying pressure, but when performed carefully, arising air bubbles were prevented or eliminated in this step. When all slides were sealed, everything was covered with a layer of parafilm. Since the polymerization of FluoromountG requires constant pressure, some weight (e.g., a 1 L bottle PBS on top of a book) was applied on top of it for at least 4 h but optimally ON. Prior to imaging or storage at 4 °C, all slides were cleaned using paper tissues and 70% ethanol in dH₂O to remove dirt and redundant mounting medium.

SHG and Epifluorescence Microscopy: COL fibres in the tissue were visualized using SHG generated by a Zeiss LSM 880 confocal microscope with a two-photon femtosecond pulsed laser (Chameleon Vision I, Coherent, Santa Clara, CA (USA)) set at 900 nm wavelength for excitation. The emitted fluorescent signal was detected before the pinhole using Zeiss Big.2 non-descanned NDD detectors in combination with a 380–430 nm band pass filter. Images were obtained using 8% laser power, with a pixel dwell time of 8.24 µs with 4x averaging, and the detector gain set at 500. The resulting image had a size of 512x512 pixels with a pixel size of 1.38 µm. Images were taken with a Plan-Apochromat 20x/0.8 NA objective in the dermal region of the skin. Z-stack imaging was performed by selection of a representative spot in the plane with the highest SHG signal, followed by defining the first and a last plane, resulting in a Z-stack with 10 slices spanning 45 µm. Maximum intensity projections were then generated in ImageJ using the Z-project function.

Epifluorescence imaging was performed using a Nikon-Ti Eclipse inverted microscope coupled with a Lumencor SOLA white light lamp for epifluorescence. Images were captured using an Andor Clara DR-5434 camera, with filtercubes for DAPI at 365 nm staining the nuclei and the secondary antibody AF647 conjugate, which labeled COL antibodies at 640 nm. To get a good view throughout the whole skin thickness, large images with a scan area of 2x1 fields of view (10% overlapping) were captured using the Perfect Focus System. Parameters such as light intensity, exposure time, magnification, and tile scan area were adjusted individually for each COL type antibody. Thus, only treated and non-treated samples for one particular COL type immunostaining can be directly compared. For illustration purposes, a LUT threshold for each subtype was selected with the non-treated control of each condition and applied on all images of the related subtype. For a summary of the imaging conditions used, please see Table S1, Supporting Information. Triplicates of all samples were measured.

In vitro Cell-Based Assay: NHDF (Promo Cell C-12302) and HaCaT (ATCC® PCS-200-011) were purchased from commercial suppliers. 50000 cells per well of NHDF and HaCaT were seeded in 96-well plate (Greiner) with DMEM medium (Gibco) including 10% (v/v) fetal bovine serum (FBS, Gibco) and 1% (v/v) Penicillin-Streptomycin (Pen-Strep) antibiotic. The cells were incubated at 37 °C for 24 h

with 5% CO₂ prior to the treatment. Next, cells were incubated with varying amounts of *B. cereus* csn (0–15%) in a total volume of 200 µL containing csn, cells, DMEM. To inhibit the collagenolytic activity of *B. cereus* csn compounds **1** and **2** were added to the culture along with 1.25% (v/v) *B. cereus* csn having 1% DMSO and incubated for 24 h. On the next day, cell viability was evaluated using MTT and live/dead staining assays. The MTT assay is based on the reduction of tetrazolium dye to purple insoluble formazan by mitochondrial succinate dehydrogenase. Live/dead imaging depends on staining the live cells with fluorescein diacetate (FDA) and dead cells with propidium iodide (PI). The MTT assay and live/dead staining were performed after 24 h and 48 h incubation for csn treatment and 24 h incubation after collagenase inhibitor treatment. To conduct the MTT assay, we removed the medium and washed the cells 2 x with sterile PBS buffer. Afterwards, we added 200 µL of a mixture containing fresh DMEM and 5 mg mL⁻¹ MTT reagent in each well and incubated the plate for 2 h at 37 °C with 5% CO₂. After the incubation, the medium was removed, and 200 µL of 100% DMSO was added to each well to dissolve the formazan crystals, and the plate was incubated at 37 °C for 30 min. Finally, the absorbance was measured using a PHERAstar plate reader (BMG Labtech, Ortenberg, Germany) at 0 nm for samples and at 620 nm for blanks with DMEM medium. The viability was also evaluated via epifluorescence microscope (Leica Microsystems CMS GmbH, Wetzlar, Germany) after the live/dead staining. Cells were seeded and treated with *B. cereus* csn similar to the procedures mentioned above and washed 3 x with sterile PBS. 0.03 mg mL⁻¹ FDA and 0.02 mg mL⁻¹ PI were added into each well and incubated at 37 °C for 5 min and 5% CO₂. Then the viability and morphology of cells were investigated with 5x magnification to obtain an overview of the quantity of live and dead cells. The morphological changes between the non-treated cells and cells treated with the csn, treated with csn was captured at bright field channel with 20x. The viability of the cells was calculated relative to non-treated controls using ImageJ Fiji software, the results were plotted with GraphPad Prism 8 for three independent experiments for each cell type and 9 images for each condition. To calculate the probability value one-way ANOVA was performed and statistical significance was analyzed by Tukey test. For display purpose, the brightness and contrast were adjusted for each image based on the values of the control image where no treatment was applied.

Galleria mellonella Virulence Assay: *Galleria mellonella* larvae (Tru-Larv) were purchased from BioSystems Technology (Exeter, United Kingdom). Injections were performed using a LA120 syringe pump (Landgraf Laborsysteme, Langenhagen, Germany) equipped with 1 mL Injekt-F tuberculin syringes (B. Braun, Melsungen, Germany) and Sterican 0.30 × 12 mm, 30G × 1.5 needles (B. Braun). The larvae were injected in the right proleg with 10 µL of different solutions (i.e., various concentrations of *B. cereus* csn or ColQ1 or with only PBS). Based on that they were classified into different groups according to the following description: untreated group, treated with sterile PBS group, treated with different amount of *B. cereus* csn (which was diluted in sterile PBS), treated with ColQ1 diluted with sterile PBS, treated group with a mixture of 100% *B. cereus* csn or 300 × 10⁻⁹ M ColQ1 and various concentrations of compounds **1** or **2** and treated group with only one of the compounds (diluted in PBS) to evaluate the toxicity level. We considered the larvae dead if they did not move and had a black color which reflected the activation of the melanization cascade due to the toxic effect induced by virulence factors. The survival of the larvae was analyzed using GraphPad Prism 8 using Kaplan-Meier analysis followed by equality test called log-rank test. The data of three independent experiments were combined and plotted in the survival curve, 45 larvae in total were included to test compounds with the csn and 30 larvae to test compounds with ColQ1 in the three experiments.

Statistical Analysis: Graphical data in the manuscript are communicated as the means ± SDs. Statistical comparisons were performed by Tukey one-way ANOVA test, which shows significant differences between conditions. Parametric/non-parametric statistical analysis used in the study were based on normality and homogeneity of variance. A value of $p \leq 0.001$ was considered statistically significant while $p > 0.05$ was considered non-significant. The normalized measurements were statistically compared between treated and non-treated groups using generalized estimating equations model to account for correlated data arising from

repeated measures. The survival of *G. mellonella* was analyzed using the Kaplan–Meier method and log-rank test was applied to calculate the significant difference between conditions.

Supporting Information

Supporting Information is available from the Wiley Online Library or from the author.

Acknowledgements

The authors are grateful to E. Färber GmbH & Co. KG (Zweibrücken, Germany) for providing fresh pig ears. This work was supported by Helmholtz-Zentrum für Infektionsforschung GmbH, European Research Council (ERC starting grant 757913), and Austrian Science Fund (P 31843 and I 4360).

Open Access funding enabled and organized by Projekt DEAL.

Conflict of Interest

The authors declare no conflict of interest.

Data Availability Statement

The data that support the findings of this study are available in the supplementary material of this article.

Keywords

antibiotic resistance, *Bacillus cereus*, collagenase, pathoblocker, virulence factors

Received: November 9, 2021

Revised: December 15, 2021

Published online:

- [1] E. J. Bottone, *Clin. Microbiol. Rev.* **2010**, *23*, 382.
- [2] P. E. Granum, T. Lund, *FEMS Microbiol. Lett.* **1997**, *157*, 223.
- [3] M. S. P. Dryden, *J. R. Soc. Med.* **1987**, *80*, 480.
- [4] X.-Y. Wu, K.-X. Ni, L. S-B, *China J. Orthop. Traumatol.* **2013**, *26*, 9.
- [5] F. A. Drobniewski, *Clin. Microbiol. Rev.* **1993**, *1744*, 304.
- [6] C.-W. Kim, S.-H. Cho, S.-H. Kang, Y.-B. Park, M.-H. Yoon, J.-B. Lee, W.-S. No, J.-B. Kim, *J. Food Sci.* **2015**, *80*, M123.
- [7] C. Fenselau, C. Havey, N. Teerakulkittipong, S. Swatkoski, O. Laine, N. Edwards, *Appl. Environ. Microbiol.* **2008**, *74*, 904.
- [8] Centers for Disease control and prevention <https://www.cdc.gov/drugresistance/biggest-threats.html> (accessed: December 2021)
- [9] S. B. Zaman, M. A. Hussain, R. Nye, V. Mehta, K. T. Mamun, N. Hosain, *Cureus* **2017**, *9*, 1403.
- [10] O. Jim, Antimicrobial Resistance: Tackling a crisis for the health and wealth of nations, **2014**.
- [11] S. W. Dickey, G. Y. C. Cheung, M. Otto, *Nat. Rev. Drug Discovery* **2017**, *16*, 457.
- [12] M. B. Calvert, V. R. Jumde, A. Titz, *Beilstein J. Org. Chem.* **2018**, *14*, 2607.
- [13] D. A. Rasko, V. Sperandio, *Nat. Rev. Drug Discovery* **2010**, *9*, 117.
- [14] W. Keenleyside, in *Microbiology: Canadian Edition*,
- [15] M. C. Callegan, S. T. Kane, D. C. Cochran, M. S. Gilmore, *DNA Cell Biol.* **2002**, *21*, 367.
- [16] P. C. Turnbull, K. Jørgensen, J. M. Kramer, R. J. Gilbert, J. M. Parry, *J. Clin. Pathol.* **1979**, *32*, 289.
- [17] D. J. Beecher, T. W. Olsen, E. B. Somers, A. C. L. Wong, *Infect. Immun.* **2000**, *68*, 5269.

- [18] K. K. Makinen, P. L. Makinen, *J. Biol. Chem.* **1987**, *262*, 12488.
- [19] I. Negut, V. Grumezescu, A. M. Grumezescu, *Molecules* **2018**, *23*, 2392.
- [20] S. H. M. D. Hussain, B. M. D. Limthongkul, T. R. M. Humphreys, *Dermatologic Surg.* **2013**, *39*, 193.
- [21] K. Gelse, E. Pöschl, T. Aigner, *Adv. Drug Delivery Rev.* **2003**, *55*, 1531.
- [22] V. Bansal, P. K. Sharma, N. Sharma, O. P. Pal, R. Malviya, *Biol. Res.* **2011**, *5*, 28.
- [23] R. Berisio, V. Granata, L. Vitagliano, A. Zagari, *J. Am. Chem. Soc.* **2004**, *126*, 11402.
- [24] D. J. Harrington, *Infect. Immun.* **1996**, *64*, 1885.
- [25] Y. Z. Zhang, L. Y. Ran, C. Y. Li, X. L. Chen, *Appl. Environ. Microbiol.* **2015**, *81*, 6098.
- [26] S. Patel, *Understanding Wound infection and colonisation* **2007**, 2.
- [27] P. G. Bowler, B. I. Duerden, D. G. Armstrong, *Clin. Microbiol. Rev.* **2001**, *14*, 244.
- [28] H. Pîrvănescu, M. Bălăşoiu, M. E. Ciurea, A. T. Bălăşoiu, R. Mănescu, *Chirurgia* **2014**, *109*, 73.
- [29] E. Schönauer, H. Brandstetter, in *Zinc Enzyme Inhibitors: Enzymes from Microorganisms* (Eds: C. T. Supuran, C. Capasso), Springer International Publishing, Cham, Switzerland **2017**, p. 69. https://doi.org/10.1007/7355_2016_9.
- [30] A. S. Duarte, A. Correia, A. C. Esteves, *Crit. Rev. Microbiol.* **2014**, *42*, 106.
- [31] K. Voos, E. Schönauer, A. Alhayek, J. Hauptenthal, A. Andreas, R. Müller, R. W. Hartmann, H. Brandstetter, A. K. H. Hirsch, C. Ducho, *ChemMedChem* **2021**, *16*, 1257.
- [32] A. M. Kany, A. Sikandar, J. Hauptenthal, S. Yahiaoui, C. K. Maurer, E. Proschak, J. Köhnke, R. W. Hartmann, *ACS Infect. Dis.* **2018**, *4*, 988.
- [33] A. M. Kany, J. Hauptenthal, K. Hüsecken, I. J. Hoppe, K. Voos, S. Yahiaoui, B. Elsässer, C. Ducho, H. Brandstetter, R. W. Hartmann, *J. Am. Chem. Soc.* **2017**, *139*, 12696.
- [34] I. J. Hoppe, H. Brandstetter, E. Schönauer, *Sci. Rep.* **2021**, *11*, 4187.
- [35] C. M. Abfalter, E. Schönauer, K. Ponnuraj, M. Huemer, G. Gadermaier, C. Regl, P. Briza, F. Ferreira, C. G. Huber, H. Brandstetter, G. Posselt, S. Wessler, *PLoS One* **2016**, *11*, 0162433.
- [36] S. F. Altschul, W. Gish, W. Miller, E. W. Myers, D. J. Lipman, *J. Mol. Biol.* **1990**, *215*, 403.
- [37] O. Matsushita, C. M. Jung, S. Katayama, J. Minami, Y. Takahashi, A. Okabe, *J. Bacteriol.* **1999**, *181*, 923.
- [38] J. Konstantinović, S. Yahiaoui, A. Alhayek, J. Hauptenthal, E. Schönauer, A. Andreas, A. M. Kany, R. Müller, J. Köhnke, F. K. Berger, M. Bischoff, R. W. Hartmann, H. Brandstetter, A. K. H. Hirsch, *J. Med. Chem.* **2020**, *63*, 8359.
- [39] G. K. Reddy, C. S. Enwemeka, *Clin. Biochem.* **1996**, *29*, 225.
- [40] A. Logan, R. E. Neuman, *J. Biol. Chem.* **1950**, *184*, 299.
- [41] L. Mostaço-Guidolin, N. L. Rosin, T. L. Hackett, *Int. J. Mol. Sci.* **2017**, *18*, 1772.
- [42] D. Rouède, E. Schaub, J. Bellanger, F. Ezan, J.-C. Scimeca, G. Baffet, F. Tiaho, *Sci. Rep.* **2017**, *7*, 12197.
- [43] R. C. Haut, in *Accidental Injury: Biomechanics and Prevention*, Vol. 228 (Eds: A. M. Nahum, J. W. Melvin), Springer, New York **2002**.
- [44] P. D. Verhaegen, H. J. Schouten, W. Tigchelaar-Gutter, J. van Marle, C. J. van Noorden, E. Middelkoop, P. P. van Zuijlen, *Wound Repair Regen.* **2012**, *20*, 658.
- [45] S. Ricard-Blum, *Cold Spring Harbor Perspect. Biol.* **2011**, *3*, a004978.
- [46] U. Eckhard, P. F. Huesgen, H. Brandstetter, C. M. Overall, *J. Proteomics* **2014**, *100*, 102.
- [47] C. Abfalter, T. Schmidt, S. Wessler, *Br. Microbiol. Res. J.* **2015**, *7*, 62.
- [48] J. Eberhardt, D. Santos-martins, A. F. Tillack, S. Forli, *J. Chem. Inf. Model.* **2021**, *61*, 3891.
- [49] J. Pottel, E. Therrien, J. L. Gleason, M. N., *J. Chem. Inf. Model.* **2014**, *254*, 2014.
- [50] S. M. Ireland, A. C. R. Martin, *Database* **2019**, *2019*, baz006.
- [51] M. A. Nilforoushzadeh, H. R. A. Ashtiani, F. Jaffary, F. Jahangiri, N. Nikkhal, M. Mahmoudbeyk, M. Fard, Z. Ansari, S. Zare, *J. Skin Stem Cell* **2017**, *4*, 69080.
- [52] D. A. Scudiero, R. H. Shoemaker, K. D. Paull, A. Monks, S. Tierney, T. H. Nofziger, M. J. Currens, D. Seniff, M. R. Boyd, *Cancer Res.* **1988**, *48*, 4827.
- [53] C. A. Day, A. Langfald, E. H. Hinchcliffe, *Methods in Cell Biology*, *158*, Elsevier, Philadelphia **2020**, p. 43.
- [54] H. C. Stearns, V. D. Sneed, *Am. J. Obstet. Gynecol.* **1966**, *94*, 718.
- [55] M. Ito, Y. Liu, Z. Yang, J. Nguyen, F. Liang, R. J. Morris, G. Cotsarelis, *Nat. Med.* **2005**, *11*, 1351.
- [56] I. Pastar, O. Stojadinovic, N. C. Yin, H. Ramirez, A. G. Nusbaum, A. Sawaya, S. B. Patel, L. Khalid, R. R. Isseroff, M. Tomic-Canic, *Adv. Wound Care* **2014**, *3*, 445.
- [57] A. M. Wojtowicz, S. Oliveira, M. W. Carlson, A. Zawadzka, C. F. Rousseau, D. Baksh, *Wound Repair Regen.* **2014**, *22*, 246.
- [58] S. M. McCarty, S. L. Percival, *Adv. Wound Care* **2013**, *2*, 438.
- [59] L. Ovington, *Ostomy Wound Manage.* **2003**, *49*, 7A.
- [60] N. Ramarao, C. Nielsen-Leroux, D. Lereclus, *J. Visualized Exp.* **2012**, *70*, 4392.
- [61] P. Singkum, S. Suwanmanee, P. Pumeesat, N. Luplertlop, *Acta Microbiol. Immunol. Hung.* **2019**, *66*, 31.
- [62] C. J. Y. Tsai, J. M. S. Loh, T. Proft, *Virulence* **2016**, *7*, 214.
- [63] V. M. Doll, M. Ehling-Schulz, R. Vogelmann, *PLoS One* **2013**, *8*, 61404.
- [64] M. Ehling-Schulz, T. M. Koehler, D. Lereclus, *Microbiol. Spectr.* **2019**, *7*, 139.
- [65] D. Peng, J. Lin, Q. Huang, W. Zheng, G. Liu, J. Zheng, L. Zhu, M. Sun, *Environ. Microbiol.* **2016**, *18*, 846.
- [66] S. Kay, J. Edwards, J. Brown, R. Dixon, *Front. Microbiol.* **2019**, *10*, 1281.
- [67] J. Griesch, M. Wedde, A. Vilcinskas, *Insect Biochem. Mol. Biol.* **2000**, *30*, 461.
- [68] B. Altincicek, A. Vilcinskas, *Dev. Comp. Immunol.* **2006**, *30*, 1108.
- [69] M. Andrejko, M. Mizerska-Dudka, *J. Invertebr. Pathol.* **2011**, *107*, 16.
- [70] D. Peng, J. Lin, Q. Huang, W. Zheng, G. Liu, J. Zheng, L. Zhu, M. Sun, *Environ. Microbiol.* **2016**, *18*, 846.
- [71] N. M. O'Boyle, M. Banck, C. A. James, C. Morley, *J. Cheminform.* **2011**, *3*, 33.
- [72] The PyMOL Molecular Graphics System, <https://pymol.org/2/> (accessed: December 2021)
- [73] S. Guo, L. A. DiPietro, *J. Dent. Res.* **2010**, *89*, 219.

2.2.1 Supporting information

Supplementary Figures

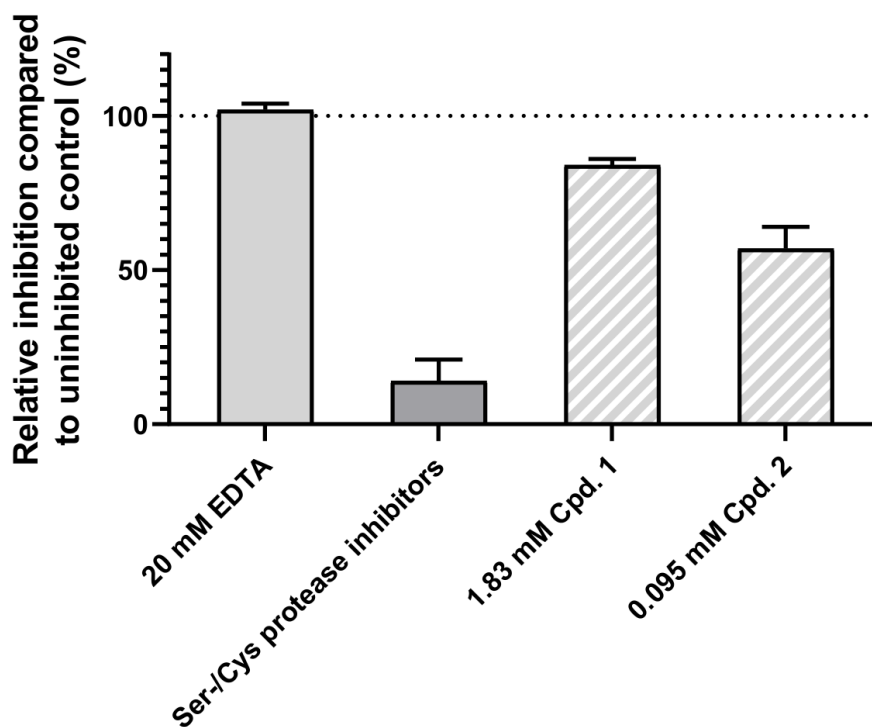
Peptidolytic activity of the *B. cereus* csn (Figure S1)

Figure S1. *B. cereus* csn activity in a collagenase-specific peptidic assay. Peptidolytic activity towards a collagenase-specific substrate by csn from *B. cereus* ATCC 14579 and inhibited with compounds **1** and **2** ($n = 3$, results are shown as mean \pm standard deviation). Compound **1** was used at a concentration of 10x its IC_{50} vs ColQ1. Due to limited solubility in the reaction buffer, compound **2** could only be tested at a concentration of 1x IC_{50} . *B. cereus*: *Bacillus cereus*, csn: culture supernatant.

Standard curve of ColQ1 (Figure S2)

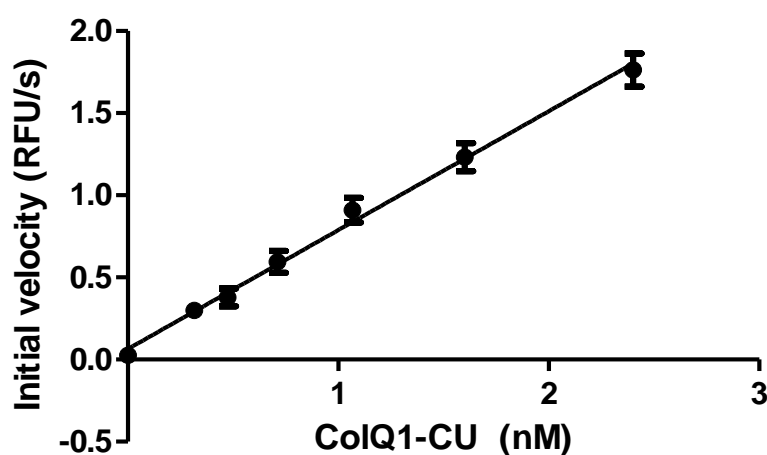


Figure S2. Representative standard curve of peptidolytic activity of ColQ1 in presence of serine and cysteine inhibitors. A 2.4 nM/ml stock solution of ColQ1 was serially diluted in the reaction buffer of the *in vitro* FRET-based peptidolytic assay. The reactions were initiated by the addition of 2 μ M FS1-1 and the reactions monitored

for 2 min (excitation: 328 nm, emission: 392 nm) at 25 °C. Initial velocities were calculated via linear regression. All experiments were performed in triplicates and results are shown as mean \pm standard deviation.

Dose-response curves for compound 1 and compound 2 vs ColQ1 (Figure S3)

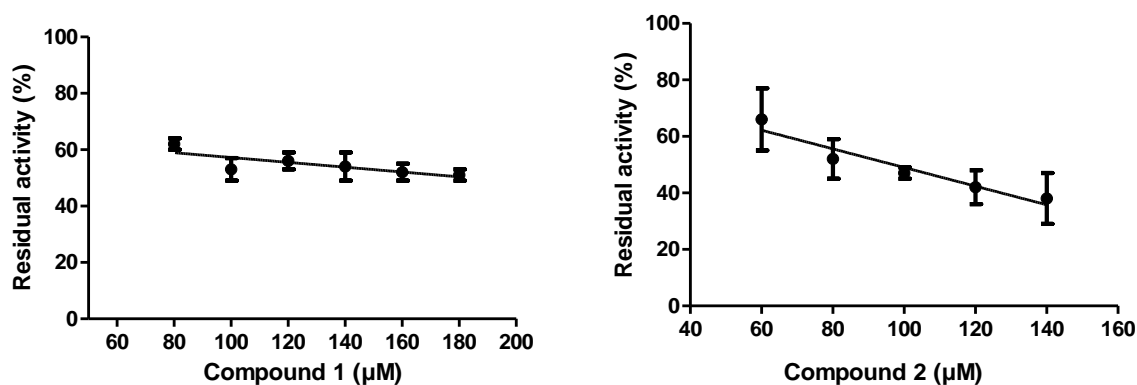
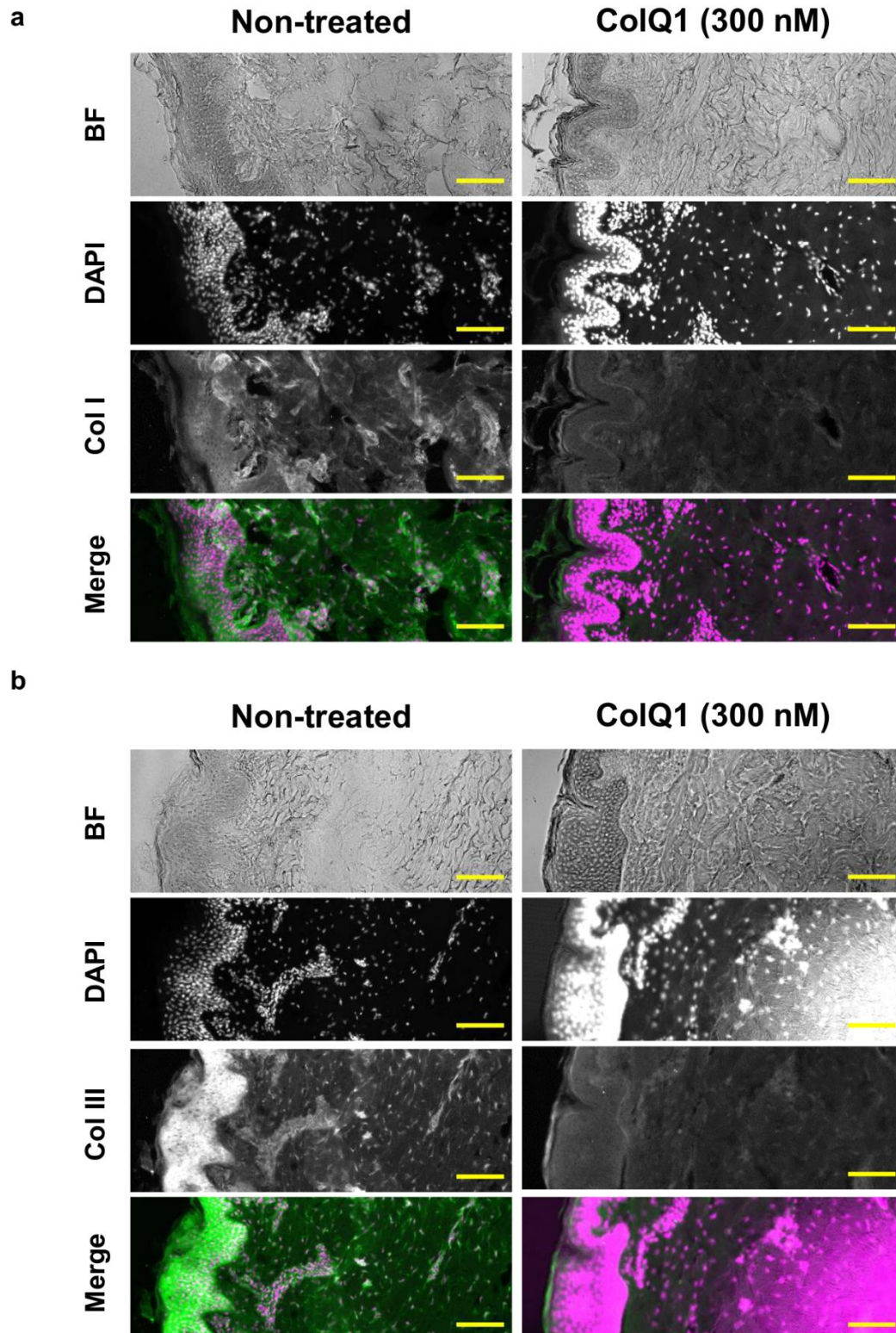


Figure S3. Representative dose-response curve for the IC_{50} value determination of compound 1 and 2 on ColQ1. Due to limited compound solubility, the IC_{50} determination had to be performed via linear regression and was limited to the linear portion of the sigmoidal response curve. The compounds were preincubated for 1 h at RT before initiating the reaction by addition of 2 μM FS1-1. The reactions were monitored for 2 min (excitation: 328 nm, emission: 392 nm) at 25 °C. Initial velocities were calculated via linear regression and normalized to a non-inhibited control reaction. All experiments were performed in triplicates and results are shown as mean \pm standard deviation.

Bright-field and DAPI signals of the tissue used for the immunostaining of fibrillar collagens (Figure S4)

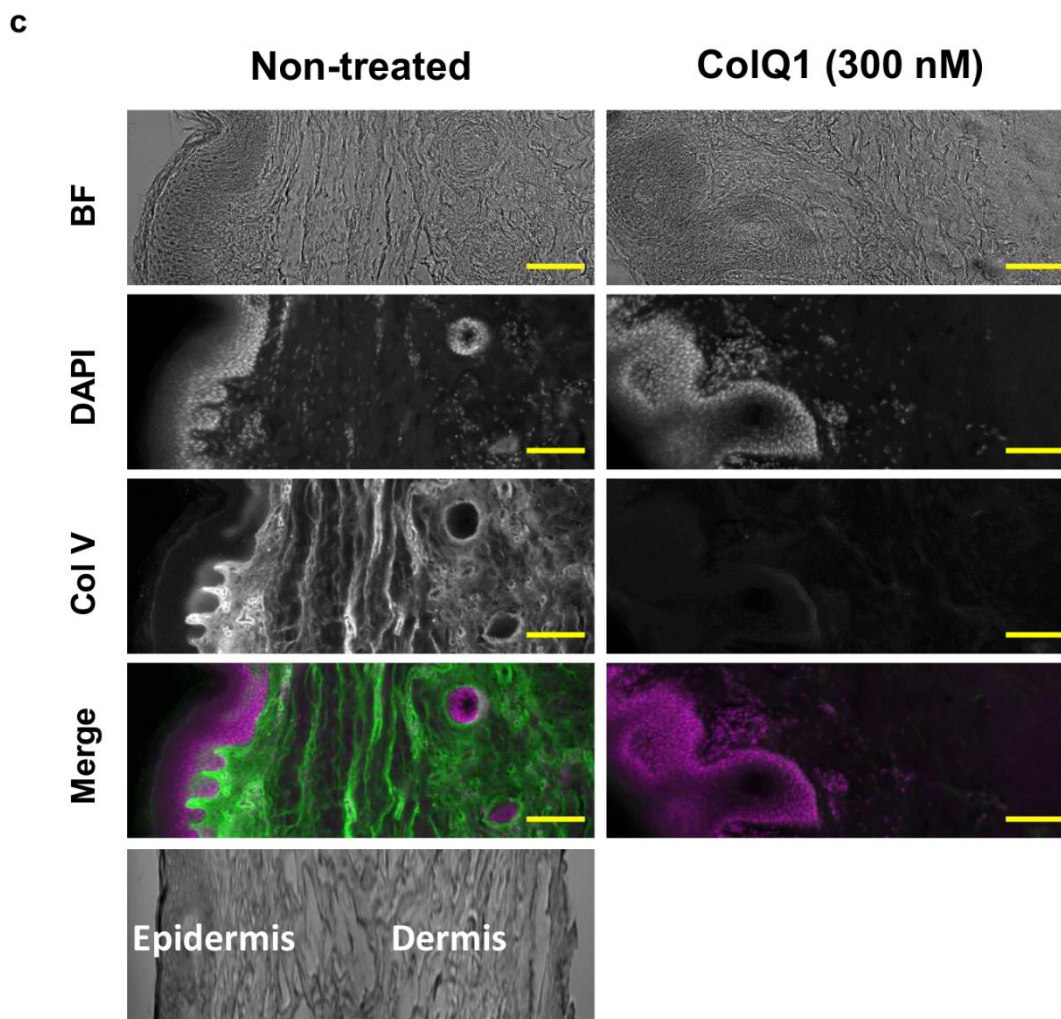


Figure S4. Bright-field and DAPI images of the non-treated tissue and ColQ1-treated tissue (a) COL I (Collagen I), (b) COL III (collagen III), (c) COL V (collagen V). Dermal and epidermal regions are labeled. Scale bar: 100 μ m.

Effect of storage conditions on skin tissue (Figure S5)

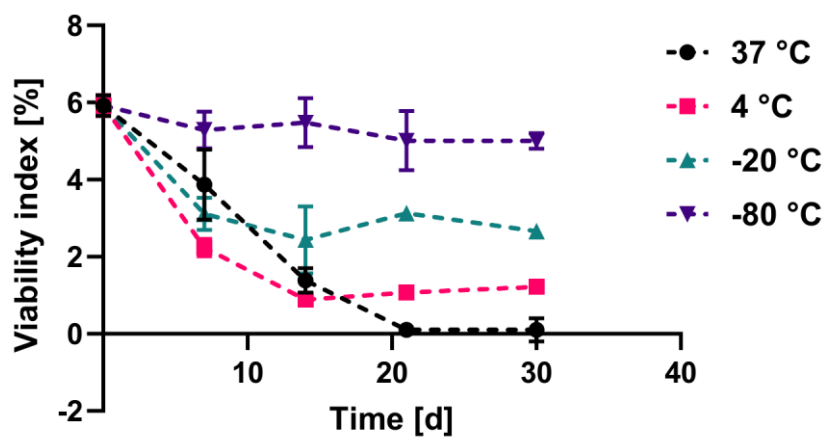


Figure S5. The influence of storage temperature on skin viability.

SHG and fibrillar collagen imaging for the tissue challenged with ColQ1 with or without compound 1 (Figure S6)

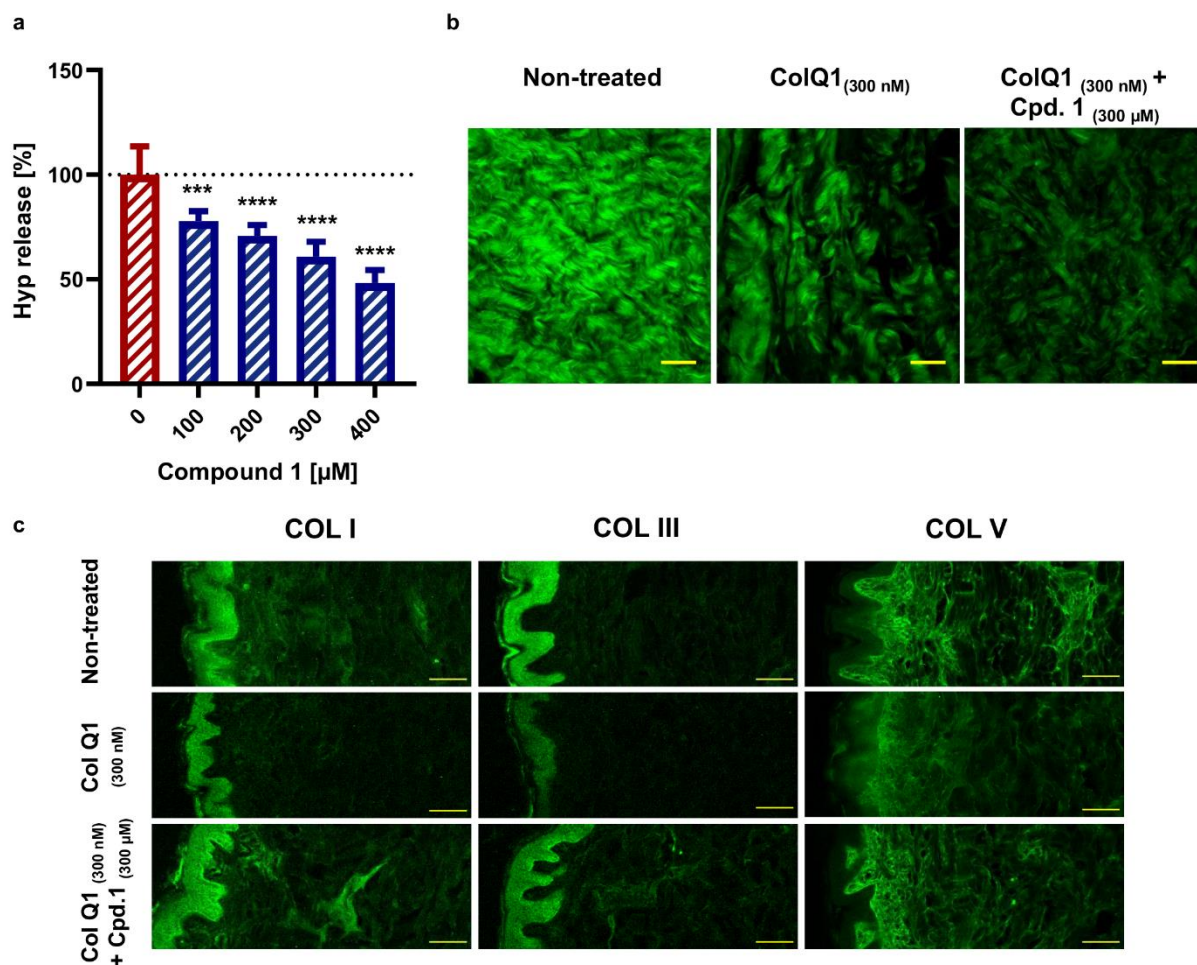


Figure S6. Compound 1 inhibited the collagenolytic effect of ColQ1 *ex vivo* in skin tissue. (a) Dose-dependent effect of compound 1 in Hyp release assay. (b) Confocal SHG images revealed an improved collagen signal with 300 μM of compound 1 (tissue challenged with 300 nM ColQ1) compared with 300 nM ColQ1 without inhibitor. (c) Immunostaining of fibrillar COLs of the non-treated skin and treated with ColQ1 with or without compound 1. Statistical analysis was performed with one-way ANOVA and statistical significance was analyzed by Tukey test. Significance was calculated by comparing non-treated *vs* treated tissue with compound 1 (mean \pm SD, **** $p \leq 0.0001$, *** $p \leq 0.001$). Hyp: hydroxyproline, COLs: collagens, SHG: second-harmonic generation. Scale bar: 100 μm for SHG images and for the immunostained images.

Viability and imaging data of fibroblast and keratinocyte cells challenged with *B. cereus* csn (Figure S7–S9)

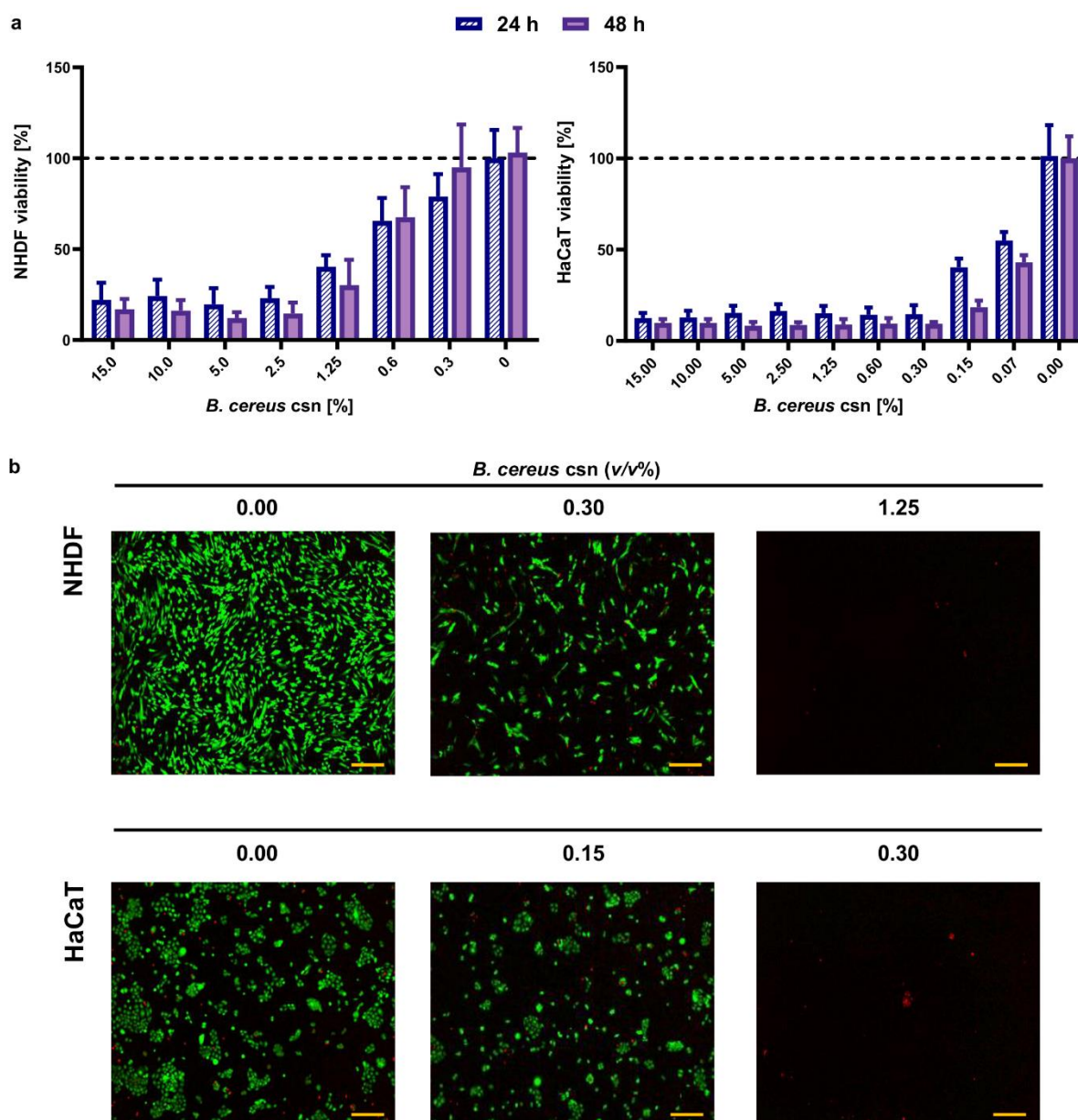


Figure S7. Viability data of fibroblast (NHDF) and keratinocyte (HaCaT) cells upon the treatment with *B. cereus* csn. (a) Representations of MTT data of skin cells after 1 and 2 days of incubation with various concentrations of *B. cereus* csn. (b) Composite signal of live and dead skin cells challenged with various concentrations of *B. cereus*. Green signals: living cells and red signals: dead cells, red signal in some cases was lost because the detached cells were washed away after the rinsing step with PBS. ($n = 3$, results are shown as mean \pm standard deviation), *B. cereus*: *Bacillus cereus*, csn: culture supernatant. Scale bar: 200 μm .

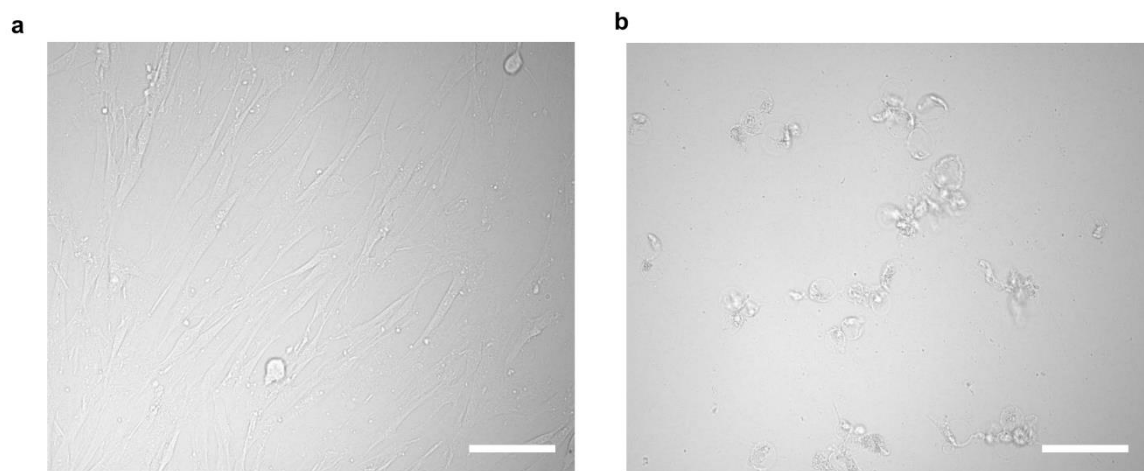


Figure S8. Bright-field signals of skin cells challenged with *B. cereus* csn visualized with 20X objective. (a) Non-treated NHDF cells compared with **(b)** NHDF cells treated with 1.25% (v/v) *B. cereus* csn. *B. cereus*: *Bacillus cereus*, csn: culture supernatant Scale bar: 100 µm

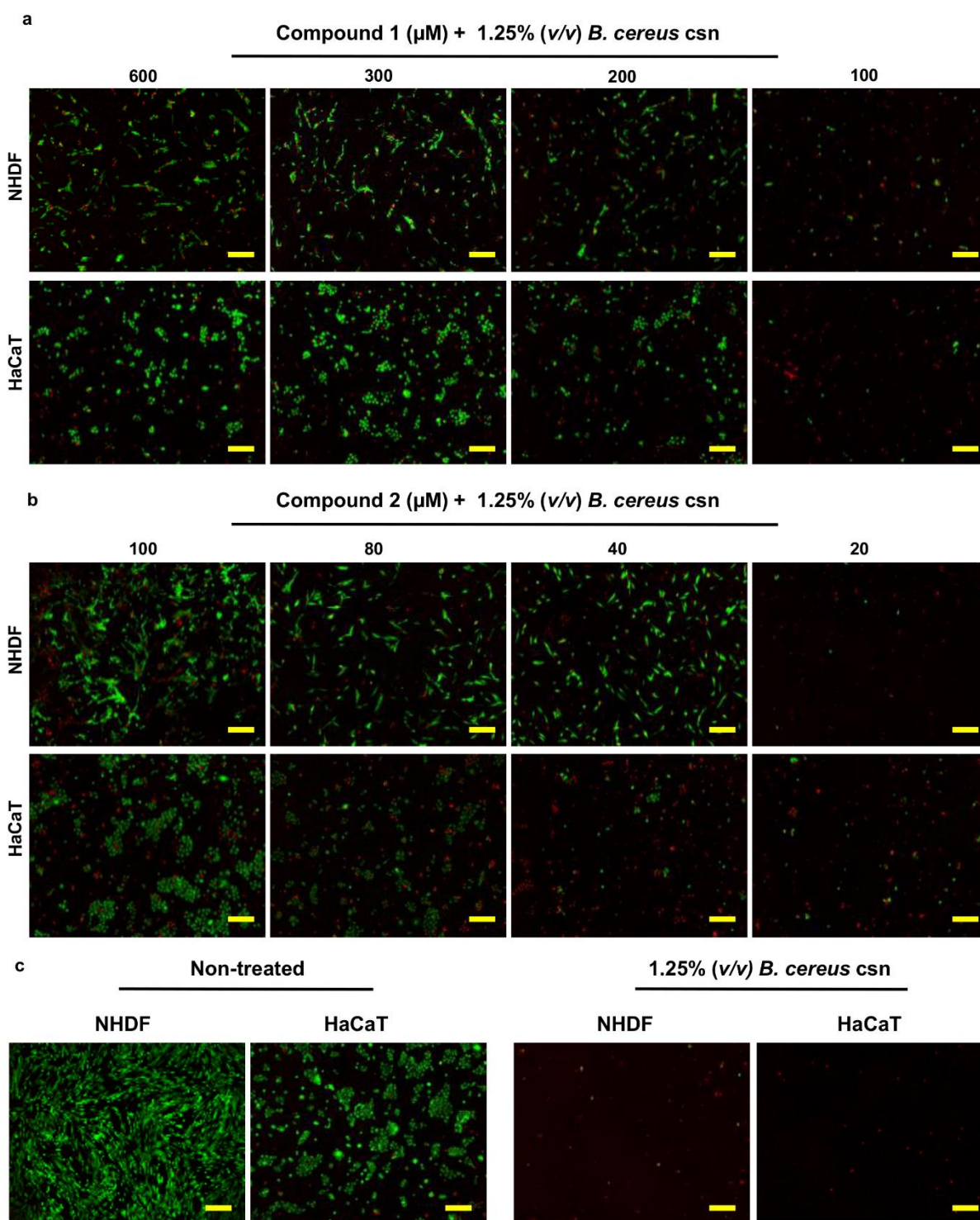
Live/dead imaging of the effect of compounds 1 and 2 on skin cells challenged with *B. cereus* csn (Figure S9)

Figure S9. Compounds 1 and 2 maintained the viability of skin cells upon the treatment with 1.25% (v/v) of *B. cereus* csn. Live/dead imaging with fibroblasts (NHDF) and keratinocytes (HaCaT) challenged with 1.25% (v/v) of *B. cereus* csn with and without compounds (a) 1 and (b) 2 and (c) non-treated cells. Green signals: living cells and red signals: dead cells, red signals in some cases were lost because the detached cells were washed away after the rinsing step with PBS. *B. cereus*: *Bacillus cereus*, csn: culture supernatant. Scale bar: 200 μm for images.

G. mellonella survival analysis of the larvae challenged with *B. cereus* csn or with ColQ1 (with or without compound 1) and its inactive mutant version (Figure S10–S11)

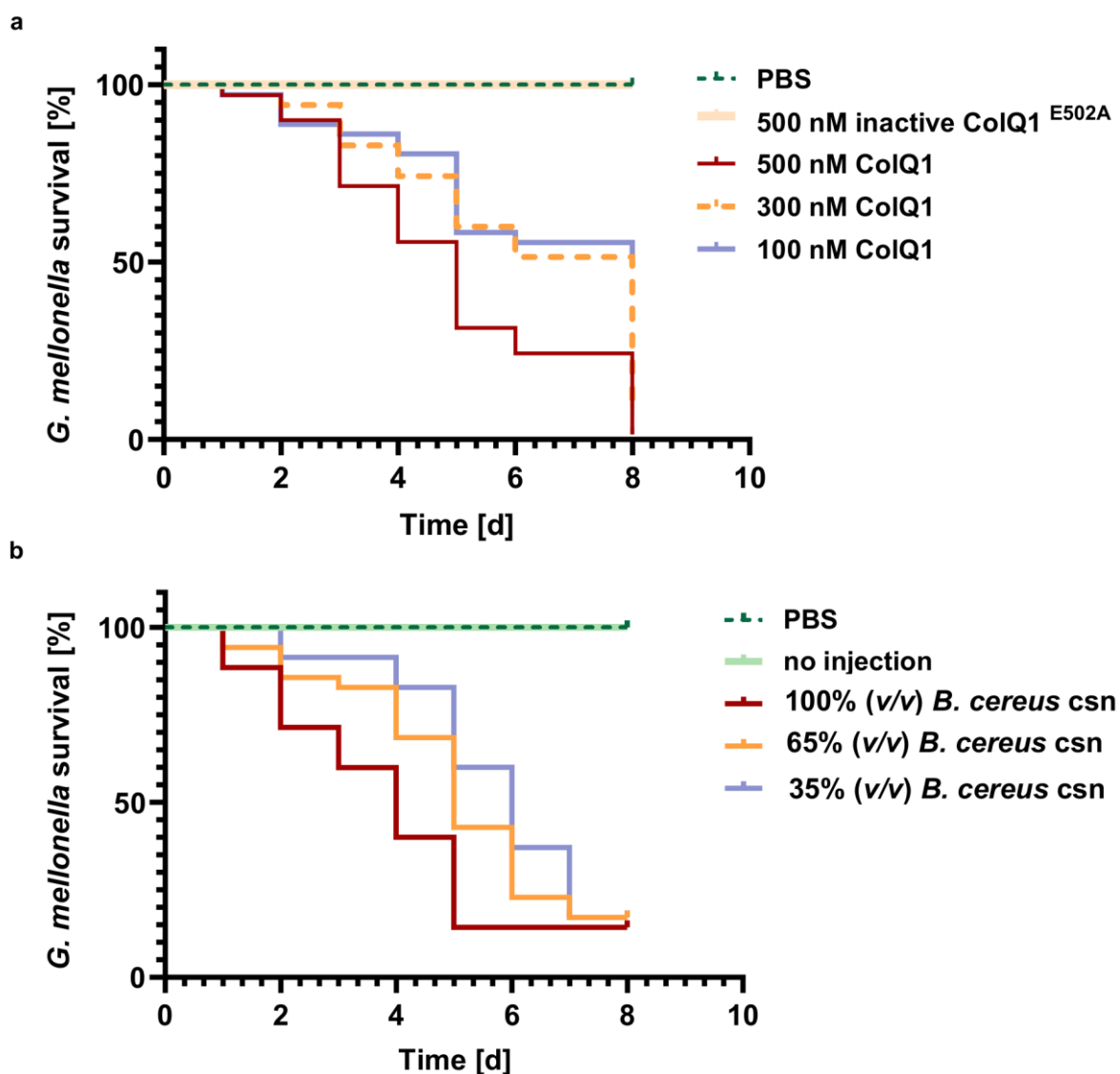


Figure S11. Probability of survival of the *Galleria mellonella* larvae treated *B. cereus* csn or ColQ1. (a) The survival of larvae challenged with different concentrations of ColQ1 (active and inactive mutant), the survival rate of larvae treated with 300 and 100 μ M of the inactive mutant ColQ1 E502A was 100%. (b) The survival of larvae challenged with different concentrations of *B. cereus* csn. *B. cereus*: *Bacillus cereus*, csn: culture supernatant. Each curve represents results of three independent experiments.

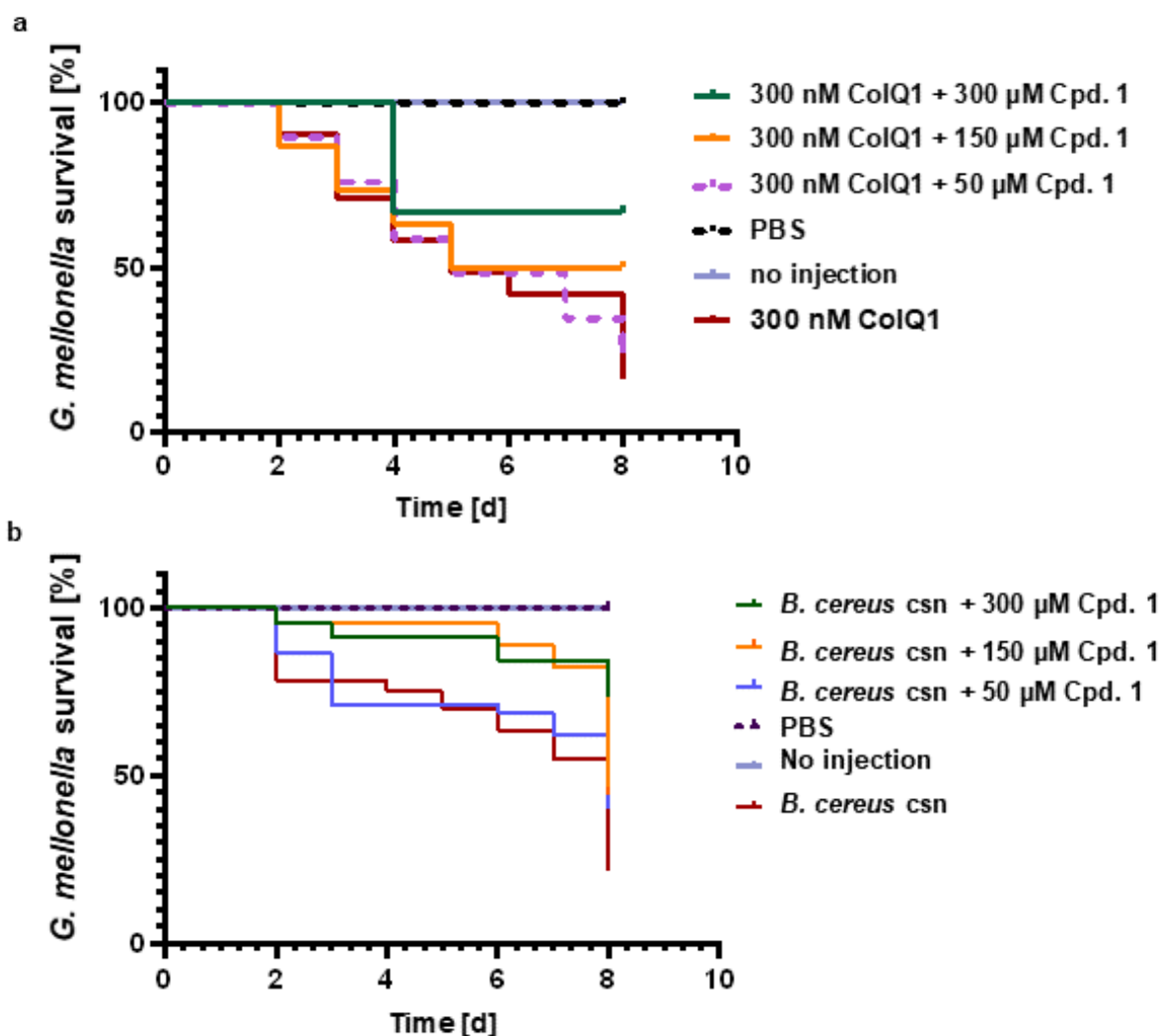


Figure S11. Kaplan–Meier survival analysis of larvae treated with *B. cereus* csn with and without compound 1. (a) Survival analysis of larvae treated with 300 nM ColQ1 and with various concentrations (50–300 μ M) compound 1. (b) The improvement in the survival of larvae challenged with 100% (v/v) *B. cereus* csn and various concentrations of compound 1 (50–300 μ M). The statistical difference between groups treated with 300, 150, and 50 μ M of compound 1 and treated with only 300 nM ColQ1 is $p = 0.0002$, $p = 0.0510$, and $p = 0.7593$, sequentially (log-rank). The statistical difference between groups treated with 300, 150, and 50 μ M of compound 1 and treated with only 100% (v/v) *B. cereus* csn is $p < 0.0001$, $p = 0.0096$, and $p = 0.0107$, respectively. The survival rate for the larvae treated with compound 1 in PBS was 100%. *B. cereus*: *Bacillus cereus*, csn: culture supernatant.

Supplementary Table

Table S1. Summary of epifluorescence imaging conditions

Imaging conditions Collagen	Objective	Exposure time	LUT settings (Min–Max)
Fig 1 – ColQ1 effect			
COL I	Plan Apo λ 10x	700 ms	500–1200
COL III	Plan Apo λ 10x	700 ms	500–1200
COL V	SPlanFluor 20x LWD Dry	200 ms	500–5600
Fig 3 – (compound 2)			
COL I	SPlanFluor 20x LWD Dry	200 ms	500–8000
COL III	SPlanFluor 20x LWD Dry	200 ms	500–1400
COL V	SPlanFluor 20x LWD Dry	1 s	500–1600
S4 Fig – (compound 1)			
COL I	SPlanFluor 20x ELWD DIC N1	200 ms	500–560
COL III	SPlanFluor 20x ELWD DIC N1	200 ms	500–560
COL V	SPlanFluor 20x ELWD DIC N1	1 s	500–800

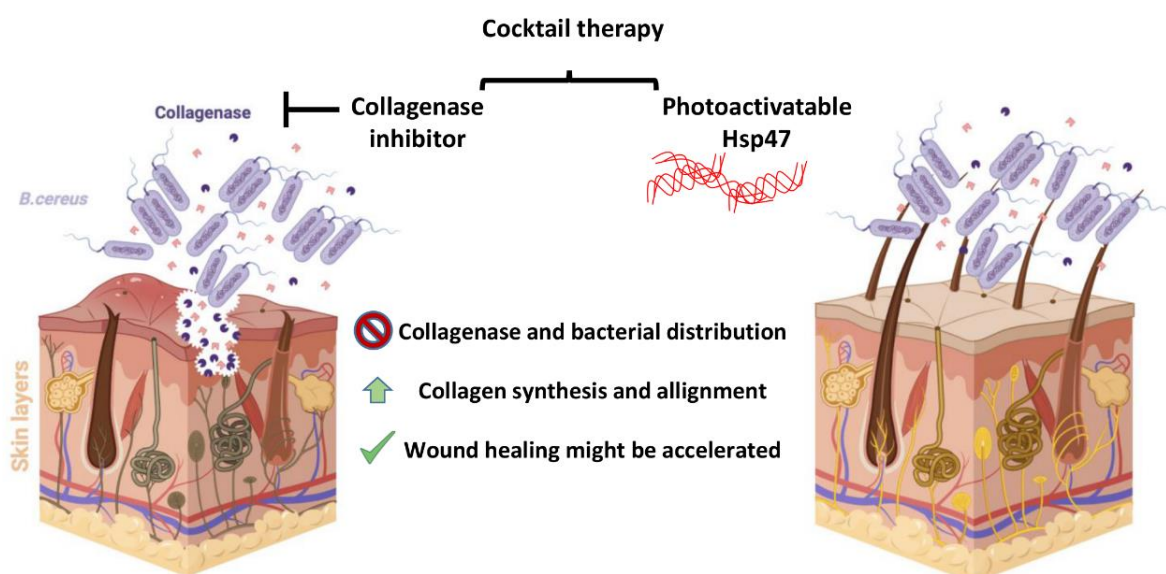
2.3 Chapter C

Cocktail therapy approach to treat wound infections induced by collagenase-producing bacteria

Alaa Alhayek[⊥], *Essak S. Khan*[⊥], *Uwe Hansen*, *Esther Schönauer*, *Tobias Däinghaus*, *Katrin Voos*,
Christian Ducho, *Hans Brandstetter*, *Jörg Hauptenthal*, *Aránzazu del Campo*, and *Anna K. H. Hirsch*

⊥these authors contributed equally

This part of the thesis will be submitted



Abstract

Bacterial wound infections are one of the major causes of mortality and morbidity in humans. This is due to the increase of antibiotic resistance, which has reduced significantly the available options to treat wound infections. The severity of wound infections is associated with the secreted virulence factors, which help to digest the extracellular matrix (ECM) during the invasion phase, facilitating bacterial dissemination. Bacterial collagenases are one of these virulence factors. Such collagen-degrading enzymes are able to digest the collagen of the ECM, enabling the infection to persist and the wound to heal slowly.

Here we describe a cocktail therapy containing collagenase inhibitor and a collagen inducer molecule named heat shock protein 47 (Hsp47). This combination showed improvement in the intensity of collagen, collagen production and alignment as evidenced by several microscopic and bio-analytical techniques.

Introduction

Bacterial wound infection is the colonization of exposed skin by a large number of proliferating bacteria.^[1] The bacteria penetrate the tissue *via* their secreted virulence factors, which assist them in reaching anaerobic areas, resulting in the production of pro-inflammatory mediators, slowing wound healing and provoking a cascade of subsequent responses.^[2-4] Purulent discharge or painful spreading erythema are examples of these local responses.^[5] The wound healing occurs by overlapping four key processes, (i) hemostasis (ii) inflammation (iii) proliferation and (iv) remodeling.^[6] Multiple cell types, ECM, and mediators (*e.g.*, growth factors and cytokines) are all employed to control each phase of wound healing.^[6] To allow a proper wound healing process to occur, all factors that impede healing must be stopped, including the activity of the released virulence factors of pathogenic bacteria secreted during invasion.^[7,8] Bacterial proteases (such as elastase B, collagenase, hyaluronidase, and others) have been demonstrated in several studies to have a negative impact on wound healing.^[8] Acute wound infections are caused by external injuries and anticipated to heal within a short time. Although, in some severe instances, especially when the wound is colonized by multiple-resistant bacteria, the treatment choices might be limited or non-effective.^[1]

Antibiotics are one of the most widely prescribed medicines for the treatment of bacterial wound infections.^[1,9] Due to the abuse of these medicines and the significant selective pressure on the bacteria, many pathogenic bacteria evolved multi-drug resistance.^[10,11] Therefore, new techniques to combat wound infections and to limit the propagation of resistance are required.^[12] The inhibition of virulence factors produced by bacteria is one possible treatment approach for wound infections.^[13,14] This is because several virulence factors target the

structural protein components of the ECM, including collagen, elastin, laminin, and fibrillin.^[3,18] Bacterial collagenases, for instance, have the potential to cause uncontrolled tissue damage during wound invasion, potentiating the bacterial dispersion and amplifying the effect of other released toxins.^[3,23,24] Furthermore, they operate as pathogenic components and keep the wound in the inflammatory phase, delaying healing.^[19,28] Also their effect on numerous immunological components such as immunoglobulins and antimicrobial peptides, might delay wound recovery.^[19,28] These collagen-degrading enzymes target the fibrous protein collagen, which accounts for 90% of the ECM and 30% of the total protein in the body.^[24,29] This protein can be degraded by bacterial collagenases at multiple sites, causing it to disintegrate into small peptides and amino acids, which can be used by the bacteria as a carbon and energy source.^[30] Collagen is an interwoven structural protein that is produced by fibroblasts in a complex of intra- and extracellular events.^[31] The biosynthesis of collagen starts in the endoplasmic reticulum (ER), where alpha-chains of procollagen are assembled with the assistance of heat shock proteins and post translational modifications.^[32] Collagen is composed of the three repeated amino acids Gly-X-Y, with X usually being proline and Y hydroxyproline (Hyp). These amino acids are linked together to create a triple helix of the collagen molecule.^[33] Besides its supportive function, collagen (such as I and III) is important for the wound-healing process. It attracts fibroblasts and stimulates them to generate and deposit more collagen to the wound bed.^[32,33,37] Collagen also triggers the clotting cascade and platelet aggregation, as well as the production of growth factors and cytokines.^[35,40,41] Therefore, if collagen is destroyed by the action of bacterial collagenases, the wound becomes weak and may split, delaying healing.^[35,40,41]

Hsp47 is an ER-resident collagen binding Hsp, that is essential for the formation and stabilization of collagen.^[42-44] It functions by guiding the correct folding of the triple-helix of procollagen before it is secreted outside the cell.^[42-44,49] Hsp47 binds to type I, II, III, IV, and V collagens, specifically to the arginine at the Y position of Gly-X-Y.^[48] The function of Hsp47 in disease promotion has been previously described using *in vitro* and *in vivo* models, which revealed that high Hsp47 levels are associated with the occurrence of fibrosis due to collagen overproduction and accumulation.^[44,50,51] Low Hsp47 levels, on the other hand, cause an incorrect collagen assembly and inappropriate synthesis in the cell.^[45] Since Hsp47 is involved in the regulation of collagen synthesis, secretion, and alignment, it is expected to play a role in wound healing.^[43,52]

Here, we report the characterization of a cocktail therapy involving a photoactivatable variant of Hsp47 (photoactivation of Hsp47 allows light-mediated regulation of collagen biosynthesis

within mammalian cells and ensure the delivery of Hsp47 into the ER) and collagenase inhibitors. The characterization was performed by an *ex vivo* pig-skin model challenged with bacterial collagenase Q1 (ColQ1, secreted by *Bacillus cereus* bacteria).^[53,54] The activity of this combination was studied by bio-analytical methods including enzyme-immunosorbent (EI), and LC-MS/MS-based Hyp assays as well as with microscopic methods including second-harmonic generation (SHG) confocal, polarization (PLM), and transmission electron microscopy (TEM). Our data from these assays revealed that the cocktail therapy inhibited the activity of ColQ1 and improved the deposition of the well-aligned collagen. This suggests that using this therapeutic tool to address wound infections could be promising to speed up wound healing.

Results and discussion

Collagen matrix protection and recovery after cocktail treatment

To study the effect of ColQ1 inhibitors and the photoactivated variant of Hsp47 (H_{47Y<ONBY}h_v) we tested them on an *ex vivo* pig-skin model pre-treated with *B. cereus* ColQ1. H_{47Y<ONBY} has no affinity to collagen due to the presence of a photoactivatable o-nitro benzyl tyrosine (ONBY). At Tyr383, the light cleaves the ONBY group (H_{47Y<ONBY}h_v), which restores the protein's ability to bind to collagen.^[46,55] We hypothesized that a photoactivatable combination treatment would not only protect the skin from progressive degradation by ColQ1, but also assist the skin to regenerate a healthy collagen matrix. Therefore, mixtures of H_{47Y<ONBY}h_v with either compound **1** or compound **2** were added to the *ex vivo* skin tissue after one day of treatment with 300 nM of the *B. cereus* ColQ1. Compounds **1** and **2**, H_{47Y<ONBY}h_v and its other variants (*i.e.*, H₄₇: wild-type Hsp47 and H_{47Y<ONBY}: inactive variant of Hsp47) were included as controls. Next, all samples were fixed and prepared for microscopic and biochemical analysis. The molecular structure of label-free collagen can be visualized *via* SHG imaging.^[56] The SHG imaging of non-treated healthy skin showed straight coiled collagen fibrils with interconnected wave-like structure (**Figure 1**). The ColQ1-treated sample, on the other hand, showed a low SHG signal with large gaps between the collagen fibers, indicating the collagenolytic activity of ColQ1 (**Figure 1**). Concentrations of 200 μM of compound **1** and 5 μM of compound **2** were used in this study due to their previously reported activity on tissue.^[53] Compound **1** at 200 μM and compound **2** at 5 μM increased the SHG signal and reduced the space between collagen fibers (**Figure 1**). While the H₄₇ and H_{47Y<ONBY} at 0.2 μM resulted in no effect on the recovery of collagen due to difficulties in their delivery into the ER, 0.2 μM of H_{47Y<ONBY}h_v led to partial collagen matrix recovery and fewer gaps between the collagen fibers (**Figure 1**). The concentration of H_{47Y<ONBY}h_v (*i.e.*, 0.2 μM) was determined based on the moderate effect on

improving collagen I (COL I) of treated skin with ColQ1 as measured by the EIA (**Figure S1**). When the inhibitors and the H_{47Y<ONBY} were combined (*i.e.*, non-photo-activated cocktails **1** and **2**), the collagen matrix was protected to some extent, similar to the effect with each compound alone. In contrast, the combined compounds with H_{47Y<ONBYhv} (*i.e.*, photo-activated cocktails **1** and **2**) showed dense wavy collagen bundles with a high SHG signal and fewer gaps, similar to the morphology of the non-treated healthy skin (**Figure 1**).

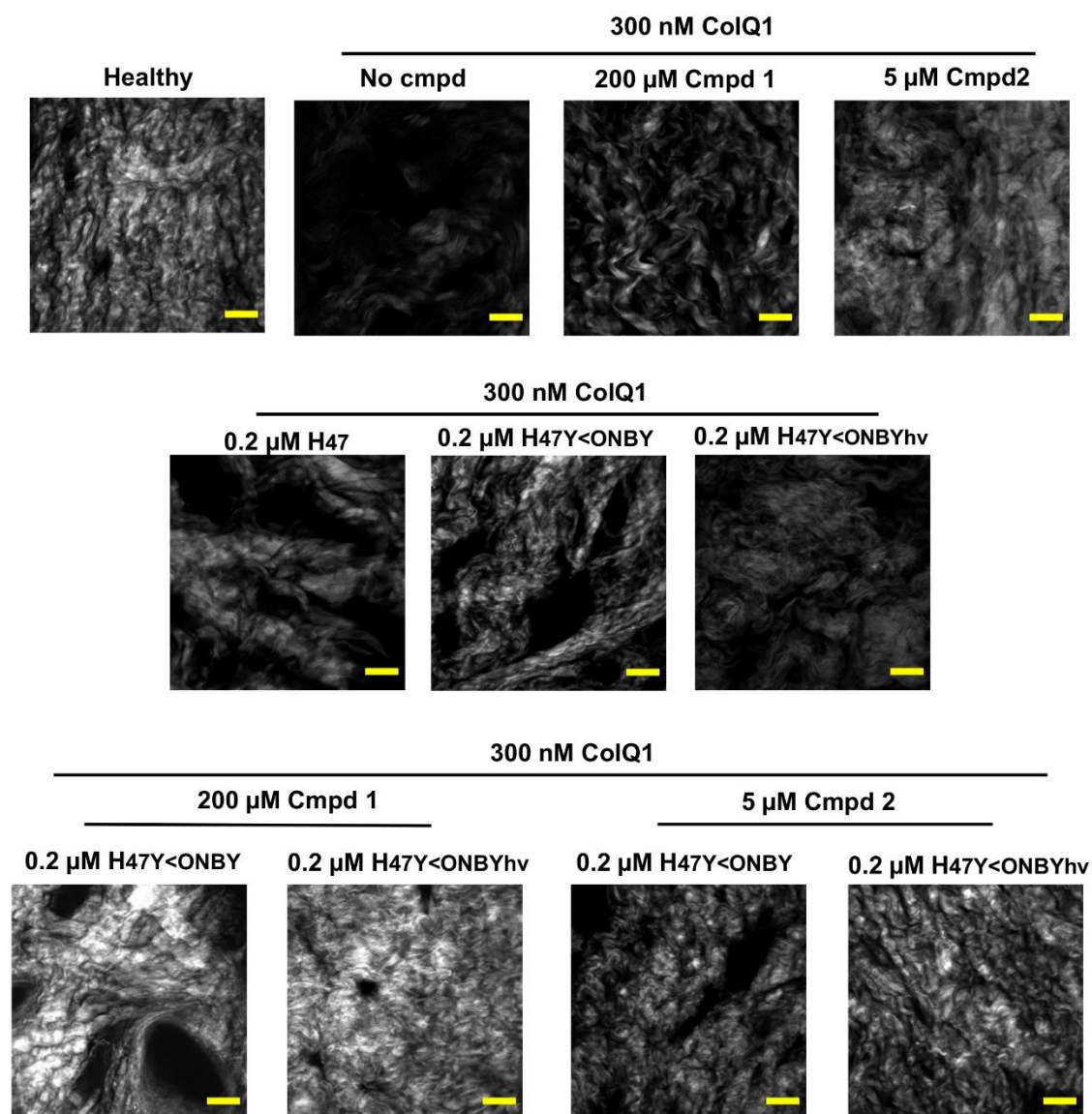


Figure 3. Photoactivated cocktails 1 and 2 suppressed the collagenolytic effect of *Bacillus cereus* collagenase Q1 (ColQ1) and increased the collagen deposition. Confocal SHG images show improvement in collagen signal upon the treatment with 200 μ M compounds **1** and 5 μ M **2** together with H_{47Y<ONBYhv}. H47: wild-type Hsp47, H_{47Y<ONBY}: inactive variant of Hsp47. H_{47Y<ONBYhv}: photo-activatable variant of Hsp47. $n = 3$, Scale bar: 100 μ m.

To quantify the effect of the treatments, the DMEM supernatant of the tissue was collected, followed by quantification of the released Hyp by LC-MS/MS. After 1 day of incubation with

ColQ1, the quantity of released Hyp into the medium was similar (~ 800 nM) for all samples (**Figure S2**). Compounds **1** and **2** reduced the release of Hyp to ~ 300 nM after 1 day of treatment. In contrast, the tissue treated with H47, H_{47Y<ONBY}hv, H_{47Y<ONBY}, and ColQ1 demonstrated an increased Hyp release over the four days of the experiment due to the activity of the non-inhibited ColQ1. The effect of the photo-activated cocktails **1** and **2** were comparable to the treatment with only compounds. This might be due to the fact that Hsp47 activity occurs inside the tissue, therefore the increase in Hyp may not be reliably quantified outside the tissue. These data support the inhibitory effect of the compounds against ColQ1, but they do not support the efficacy of cocktails **1** and **2**. Therefore, the tissue-derived Hyp was evaluated in more detail for cocktail-treated tissue samples. After 4 days of incubation, the ColQ1-treated tissue showed a reduction in Hyp levels (3 ± 1 μ M/mg) (**Figure 2**). The treatment with the non-photo-activated cocktails **1** and **2** enhanced the Hyp in the tissue from 3 ± 1 μ M/mg to 5 ± 2 μ M/mg on day four. The photo-activated cocktails **1** and **2** boosted the amount of Hyp further. Both increased the Hyp levels from 3 ± 1 μ M/mg to 10 ± 4 μ M/mg, which was equivalent to the amount measured in the healthy tissue (**Figure 2**). These findings confirm the SHG imaging data and indicate the activity of the combined treatments in inhibiting ColQ1 and depositing collagen in the tissue.

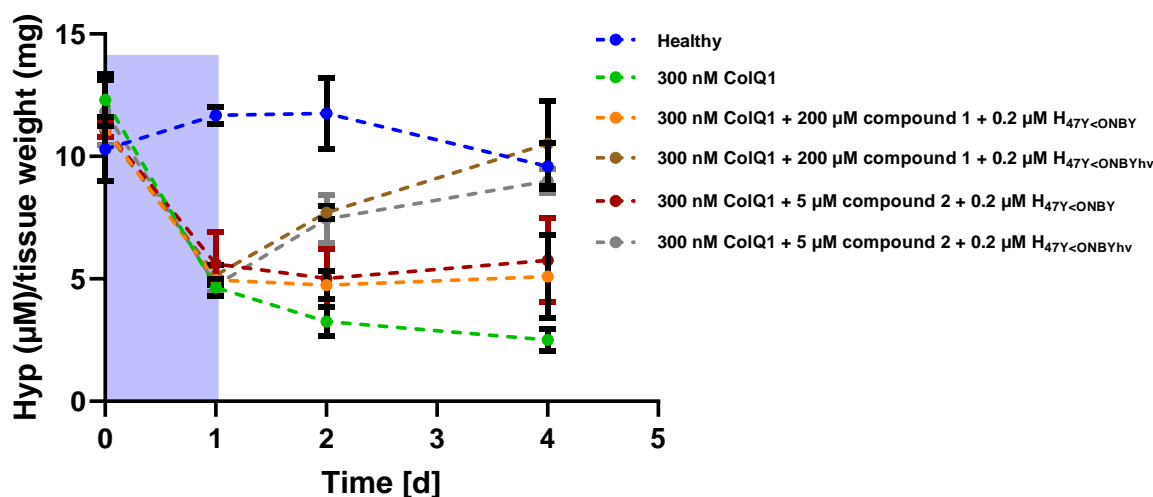


Figure 4. The amount of hydroxyproline (Hyp) in the tissue treated with 300 nM of the *Bacillus cereus* collagenase Q1 (ColQ1) and cocktails **1** and **2**. The skin was treated with 300 nM ColQ1 for one day (background is highlighted in violet). Then, the cocktails of H_{47Y<ONBY} with compound **1** or compound **2** were added on day 2, exposed to light, and kept until day 4. Upon light exposure, H_{47Y<ONBY} was converted to its active version H_{47Y<ONBY}hv. Data point represents mean value of three independent experiments \pm SD

Cocktail therapies improve alignment and intensity of collagen fibers

The mechanical behavior of skin is influenced by the orientation of collagen fibers. To investigate the degree of alignment and molecular order of dermal collagen fibers of skin we used polarization light microscopy (PLM).^[57,58] We also evaluated the optical retardance of the

skin collagen, which is an indicator of the molecular order of the birefringent polymer, collagen.^[57,58] Mean values of optical retardation were normalized to the highest measurement of all healthy samples as 100%.

The PLM imaging of the non-treated healthy skin showed a good signal intensity in the heat map (yellow to red color) (**Figure 3a**), ordered vector directionality (**Figure S3**), and high optical retardation values (*i.e.*, 100%) (**Figure 3b**), reflecting a high degree of alignment. A substantial decrease in the intensity of collagen signals confirmed by heat map (cyan to blue color) (**Figure 3a**), random directionality of the vectors (**Figure S3**), and 50% drop in the optical retardance (**Figure 3b**) was observed in the ColQ1-treated sample, suggesting that collagen fibers were interrupted and disordered (**Figure 3**). In contrast, treatment with each individual compound, as well as photo-activated or non-photo-activated cocktails **1** and **2** showed moderate to high collagen in the heat maps, fewer random vector directions, and improvement in the optical retardance in a range of 70–100%. Interestingly, the photo-activated samples exhibited a similar appearance as the healthy sample (**Figures 3 and S3**). The unusual gaps were filled and the collagen fibers were arranged in a dense web (**Figure 3**). This indicates the potency of the photo-activated cocktails **1** and **2** in inhibiting ColQ1 and generating new well-aligned collagen.

To further assess the morphology of the matrix collagen fibrils, and the three-dimensional appearance of the skin, we used transmission electron microscopy (TEM).^[59] The collagen fibrils in the non-treated healthy samples were highly aligned with consistent interfibrillar spacing and grouped in basket-weaves shape, as described before for skin (**Figure 4**). Collagen fibrils were poorly aligned and the interfibrillar gaps were large when treated with ColQ1. Upon treatment with only compound **1**, compound **2**, or the photo-activated H_{47Y<ONBY}h_v in presence of ColQ1, the amount of collagen fibrils increased, resulting in fewer gaps. This effect increased further when both (*i.e.*, ColQ1 inhibitor and photo-activatable H_{47Y<ONBY}h_v) were combined, as this led to a remarkable increase in the collagen fibril density and organization. In addition, interfibrillar gaps were reduced to the level of non-treated healthy samples (**Figure 4**). The controls, non-photo-activated cocktails **1** and **2**, showed similar effects to the samples with only compounds. H47 and H_{47Y<ONBY}, on the other hand, showed more spacing and fewer collagen fibrils (**Figure 4**). These data indicate that upon treatment with cocktails, the effect of ColQ1 is inhibited and new deposited collagen is formed with a structure similar to that of an untreated healthy sample.

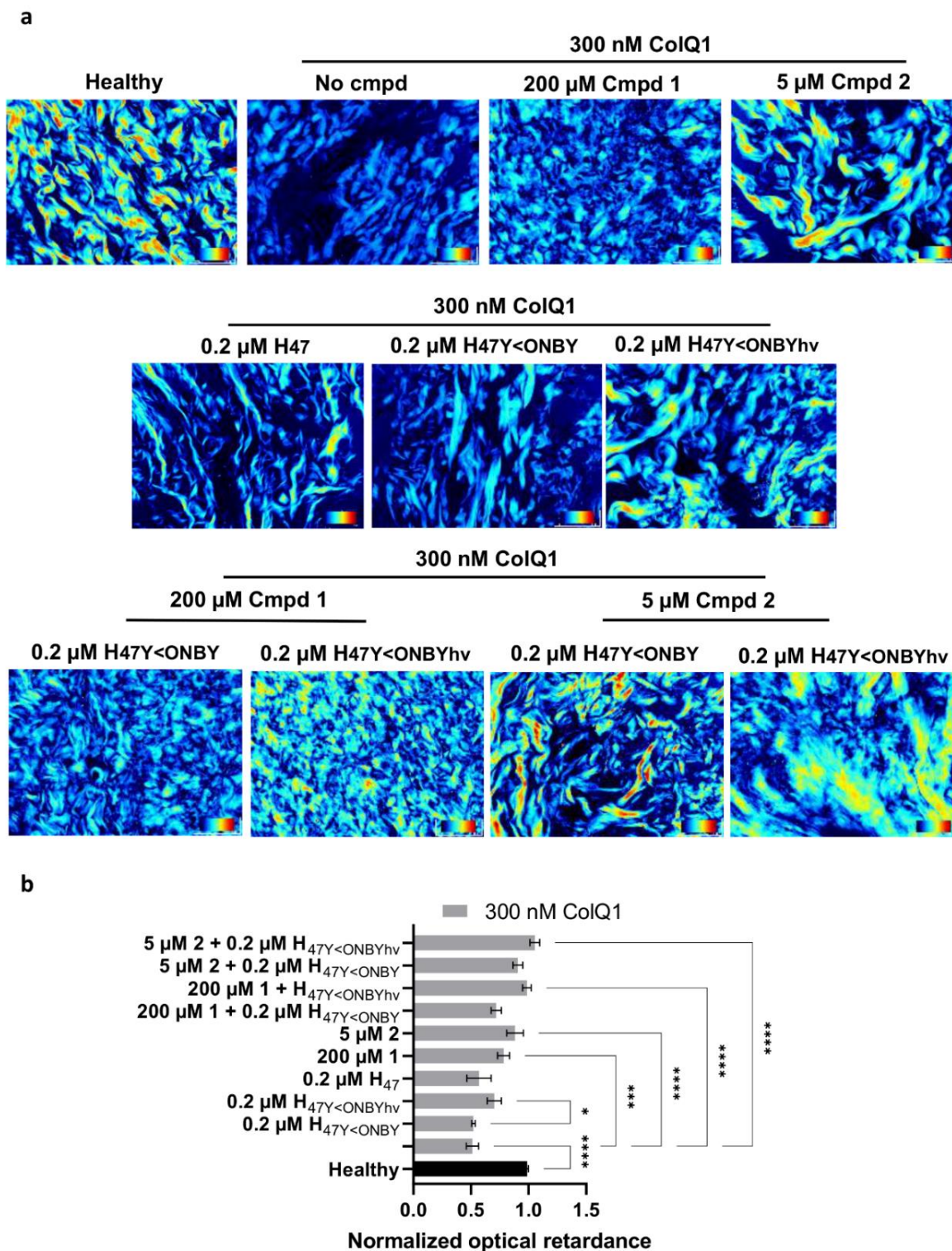


Figure 5. Intensity of dermal collagen fibers in ColQ1-treated skin tissue, and with and without cocktails 1 and 2, visualized with a polarization light microscope. a) Heat map images indicate the high (red to yellow) and the low (cyan to blue) intensity of collagen of the skin. **b)** Relative values of the optical retardance calculated for healthy and ColQ1-treated skin tissues ($n = 3$). The data represent the mean values of each experiment \pm SD, ANOVA; statistical significance was analyzed by Tukey test, *** $p < 0.001$).

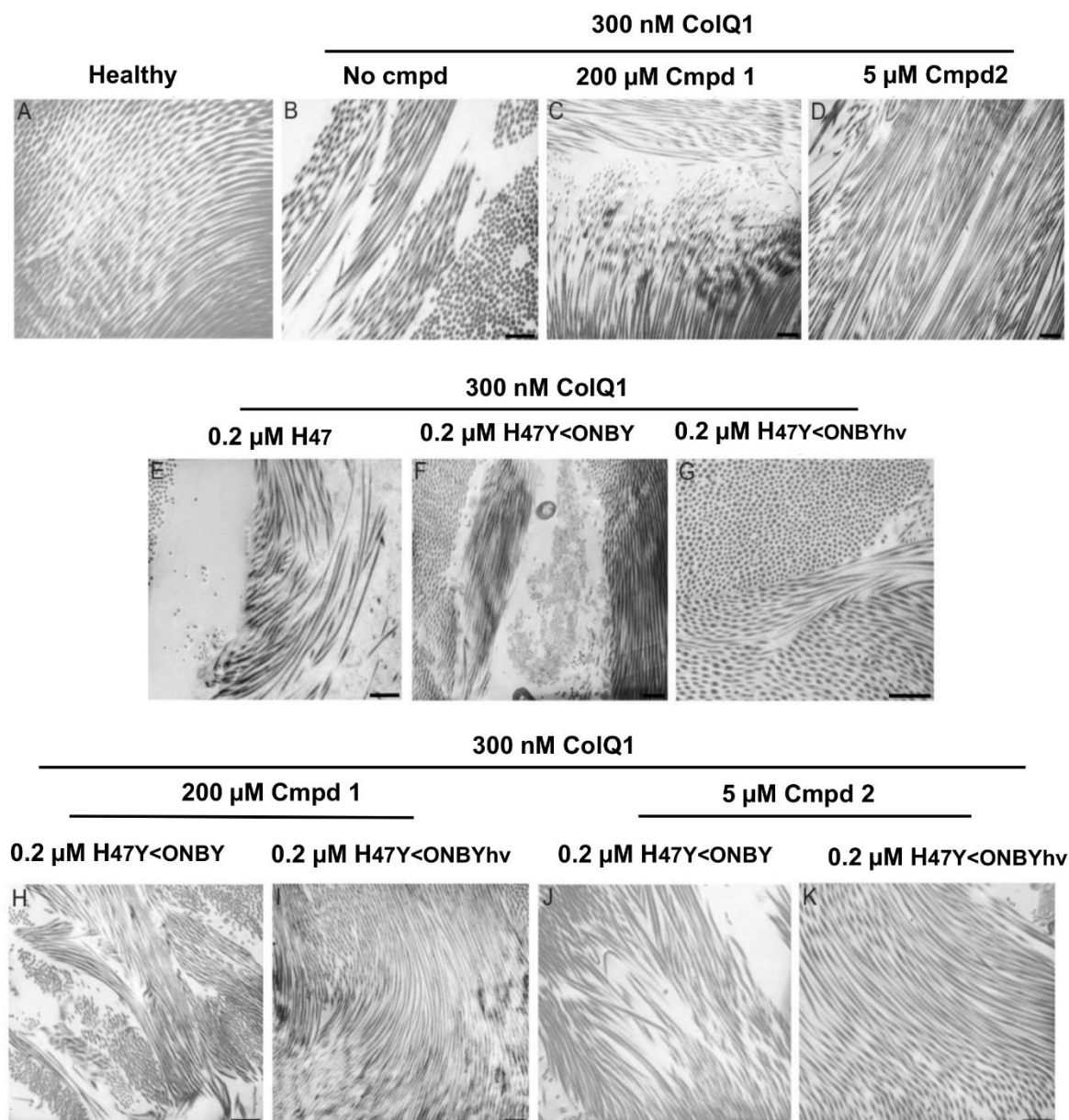


Figure 6. Representative electron micrographs of the morphology of dermal collagen networks in human skin. Normal human skin sample with densely packed collagen fibrils (A). The number of collagen fibrils is decreased and their suprastructural organization disrupted in the presence of 300 nM of ColQ1 (B). In contrast, the dermal collagenous network is more like in normal skin in the presence of compound 1 (C) and even better in the presence of compound 2 (D). In the presence of the photo-activated collagen inducer H47Y<ONBYhv, the dermal matrix was improved although the skin was treated with ColQ1 (compare E-G). This effect is even more pronounced in a combination of the photo-activated collagen inducer and compounds 1 or 2 (compare H-K). $n = 5$, all scale bars: 1 μm .

Cocktail treatments inhibit ColQ1 and enhance the amount of fibrillar collagen I of the tissue

COL I is the most common collagen found in skin, representing 80–90% of skin collagen.^[47] To quantify the effects of the cocktail therapies on COL I, an enzyme immunoassay (EIA) was performed. As plotted in **Figure 5**, the non-treated healthy sample showed no

significant changes in the relative COL I amount per tissue weight. ColQ1-treated samples lost 70% and 100% of their relative COL I amount within 24 h and 48 h, respectively. Each individual compound was able to inhibit the collagenolytic effect of ColQ1; the COL I level increased to about 50% after 48 h of incubation. The photo-activated H_{47Y<ONBY}h_v slowed the degradation, indicating its activity in synthesizing COL I after 48 h of incubation. The non-photo-activated cocktail-treated samples showed similar COL I recovery as the compounds. Encouragingly, incubation with photoactivated cocktails **1** and **2** led to significantly increased COL I levels back to 100%, indicating enhanced collagen deposition. These results corroborate our microscopic observations, and allowed to examine the effects of all treatments over time.

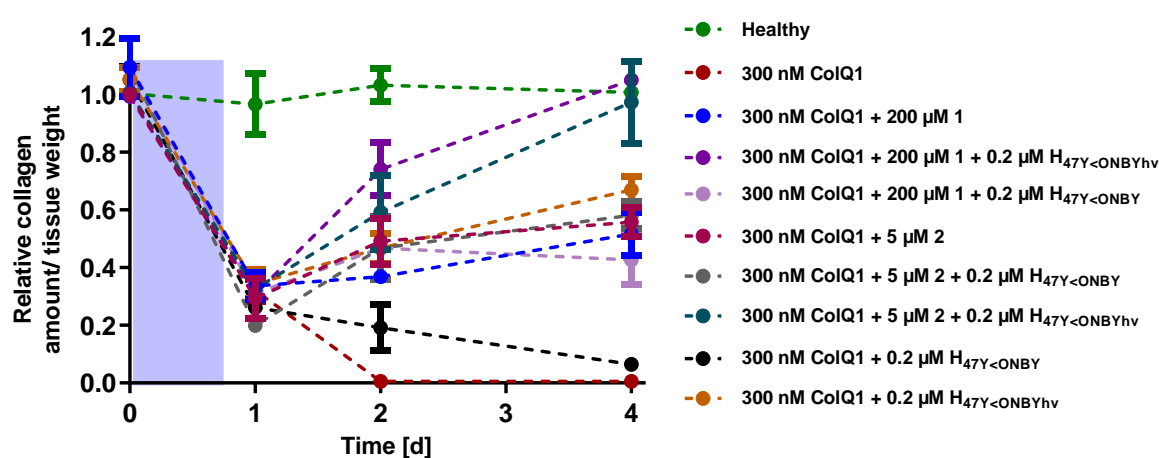


Figure 7. The relative amount of collagen I per mg tissue measured over time using enzyme immunosorbent assay. The skin was treated with 300 nM for one day (background is highlighted in violet), then the cocktails of H_{47Y<ONBY} with compound **1** or compound **2** were added on day 2, exposed to light, and kept until day 4. Upon light exposure, H_{47Y<ONBY} was converted to its active version H_{47Y<ONBY}h_v. Data points represent mean values of three independent experiments \pm SD.

Conclusions

Since collagen is involved in wound healing, it is important to protect it from the collagenolytic activity of bacterial collagenases.^[26,60] One strategy to prevent collagen breakdown is the use of small-molecule collagenase inhibitors.^[61] Hsp47 is a heat shock protein involved in collagen synthesis and assembly.^[42,52] Here, we investigated the biological activities of a combined treatment of wound infections by collagenase inhibitors and Hsp47. This combination therapy led to high SHG signals and less spacing between collagen fibers in an *ex vivo* pig-skin model, pre-treated with the *B. cereus* ColQ1. Additionally, we revealed that the tissue treated with the cocktails **1** and **2** showed a significant increase in Hyp levels inside the tissue. Furthermore, PLM and TEM imaging revealed that well-aligned deposited collagen and less interfibril spacing after treatment with photo-activated cocktails **1** and **2**. Finally, our data were further verified on the level of the fibrillar COL I deposited in the tissue using EIA. The data of this assay underlined that cocktail treatment enhanced COL I in the tissue pre-challenged with

ColQ1 comparable to what is seen in non-treated healthy tissue. The effects of this combination require further research to study the effect of the cocktails in other models and biochemical assays. Other collagen-enhancing molecules such as ascorbic acid^[62] or retinol^[63] in conjugation with collagenase inhibitors could also be investigated.

Materials and Methods

Production of photo-activatable H47 and H47Y<ONBY. Expression and purification of H47 and H47Y<ONBY were carried out as previously described.^[46]

Expression and purification of *B. cereus* ColQ1. The collagenase unit of ColQ1 from *B. cereus* strain Q1 (Uniprot: B9J3S4; Tyr94-Gly765) was produced as reported before.^[64]

Synthesis of compounds 1 and 2. The synthesis was performed according to the previously reported synthetic route.^[53]

***Ex vivo* pig-skin model.** The *ex vivo* pig-skin model was carried out as described before with some modifications.^[53,54] The 15 mm sterile skin punches were acclimatized for 24 h in the DMEM medium and stored at 37 °C, 5% CO₂ with shaking at 300 rpm. The next day, the skin was rinsed 3x with PBS and used for subsequent experiments.

For cocktail therapy application, the skin was treated with 300 nM ColQ1 in 300 μl DMEM supplemented with 4 mM Ca²⁺ and 10 μM Zn²⁺ for 24 h at 37 °C, 5% CO₂ with shaking at 300 rpm. The next day, the tissues were treated with the following treatments for 5 h in the dark: **1)** DMSO **2)** 200 μM compound **1** and 5 μM compound **2** **3)** 0.2 μM H47Y<ONBY **4)** 200 μM compound **1** or 5 μM compound **2** with 0.2 μM H47Y<ONBY, two controls were included one non-treated with ColQ1 and the other treated with 300 nM ColQ1. Skin tissue treated with cocktail **1** (200 M compound **1** + 0.2 μM H47Y<ONBY) and **2** (5 M compound + 0.2 μM H47Y<ONBY) were illuminated with 0.48 J/cm² UV of a custom-made apparatus (6 cm distance to the sample) for 60 seconds within a separate 24-well plate to activate H47Y<ONBY. Following the activation step, all samples were incubated for 72 h at 37 °C, 5% CO₂, with 300 rpm shaking without any medium changes. Next, the biopsy punches were washed 1x PBS and incubated for 3 days in 300 μL DMEM supplemented with 4 mM Ca²⁺ and 10 μM Zn²⁺ and 1% pen/strep. Afterwards, the tissue samples were fixed using 4% PFA and stored at 4 °C for microscopic analysis and the DMEM medium was collected for the Hyp assay or kept at -20 °C.

Sample preparation for SHG microscopy. The sample preparation and imaging was carried out as described before.^[53]

Sample preparation for polarization microscopy. The samples were prepared following the published method for SHG and with 20 μm thickness.^[53] A Zeiss inverse Observer microscope (Zeiss Observer Z1, Göttingen, Germany) with a LC-PolScope image processing system (CRI,

LOT-Oriel, Darmstadt, Germany) equipped with an A-Plan 10x/0.25Phl objective was used together with CRI's Abrio imaging software was used to study alignment of collagen fibers in skin cryosections. A standard 546 nm band filter was used for all images. Prior to the analysis of each sample, even for different samples on the same slide, the background images were acquired. The background serves as a system calibration and subtraction of the actual signal which therefore facilitates comparison of all images taken. To acquire these background images, a spot without any signal and no traces of hydrophobic PAP-pen circuit must be selected. Simultaneously to the image recording, the pictures optical retardance intensity is recorded by the software which is further used to statistically analyze the difference between each condition. Each image was captured to derive grayscale, heat map, and pseudo-orientation with 10 nm vector grid. Grayscale indicates the intensity of optical retardance from black to white (weak to strong). Heat map shows the collagen content from blue to red (low to high). Pseudo-orientation illustrates the direction of the imaged collagen fibers, which is shown by the color code of a pie diagram. Vectors illustrate continuous or interrupted fibers of a decent length (here 10 μm). For calculation of the relative retardance in the polarization measurement, the mean optical retardance values of all images from three independent experiments were normalized to the highest optical retardance mean value from healthy pig skin, which was considered as 100%. The statistical significance was analyzed by the Tukey test, which illustrates the significant differences between conditions. Significance was calculated by comparing non-treated *vs* treated samples (mean \pm SD, ANOVA, *** $p < 0.001$).

Sample preparation for electron microscopy. Small skin samples were fixed in 2% (v/v) formaldehyde and 2.5% (v/v) glutaraldehyde in 100 mM cacodylate buffer, pH 7.4, at 4 °C overnight. After washing in PBS, samples were postfixated in 0.5% (v/v) osmiumtetroxide and 1% (w/v) potassium hex-acyanoferrate (III) in 0.1 M cacodylate buffer for 2 h at 4 °C followed by washing with H₂O. After dehydration in an ascending ethanol gradient ranging from 30 to 100%, specimens were incubated 2x in propyleneoxide for 15 min each time and embedded in Epon using flat embedding molds. Ultrathin sections were cut with an ultramicrotome, collected on copper grids, and stained with 2% uranyl acetate for 10 min. Electron micrographs were taken at 60 kV with a Phillips EM-410 electron microscope using imaging plates (Ditabis, Pforzheim, Germany).

LC-MS/MS-based hydroxyproline assay. The collected DMEM medium of the *ex vivo* experiments after 0, 1, 2, 4 days were tested to quantify the released Hyp of each condition. A 500 μL master mix solution of 20% H₂O, 80% acetonitrile, and 500 nM epinephrine (Sigma) was used to dilute 5 μL of each sample. The epinephrine served as internal standard. All samples

were centrifuged two times for 10 min at 14,000 rcf and 4 °C to remove the ColQ1 protein. A volume of 120 µL supernatant was filled into inserts in the MS vials then submitted to the LC-MS/MS. To generate a calibration curve, a hydroxyproline standard (Sigma) of 10 mM in DMEM medium was stepwise diluted 1:1 until a concentration of 0.078 nM was achieved, and 5 µL of each diluted standard were added to 500 µL master mix (**Figure S4**). The measurement was carried out using a TF UltiMate 3000 binary RSLC UHPLC (Thermo Fisher, Dreieich, Germany) connected to a TF TSQ Quantum Access Max mass spectrometer with heated electro-spray ionization source (HESI-II). For gradient elution, a Ymc-Triart Diol HILIC column (5 µm, 150 X 4.6 mmI.D., Ymc Europe GMPH) was used at flow rate of 200 µL/min with a mobile phase composed of acetonitrile containing 1‰ formic acid (FA) (v/v; eluent A) and H₂O containing 1‰ FA (v/v; eluent B) under the following conditions: 0–1.3 min 10% B, 1.3–5.5 min 60–90% B, 5.5–6 min 90–10% B, 5.5–6 min hold, and 7–12 min 10% B with 400 µL/min flow rate and a total run time of 12 min. The injection volume was 2 µL. The divert valve was set to 1.6 min. The temperature of the autosampler was set to 20 °C. The following MS settings were used: electrospray ionization (ESI); positive mode; sheath gas nitrogen at a flow rate of 60 arbitrary units; auxiliary gas nitrogen at flow rate of 30 arbitrary units; vaporizer temperature 300 °C; ion transfer capillary temperature 250 C, spray voltage: 3500 V.

The mass spectrometer was operated in the SRM mode with the following masses: 68.170 m/z Hyp product (tube lens offset 66 V and collision energy 17 eV); epinephrine, 77.089 m/z (product a) and 166.043 m/z (product b) (tube lens offset 66 V for both and collision energy 36 and 9 eV, respectively) with a scan width of 0.010 m/z and a scan time of 0.1 s, respectively. Observed retention times were as follows: hydroxyproline 5.07 min; epinephrine 5.07 min for products a and b (**Figure S4**). MS-peak areas were determined using TF Xcalibur Software then Hp peak areas were normalized by the internal standard (*i.e.*, epinephrine) peak area and the concentration of Hp was calculated using the calibration curve. Measurements were performed in duplicates, repeated at least two times from three independent experiments.

To quantify the hydroxyproline in tissue, the procedure above was used with minor modifications. The flash-frozen tissue was homogenized by sonicating (20% power for 5 min, 60 sec on and 15 sec off) following with acid hydrolysis with 37% (v/v) HCl for 3 h at 120 °C, the homogenized tissue was then centrifuged 14,000, 10 min, 20 °C. The supernatant was collected and diluted 1:10 in H₂O followed with 1:100 dilution in the master mix mentioned before. The instrument set up was the same as above. The Hyp amount was divided by the weight of the subsequent sample.

Enzyme-immunosorbent assay. The tissue samples were transferred into 2 mL Eppendorf tubes, and they were weighed to correct weight differences of samples used for further measurements. The biopsy punch quarters were labeled with 200 μ L of an 1:500 diluted rabbit anti human COL I antibody (Collagen Type I Antibody 600-401-103-0.5, Rockland INC.) in PBS per tube and incubated for 1 h at room temperature. Then the antibody solution was removed, and the samples were washed with 3x 200 μ L PBS with 5 min incubation time in between each step. After washing, the samples were incubated with 200 μ L horseradish-peroxidase (HRP) conjugated secondary antibody (anti-rabbit IgG HRP-conjugated Antibody) (1:500 diluted in PBS) for 1 h. The samples were then washed with 1x 200 μ L PBS to remove unbound antibody. Next, the samples were incubated with 300 μ L of a pre-warmed 1:1 mixture of substrate A (stabilized hydrogen peroxide) and substrate B (stabilized 3, 3', 5, 5'-tetramethylbenzidine) for 20 min in the dark, at 200 rpm and at room temperature. Then, a volume of 150 μ L stop solution (2 N H₂SO₄) was added into each Eppendorf tube. The tissue-free Eppendorf tube containing substrate mix and stop solution was used to blank the absorbance measurement at 450 nm using a SpectraMax spectrophotometer. Each biopsy punch quarter series absorbance per weight value was normalized to its healthy sample.

Statistical analysis

The datasets of all conditions were plotted and their statistical significance was analyzed using GraphPad Prism v9. All graphical data in this work is reported as the mean(s) \pm SD(s). The comparisons of multiple conditions are performed by Tukey one-way ANOVA test to show significant differences between conditions. Thereby, the values of untreated vs treated samples were compared. A $p < 0.001$ was considered as statistically significant. The highest value of all non-treated healthy samples was assumed as 1 (*i.e.*, 100%), and all other conditions were normalized to that value.

References

1. Lack, M. & Sant, G. Wound Microbiology and Associated Approaches to Wound Management. *TRAFFIC Int.* **14**, 35 (2006).
2. Bessa, L. J., Fazii, P., Di Giulio, M. & Cellini, L. Bacterial isolates from infected wounds and their antibiotic susceptibility pattern: Some remarks about wound infection. *Int. Wound J.* **12**, 47–52 (2015).
3. Singh, B., Fleury, C., Jalalvand, F. & Riesbeck, K. Human pathogens utilize host extracellular matrix proteins laminin and collagen for adhesion and invasion of the host. *FEMS Microbiol. Rev.* **36**, 1122–1180 (2012).
4. Tom, I. M. *et al.* Infection of Wounds by Potential Bacterial Pathogens and Their Resistogram. *OALib* **06**, 1–13 (2019).
5. Aftab, S., Tarik, M. M., Siddique, M. A. & Yusuf, M. A. Clinical and Microbiological Aspect of Wound Infection: A Review Update. *Bangladesh J. Infect. Dis.* **1**, 32–37 (2015).
6. Velnar, T., Bailey, T. & Smrkolj, V. The wound healing process: An overview of the cellular and molecular mechanisms. *J. Int. Med. Res.* **37**, 1528–1542 (2009).
7. Maheswary, T., Nurul, A. A. & Fauzi, M. B. The insights of microbes' roles in wound healing: A comprehensive review. *Pharmaceutics* **13**, (2021).
8. Lindsay, S., Oates, A. & Bourdillon, K. The detrimental impact of extracellular bacterial proteases on wound healing. *Int. Wound J.* **14**, 1237–1247 (2017).
9. NHS. *Wound Management Guidelines*. (2016).
10. Cansizoglu, M. F. & Toprak, E. Fighting against evolution of antibiotic resistance by utilizing evolvable antimicrobial drugs. *Curr. Genet.* **63**, 973–976 (2017).
11. Centers for Disease control and prevention. Antibiotic/ Antimicrobial resistance (AR/ AMR) Biggest Threats and Data. (2019). Available at: <https://www.cdc.gov/drugresistance/biggest-threats.html>.
12. Kumar, M. *et al.* Futuristic Non-antibiotic Therapies to Combat Antibiotic Resistance: A Review. *Front. Microbiol.* **12**, 1–15 (2021).
13. Dickey, S. W., Cheung, G. Y. C. & Otto, M. Different drugs for bad bugs: Antivirulence strategies in the age of antibiotic resistance. *Nat. Rev. Drug Discov.* **16**, 457–471 (2017).
14. Calvert, M. B., Jumde, V. R. & Titz, A. Pathoblockers or antivirulence drugs as a new option for the treatment of bacterial infections. 2607–2617 (2018). doi:10.3762/bjoc.14.239
15. Avishai, E., Yeghiazaryan, K. & Golubnitschaja, O. Impaired wound healing: Facts and hypotheses for multi-professional considerations in predictive, preventive and personalised medicine. *EPMA J.* **8**, 23–33 (2017).
16. Menke, N. B., Ward, K. R., Witten, T. M., Bonchev, D. G. & Diegelmann, R. F. Impaired wound healing. *Clin. Dermatol.* **25**, 19–25 (2007).
17. Lantz, M. S. Are bacterial proteases important virulence factors? (1997).
18. Matsushita, O. & Okabe, A. Clostridial hydrolytic enzymes degrading extracellular components. **39**, (2001).
19. Supuran, C. T., Scozzafava, A. & Mastrolorenzo, A. Bacterial proteases: Current therapeutic use and future prospects for the development of new antibiotics. *Expert Opin. Ther. Pat.* **11**, 221–259 (2001).
20. McCarty, S. M., Cochrane, C. A., Clegg, P. D. & Percival, S. L. The role of endogenous and exogenous

- enzymes in chronic wounds: A focus on the implications of aberrant levels of both host and bacterial proteases in wound healing. *Wound Repair Regen.* **20**, 125–136 (2012).
21. Endotoxins, B. Mechanisms of bacterial pathogenicity. *Postgr. Med J* **78**, 216–225 (2002).
 22. Casadevall, A. & Pirofski, L. anne. Host-pathogen interactions: The attributes of virulence. *J. Infect. Dis.* **184**, 337–344 (2001).
 23. Matsushita, O. & Okabe, A. Clostridial hydrolytic enzymes degrading extracellular components. *Toxicon* **39**, 1769–1780 (2001).
 24. Duarte, A. S., Correia, A. & Esteves, A. C. Bacterial collagenases - A review. *Crit. Rev. Microbiol.* **42**, 106–126 (2016).
 25. Mary Mathew, S., Ravisanker, V. & Potluri, T. Delayed Diabetic Wound Healing: a Focus on Bacterial Proteases in Chronic Wound and Foot Ulcer. *Int J Cur Res Rev* **7**, 36–43 (2015).
 26. Guo, S. & DiPietro, L. A. Factors affecting wound healing. *J. Dent. Res.* **89**, 219–229 (2010).
 27. Why Wounds Fail To Heal.
 28. McCarty, S. M. & Percival, S. L. Proteases and Delayed Wound Healing. *Adv. Wound Care* **2**, 438–447 (2013).
 29. Rosenberg, G. A., Estrada, E., Kelley, R. O. & Kornfeld, M. Bacterial collagenase disrupts extracellular matrix and opens blood-brain barrier in rat. *Neurosci. Lett.* **160**, 117–119 (1993).
 30. Brandstetter, H. and Schönauer, E. Inhibition and Activity Regulation of Bacterial Collagenases. in *Zinc Enzyme Inhibitors: Enzymes from Microorganisms* 156 (2017).
 31. Theocharis, A. D., Skandalis, S. S., Gialeli, C. & Karamanos, N. K. Extracellular matrix structure. *Adv. Drug Deliv. Rev.* **97**, 4–27 (2016).
 32. Gelse, K., Pöschl, E. & Aigner, T. Collagens - Structure, function, and biosynthesis. *Adv. Drug Deliv. Rev.* **55**, 1531–1546 (2003).
 33. Gordon, M. K. & Hahn, R. A. Collagens. *Cell Tissue Res.* **339**, 247–257 (2010).
 34. Kadler, K. E., Baldock, C., Bella, J. & Boot-Handford, R. P. Collagens at a glance. *J. Cell Sci.* **120**, 1955–1958 (2007).
 35. Aravindan Rangaraj, Keith Harding & David Leaper. Role of collagen in wound management. *Wounds UK* **7**, 54–63 (2011).
 36. Mathew-Steiner, S. S., Roy, S. & Sen, C. K. Collagen in wound healing. *Bioengineering* **8**, (2021).
 37. Hulmes, D. J. S. Collagen diversity, synthesis and assembly. *Collagen Struct. Mech.* 15–47 (2008). doi:10.1007/978-0-387-73906-9_2
 38. Diegelmann, R. F. & Evans, M. C. WOUND HEALING: AN OVERVIEW OF ACUTE, FIBROTIC AND DELAYED HEALING. *Front. Biosci.* 283–289 (2004).
 39. PODIATRY MANAGEMENT. *Collagen: Its Role in Wound Healing.* (2014).
 40. Ross, R. Wound healing and collagen formation. 533–551 (1962).
 41. Barrientos, S., Stojadinovic, O., Golinko, M. S., Brem, H. & Tomic-Canic, M. Growth factors and cytokines in wound healing. *Wound Repair and Regeneration* **16**, 585–601 (2008).
 42. Natsume, T., Koide, T., Yokota, S. I., Hirayoshi, K. & Nagata, K. Interactions between collagen-binding

- stress protein HSP47 and collagen. Analysis of kinetic parameters by surface plasmon resonance biosensor. *J. Biol. Chem.* **269**, 31224–31228 (1994).
43. Howard, J. C. *et al.* Wound healing-associated proteins Hsp47 and fibronectin are elevated in Dupuytren's contracture. *J. Surg. Res.* **117**, 232–238 (2004).
 44. Taguchi, T., Nazneen, A., Al-Shihri, A. A., Turkistani, K. A. & Razzaque, M. S. Heat shock protein 47: A novel biomarker of phenotypically altered collagen-producing cells. *Acta Histochem. Cytochem.* **44**, 35–41 (2011).
 45. Widmera, C. *et al.* Molecular basis for the action of the collagen-specific chaperone Hsp47/SERPINH1 and its structure-specific client recognition. *Proc. Natl. Acad. Sci. U. S. A.* **109**, 13243–13247 (2012).
 46. Khan, E. S. *et al.* Photoactivatable Hsp47: A Tool to Regulate Collagen Secretion and Assembly. *Adv. Sci.* **6**, (2019).
 47. Ricard-Blum, S. The Collagen Family. *Cold Spring Harb. Perspect. Biol.* **3**, 1–19 (2011).
 48. Koide, T., Takahara, Y., Asada, S. & Nagata, K. Xaa-Arg-Gly triplets in the collagen triple helix are dominant binding sites for the molecular chaperone HSP47. *J. Biol. Chem.* **277**, 6178–6182 (2002).
 49. Chen, J. J. *et al.* Effect of heat shock protein 47 on collagen synthesis of keloid in vivo. *ANZ J. Surg.* **81**, 425–430 (2011).
 50. Nagai, N. *et al.* Embryonic lethality of molecular chaperone Hsp47 knockout mice is associated with defects in collagen biosynthesis. *J. Cell Biol.* **150**, 1499–1505 (2000).
 51. Ishikawa, Y., Holden, P. & Bächinger, H. P. Heat shock protein 47 and 65-kDa FK506-binding protein weakly but synergistically interact during collagen folding in the endoplasmic reticulum. *J. Biol. Chem.* **292**, 17216–17224 (2017).
 52. Wang, J. F. *et al.* Molecular and cell biology of porcine HSP47 during wound healing: Complete cDNA sequence and regulation of gene expression. *Wound Repair Regen.* **10**, 230–240 (2002).
 53. Alhayek, A. *et al.* Inhibition of Collagenase Q1 of *Bacillus cereus* as a Novel Antivirulence Strategy for the Treatment of Skin-Wound Infections. *Adv. Ther.* 2100222 (2022). doi:10.1002/adtp.202100222
 54. Konstantinović, J. *et al.* N-Aryl-3-mercaptosuccinimides as Antivirulence Agents Targeting *Pseudomonas aeruginosa* Elastase and *Clostridium* Collagenases. *J. Med. Chem.* **63**, 8359–8368 (2020).
 55. Khan, E. S., Sankaran, S., Lloncop, L. & del Campo, A. Exogenous supply of Hsp47 triggers fibrillar collagen deposition in skin cell cultures in vitro. *BMC Mol. Cell Biol.* **21**, 1–13 (2020).
 56. Mostaço-Guidolin, L., Rosin, N. L. & Hackett, T. L. Imaging collagen in scar tissue: Developments in second harmonic generation microscopy for biomedical applications. *Int. J. Mol. Sci.* **18**, (2017).
 57. Yamamoto, N., Nishioka, S. & Sasai, Y. Polarization microscopic investigation of collagen and acid glycosaminoglycans in the skin of progressive systemic sclerosis (PSS). *Acta Histochem.* **97**, 195–202 (1995).
 58. Junqueira, L. C. U., Cossermelli, W. & Brentani, R. Differential Staining of Collagens Type I, II and III by Sirius Red and Polarization Microscopy. *Arch. Histol. Jpn.* **41**, 267–274 (1978).
 59. Starborg, T. *et al.* Using transmission electron microscopy and 3View to determine collagen fibril size and three-dimensional organization. *Nat. Protoc.* **8**, 1433–1448 (2013).
 60. Liza Ovington. Bacterial toxins and wound healing. *Ostomy. Wound. Manage.* **49,7A Supp**, (2003).
 61. Schönauer, E. & Brandstetter, H. Inhibition and Activity Regulation of Bacterial Collagenases. in *Zinc Enzyme Inhibitors: Enzymes from Microorganisms* (eds. Supuran, C. T. & Capasso, C.) 69–94 (Springer

International Publishing, 2017). doi:10.1007/7355_2016_9

62. Traikovich, S. S. Use of topical ascorbic acid and its effects on photodamaged skin topography. *Arch. Otolaryngol. - Head Neck Surg.* **125**, 1091–1098 (1999).
63. Varani, J. *et al.* Vitamin A antagonizes decreased cell growth and elevated collagen- degrading matrix metalloproteinases and stimulates collagen accumulation in naturally aged human skin. *J. Invest. Dermatol.* **114**, 480–486 (2000).
64. Hoppe, I. J., Brandstetter, H. & Schönauer, E. Biochemical characterisation of a collagenase from *Bacillus cereus* strain Q1. *Sci. Rep.* **11**, 1–15 (2021).

2.3.1 Supporting information

Supplementary Table

Table SI. Second harmonic generation confocal acquisition raw data

Z-stack	10 slices (45 μm)
Scaling	1.38 μm x 1.38 μm x 5.00 μm
Bit depth	12 bit
Zoom	0.6 x 0.6
Pixel time	8.24 μs
Averaging	4
NDD detector	
Laser power	8.0%
Laser wavelength	900
Detector gain	500

Supplementary Figures

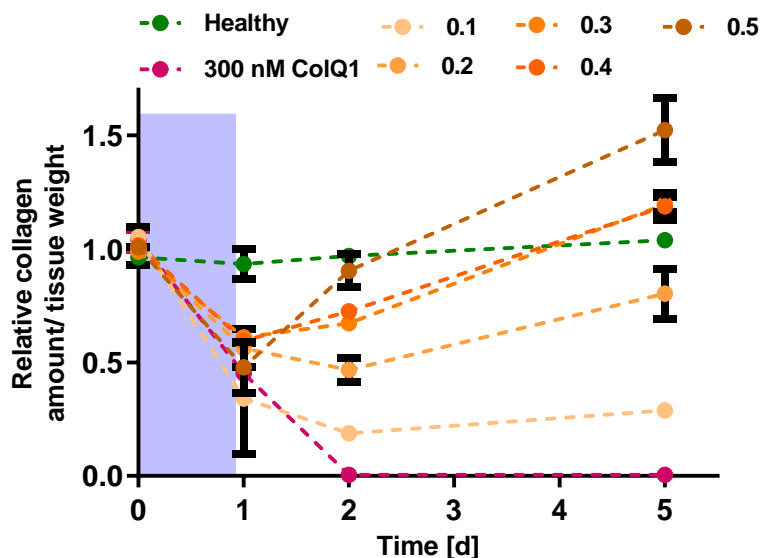


Figure S1. The amount of collagen 1 deposited in the tissue upon the treatment with 300 nM of the *Bacillus cereus* collagen Q1 (ColQ1) and different concentrations of the photoactivatable H47Y<ONBYhv. The skin was treated with 300 nM for one day (background is highlighted in violet) then the cocktails of H47Y<ONBY with compound 1 or compound 2 were added on day 2, exposed to light, and kept until day 4. Upon light exposure, H47Y<ONBY was converted to its active version H47Y<ONBYhv. Data points represent mean values of three independent experiments \pm SD.

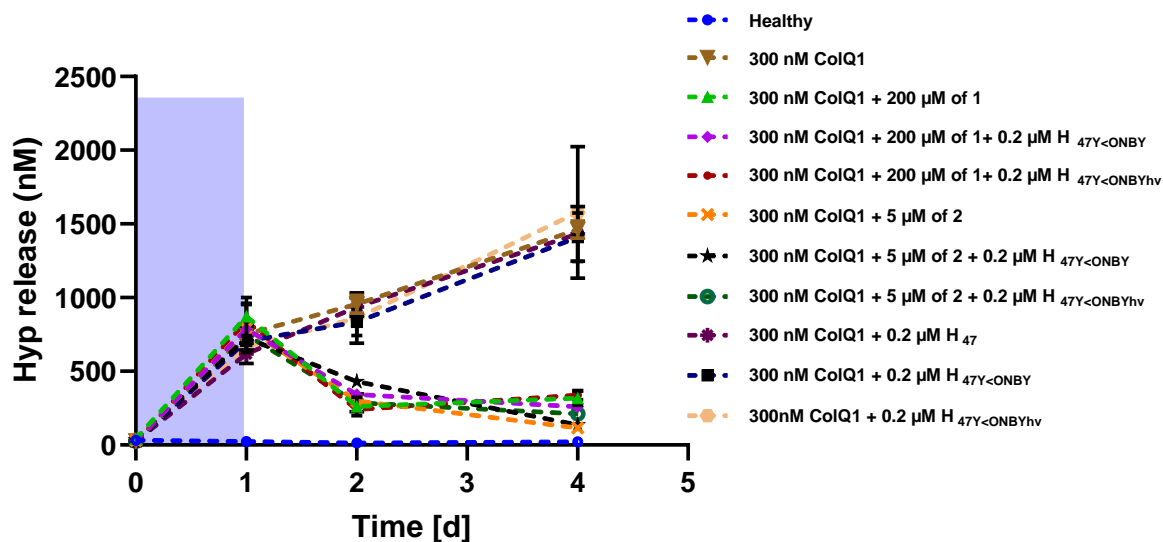


Figure S2. The release of hydroxyproline (Hyp) over time into the DMEM medium of the skin tissue. The skin was treated with 300 nM for one day (background is highlighted in violet) then the cocktails of H47Y<ONBY with compound 1 or compound 2 were added on day 2, exposed to light, and kept until day 4. Upon light exposure, H47Y<ONBY was converted to its active version H47Y<ONBYhv. Data points represent mean values of three independent experiments \pm SD.

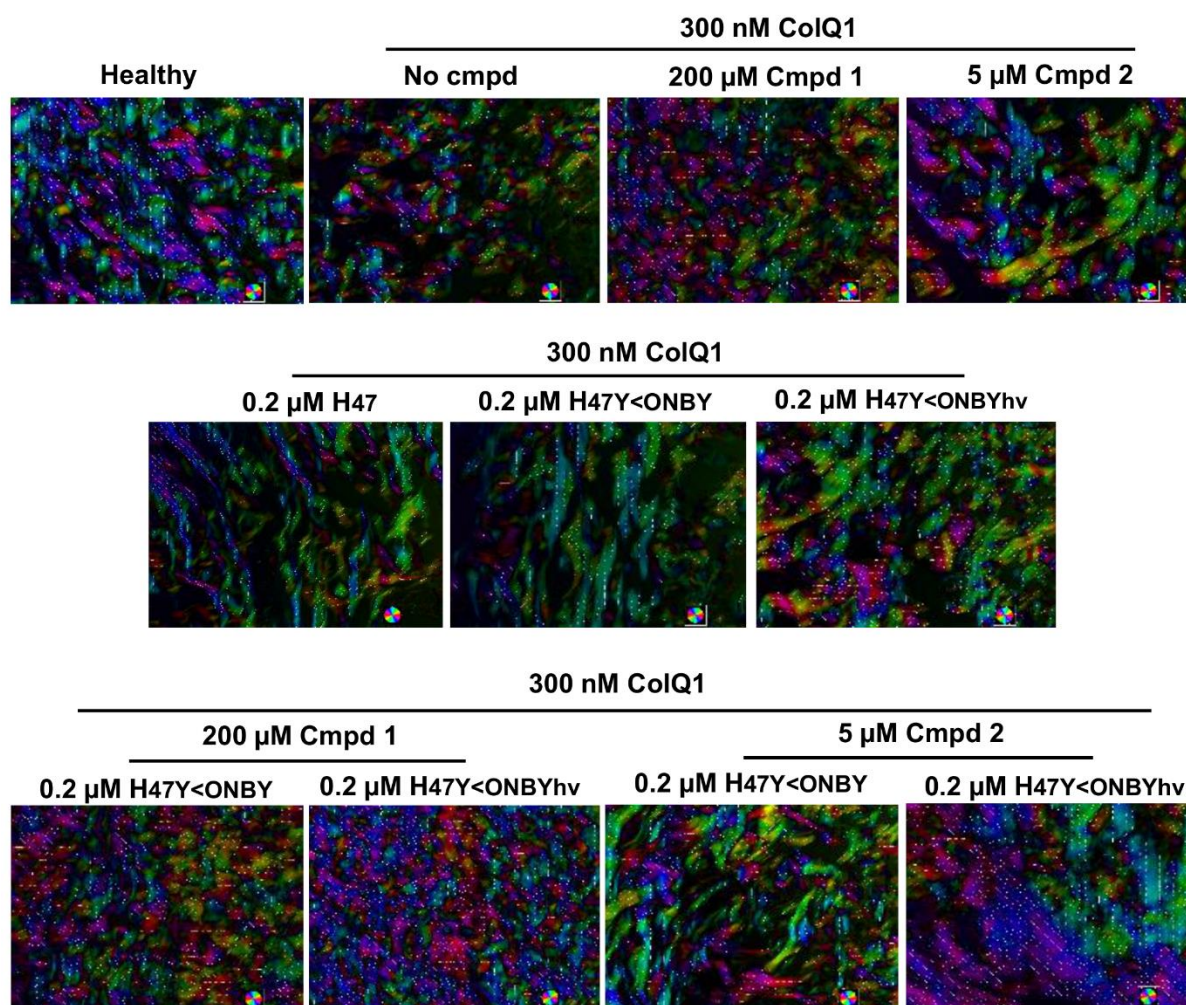


Figure S3. Alignment of dermal collagen fibers in ColQ1-treated skin tissue and with and without cocktails 1 and 2 visualized with polarization light microscope. The analysis of LC-PolScope orientation images encoding the slow optical axis per pixel are shown as pie diagram. Vectors directions indicate the orientation of collagen fibers.

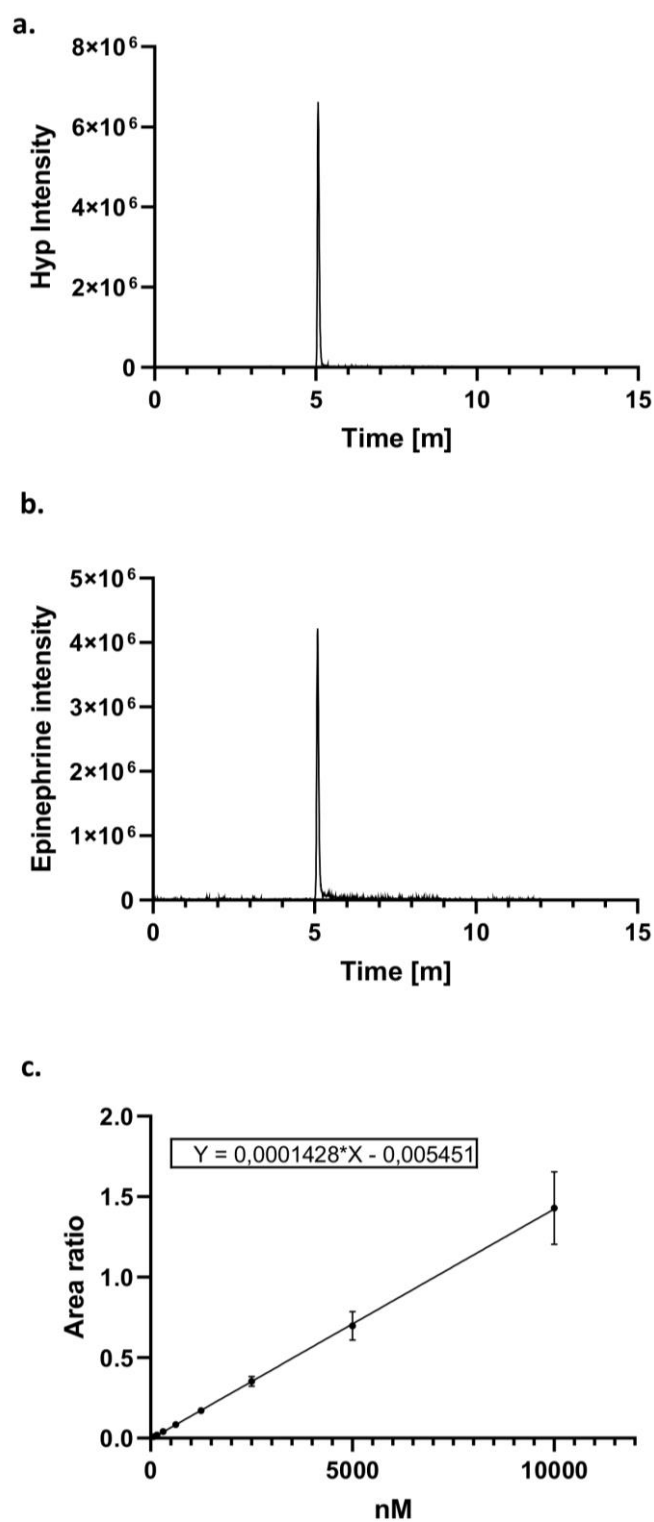


Figure S4. The LC-MS spectra of hydroxyproline (Hyp) (a) and epinephrine (internal standard of the LC-MS/MS-based hydroxyproline assay) and the calibration curve of the hydroxyproline (c), which was used to estimate the concentration of hydroxyproline of the unknown samples.

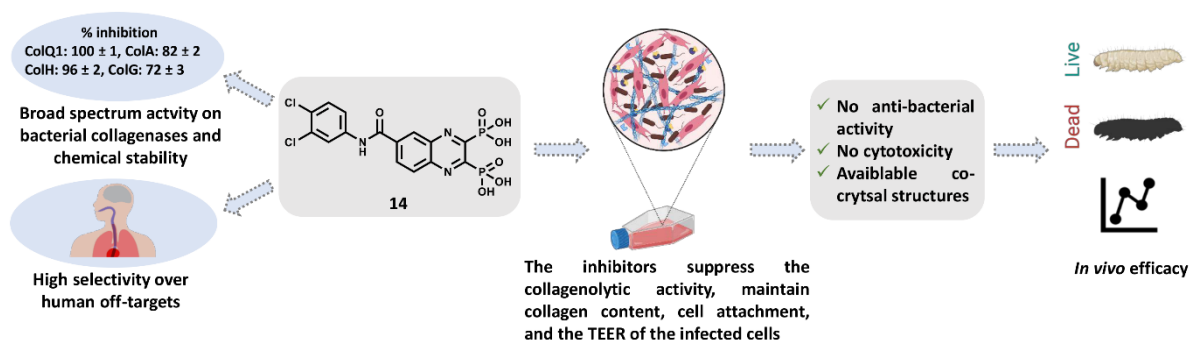
2.4 Chapter D

Discovery and Characterization of Novel, Potent Inhibitors of Clostridial and Bacillary Collagenases

Alaa Alhayek, Ahmed S. Abdelsamie, Esther Schönauer, Virgyl Camberlein, Evelyn Hutterer, Gernot Posselt, Jamil Serwanja, Constantin Blöchl, Christian Huber, Jörg Hauptenthal, Hans Brandstetter, Silja Wessler, and Anna K. H. Hirsch**

* these authors contributed equally

This part of the thesis will be submitted



Abstract

In view of the worldwide bacterial infection and antimicrobial resistance threats, new bacterial targets and innovative anti-infective agents with novel mechanisms of action are urgently needed. Since important roles in bacterial pathogenesis have been demonstrated for the Collagenases H and G (ColH and ColG) from *Clostridium histolyticum*, collagenases Q1 and A (ColQ1 and ColA) from *Bacillus cereus* represent attractive antivirulence targets.

Here, we report on novel, potent and chemically stable bacterial collagenase inhibitors. Two chemical classes were discovered: synthesized and FDA-approved diphosphonates and hydroxamates. Both classes showed high *in vitro* activity against clostridial and bacillary collagenases (ColH, ColG, ColA, and ColQ1) accompanied by high selectivity over human metalloproteases. Furthermore, the inhibitors showed no cytotoxicity on several human cell lines and no inhibition of the ColQ1 and ColA-positive *B. cereus* AH187 strain growth. The biological activity of the most active inhibitors were also characterized in infection models. The most active diphosphonate compounds showed remarkable efficacy on the activity of collagenases (*i.e.*, ColQ1 and ColA) secreted by AH187 strain. They reduced *B. cereus*-mediated detachment of fibroblast cells, enhanced cell viability and prevented fibrillar collagen degradation. They also preserved cell polarity of the infected epithelial cells as measured by the transepithelial electrical resistance (TEER). The potent diphosphonate compounds improved the survival rate of AH187-infected *Galleria mellonella* larvae. The hydroxamate class was also tested in a similar manner. Interestingly, despite similar activity in enzyme inhibition assays, they did not have the same inhibitory effect in infection models. This might be due to their fast binding kinetics to clostridial and bacillary collagenases. By contrast, diphosphonates showed different and significantly slower binding kinetics towards the bacterial target collagenases.

Introduction

Bacterial resistance is on the rise and a worldwide economic and health crisis might be on the horizon as a result of the high incidence of death caused by multi-drug resistant bacteria.^[1,2] This also comes together with the slow discovery of new antibiotics. If this trend continues, mild infections of today might become lethal in the future.^[1,2] To tackle the rise in antibiotic resistance, alternative non-antibiotic treatment approaches are urgently needed. Antivirulence agents, which selectively inhibit pathogenicity factors of bacteria, and hence prevent or delay infection, are one potential strategy.^[3,4] This could – without exerting selective pressure – harness the host's immune system to fight the infection.^[3,4]

Clostridium histolyticum (*C. histolyticum*) and *Bacillus cereus* (*B. cereus*) are Gram-positive bacteria and the epitome of many serious opportunistic infections including wound, corneal, gas gangrene, and also gastrointestinal infections.^[5,6] The pathogenicity of these microorganisms is linked to their secreted toxins and proteases, which assist them to elude defensive mechanisms, reach deep locations for nourishment, and consequently reduplicate and persist in the infection site.^[7] This might also enhance bacterial histotoxicity by promoting toxin diffusion.^[7] Bacterial collagenases are calcium- and zinc-dependent metalloproteases and the etiologic feature of the aforementioned pathogens; they destroy tissue by demolishing extracellular matrix (ECM) collagen.^[8,9] Fibrillar collagen is the most common protein in the ECM (up to 90%). It has a stable structure that resists proteolysis and can only be broken down by true bacterial and mammalian collagenases.^[8,9] True bacterial collagenases process triple helical collagen under physiological conditions into small peptides and amino acids by targeting multiple sites.^[8,9] True mammalian collagenases, on the other hand, such as the collagenolytic matrix metalloproteinases, cleave the collagen at a single site. After this initial cut, other enzymes assist in the further proteolysis of the collagen fragments.^[9] Collagen is involved in many vital physiological processes such as tissue regeneration and wound healing, in addition to its tissue-supporting functions.^[9] Therefore, any bacterial collagenase-induced imbalance in collagen structure or quantity will have detrimental effects on tissue regeneration and wound healing besides the formation of voids in the ECM, that allow the bacteria to invade and gain access to anaerobic areas.^[10] Consequently, protecting collagen from bacterial collagenase represents a promising approach for developing antivirulence agents that can be used to treat collagenase-positive infections.

C. histolyticum collagenases have been well studied in contrast to the homologous *B. cereus* collagenases. They are composed of two main structural modules; collagenase unit and collagen recruitment domains. The collagenase unit is composed of an activator and peptidase domains.^[11,12] In the latter, two histidine residues in a HEXXH motif and a downstream glutamate coordinate the catalytic zinc ion. The general-acid base glutamate and the zinc ion polarize the water molecule in the active site and activate it for the nucleophilic attack.^[11-14] The collagen recruitment domains are suggested to be involved in collagen swelling and binding to fibrillar and insoluble collagen.^[11-14] High-resolution crystal structures are available for *C. histolyticum* collagenases, but not for *B. cereus* collagenases, which share a high sequence similarity (*i.e.*, 70%).^[15,16,13,17]

We focused in this study on *C. histolyticum* collagenase H and G (ColH and ColG) and *B. cereus* collagenase Q1 and A (ColQ1 and ColA). These bacterial collagenases are attractive

candidates for antivirulence development because of their role in bacterial pathogenicity as well as their extracellular localization.^[10] The penetration of the bacterial cell wall is generally a key problem for antibacterial agent development, however in this instance it can be avoided.

Distinct collagenase inhibitors have been identified to date, the majority of which include a zinc-binding group (ZBG) that binds to the catalytic zinc ion, displacing the catalytic water molecule from the coordination and turning the enzyme inactive. **Figure 1a** shows examples of known ColH inhibitors.^[18–20] The lack of selectivity over human matrix metalloproteases (MMPs) is the primary drawback that prevents further development of these existing potent inhibitors.

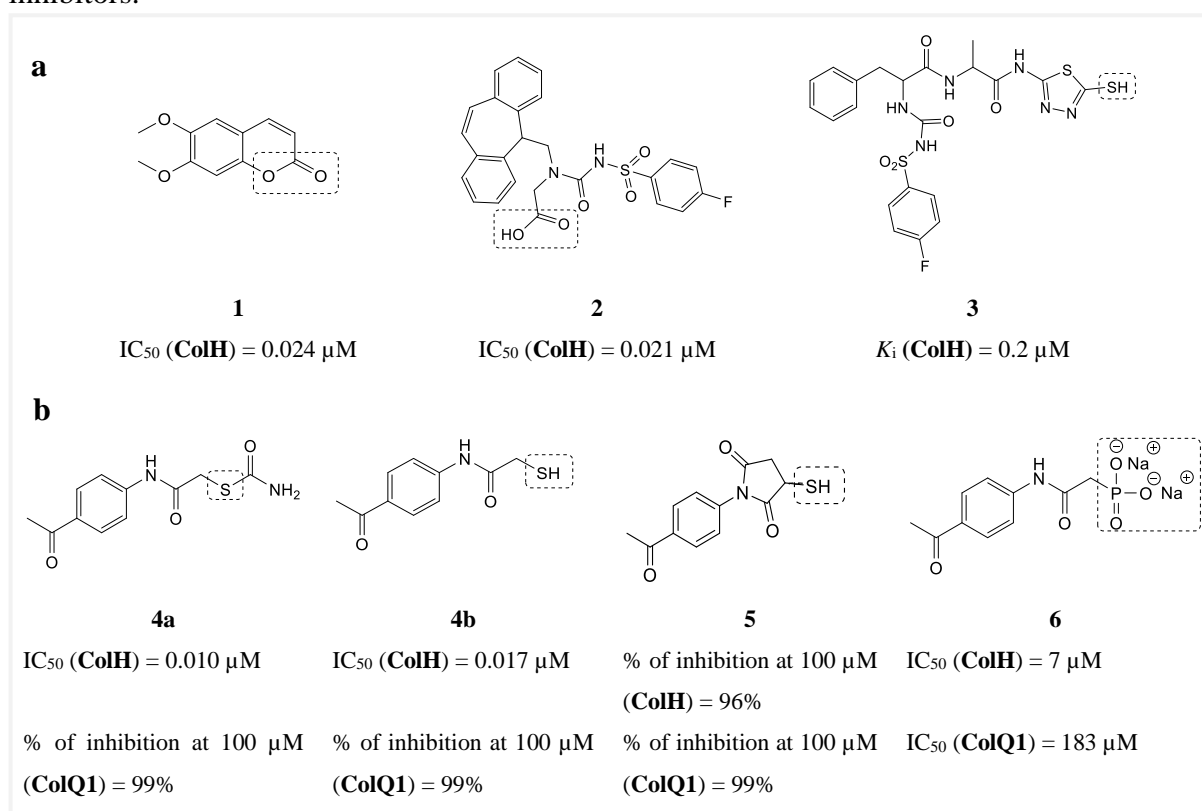


Figure 8. Example of known bacterial collagenase H (ColH) inhibitors. a) Structures of bacterial collagenase H.^[18–20] **b)** Structures of the recently identified collagenases H and Q1 (ColH and ColQ1 inhibitors).^[21,22,23,24] Zinc binding groups are highlighted by a dashed rectangles.

Recently, we were able to develop selective inhibitors of bacterial collagenases. Compound **4a**, a thiocarbamate, serves as a prodrug. By conversion into a free thiol group **4b** it can bind to the zinc ion (**Figure 1b**).^[21] The rest of the molecule binds to the conserved clostridial non-primed edge strand, explaining the selectivity for the bacterial collagenases over the human off-targets MMPs.^[21] Succinimide **5** is a more rigid derivative of compound **4b** (**Figure 1b**).^[22] Similarly to thiocarbamate, this class has been validated for its high selectivity for several bacterial collagenases, including ColH and ColG from *C. histolyticum*, ColT from *C. tetani*, and ColQ1

from *B. cereus*, over the unwanted inhibition of human MMPs. The main drawback of these two compound classes is their chemical instability due to the oxidation of the thiol group into disulfide, which leads to the loss of their activity.

Replacing the thiol group with another stable ZBG to maintain the chemical stability of the inhibitor is necessary, in addition to maintaining the high selectivity towards bacterial metalloproteases. The first stable and selective inhibitor (*i.e.*, compound **6**) (**Figure 1b**) of ColH was recently reported. Among various ZBGs, a phosphonate group has high stability and selectivity but moderate activities on ColH and ColQ1.^[23,24]

In this work, we aimed to find chemically stable, potent, and selective bacterial collagenase inhibitors. Furthermore, we set out to characterize a range of compounds bearing several different ZBGs regarding their biological activity in infection models that mimic the damage caused by collagenase during infection. We identified two chemical classes, namely diphosphonates (including FDA-approved drugs) and hydroxamates with excellent selectivity, low cytotoxicity, and remarkable micro- to submicromolar activity *in vitro* against *B. cereus* ColQ1, ColA and *C. histolyticum* ColH and ColG, demonstrating broad-spectrum activity towards a variety of disease-causing bacteria. In addition, activity in increasingly complex whole-cell assays and efficacy in a simple *Galleria mellonella* infection model. Hydroxamates compounds were tested analogously. Surprisingly, they did not demonstrate the same inhibitory impact in the infection models, despite similar potencies in enzyme-inhibition studies.

Results and discussion

Screening of compounds with various ZBGs on ColQ1 and ColH

To discover new small-molecule inhibitors with a stable ZBG, a total of 38 compounds with distinct ZBGs were screened at 100 μ M in an *in vitro* peptidolytic assay using a custom-made collagenase-specific quenched fluorescence substrate (**Table S1 and Figure S1**). Two compounds (**13** and **27**) showed strong inhibition against the collagenase unit of ColQ1 (ColQ1-CU) ($98 \pm 1\%$ inhibition and $97 \pm 2\%$ inhibition) and the peptidase unit of ColH (ColH-PD) ($83 \pm 9\%$ inhibition and $84 \pm 2\%$ inhibition), respectively. Both compounds were selected for further studies and a small library based on **13** and **27** structures was designed and synthesized (*i.e.*, eighteen diphosphonates and seven hydroxamates).

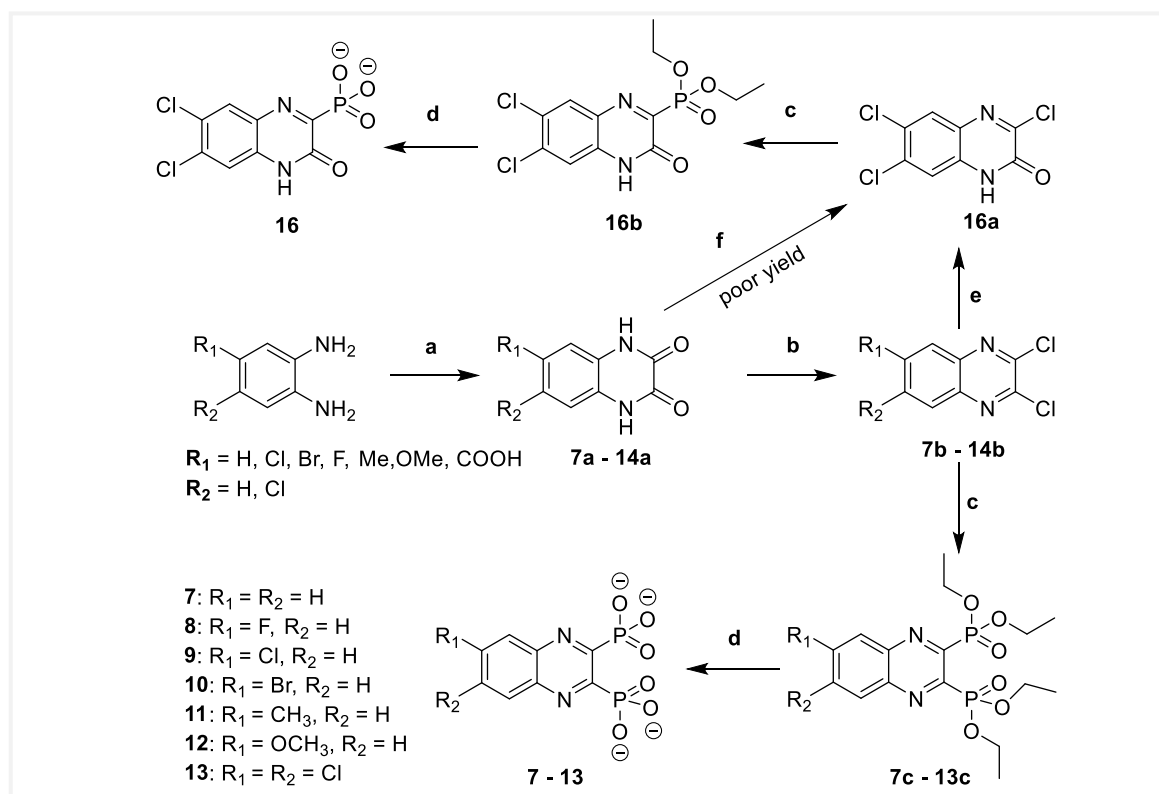
Synthesis of new anti-collagenase pathoblocker agents

Diphosphonate synthesis

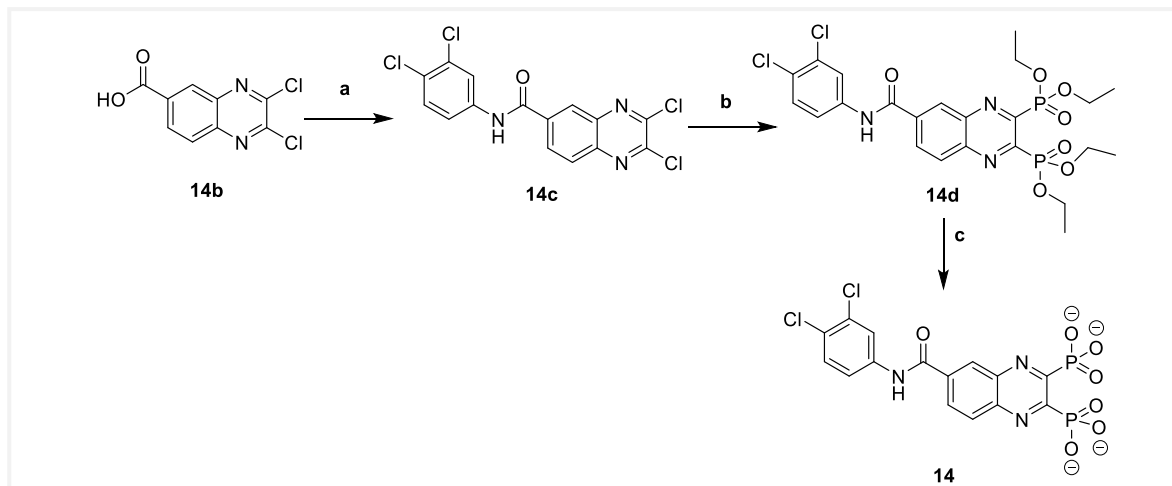
As described in **Schemes 1–3**, the substituted 2,3-dihydroxy quinoxalines **7a–14a**, and **15b** were obtained by refluxing oxalic acid and the diamine derivative in 4 N hydrochloric acid. These dihydroxy quinoxalines were directly reacted with POCl_3 in DMF in a one-pot reactor,

to provide 2,3-dichloroquinoxalines **7b–14b** and **15c**, respectively, which were used in the following step without additional purification.^[25,26] The resulting mono **16a** or di-chloro quinoxalines **7b–14b**, **14c**, and **15b** were subjected to Arbuzov reaction with triethylphosphite in a sealed tube at 150 °C. TMSBr was employed to cleave the diethylphosphonate esters to their corresponding phosphonic acid **7–16** in good yield. Compound **14c** was synthesized by reacting of 2,3-dichloroquinoxaline-6-carboxylic acid **14b** with 3,4-dichloroaniline in DCM at RT for 18 h using EDC·HCl as a coupling reagent (**Scheme 2**). Using LiOH in a dioxane/ water mixture, the di-chloro **13b** was converted into its mono-chloro derivative **16a**, as described by Yang *et al.* (**Scheme 1**).

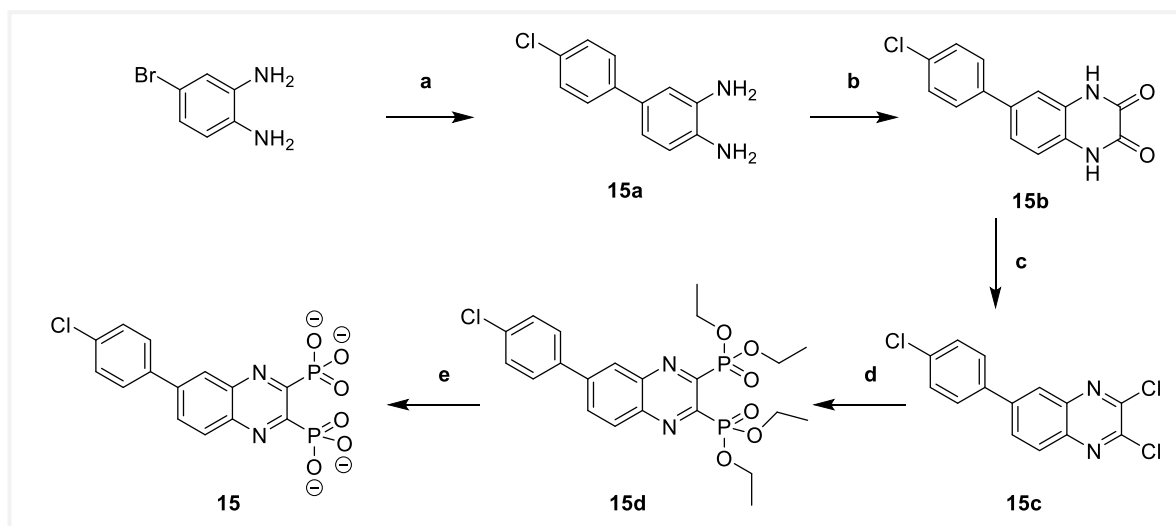
15a was produced by reacting 4-bromobenzene-1,2-diamine and (4-chlorophenyl)boronic acid in presence of 2 M sodium carbonate and (1,1'-bis(diphenylphosphino)ferrocene)palladium(II) dichloride [Pd(dppf)Cl₂] as a catalyst in a mixture of dioxane/H₂O (4:1) under microwave irradiation (150 °C, 150 W) for 20 min (**Scheme 3**).^[27]



Scheme 1. Synthesis of 5797 and its Analogues. Reagents and conditions: a) oxalic acid, 4 N HCl, reflux, 6 h; b) POCl₃, DMF, 50 °C, 6 h; c) triethyl phosphite, sealed tube, 150 °C, 18h; d) bromotrimethylsilane, dry DCM, st., rt, 18 h; e) dioxane/H₂O (1:1), LiOH, 55 °C, 24 h; f) POCl₃, DMF, 0 °C to RT, 5 min.



Scheme 2. Synthesis of compound 14. Reagents and conditions: a) 3,4-dichloroaniline, EDC.HCl, DCM, 18 h; b) triethyl phosphite, sealed tube, 150 °C, 18 h; d) bromotrimethylsilane, dry DCM, st., RT, 18 h.

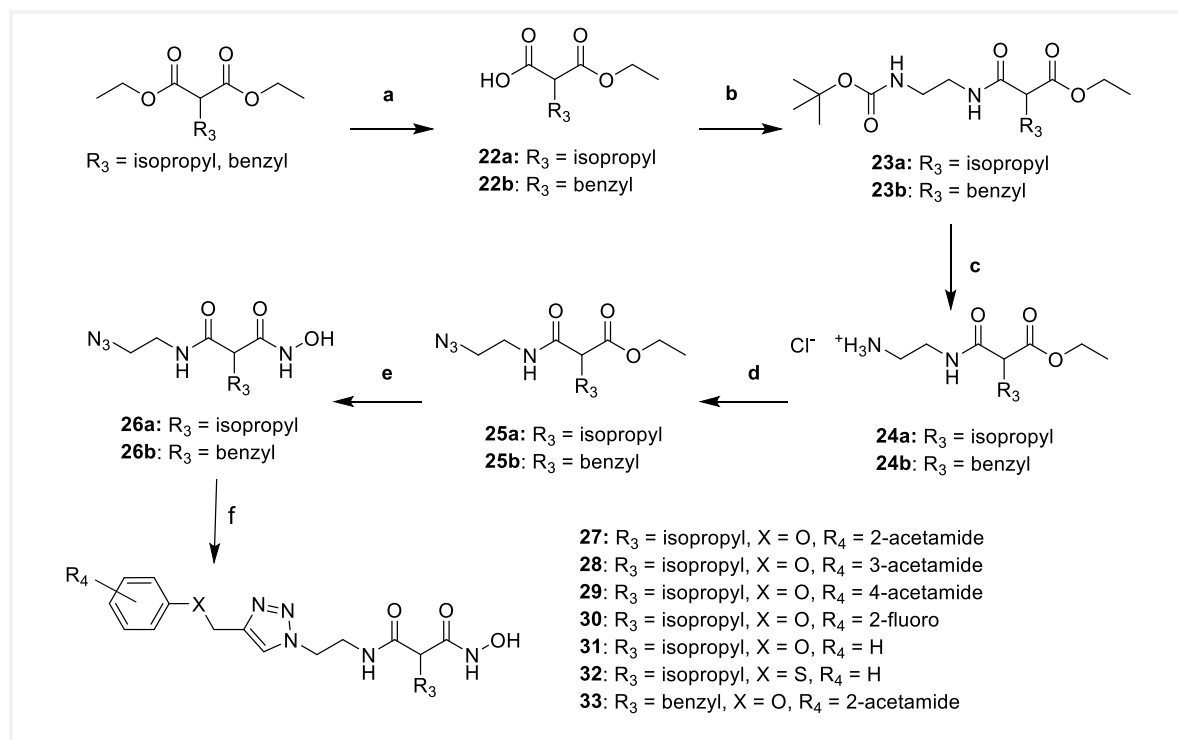


Scheme 3. Synthesis of compound 15. Reagents and conditions: a) (4-chlorophenyl)boronic acid, dioxane/ H₂O (4:1), Na₂CO₃ (2 M), Pd(PPh₃)₄, microwave, 20 min; b) Oxalic acid, 4 N HCl, reflux, 6 h; c) POCl₃, DMF, 50 °C, 6 h; d) triethyl phosphite, sealed tube, 150 °C, 18 h; e) bromotrimethylsilane, dry DCM, st., RT, 18 h.

Hydroxamate synthesis

As described in **Scheme 4**, the hydroxamates **27–33** were synthesized in six steps. The mono carboxylic acids **22a** and **22b** were first obtained through a monosaponification using sodium hydroxide in a mixture of ethanol and water. These intermediates were then activated using EDC.HCl and HOBT, in dichloromethane with diisopropylethylamine, to form the desired amides **23a** and **23b** by reacting them with the free amine. Then, an addition of hydrochloric acid (4 N in dioxane) afforded the free amines **24a** and **24b**, and these react with the diazo transfer reagent to form the azides **25a** and **25b**. The ethyl esters were engaged in a KCN-

catalyzed aminolysis reaction, which lead to the formation of the azido hydroxamic acids **26a** and **26b**. The final step is a copper-catalyzed Huisgen 1,3-dipolar cycloaddition to give the desired 1,2,3-triazole 1,4-disubstituted **27–33**, the needed alkynes **34a–34d** being previously synthesized by nucleophilic substitution of phenols on the propargylbromide.



Scheme 4. Scheme 4. Synthesis of hydroxamic acid compounds. Reagents and conditions: NaOH, EtOH/H₂O (4:1), rt., 18 h; b) tert-butyl *N*-(2-aminoethyl)carbamate, EDC.HCl, HOBT, DIPEA, CH₂Cl₂, rt., 18 h; c) 4 N HCl, EtOH, 0°C to rt., 18 h; d) azide-*N*-diazoimidazole-1-sulfonamide hydrogen sulfate, K₂CO₃, ZnCl₂, DIPEA, MeOH, rt., 18 h; e) aq. hydroxylamine (50% in water *w/w*), KCN (cat.), MeOH, rt., 18 h; f) Alkyne **34a–34d**, prop-2-ynoxybenzene or prop-2-ynylsulfanylbenzene, CuSO₄ (5H₂O), NaAsc, *N,N*-dimethylformamide/H₂O (1.2:1), rt., 18 h.

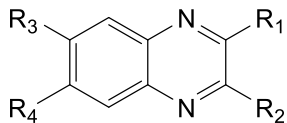
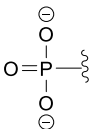
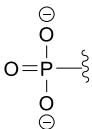
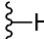
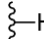
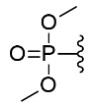
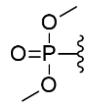
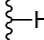
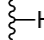
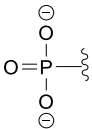
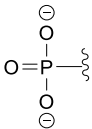
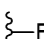
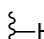
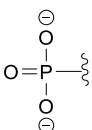
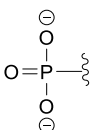
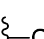
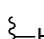
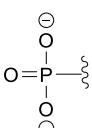
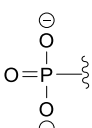
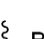
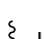
Activity on *B. cereus* ColQ1

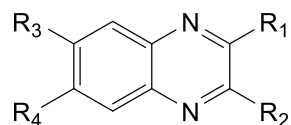
Structure–activity relationships of the synthesized and FDA-approved diphosphonate compounds on ColQ1. The initial screening of the diphosphonate **13** and its synthesized derivatives using ColQ1-CU showed that the presence of both phosphonate groups with free hydroxyl groups is indispensable for inhibition (**Table 1**), indicating that the phosphonate groups acts as ZBG to the catalytic zinc ion. Replacing the 3,4-chloro of **13** with 3-methoxy group and 4-hydro (**12c**) or with 3,4-dihydro lead to loss of the activity as shown in compound **7c**. Replacing the 4-chloro of **13** with 4-hydro reduced the activity of **12**. Compound **8** with 3-fluoro instead of 3-chloro had a low activity. While compound **10** with 3-bromo regained the loss in the activity. Compound **15** with 3-chlorophenyl was more active than its 3-chloro derivative **9**. The elongation of the 3-chlorophenyl into 3-dichlorophenylamide in compound

14 maintained the activity of **15**. Quinoxaline (**21**) and *N*-di-methyl quinoxaline (**b21**) derivatives showed a much lower activity.

In case of ColG-PD, this SAR could be rationalized by a crystal structure in complex with compound **13** determined at 1.95 Å resolution (**Figure 3 and Table S2**). In addition to a non-functional binding site at the rear of the peptidase domain, we could detect **13** in the primed binding pocket, albeit at relatively low occupancy/high mobility. The inhibitor could be modeled into the active site with the help of a polder map. One of the phosphonate groups acted as ZBG and simultaneously interacted with Glu555 and Tyr607, while the aromatic scaffold of **13** and the chlorides established hydrophobic interactions in the primed binding pockets with Phe515, His523 and Ile576.

Table 1. Inhibition of ColQ1-CU by diphosphonates and derivatives at 100 μM concentration^a

					
Cpd.	R ₁	R ₂	R ₃	R ₄	Inhibition (%)
7					40 ± 7
7c					0 - 8
8					38 ± 3
9					88 ± 2
10					95 ± 5



Cpd.	R ₁	R ₂	R ₃	R ₄	Inhibition (%)
11					58 ± 4
11c					0 - 8
12					23 ± 6
12c					0 - 8
13					98 ± 1
14					100 ± 1
15					96 ± 4
16					5 ± 2
17					17 ± 6
18					8 ± 2

Cpd.	R ₁	R ₂	R ₃	R ₄	Inhibition (%)
19					8 ± 4
20					21 ± 4
21					35 ± 4
21b					58 ± 3

^aMeans and SD of three independent experiments.

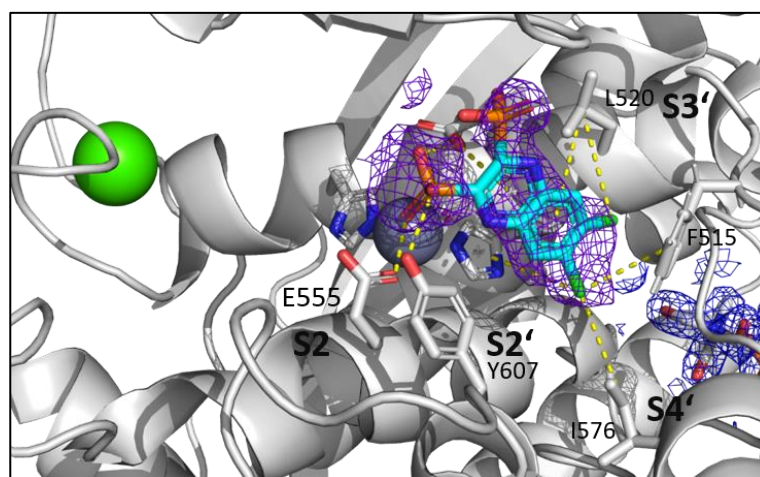


Figure 9. Crystal structure of ColG-PD in complex with 13 solved at 1.95 Å resolution. Close-up view of the active site in ball-and-stick representation. The inhibitor (cyan) is shown in sticks with polder map contoured at 2.5 σ above background. The catalytic zinc ion (dark gray) and the calcium ion (green) are shown as spheres.

As diphosphonates are routinely used in the treatment of bone diseases,^[28] we also screened a number of FDA-approved diphosphonates regarding their effect on ColQ1-CU (**Table 2**).

Tiludronate disodium and **alendronate sodium** resulted in moderate inhibition of ColQ1-CU (63 ± 3 and $76 \pm 1\%$, respectively) at $100 \mu\text{M}$ concentration.

Table 2. Inhibition of ColQ1-CU by selected FDA-approved disphosphonates at $100 \mu\text{M}$ concentration^a

Cpd.	Structure	Inhibition (%)	Cpd.	Structure	Inhibition (%)
Clodronate disodium		n.i.	Alendronate sodium		76 ± 1
Tiludronate disodium		63 ± 3	Ibandronate sodium		n.i.
Neridronate		n.i.	Risedronate sodium		n.i.

^aMeans and SD of three independent experiments, n.i.: no inhibition.

Structure–activity relationships of hydroxamate compounds on ColQ1. An initial screening of hydroxamate **27** and its six derivatives using ColQ1-CU from *B. cereus* strain Q1 was performed (**Figure S2** and **Table 3**). The compounds differed structurally in the *alpha*-substituent relative to the hydroxamic acid group and the terminal moiety. The screen revealed that the *o*-acetamide substituted phenoxy group present in **27** and **33** was the most favored terminal group and that small variations in the *alpha*-position were tolerated. Next, we evaluated the potential of the most potent compounds **27** and **33** as broad-spectrum inhibitors of bacterial collagenases and determined the inhibition constants using ColG-CU and ColH-PD from *C. histolyticum*, and ColA-CU from *B. cereus* strain ATCC14579 and ColQ1-CU (**Table 4**). The results revealed that both compounds inhibited clostridial and bacillary collagenases in the low micro- to submicromolar range.

Table 3. Inhibition of ColQ1-CU by hydroxamates at 100 μM concentration^a

Cpd.	R ₁	R ₂	R ₃	R ₄	R ₅	Inhibition (%)
27				O		97 ± 2
28				O		81 ± 3
29				O		87 ± 3
31				O		93 ± 1
30				O		92 ± 5
32				S		71 ± 3
33				O		101 ± 1

^aMeans and SD of three independent experimentsTable 4. Inhibition of bacterial collagenases by 27 and 33^a

		6007	6193
Protein		K _i (μM)	K _i (μM)
<i>C. histolyticum</i>	ColH-PD	11.6 ± 0.4	1.7 ± 0.2
	ColG-CU	31 ± 1	18.4 ± 0.6
<i>B. cereus</i>	ColQ1-CU	0.10 ± 0.02	0.82 ± 0.07
	ColA-CU	3.4 ± 4	4.7 ± 0.3

^aMeans and SD of three independent experiments

We rationalized the screening results based on the crystal structure of **27** in complex with the peptidase domain of ColG, a close homologue of ColQ1, solved at 1.80 Å resolution (**Figure 4 and Table S2**). The bound inhibitor occupied the active site from the S3 pocket to the S2' binding site. In the S3 binding pocket, the *ortho*-acetamide group directly interacted with the edge strand *via* a hydrogen bond to the backbone amide of Glu498, while the aromatic phenoxy ring established π - π stacking interactions with the sidechain of Trp539. This explains the observed preference for the *ortho*-configuration of the acetamide group.

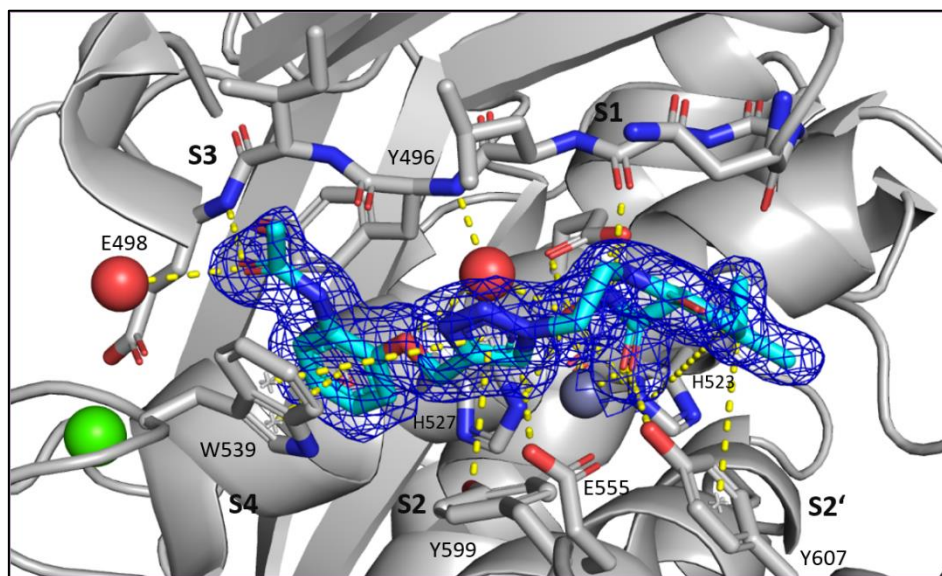


Figure 4. Crystal structure of ColG-PD in complex with **27 solved at 1.80 Å resolution.** Close-up view of the active site in ball-and-stick representation. The inhibitor (cyan) is shown in sticks with the maximum likelihood weighted $2F_o - F_c$ electron density map contoured at 1σ . The catalytic zinc ion (dark gray) and the calcium ion (green) and water molecules (red) are shown as spheres.

The central triazole ring hydrogen-bonded with Glu555 and formed a π -hydrogen interaction with Tyr599 in the S2 binding pocket. The hydroxamate group coordinated, as expected, the catalytic zinc ion. The isobutyl group in the *alpha*-position formed hydrophobic interactions with Tyr607 and His523 in the S2' pocket. The hydrophobic benzyl group of **33** can be expected to fit similarly into the S2' pocket.

Selectivity over human MMPs and activity on other bacterial virulence factor collagenases

To assess the selectivity of the compounds towards human MMPs and other bacterial collagenases, compounds **13**, **14**, **15**, **27**, **tiludronate disodium**, and **alendronate sodium** were tested against ColG-CU and ColH-PD from *C. histolyticum*, and ColA-CU from *B. cereus* strain ATCC14579. In addition, the compounds were tested on catalytic domains of several human MMPs including MMP-1, -2, -3 and other important human off-targets which are involved in

gene expression and the processing of TNF- α , these include HDAC-3, -8, TACE (ADAM-17).^[29,30] For advanced safety screen COX-1 was also tested.

Our data showed that the most potent inhibitors of ColQ1 possess a high selectivity over most of the tested human off-targets (except for **13** against MMP-1, -2, and -3 and **tiludronate disodium** against MMP-1) (Tables 5 and S3). Their activity against most tested bacterial collagenases, on the other hand, proved to be high which confirms their broad-spectrum inhibitory potency against bacterial targets (Table 6). This broad activity is comparable to that previously observed for compounds carrying thiol or phosphonate ZBGs.^[21,22,23]

Table 5. Inhibition of three MMPs in presence of 100 μ M of compounds 13 14, 15, 27, tiludronate disodium, and alendronate sodium^a

Class	Cpd.	MMP-1	MMP-2	MMP-3
Synthesized diphosphonates	13	53 \pm 3	79 \pm 2	33 \pm 11
	14	>100	>100	>100
	15	>100	>100	>100
FDA-approved diphosphonates	Tiludronate disodium	50 \pm 10	>100	>100
	Alendronate sodium	>100	>100	>100
Hydroxamate	27	>100	>100	>100

^aMeans and SD of two independent experiments.

Table 6. Inhibition of ColA-CU, ColH-PD, and ColG-CU in presence of 100 μ M of compounds 13 14, 15, 27, tiludronate disodium, and alendronate sodium^a

Class	Cpd.	ColA-CU	ColH-PD	ColG-CU
Synthesized diphosphonates	13	71 \pm 4	83 \pm 9	68 \pm 4
	14	82 \pm 2	96 \pm 2	72 \pm 3
	15	86 \pm 8	97 \pm 5	70 \pm 8
FDA-approved diphosphonates	Tiludronate disodium	72 \pm 2	91 \pm 2	28 \pm 7
	Alendronate sodium	18 \pm 4	25 \pm 5	28 \pm 7

Class	Cpd.	ColA-CU	ColH-PD	ColG-CU
Hydroxamate	27	93 ± 2	84 ± 2	71 ± 7

^aMeans and SD of at least two independent experiments.

Cytotoxicity against human cell lines. Besides the selectivity, cytotoxicity is also an important criterium, especially when it comes to a potential therapeutic use in humans. In this context, we evaluated the cytotoxicity of **13**, **14**, **15**, and **6007** against four human cell lines – HepG2 (hepatocellular carcinoma), HEK293 (embryonal kidney), NHDF (Normal Human Dermal Fibroblasts), and MDCK II (Madin-Darby Canine Kidney II). The compounds did not show cytotoxic effects (IC₅₀ values > 100 μM or 200 μM) against these cell lines (**Table S4**). This makes them suitable for further investigation to study their ADMET profile.

Small-molecule inhibitors prevent collagen I degradation

***B. cereus* collagenase inhibitors prevent collagen I cleavage.** We examined collagen I (Col I) cleavage induced by the full length ColQ1-FL with and without inhibitors to investigate whether the compounds have an anti-collagenolytic effect on the collagenase's natural substrate. After 4 h of co-incubation of ColQ1 with Col I, in the absence and presence of inhibitor, Col I breakdown was investigated. On reducing polyacrylamide gels, the hallmark bands of Col I (*i.e.*, alpha 1, alpha 2, and beta chains) were clearly visible. Compared to the negative control (no inhibitor), **13** and **27** displayed considerable anti-ColQ1 activity and maintained the chains of Col I as shown at concentrations above 3 μM and 0.8 μM, respectively. Below these concentrations substantial chain disintegration was detected (**Figure 5**). The diphosphonate derivatives **11**, **10**, **14**, and **15** inhibited the collagenase activity at all concentrations tested (12.5–1.5 μM) and protected Col I chains from cleavage (**Figure 5**). Similar findings were observed for other diphosphonate derivatives **7**, **9**, **11** and the hydroxamate derivative **33** (**Figure S3**). While severe degradation was visible at all tested concentrations (12.5–1.5 μM) of compounds **16**, **21**, **b21**, and the hydroxamate derivatives **28**, **29**, **31**, and **32** (**Figure S3**), indicating their low activity on ColQ1. These findings are corroborated by the previously determined inhibition data derived with the peptidolytic substrate. This highlights that several of our hydroxamate and diphosphonate compounds are *in vitro* able to prevent cleavage of the large, structurally more complex physiological substrate of collagenases *i.e.*, Col I, which accounts for 80–90% of the collagen in the body.^[31] Based on

these findings, we next investigated whether this protective effect would also prevail in a more complex cellular setting.

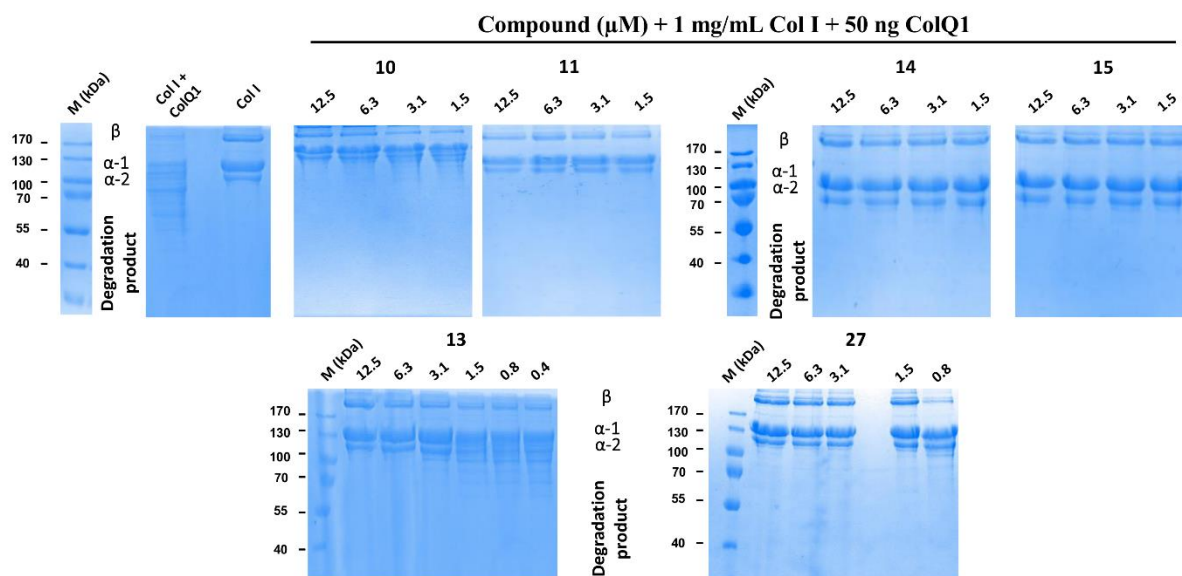


Figure 5. Activity of ColQ1 inhibitors against the collagenolytic activity of ColQ1. Inhibitors prevented cleavage of 1 mg/mL of Col I chains (i.e., beta, alpha-1, and alpha-2). The *Bacillus cereus* collagenase Q1 ColQ1 full length (50 ng) was incubated with 1 mg/mL Col I for three hours and the degradation was then visualized on 12% SDS-PAGE. Col I: 1 mg/mL Col I without any protease. M (kDa): molecular weight standards, Col I: type I collagen.

Small-molecule inhibitors inhibit collagenase activity and preserve fibroblast cell integrity

Collagenase release during *B. cereus* infection of NHDF cells. To investigate a potential antivirulence activity of ColQ1 inhibitors, we developed an *in vitro* infection model using the common connective tissue cell line NHDF in the ECM. There they have crucial functions, as they synthesize the main components of the ECM (such as collagen) and maintaining the ECM homeostasis.^[32] Previous reports revealed that bacillary ColQ1 and ColA have prominent collagenolytic activity that is greater than or similar with the well-studied clostridial ColG and ColH.^[16] Therefore, *B. cereus* collagenases were used as model proteases to further evaluate the inhibitors' effects on infection settings.

To establish the model, the release of *B. cereus* collagenases was investigated, in order to determine the duration needed for the BC AH187 strain (expresses two collagenases: B7HV61 (sequence identical to ColQ1) and B7HZW5 (ColA)) to secrete considerable amounts of collagenase into the surrounding DMEM of NHDF cells. To inspect the release of collagenase, the DMEM medium was collected at various time points and investigated by gelatin zymography. The zymography analysis revealed that the bacteria required at least 4 h to release

substantial amounts of collagenases, which rose over time as seen in **Figure S4**. In the zymograms, besides the bands of the full-length ColQ1 and ColA (109 kDa), also truncated isoforms (100–40 kDa) were detected (**Figure S4**). This phenomenon has been previously reported for other bacterial collagenases.¹⁵ After 4 h of infection, we could also observe a massive reduction (>50%) in fibrillar collagen in the ECM quantified with the picosirius red assay (**Figure S4**).^[33,34] Concomitantly, NHDF cells started to detach and their morphology changed from spindle-shaped to round, evidenced by light microscopy studies and SDS-PAGE analysis of the cell lysate (**Figure S4**). In addition, we monitored the release of lactate dehydrogenase (LDH)^[35] enzyme into the DMEM to detect cells undergoing cell death. Significant amounts of LDH were excreted after 4 h and the excretion increased over time (**Figure S4**). Studies showed that *B. cereus* protein complexes hemolysin BL and nonhemolytic enterotoxin also induced cytotoxicity and cell detachment, which means their release could also induce cytotoxicity.^[36,37] These results suggest that bacterial collagenases may also play a role in inducing cellular necrosis. Based on these findings, we chose a time window of 4–6 h was chosen for testing the efficacy of collagenase inhibitors in the NHDF infection model.

Collagenase inhibitors suppress the gelatinolytic activity of *B. cereus* collagenases released in the NHDF infection model. We investigated the most potent compounds from our *in vitro* cleavage assays in the NHDF infection model at 0, 25, 50, 100, and 200 μ M concentrations. We observed a dose-dependent inhibitory effect on the activity of the secreted collagenases into the supernatant of infected cells detected by gelatin zymography. At 200 μ M, **13** completely suppressed the gelatinolytic activity, while for **14** complete inhibition was already observed at 100 μ M concentration (**Figure 6**). The other diphosphonate derivatives (**10**, **11**, and **15**) were also evaluated. Compound **15** demonstrated also a clear dose-dependent inhibitory effect on gelatin turnover (**Figure S7**), while this was less evident for **10** and **11**, which inhibited the collagenase' activity towards gelatin only marginally at 100 μ M (**Figure S7**).

The most promising FDA-approved diphosphonate drugs from the *in vitro* enzyme assays were also tested. **Tiludronate disodium** and **alendronate sodium** could completely inhibit gelatin turnover in the zymography at a concentration of 100 μ M and 200 μ M, respectively, (**Figure S9**). Interestingly, the hydroxamate compounds (**27**, **28**, **29**, **30**, **31**, **32**, and **33**) showed no inhibitory effect on the collagenase in the zymography at all tested concentrations (**Figures S10 and S11**).

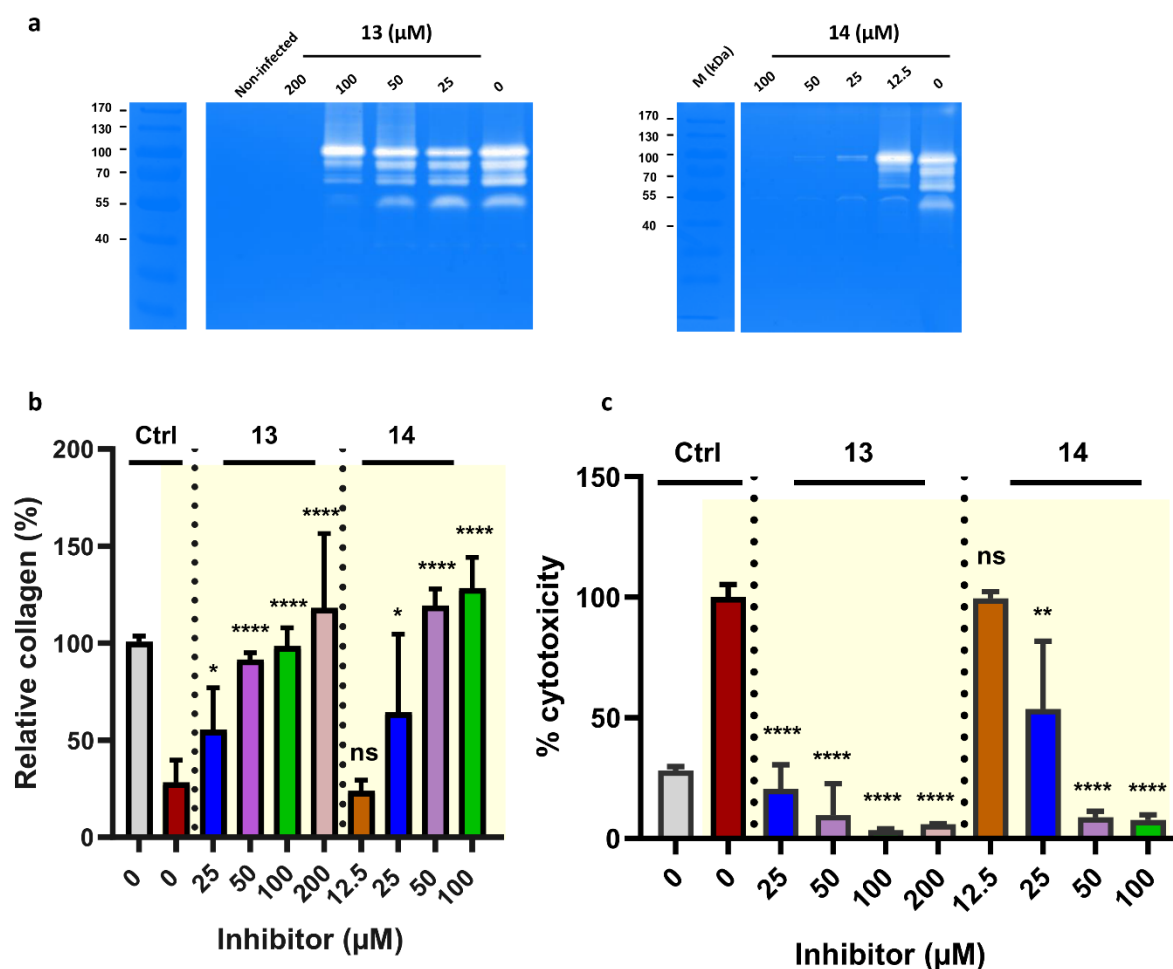


Figure 6. The activities of **13** and **14** on the fibroblast (NHDF) cells infected with *Bacillus cereus*. **a**) The anti-gelatinolytic activities of compounds **13** and **14** against *B. cereus* collagenases. The DMEM supernatants of the infected NHDF cells were applied on the zymograms. Clear regions against blue background indicate gelatin in the gel has been cleaved. **b**) The amount of fibrillar collagens maintained by **13** and **14** in the infected NHDF cells (highlighted in yellow). **c**) The cytotoxicity of *B. cereus* infection (highlighted in yellow) into NHDF cells treated with **13** and **14**. Statistical analysis was performed with one-way ANOVA and statistical significance was analyzed by Tukey test. Significance was calculated by comparing non-treated *vs* treated cells with compounds (mean \pm SD, **** $p < 0.0001$, ** $p < 0.01$, ns non-significant). Ctrl: control. M (kDa): molecular weight marker.

Collagenase inhibitors prevent NHDF cell detachment and cleavage of fibrillar collagens of the ECM. We further evaluated the effect of the diphosphonate and hydroxamate compounds on cell morphology, the fibrillar collagen content of the ECM, and cell viability in the infection model. As shown in **Figure 6**, the diphosphate compounds **13** and **14** showed a dose-dependent effect on the NHDF cell. Above a concentration of 25 μM , they were both able to sustain the cells. The cells stayed attached and maintained their spindle shape (**Figures S5 and S6**) and above 50 μM concentration we observed a significant reduction in LDH releases, indicating higher cell viability. The diphosphonate derivative **15** and the FDA-approved diphosphonate drugs **tiludronate disodium** and **alendronate sodium** also showed dose-dependent effects on NHDF morphology, fibrillar ECM collagen content, and LDH release, however, at concentration $\geq 100 \mu\text{M}$ (**Figures S6-S9**). While the diphosphonate **10** and **11** showed less of

an effect at all tested concentrations (except for **10** which at 100 μM resulted in higher cell viability) (**Figures S6 and S7**).

We also examined the hydroxamate compounds **27**, **28**, **29**, **31**, **32**, and **33**. Interestingly, none of them showed the expected effects. They were neither able to rescue cell morphology, nor to maintain the collagen content of the ECM. Also no inhibition of the collagenase in the gelatin zymography was detected at all concentrations tested (**Figures S10 and S11**). Puzzled by the results of the hydroxamate compounds, we investigated their stability in the conditions of the NHDF infection model to obtain a potential explanation for the observed findings. We used **27** as representative example for this compound class. The LC-MS spectra (**Figure S12**) confirmed, however, the stability of **27** under the assay conditions. We, therefore, speculate that the hydroxamate compounds bind to the collagen and gelatin substrates with high effective affinity/avidity, thus reducing the free inhibitor concentration.

To sum up, in the NHDF infection model, the potent diphosphonate compounds from the *in vitro* enzyme assays were shown to have anti-collagenolytic activity, by inactivating the bacterial collagenases. Furthermore, they reduced the cytotoxicity induced directly or indirectly by the released collagenases and maintained the spindle-shaped morphology of the cells. In contrast, the hydroxamate-based compounds displayed almost no anti-collagenolytic activity in the infection model, despite their inhibitory activity in the *in vitro* enzyme assays.

Rapid, slow or very slow reversibility of diphosphonate inhibitors depends on target collagenase

Next, we compared the inhibition mechanism of the diphosphonate compounds and the hydroxamate compounds to the bacterial collagenases. For this purpose, we performed rapid dilutions assays to test the reversibility of compound inhibition with ColA-CU and ColQ1-CU from *B. cereus* and ColH-PD and ColG-CU from *C. histolyticum*.^[36] Upon rapid dilution, rapidly reversible inhibitors quickly dissociate from the enzyme and progress curves similar to the uninhibited control are observed, while irreversible or very slowly dissociating inhibitors remain bound to the enzyme and only very gradually recover activity.

Intriguingly, as demonstrated in **Figure S13**, we observed clear differences between the compound classes. While the hydroxamates **27** and **33** behaved towards both bacillary and clostridial collagenases like rapidly reversible inhibitors – as expected from active-site directed competitive inhibitors –, the diphosphonate compounds showed a more varied response. In case of ColQ1-CU, both **13** and **15** displayed progress curves with approximately less than 9% residual activity, which is typical for irreversible or very slowly dissociating inhibitors.^[36] Therefore, we examined ColQ1-CU treated overnight with **13** by mass spectroscopy and could

confirm that the compound did not result in covalent protein modification (**Figure S14**). This leads to the conclusion that **13** must be a very slowly dissociating reversible binder of ColQ1. In case of ColA-CU, the rapid dilution assay revealed only a minimal inhibition in presence of **13**, but **15** displayed a progress curve typical for slowly dissociating inhibitors. In case of ColH, the effect of **13** and **15** were reversed compared to ColA, and in case of ColG, both diphosphonates behaved like rapidly reversible inhibitors. Slowly and very slowly dissociating inhibition are an interesting mechanism for reducing enzyme activity, as they increase the lifetime of the enzyme-inhibitor complex. Its advantages appear in the latter phases of drug development when pharmacological properties (*i.e.*, dosing interval and patient safety) need to be optimized.^[36,37] We speculate that the differential behavior observed in the infection models between the diphosphonate and hydroxamate compounds is caused by their different dissociation properties, which results in different enzyme–inhibitor complex lifetimes. The exact mechanism underlying the slow dissociation behavior, however, remains currently elusive, as we could not get a crystal structure of a diphosphonate inhibitor complex with ColA or ColQ1.

Small-molecule inhibitors reduce collagenase activity and maintain epithelial cell integrity

Collagenase inhibitors maintain the TEER of MDCK II cells. Epithelial cells form intracellular tight junctions establishing a sealed epithelium to control diffusion of membrane proteins, uptake of small molecules, and protect the body from hazardous substances.^[38,39] *B. cereus*-mediated cell detachment severely destroys the epithelial barrier function, allowing access to deeper areas of the tissue. To quantify the effect on the epithelial barrier function, we investigated selected compounds regarding their effect on the TEER of polarized Madin–Darby Canine Kidney (MDCK) cells. We treated MDCK II cells with our target compounds followed by the infection with *B. cereus* AH187 strain or co-incubation with supernatant from BC AH187 strain culture, which contains ColQ1 and ColA. In comparison to the no inhibitor control, the TEER of the infected MDCK cells (**Figures 7a and S15**) was maintained with compounds **14**, **15**, **tiludronate disodium** and **alendronate sodium** at 100 μ M concentration. While compounds **13** and **10** failed to sustain the TEER of the infected cells at 200 μ M concentration (**Figure S15**) but they retain the TEER of the challenged cells with 50% (*v/v*) supernatant (**Figure 7b**).

This discrepancy might be due to the lower quantities of collagenases secreted in the supernatant than compared to the potentially very high bacterial densities during infection events, resulting in high collagenase secretion. This might have disrupted the optimum

inhibitor/collagenase ratio and resulted in lower efficacy of some inhibitors. Despite these variations in effect, our findings support the notion that collagenases are involved in attacking epithelial barriers and that our inhibitor compounds can help to preserve the cellular junction, thereby reducing bacterial invasion. Thus, the effect of some inhibitors might be less in this case. These findings corroborate the theory that collagenases are one of the factors that might be involved in disturbing the TEER of epithelial cells. Our collagenase inhibitors proved their potential to preserve the cell attachment and the junction between them, subsequently reducing bacterial invasion.

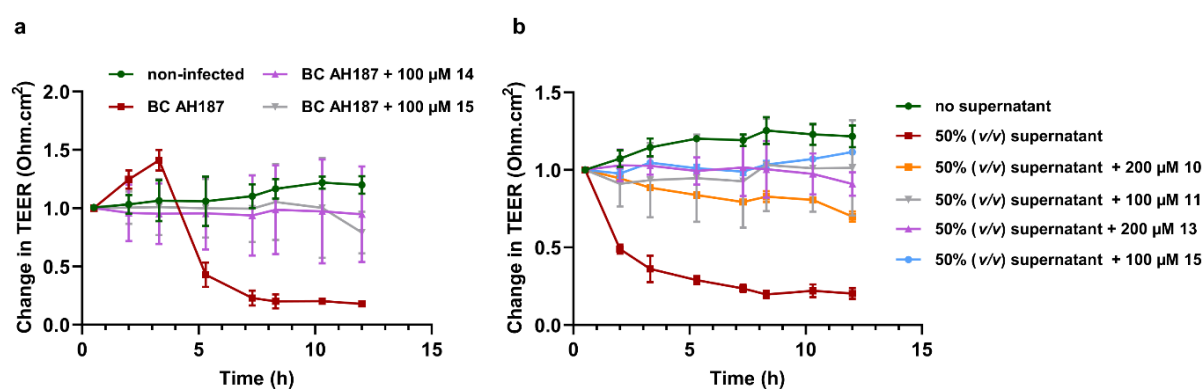


Figure 7. The change in the transepithelial electrical resistance (TEER) of the Madin–Darby Canine Kidney (MDCK) cells challenged with *Bacillus cereus* or 50% (v/v) culture supernatant. **a)** 14 and 15 preserve the TEER value of the MDCK infected with *B. cereus* compared with the non-treated conditions with inhibitor. **b)** Compounds 10, 13, 14, and 15 maintained the TEER of MDCK cells challenged with *B. cereus* supernatant. Each curve represents average \pm standard deviation of at least three independent experiments.

Compounds do not interfere with *B. cereus* growth. The aim of this work was to develop antivirulence agent that prevent bacteria from causing damage rather than killing them.^[3] Therefore, we tested the compounds on *B. cereus* growth to rule out antibacterial activity and ensure that the effects shown in the *in vitro* infection models were not caused by influencing bacterial viability. For this purpose, we selected the most potent compounds and tested them against the BC AH187 strain. As shown in **Table S5**, compound had no effect on BC AH187 growth and their minimum inhibitory concentration (MIC) was >200 μ M or >100 μ M. These data support that the antivirulence activity, not an antibacterial activity, was responsible for the observed effect in the infection experiments.

ColQ1 inhibitors maintain the survival of *G. mellonella* larvae. Finally, we evaluated selected compounds in an *in vivo* infection model. *G. mellonella* larvae are one of the most frequently used models to evaluate effectiveness of newly discovered inhibitors and is well established for assessing *B. cereus* cytotoxicity.^[40] We reported previously that treating the *G. mellonella* larvae with ColQ1 caused larvae death.^[24] We established *B. cereus* infection of *G. mellonella* by injecting BC AH187 strain into the larvae in presence or absence of our

compound. The larvae were incubated at 37 °C throughout the experiment and the larvae survival was monitored twice a day. Three synthesized inhibitors and two FDA-approved drugs were tested. Compounds **13**, **14**, **15**, **tiludronate disodium** and **alendronate sodium** ameliorated the survival of the larvae in a dose-dependent manner when compared to a control where no inhibitor was administered. At 100 μM , compounds **14** and **15** boosted the survival by around 50% and 35%, respectively. At lower concentration (*i.e.*, 25 μM), both had a reduced effect (**Figures 8 & S16**). Compounds **tiludronate disodium** and **alendronate sodium** increased the survival by 40% at 100 and 200 μM , respectively (**Figure S16**). A concentration of 200 μM of **13** showed the highest effect, increasing the survival by about 35% while 50 μM showed the smallest effect and only improved survival by 5% (**Figure S16**). Overall, the data revealed the protective effect of the collagenase inhibition during *B. cereus* infection. As a result, these antivirulence compounds may be evaluated as a promising therapeutic agents in the future.

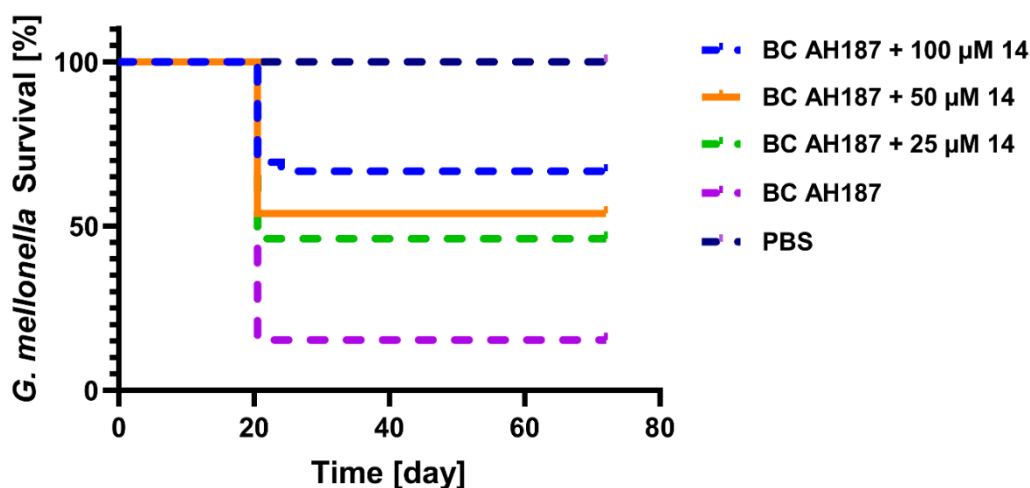


Figure 8. Survival analysis of *Galleria mellonella* larvae treated with *Bacillus cereus* AH187 strain with and without **14**. Each curve represents results of three independent experiments, statistical difference between groups treated with 100, 50, and 25 μM of compound **14** and *B. cereus* AH187 and with group treated only with *B. cereus* AH187 is $p < 0.0001$, $p = 0.0039$ and $p = 0.0173$, respectively, (log-rank test). The survival rate for the larvae treated with compound **14** in PBS was 100%.

Conclusions

To tackle the antibiotic resistance crisis, alternative, non-antibiotic therapies are urgently needed. One potential approach is the use of antivirulence agents, which inhibit the pathogenicity factors of bacteria and thus prevent or delay infection without exerting selective pressure. Bacterial collagenases are one of the antivirulence targets that are currently gaining wide attention. In this study, we identified two classes of inhibitors (synthesized and FDA-

approved diphosphonates and hydroxamates) that target clostridial and bacillary collagenases. Among these compounds **13**, **14**, **15**, **tiludronate disodium** and **alendronate sodium** of the diphosphonate class and **27** and **33** of the hydroxamate class displayed high and broad-spectrum *in vitro* inhibition of clostridial collagenases ColH, ColA, and on bacillary collagenases ColA and ColQ1. Furthermore, the majority of them demonstrated adequate selectivity over human MMPs and other off-targets. These compounds also showed no cytotoxicity in four human cell lines. We also studied the biological effect of these compounds in infection models where *B. cereus* was used as a representative bacterium-producing collagenases. In this context, we developed fibroblast- and epithelial-cell infection models to characterize the effect of *B. cereus* collagenases and their inhibition. Our findings suggest that the inhibition of *B. cereus* collagenases by the most potent diphosphonate compounds maintain the fibroblast cell attachment, cell morphology, cell viability, preserved the fibrillar collagen content, and sustained the TEER of epithelial cells. We also tested the compound *in vivo* in the *G. mellonella* larvae infection model, where the compounds enhanced the survival rate. The hydroxamates did not display any inhibition in the infection models, however, they showed similar potency as diphosphonates in the enzyme cleavage assays. This could be explained by their reversible binding mode, which we determined on clostridial and bacillary collagenases. In contrast, the most active diphosphonate demonstrated high potency in both enzyme assays and infection models which might be due to their slow to very slow dissociation binding with *B. cereus* collagenases. These findings offer insight on the role of bacterial collagenases in infections and on the significance of their inhibition with small-molecule inhibitors, which might represent a potential treatment strategy in the future.

Materials and methods

Chemistry for the diphosphonate compounds. Chemistry for the diphosphonate compounds. Chemical names follow the IUPAC nomenclature. Starting materials were purchased from Chempur, Aldrich, Acros, Combi-Blocks or Fluorochem and were used without purification. Column chromatography was performed using the automated flash chromatography system Combiflash Rf+ (Teledyne Isco) equipped with RediSepRf silica columns. Final products were dried in high vacuum. ^1H NMR and ^{13}C NMR-spectra were measured on a Bruker AM500 spectrometer (at 500 MHz and 125MHz, respectively) at 300 K and on a Bruker Fourier 300 (at 300 MHz and 75 MHz, respectively) at 300 K. Chemical shifts are reported in δ (parts per million: ppm), by reference to the hydrogenated residues of deuterated solvent as internal standard: 2.05 ppm (^1H NMR), 29.8, and 206.3 ppm (^{13}C NMR) for acetone- d_6 , 2.50 ppm (^1H NMR) and 39.52 ppm (^{13}C NMR) for DMSO- d_6 . Signals are described as br (broad), s (singlet),

d (doublet), t (triplet), dd (doublet of doublets), ddd (doublet of doublet of doublets), dt (doublet of triplets) and m (multiplet). All coupling constants (J) are given in Hertz (Hz). Mass spectrometry was performed on a TSQ Quantum (ThermoFisher, Dreieich, Germany). The triple quadrupole mass spectrometer was equipped with an electrospray interface (ESI). Purity of compounds was determined by LC-MS using the area percentage method on the UV trace recorded at a wavelength of 254 nm and found to be > 95%. The Surveyor-LC-system consisted of a pump, an auto sampler, and a PDA detector. The system was operated by the standard software Xcalibur. An RP C18 NUCLEODUR 100-5 (3 mm) column (Macherey-Nagel GmbH) was used as stationary phase. All solvents were HPLC-grade. In a gradient run, using acetonitrile and water the percentage of acetonitrile (containing 0.1% trifluoroacetic acid) was increased from an initial concentration of 0% at 0 min to 100% at 13 min and kept at 100% for 2 min. The injection volume was 15 μ L and the flow rate was set to 800 μ L/min. MS analysis was carried out at a needle voltage of 3000 V and a capillary temperature of 350 °C. Mass spectra were acquired in positive mode, using an electron spray ionization method, from 100 to 1000 m/z and UV spectra were recorded at the wave length of 254 nm and in some cases at 360 nm. High-resolution mass spectrometry (HRMS) measurements were recorded on a SpectraSystems-MSQ LC-MS system (Thermo Fisher).

General procedure A: preparation of 1,4-dihydro-2,3-quinoxalinedione derivatives 7a–14a and 15b

A mixture of 1,2-phenyldiamine derivative (1 eq.) and oxalic acid (1.2 eq.) was refluxed in 4 N HCl (20 mL) for 6 h, cooled to RT, poured over ice, and filtered. The product was washed with water and dried to give the titled compound. The product was used in the next step without further purification.

General procedure B: preparation of 2,3-dichloroquinoxaline derivatives 7b–14b and 15c

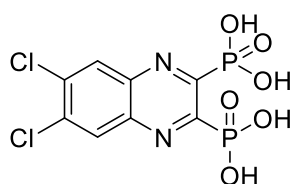
A mixture of 1,4-dihydro-2,3-quinoxalinediones **7a–14a**, and **15b** (2 mmol) and POCl₃ (10 mL) was stirred at 50 °C in DMF for 2 h, cooled to RT, poured over ice, and filtered. The product was washed with water and dried to give the title compound. The product was used in the next step without additional purification.

General procedure C: preparation of diethyl phosphonate derivatives 7c–13c, 14d, 15d, and 16b

2,3-dichloroquinoxaline derivatives **7b–14b**, **15c**, and **16a** (1 eq) was suspended in triethyl phosphite (10 eq) and heated to 150 °C in a sealed tube for 18 h. Most of unreacted triethyl phosphite was evaporated *in vacuo* and the resultant oil was purified by column chromatography.

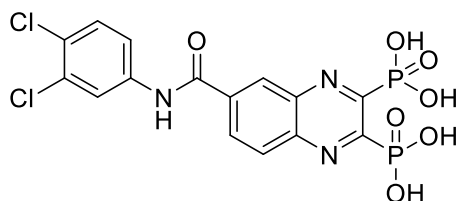
General procedure D: preparation of phosphonic acid derivatives 7–16

To a solution of diethyl phosphonate (1 eq) in dry DCM, bromotrimethylsilane (10 eq) was added dropwise over a period of 15 min. The reaction mixture was stirred at RT overnight. Then MeOH was added and stirred at RT for 30 min. Solvents were concentrated *in vacuo* and the resultant oil was purified by preparative HPLC.

(6,7-Dichloroquinoxaline-2,3-diyl)bis(phosphonic acid) (13) Compound **13** was synthesized

according to general procedure D, using tetraethyl (6,7-dichloroquinoxaline-2,3-diyl)bis(phosphonate) **13c** (80 mg, 0.17 mmol), bromotrimethylsilane (222 μ L, 1.7 mmol) and DCM (15 mL). The reaction was stirred at RT overnight. The crude product

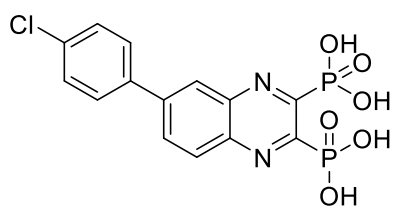
was purified using preparative HPLC (CH₃CN (HCOOH 0.05 %)/H₂O (HCOOH 0.05 %) = 0.2:9.8 to 10:0). The product was obtained as white solid (39 mg, 65%). ¹H NMR (500 MHz, DMSO) δ 8.51 (s, 2H). ¹³C NMR (126 MHz, DMSO) δ 155.1 (dd, J_{C-P} = 199.4, 29.9 Hz), 139.6 (dd, J_{C-P} = 19.9, 3.9 Hz), 135.6, 130.6. ³¹P NMR (202 MHz, DMSO) δ 4.49. HRMS (ESI⁻) calculated for C₈H₅Cl₂N₂O₆P₂ [M-H]⁻ 356.90054, found 356.90056.

(6-((3,4-Dichlorophenyl)carbamoyl)quinoxaline-2,3-diyl)bis(phosphonic acid) (14).

Compound **14** was synthesized according to general procedure D, using tetraethyl (6-((3,4-dichlorophenyl)carbamoyl)quinoxaline-2,3-diyl)bis(phosphonate) **14d** (100 mg, 0.17 mmol),

bromotrimethylsilane (222 μ L, 1.7 mmol) and DCM (15 mL). The reaction was stirred at RT overnight. The crude product was purified using preparative HPLC (CH₃CN (HCOOH 0.05 %)/H₂O (HCOOH 0.05 %) = 0.2:9.8 to 10:0). The product was obtained as a white solid (43 mg, 53%). ¹H NMR (500 MHz, DMSO) δ 10.99 (s, 1H), 8.87 (d, J = 1.8 Hz, 1H), 8.45 (dd, J = 8.8, 1.9 Hz, 1H), 8.33 (d, J = 8.8 Hz, 1H), 8.25 (d, J = 2.4 Hz, 1H), 7.84 (dd, J = 8.8, 2.4 Hz, 1H), 7.68 (d, J = 8.8 Hz, 1H). ¹³C NMR (126 MHz, DMSO) δ 164.9, 155.7 (dd, J_{C-P} = 70.9, 29.7 Hz), 154.1 (dd, J_{C-P} = 71.9, 30.0 Hz), 141.8 (dd, J_{C-P} = 18.3, 2.7 Hz), 139.9 (dd, J_{C-P} = 18.4, 2.6 Hz), 139.5, 137.3, 131.4, 131.3, 131.2, 130.1, 129.3, 126.0, 122.0, 120.9. ³¹P NMR (202 MHz, DMSO) δ 4.95 (d, J = 4.8 Hz), 4.71 (d, J = 6.0 Hz). HRMS (ESI⁻) calculated for C₁₅H₁₀Cl₂N₃O₇P₂ [M-H]⁻ 475.93765, found 475.93766.

(6-(4-Chlorophenyl)quinoxaline-2,3-diyl)bis(phosphonic acid) (15). Compound **15** was



synthesized according to general procedure D, using tetraethyl (6-(4-chlorophenyl)quinoxaline-2,3-diyl)bis(phosphonate) **15d** (70 mg, 0.13 mmol), bromotrimethylsilane (170 μ L, 1.3 mmol) and DCM (15 mL).

The reaction was stirred at RT overnight. The crude product was purified using preparative HPLC (CH₃CN (HCOOH 0.05 %)/H₂O (HCOOH 0.05 %) = 0.2:9.8 to 10:0). The product was obtained as a white solid (24 mg, 44%). ¹H NMR (500 MHz, DMSO) δ 8.45 (d, J = 1.9 Hz, 1H), 8.37 (dd, J = 8.8, 2.0 Hz, 1H), 8.29 (d, J = 8.8 Hz, 1H), 8.04 – 7.96 (m, 2H), 7.67 – 7.59 (m, 2H). ¹³C NMR (126 MHz, DMSO) δ 154.5 (dd, J_{C-P} = 88.9, 30.6 Hz), 152.9 (dd, J_{C-P} = 89.0, 29.9 Hz), 142.8, 140.9 (dd, J_{C-P} = 20.3, 5.2 Hz), 140.1 (dd, J_{C-P} = 20.4, 5.1 Hz), 137.4, 134.3, 131.9, 130.3, 129.9, 129.7, 126.5. ³¹P NMR (202 MHz, DMSO) δ 5.31, 5.27. HRMS (ESI⁻) calculated for C₁₄H₁₀ClN₂O₆P₂ [M-H]⁻ 398.97081, found 398.97078.

Expression and purification of ColQ1, ColA, ColH, and ColG. The collagenases were produced and purified as previously described.^[16]

In vitro FRET-based proteolytic assay (ColQ1, ColA, ColG, and ColH). For all targets, the percent of inhibition and IC₅₀ measurements were carried out as previously described.^{16,21,22} Experiments were performed in triplicate, and the results are provided as means \pm standard deviation. For the determination of the inhibition constant (K_i), similar assay conditions were chosen. However, nominal final enzyme concentrations of 1 nM ColQ1-CU, 10 nM ColH-PD, 35 nM ColA, 60 nM ColG were used and the reactions were monitored for 2 min 24 s. Regression analysis was performed using GraphPad Prism v 9.0.0 (Graph Pad Software, San Diego, CA, USA). The experiments were performed under first-order conditions ($[S_0] \ll K_M$), which resulted in an approximation of the K_i^{app} to the true inhibition constant (K_i), therefore, the results are reported as K_i values.

Reversibility assays by rapid dilution. The recovery of enzymatic activity after a rapid large dilution was performed following Copeland, 2013.^[28] In short, ColA, ColG, ColH, and ColQ1 were incubated for 30 min at 100-fold the concentration required for the activity assay (*i.e.*, 4.375 μ M, 7.500 μ M, 1.250 μ M and 0.125 μ M, respectively) with a concentration of inhibitor equivalent to 10-fold the IC₅₀. The mixture was then diluted 100-fold into the reaction buffer. The reaction was immediately initiated by addition of the quenched-fluorescent substrate FS1-1 at a final concentration of 2 μ M. The reaction was monitored for 2 min (excitation: 328 nm, emission: 392 nm) at 25 °C in an Infinite M200 plate reader (Tecan, Grödig, Austria).

Selectivity toward human MMPs. The MMPs inhibition assay (Sigma-Aldrich, Saint Louis, MO) was performed as previously reported and in accordance with the manufacturer's instructions. The Fluorescence signals were measured in a CLARIOstar plate reader (BMG LABTECH, Ortenberg, Germany) at a concentration of 100 μ M.

Compound toxicity. Cytotoxicity assays on HepG2, HEK293, NHDF, and MDCK cells were carried out as described previously.^[21]

***In vitro* collagen cleavage assay.** The experiments were done as described before.^[16,24] Briefly, in a buffer containing 250 mM HEPES, 150 mM NaCl, 5 mM CaCl₂, 5 μ M ZnCl₂, pH 7.5, 1 mg/mL acid-soluble type I collagen from bovine tail (Thermo Fischer Scientific) was incubated with 50 ng full length ColQ1. Compounds were evaluated at various concentrations, and incubated together with collagen, and ColQ1 at 25 °C for 3 h. After stopping the reaction with 50 mM EDTA, the mixture was loaded on 12% SDS-PAGE gel and stained with colloidal coomassie G-250 stainer.^[41] Two separate experiments were carried out for each compound.

***In vitro* NHDF infection model.** A number of NHDF (Promo Cell C-12302) 1×10^5 cells/well were seeded in 24-well plates (Greiner) with DMEM medium (Gibco) containing 10% (v/v) fetal calf serum (FCS, Gibco) and 1% (v/v) glutamine (Gibco). Prior to the treatment, the cells were cultured at 37 °C for 24 h with 5% CO₂. In brain heart infusion (BHI) medium, *B. cereus* AH187 bacteria were cultivated to a mid-exponential phase. The culture was centrifuged at 4,000 x g for 7 min at RT before being rinsed and diluted in PBS. Then, *B. cereus* suspension was added on the cells to give an MOI (multiplicity of infection) of 0.03. Before the infection, cells were starved for 1 h with DMEM containing only 1% (v/v) glutamine and no FCS. The cells were infected with *B. cereus* for 1, 2, 4, and 6 h to examine the kinetics of collagenase release. The DMEM supernatant was collected and harvested by centrifugation at 4,000 x g at 4 °C for 10 min. After the cells were washed, they were lysed using a lysis buffer (20 mM Tris pH 7.5, 1 mM EDTA, 100 mM NaCl, 1% Triton 100, 0.5% Na-deoxycholat, 0.1 % SDS, 1 x PIT, 1 mM Na₃VO₄, 1 mM Na-molybdate, 20 mM NaF, 20 mM β -glycerophosphate). Cell debris was removed by centrifugation with 12,000 x g at 4 °C for 10 min. The DMEM supernatants and cell lysates were stored at -80 °C for further investigation. The cell morphology was monitored with a light microscope (Olympus) using 20X objective. The kinetic study was performed in three independent experiments. To study the behavior of ColQ1 inhibitors in this model, the experiment was done as stated above with a few changes, the compounds were added to the NHDF cells along with the bacterial suspension, and all incubated

at 37 °C for 5 h and 5% CO₂. Two controls were considered in each experiment, uninfected cells, and infected cells without inhibitor. Each experiment was repeated three times in total.

Non-reducing sodium dodecyl sulfate polyacrylamide gel electrophoresis and zymography. To perform the zymography, we collected supernatants from the NHDF infection experiments and mixed them with 1% non-reducing loading buffer. They were then electrophoretically separated after loading onto 10% SDS-PAGE gels containing 0.1% gelatin (Roth, Karlsruhe, Germany). Following separation, the gel was incubated at 4 °C for 2x 30 min with gentle agitation in a renaturation buffer (50 mM HEPES pH 7.5, 200 mM NaCl, 10 mM CaCl₂, 10 μM ZnCl₂, 2.5% Triton X-100). The gel was then treated in a developing buffer (50 mM HEPES pH 7.5, 200 mM NaCl, 10 mM CaCl₂, 10 μM ZnCl₂, 0.02% Brij-35) at 37 °C overnight. By staining the gel with 0.1% Coomassie brilliant blue R-250 dye overnight, transparent bands of gelatinolytic activity could be seen. The ChemiDoc XRS+ imaging system (Biorad, USA) was used to scan the gels and image analysis was performed with software (Li-Cor Biosciences, USA).

Reducing sodium dodecyl sulfate polyacrylamide gel electrophoresis. The cell lysate was placed onto a 12% SDS-PAGE gel with a similar total protein content and stained overnight with Coomassie brilliant blue G-250. The gel was then visualized with ChemiDoc XRS+ imaging system (Biorad, USA) and the signal analysis was exerted with Image lab software.

Picrosirius red assay. After infection, the NHDF cells were washed 3 x with PBS and then incubated with Bouin solution (Sigma) at RT for 20 min. The cells were incubated with 0.1% Picrosirius red dye (ab150681) at RT for 2 h. Then, they were washed 1 x with 0.01 N HCl and the matrix was dissolved in 0.01 N NaOH. The absorption was measured at 570 nm using a Tecan Infinite M200 plate reader (Tecan, Grödig, Austria). By dividing the absorbance of each sample by the absorbance of the healthy sample, the relative collagen quantity was determined. For each condition, the experiment was performed three times.

Lactate dehydrogenase (LDH) release assay. The manufacturer's procedure was followed to measure the released LDH amount in the supernatant of NHDF cells. Briefly, in a 96-well plate (Grenier), 50 μL of the supernatant were combined with 50 μL substrate. The plate was incubated at RT for 30 min in the dark then the reaction was stopped with 50 μL of the stop solution. The absorbance was measured at 490 nm with a Tecan Infinite M200 plate reader (Tecan, Grödig, Austria). The cytotoxicity was calculated in relative to the control (no inhibitor).

Stability of 27 with LC-MS. A concentration of 200 μM of compound **27** was incubated with DMEM medium at 37 °C for 5 h and 5% CO₂. After the incubation, 2 μL of the compound were

transferred to LC-MS vials containing 200 μ L acetonitrile and LC-MS spectra were measured. Three controls were included i) **27** in DME0 ii) **27** in DMEM without incubation iii) DMEM medium.

Transepithelial electric resistance (TEER) experiment. MDCK cells were seeded at a density of 3×10^4 cells/mL onto a Millipore hanging cell culture insert at 37 °C for 12 days with 5% CO₂. On day 5, the medium was changed. Prior to treatment, the cells were starved for 16 h in FCS free RPMI medium (Gibco). The bacteria or bacterial free supernatant were prepared, the bacteria used at MOI of 0.03 while 50% (v/v) supernatant was added. The ColQ1 inhibitors were added into the inner compartment. The TEER of the cells was measured with Millicell ERS-2 (Electrical Resistance System) over time. Three readings were recorded for each well, and the unit area resistance (UAR) was calculated using the mean values of the TEER following the equation below:

$$UAR \text{ [}[\Omega * \text{cm}^2] = (\Omega_{monolayer} - \Omega_{blank}) * \text{effective membrane area}$$

Changes in TEER were normalized to the initial UAR (t = 0), which was set to 100%.

B. cereus supernatant production. *B. cereus* AH187 strain was cultured in FCS-free DMEM medium at 37 °C. The supernatant was harvested by centrifugation and kept in –80 °C until needed. The supernatant was sterile-filtered with a 0.22 μ m filter (Greiner).

B. cereus growth inhibition assay. The effect of the compounds on *B. cereus* growth was carried out by growing the bacteria in BHI medium until the mid-growth phase. Next, the bacterial suspension was diluted until OD_{600 nm} was 0.2 and combined with compounds in a 96-well plate. The plates were subsequently incubated at 37 °C for 48 h in a Tecan Infinite M200 plate reader (Tecan, Grödig, Austria). The MIC values presented are the average of at least two independent determinations.

In vivo Galleria mellonella infection model. *G. mellonella* larvae were purchased from a fishing store. Injections were carried out using a LA120 syringe pump (Landgraf Laborsysteme, Langenhagen, Germany) equipped with 1 mL Injekt-F tuberculin syringes (B. Braun, Melsungen, Germany) and Sterican 0.30×12 mm, 30G×1.5 needles (B. Braun). The larvae were divided into five groups depending on their treatment: i) Sterile PBS ii) no injection iii) only compound iv) BC AH187 bacterial suspension v) BC AH187 bacterial suspension with compound. Larvae were incubated at 37 °C for 3 days and inspected twice daily. The total larvae used in all three experiments were 40 larvae per group. When the larvae became black and did not move when simulated with a tweezer, they were deemed dead.

Crystallization, X-ray data collection and analysis. Crystals of ColG-PD were grown in 0.1 M Tris-Bicine pH 8.5, 0.04 M pentaethylene glycol, 0.04 M diethylene glycol, 0.04 M

triethylene glycol, 0.04 M tetraethylene glycol, 10% (w/v) polyethylene glycol 20,000 and 20% (v/v) polyethylene glycol 550 monomethyl ether in sitting-vapor diffusion plates. Crystals were soaked with 10 mM **27** and **13** for 2 weeks. The crystals were cryoprotected with MiTeGen LV Cryo-oil (MiTeGen, Ithaca, NY) and immediately flash-frozen in liquid nitrogen. X-ray diffraction data were collected on beamline ID30B-at the European Synchrotron Radiation Facility (ESRF) in Grenoble, France. The data sets were indexed, integrated and scaled using XDS^[42] and AIMLESS.^[43] Molecular replacement was performed with PHASER^[44] using as search model PDB entry 2y6i (ligand and activator domain deleted). Ligand coordinates and restraints were generated using the Grade Web Server.^[45] Final structures were obtained using PHENIX^[46] together with model building in WinCoot.^[47] PyMOL v 4.0.0 was used for figure generation (The PyMOL Molecular Graphics System, Version 4.0.0 Schrödinger, LLC). The final refined structures will be deposited in the Protein Data Bank (PDB) before the submission. Data collection and refinement statistics are listed in **Table S2**.

Statistical analysis. Graphical data in the manuscript are presented as the means \pm SDs. Statistical comparisons are performed by Tukey one-way ANOVA test, which shows significant differences between conditions. Parametric/non-parametric statistical analysis used in the study were based on normality and homogeneity of variance. A value of $p \leq 0.001$ was considered statistically significant while $p > 0.05$ was considered non-significant. The normalized measurements were statistically compared between treated and non-treated groups using generalized estimating equations model to account for correlated data arising from repeated measures. The survival of *G. mellonella* was computed using the Kaplan–Meier method and log-rank test was applied to calculate the significance of differences between conditions.

References

1. WHO (World Health Organization). Antibiotic resistance. (2020). Available at: <https://www.who.int/news-room/fact-sheets/detail/antibiotic-resistance>.
2. WHO (World Health Organization). No Time to Wait: Securing the Future from Drug-Resistant Infections. Available at: https://www.who.int/docs/default-source/documents/no-time-to-wait-securing-the-future-from-drug-resistant-infections-en.pdf?sfvrsn=5b424d7_6.
3. Vale, P. F., Fenton, A. & Brown, S. P. Limiting Damage during Infection: Lessons from Infection Tolerance for Novel Therapeutics. *PLoS Biol.* 12, (2014).
4. Allen, R. C., Popat, R., Diggle, S. P. & Brown, S. P. Targeting virulence: Can we make evolution-proof drugs? *Nat. Rev. Microbiol.* 12, 300–308 (2014).
5. Bottone, E. J. *Bacillus cereus*, a volatile human pathogen. *Clin. Microbiol. Rev.* 23, 382–398 (2010).
6. MACLENNAN, J. D. The histotoxic clostridial infections of man. *Bacteriol. Rev.* 26, 177–276 (1962).
7. JW., P. Bacterial pathogenesis. in *Medical Microbiology: 4th edition* (1996).
8. Zhang, Y. Z., Ran, L. Y., Li, C. Y. & Chen, X. L. Diversity, structures, and collagen-degrading mechanisms of bacterial collagenolytic proteases. *Appl. Environ. Microbiol.* 81, 6098–6107 (2015).
9. Duarte, A. S., Correia, A. & Esteves, A. C. Bacterial collagenases - A review. *Crit. Rev. Microbiol.* 42, 106–126 (2016).
10. Harrington, D. J. Bacterial Collagenases and Collagen-Degrading Enzymes and Their Potential Role in Human Disease. 64, 1885–1891 (1996).
11. Bauer, R. *et al.* Structural comparison of ColH and ColG collagen-binding domains from *Clostridium histolyticum*. *J. Bacteriol.* 195, 318–327 (2013).
12. Eckhard, U. *et al.* Biochemical characterization of the catalytic domains of three different clostridial collagenases. *Biol. Chem.* 390, 11–18 (2009).
13. Eckhard, U., Schönauer, E., Nüss, D. & Brandstetter, H. Structure of collagenase G reveals a chew-and-digest mechanism of bacterial collagenolysis. *Nat. Struct. Mol. Biol.* 18, 1109–1114 (2010).
14. Matsushita, O., Koide, T., Kobayashi, R., Nagata, K. & Okabe, A. Substrate Recognition by the Collagen-binding Domain of *Clostridium histolyticum* Class I Collagenase. *J. Biol. Chem.* 276, 8761–8770 (2001).
15. Abfalter, C. M. *et al.* Cloning, Purification and Characterization of the Collagenase ColA Expressed by *Bacillus cereus* ATCC 14579. *PLoS One* 11, 1–19 (2016).
16. Hoppe, I. J., Brandstetter, H. & Schönauer, E. Biochemical characterisation of a collagenase from *Bacillus cereus* strain Q1. *Sci. Rep.* 11, 1–15 (2021).
17. Eckhard, U., Schönauer, E. & Brandstetter, H. Structural Basis for Activity Regulation and Substrate Preference of Clostridial Collagenases G, H, and T * □. 288, 20184–20194 (2013).
18. Oshima, N., Narukawa, Y., Takeda, T. & Kiuchi, F. Collagenase inhibitors from *Viola yedoensis*. *J. Nat. Med.* 67, 240–245 (2013).
19. Scozzafava, A. & Supuran, C. T. Protease inhibitors: Synthesis of matrix metalloproteinase and bacterial collagenase inhibitors incorporating 5-amino-2-mercapto-1,3,4-thiadiazole zinc binding functions. *Bioorganic Med. Chem. Lett.* 12, 2667–2672 (2002).
20. Scozzafava, A. & Supuran, C. T. Protease inhibitors: Synthesis of matrix metalloproteinase and bacterial collagenase inhibitors incorporating 5-amino-2-mercapto-1,3,4-thiadiazole zinc binding functions.

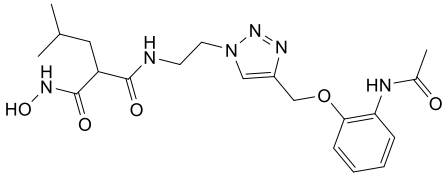
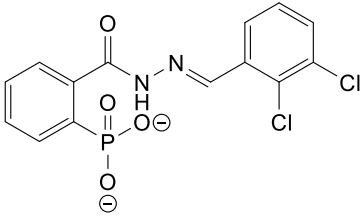
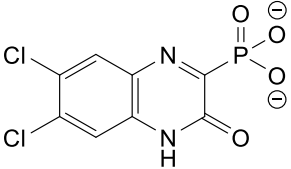
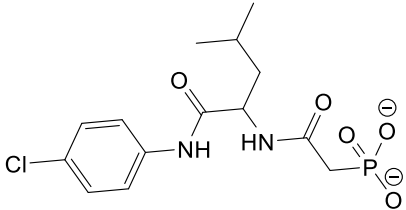
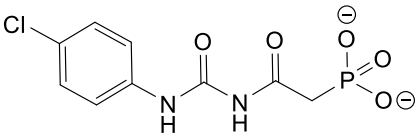
- Bioorganic Med. Chem. Lett.* 12, 2667–2672 (2000).
21. Schönauer, E. *et al.* Discovery of a Potent Inhibitor Class with High Selectivity toward Clostridial Collagenases. *J. Am. Chem. Soc.* 139, 12696–12703 (2017).
 22. Konstantinović, J. *et al.* N-Aryl-3-mercaptosuccinimides as Antivirulence Agents Targeting *Pseudomonas aeruginosa* Elastase and *Clostridium* Collagenases. *J. Med. Chem.* 63, 8359–8368 (2020).
 23. Voos, K. *et al.* Phosphonate as a Stable Zinc-Binding Group for “Pathoblocker” Inhibitors of Clostridial Collagenase H (ColH). *ChemMedChem* 1–12 (2021). doi:10.1002/cmdc.202000994
 24. Alhayek, A. *et al.* Inhibition of Collagenase Q1 of *Bacillus cereus* as a Novel Antivirulence Strategy for the Treatment of Skin-Wound Infections. *Adv. Ther.* 2100222 (2022). doi:10.1002/adtp.202100222
 25. Zhang, P.-M. *et al.* A One-pot Facile Synthesis of 2,3-Dihydroxyquinoxaline and 2,3-Dichloroquinoxaline Derivatives Using Silica Gel as an Efficient Catalyst. *J. Heterocycl. Chem.* 55, 1809–1814 (2018).
 26. Yang, Y. *et al.* An Efficient Synthesis of Quinoxalinone Derivatives as Potent Inhibitors of Aldose Reductase. *ChemMedChem* 7, 823–835 (2012).
 27. Rangarajan, M. *et al.* Topoisomerase I inhibition and cytotoxicity of 5-Bromo- and 5-Phenylterbenzimidazoles. *Bioorg. Med. Chem.* 8, 2591–2600 (2000).
 28. Lozano-Calderon, S. A., Colman, M. W., Raskin, K. A., Hornicek, F. J. & Gebhardt, M. Use of Bisphosphonates in Orthopedic Surgery. *Orthop. Clin. North Am.* 45, 403–416 (2014).
 29. Goos, M. ADAM-17: the enzyme that does it all. *Crit. Rev. Biochem. Mol. Biol.* 45, 146–169 (2010).
 30. Ropero, S. & Esteller, M. The role of histone deacetylases (HDACs) in human cancer. *Mol. Oncol.* 1, 19–25 (2007).
 31. Gelse, K., Pöschl, E. & Aigner, T. Collagens - Structure, function, and biosynthesis. *Adv. Drug Deliv. Rev.* 55, 1531–1546 (2003).
 32. Healing, W. The fibroblast. 60, 778–782 (1967).
 33. Lattouf, R. *et al.* Picrosirius Red Staining: A Useful Tool to Appraise Collagen Networks in Normal and Pathological Tissues. *J. Histochem. Cytochem.* 62, 751–758 (2014).
 34. Junqueira, L. C. U., Cossermelli, W. & Brentani, R. Differential Staining of Collagens Type I, II and III by Sirius Red and Polarization Microscopy. *Arch. Histol. Jpn.* 41, 267–274 (1978).
 35. Das C, Lucia MS, H. K. and T. J. Quantification of lactate dehydrogenase for cell viability testing using cell lines and primary cultured astrocytes. *Physiol. Behav.* 176, 139–148 (2017).
 36. Lindbäck, T. *et al.* Cytotoxicity of the *Bacillus cereus* Nhe enterotoxin requires specific binding order of its three exoprotein components. *Infect. Immun.* 78, 3813–3821 (2010).
 37. Tausch, F. *et al.* Evidence for complex formation of the *Bacillus cereus* haemolysin BL components in solution. *Toxins (Basel)*. 9, 1–18 (2017).
 38. Chen, S., Einspanier, R. & Schoen, J. Transepithelial electrical resistance (TEER): a functional parameter to monitor the quality of oviduct epithelial cells cultured on filter supports. *Histochem. Cell Biol.* 144, 509–515 (2015).
 39. Shuler, L. & Hickman, J. J. *TEER measurement techniques for in vitro barrier model systems. Journal of Laboratory Automation* 20, (2016).
 40. Ramarao, N., Nielsen-Leroux, C. & Lereclus, D. The Insect *Galleria mellonella* as a Powerful Infection Model to Investigate Bacterial Pathogenesis. *J. Vis. Exp.* 1–7 (2012). doi:10.3791/4392

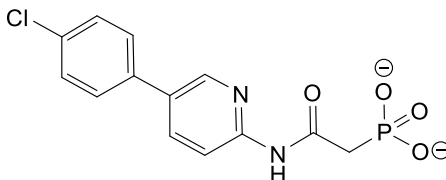
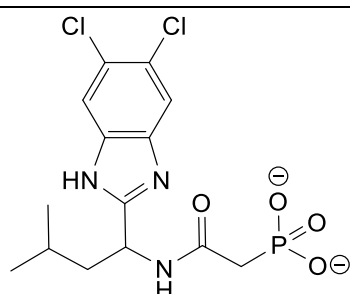
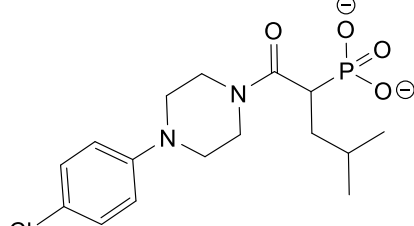
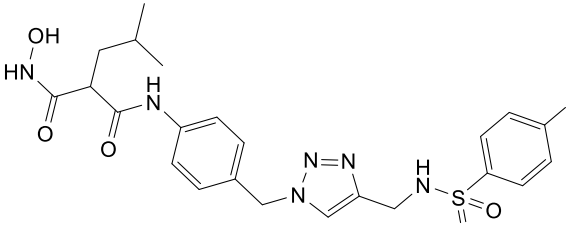
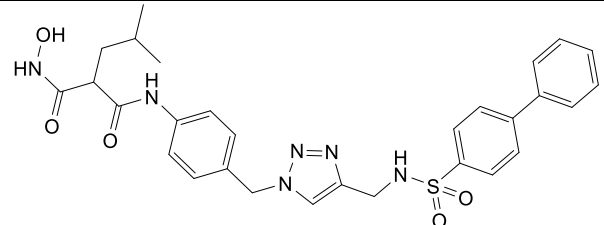
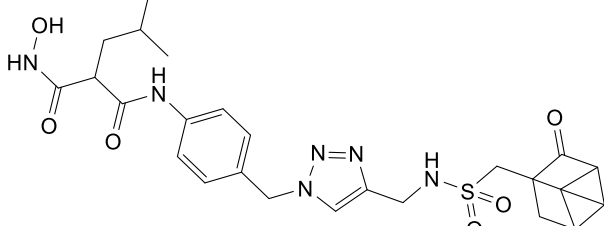
41. Dyballa, N. & Metzger, S. Fast and sensitive colloidal Coomassie G-250 staining for proteins in polyacrylamide gels. *J. Vis. Exp.* 2–5 (2009). doi:10.3791/1431
42. Kabsch, W. XDS. *Acta Crystallogr. Sect. D Biol. Crystallogr.* 66, 125–132 (2010).
43. Evans, P. R. & Murshudov, G. N. How good are my data and what is the resolution? *Acta Crystallogr. Sect. D Biol. Crystallogr.* 69, 1204–1214 (2013).
44. McCoy, A. J. Solving structures of protein complexes by molecular replacement with Phaser. *Acta Crystallogr. Sect. D Biol. Crystallogr.* 63, 32–41 (2007).
45. Smart, O. S. *et al.* Exploiting structure similarity in refinement: automated NCS and target-structure restraints in BUSTER. *Acta Crystallogr. Sect. D Biol. Crystallogr.* 68, 368–380 (2012).
46. Adams, P. D. *et al.* PHENIX: a comprehensive Python-based system for macromolecular structure solution. *Acta Crystallogr. Sect. D Biol. Crystallogr.* 66, 213–221 (2010).
47. Emsley, P., Lohkamp, B., Scott, W. G. & Cowtan, K. Features and development of Coot. *Acta Crystallogr. Sect. D Biol. Crystallogr.* 66, 486–501 (2010).

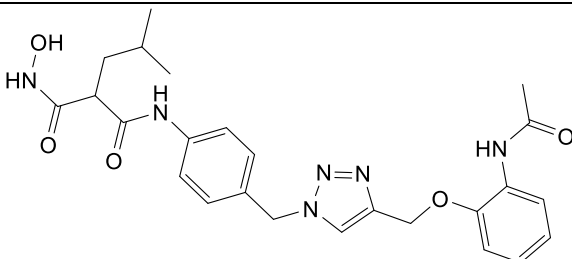
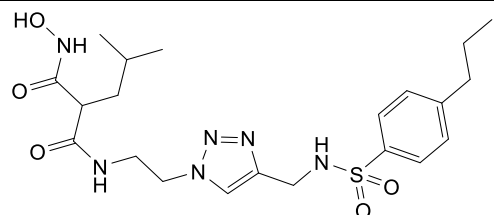
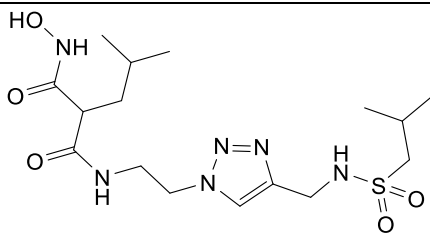
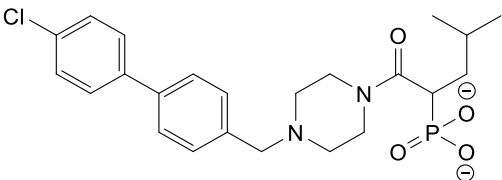
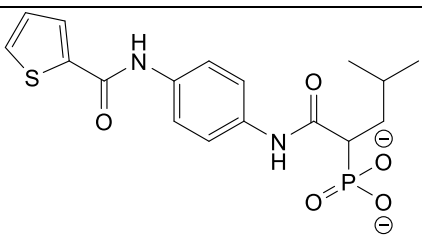
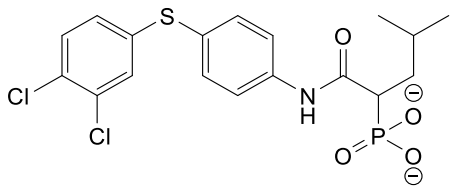
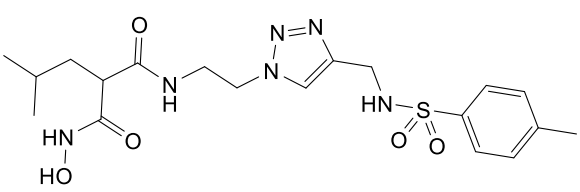
2.4.1 Supporting information

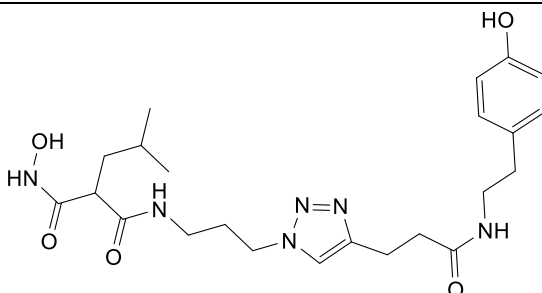
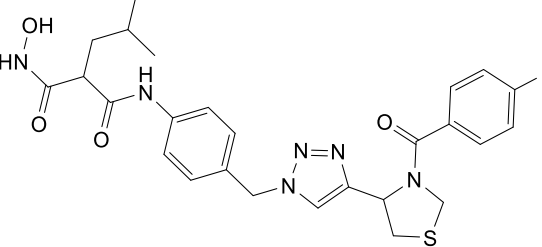
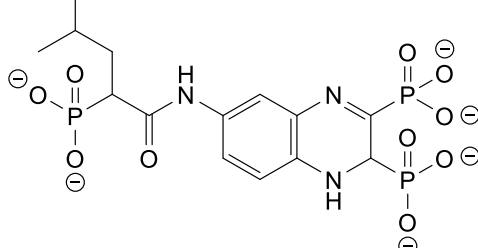
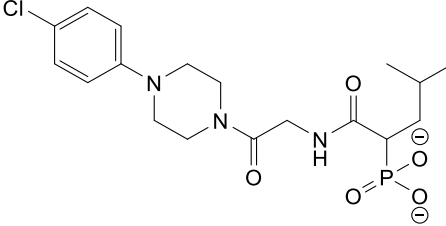
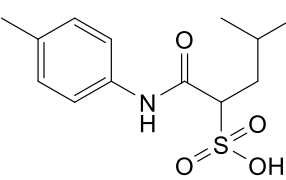
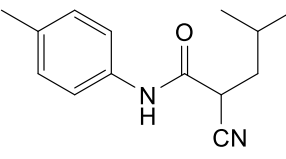
Supplementary Tables

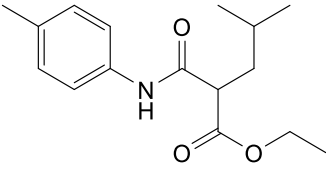
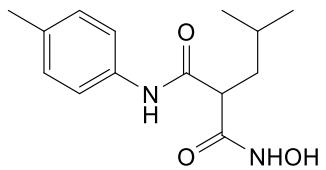
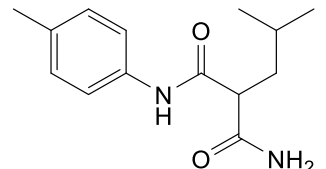
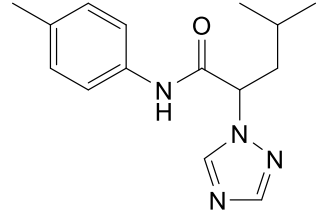
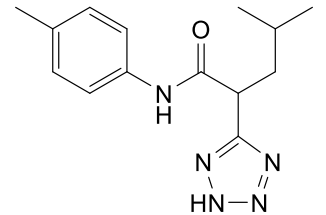
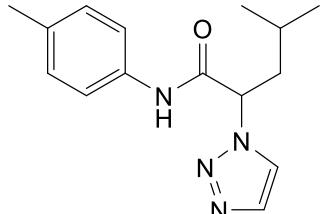
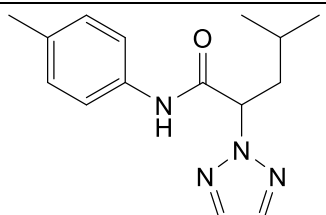
Table S1. Screening results for peptidase domain (PD) of ColH and collagenase unit (CU) of ColQ1 inhibitors discovery. The testing was performed at 100 μ M.

Compound	% Inhibition (ColH-PD)		% Inhibition (ColQ1-CU)		Structure
	Mean	SD	Mean	SD	
13	83	9	98	1	
27	84	2	97	2	
35	32	12	23	3	
36	86	5	72	5	
37	24	8	4	2	
38	19	7	3	1	

Compound	% Inhibition (ColH-PD)		% Inhibition (ColQ1-CU)		Structure
	Mean	SD	Mean	SD	
39	30	14	3	10	
40	0	7	-1	1	
41	23	9	13	6	
42	102	3	98	7	
43	63	1	87	4	
44	82	5	90	2	

Compound	% Inhibition (ColH-PD)		% Inhibition (ColQ1-CU)		Structure
	Mean	SD	Mean	SD	
45	67	4	84	2	
46	18	8	88	2	
47	43	5	53	2	
48	30	9	-4	5	
49	-5	6	10	7	
50	17	7	2	3	
51	47	8	84	5	

Compound	% Inhibition (ColH-PD)		% Inhibition (ColQ1-CU)		Structure
	Mean	SD	Mean	SD	
52	42	6	59	2	
53	84	7	85	1	
54	7	16	16	4	
55	34	8	0	3	
56	-16	3	0	2	
57	-8	21	0	3	

Compound	% Inhibition (ColH-PD)		% Inhibition (ColQ1-CU)		Structure
	Mean	SD	Mean	SD	
58	-16	16	-4	7	
59	61	0	64	1	
60	1	14	-3	1	
61	-5	6	-8	2	
62	4	10	-2	1	
63	24	9	-4	5	
64	18	16	5	3	

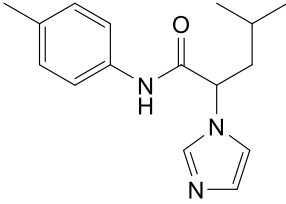
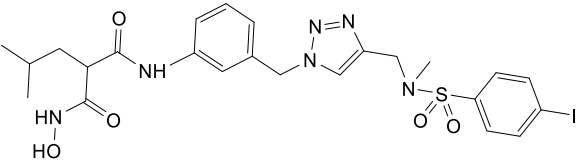
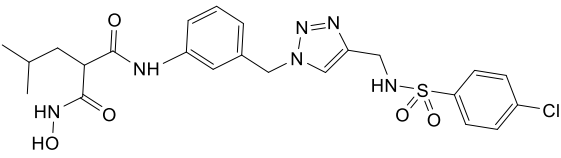
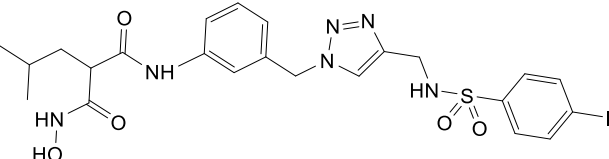
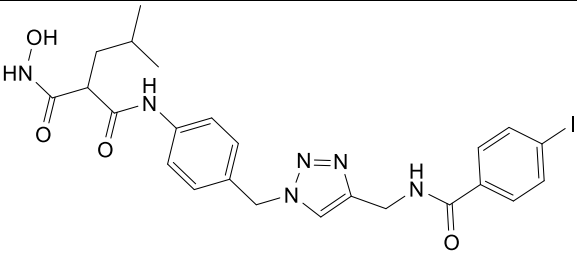
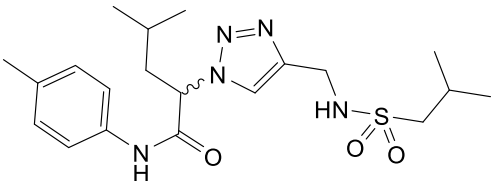
Compound	% Inhibition (ColH-PD)		% Inhibition (ColQ1-CU)		Structure
	Mean	SD	Mean	SD	
65	72	7	-3	4	
66	95	4	92	2	
67	105	3	89	2	
68	58	6	Ki 6.9	0.2	
69	75	2	84	8	
70	32	16	-8	3	

Table S2. Data collection and refinement statistics for ColG-PD in complex with compound 27 and 13

Data collection	27	13
Wavelength (Å)	0.976254	0.976254
Resolution range (Å)	41.06 – 1.80 (1.86 – 1.80) ^a	41.25 – 1.95 (2.02 – 1.95)
Space Group	P 2 ₁ 2 ₁ 2 ₁	P 2 ₁ 2 ₁ 2 ₁
Cell dimensions		
a, b, c (Å)	59.31, 78.39, 96.41	60.27, 77.79, 97.32
α, β, γ (°)	90.00, 90.00, 90.00	90.00, 90.00, 90.00
No. of unique reflections	38367 (3832)	33936 (3303)
R _{merge}	0.0400 (0.3339)	0.0372 (0.3959)
Mean I/sigma(I)	11.09 (2.20)	12.33 (2.06)
Completeness (%)	90.52 (91.91)	99.69 (99.70)
Multiplicity	1.9 (1.9)	2.0 (2.0)
CC _{1/2}	0.998 (0.773)	0.998 (0.699)
CC*	0.999 (0.934)	1.000 (0.907)
Wilson B-factor	23.35	30.71
Refinement		
Resolution range (Å)	42.46 – 1.80 (1.86 – 1.80)	41.25 – 1.95 (2.02 – 1.95)
R _{work} / R _{free}	0.1789 (0.2467) / 0.2067 (0.2934)	0.1842 (0.2627) / 0.2291 (0.3104)
No. of non-hydrogen atoms	3293	3292
Protein	3110	3167
Ligand	61	74
Solvent	150	75

Data collection	27	13
B factors		
Protein	34.04	36.16
Ligand	25.07	57.38
Solvent	34.45	34.06
RMSD		
Bond lengths (Å)	0.017	0.018
Bond angles (°)	1.29	1.36
Ramachandran favored (%)	98.69	98.71
Ramachandran allowed (%)	1.05	1.29
Ramachandran outliers (%)	0.26	0.00

^aStatistics for the highest-resolution shell are shown in parentheses.

Table S3. Activity of compounds 13, 14, 15, 27, tiludronate disodium, and alendronate sodium at 100 μ M against HDAC-3, HDAC-8, TACE, and COX-1^a

Class	Cpb.	HDAC-3	HDAC-8	TACE	COX-1
Synthesized diphosphonates	13	>100	>100	>100	>100
	14	>100	>100	>100	>100
	15	>100	>100	>100	>100
FDA-approved diphosphonates	Tiludronate disodium	>100	>100	>100	>100
	Alendronate sodium	>100	>100	>100	>100
Hydroxamate	27	>100	>100	>100	n.d.

^aMeans and SD of two independent experiments, n.d.: not determined.

Table S4. Cytotoxicity of compounds 13, 14, 15, and 27 at 100 μ M or 200 μ M against HepG2, HEK293, NHDF, and MDCKII cell lines^a

Class	Cpb.	HepG2	HEK293	NHDF	MDCK II
Synthesized diphosphonates	13	>100	=100	>200	>200
	14	>100	>100	>100	>100
	15	>100	>100	>200	>200
Hydroxamate	27	>100	>100	>200	>200

^aMeans and SD of two independent experiments.

Table S5. Antibacterial activity of selected compounds on BC AH 187 strain^a

Class	Cpd.	MIC (μ M) BC AH187
Synthesized diphosphonates	10	>200
	11	>200
	13	>200
	14	>100
	15	>100
FDA-approved diphosphonates	Tiludronate disodium	>200
	Alendronate sodium	>200
Hydroxamate	6007	>200

^aMeans and SD of two independent experiments.

Supplementary Figures

Inhibition of the compounds vs ColQ1-CU and ColH-PD

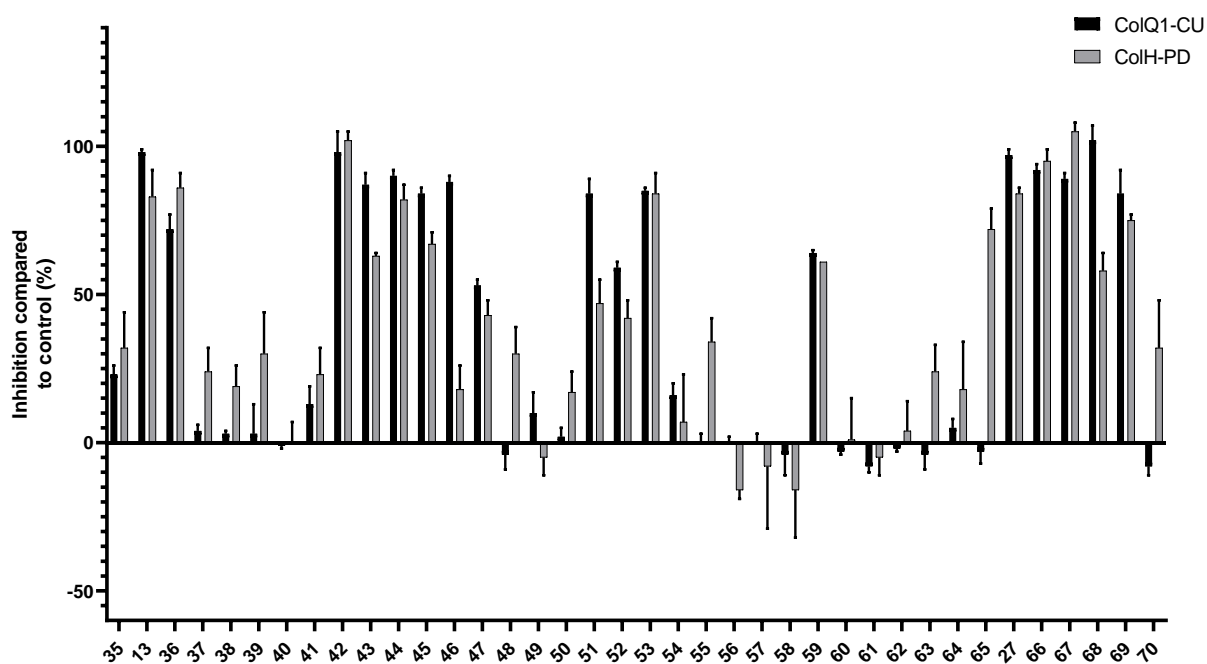


Figure S1. Inhibition of the screened compounds at 100 μ M vs collagenase unit (CU) of ColQ1 and peptidase unit (PD) of ColH.

Inhibition of the hydroxamate compounds vs ColQ1-CU at 1, 10, and 100 μM concentrations.

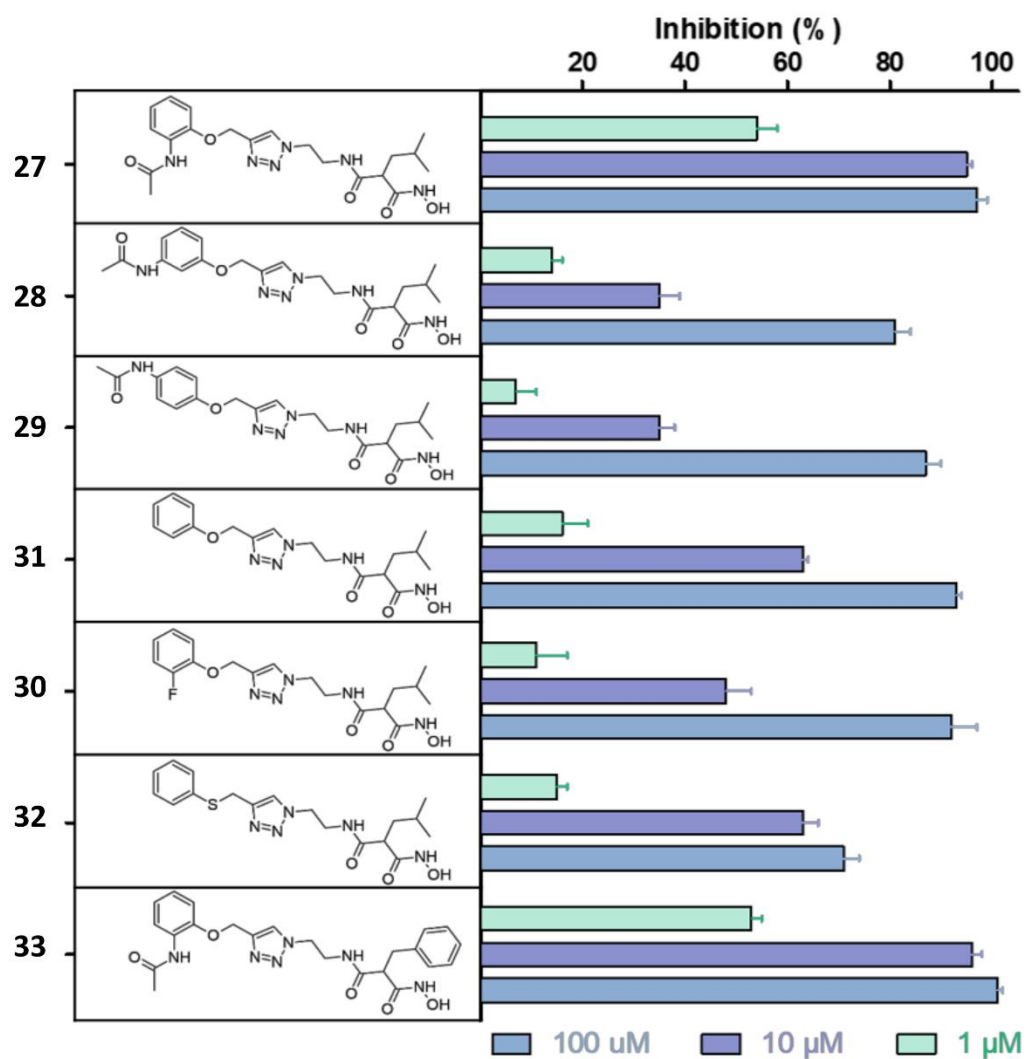


Figure S2. Inhibition of ColQ1-CU by hydroxamates at 1, 10, and 100 μM concentration.

ColQ1 inhibitors effect on collagen I cleavage

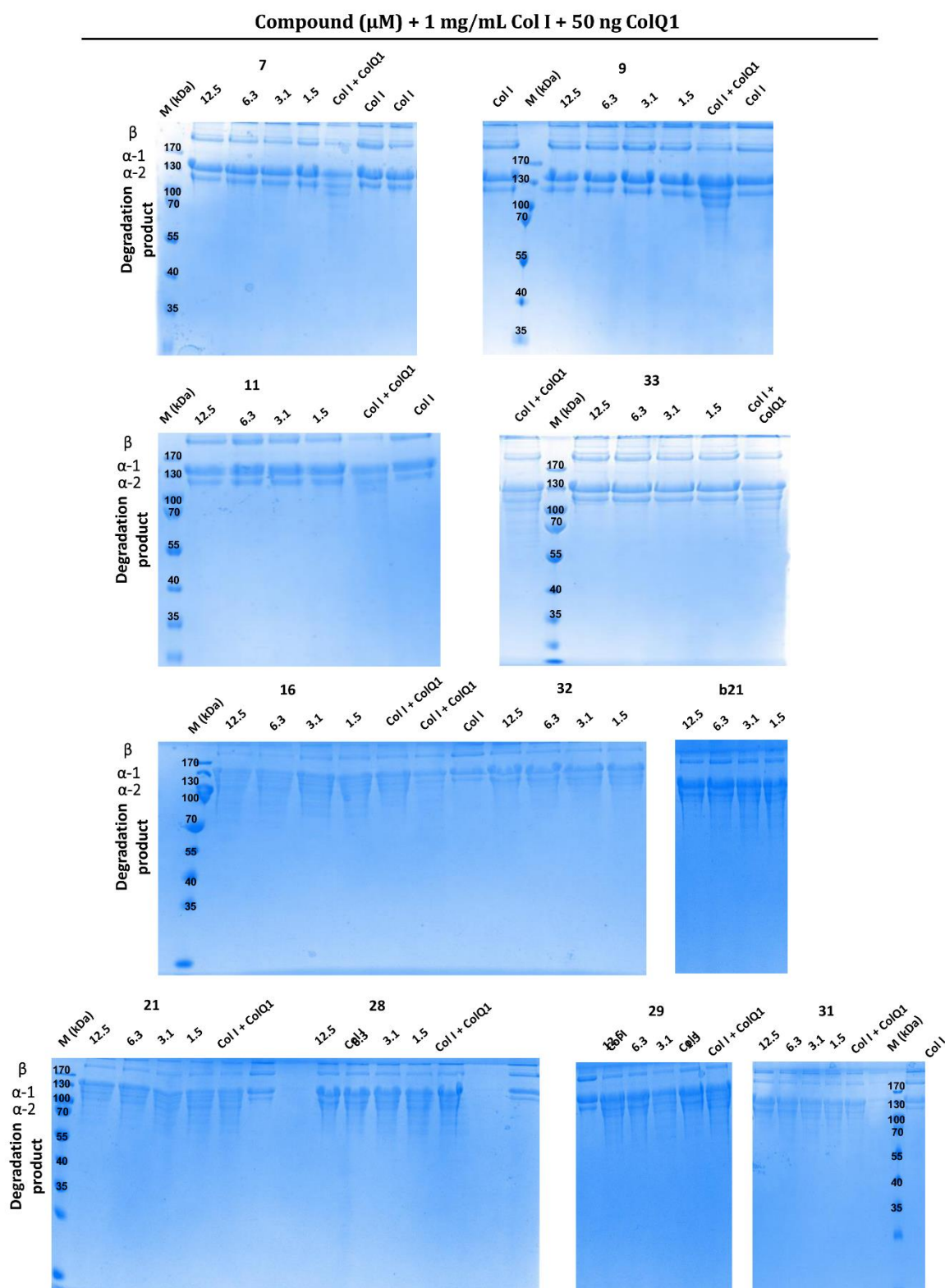


Figure S3. The effect of ColQ1 inhibitors on Col I cleavage. The *Bacillus cereus* collagenase Q1 ColQ1 full length (50 ng) was incubated with 1 mg/mL Col I for 3 h, and the degradation was then visualized on 12% SDS-PAGE. Col I: 1 mg/mL Col I without any protease. M (kDa): molecular weight standards, Col I: type I collagen.

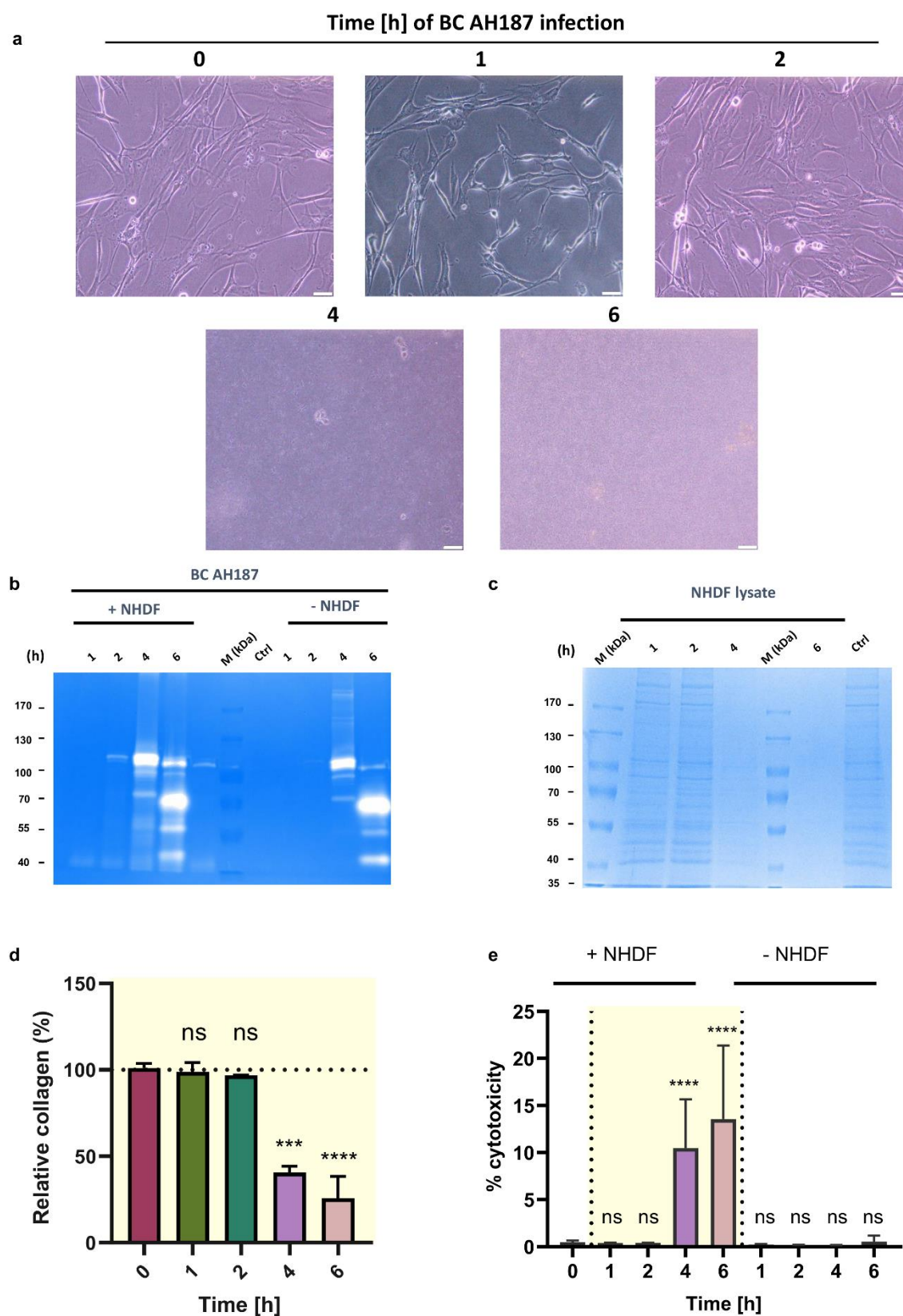
The release of *Bacillus cereus* AH187 collagenases over time

Figure S4. The release of collagenases of *Bacillus cereus* AH187 over 6 h period of time. a) The morphological changes in the fibroblast (NHDF) cells and their detachment over time. **b)** Gelatin zymogram represents the activity of *Bacillus cereus* collagenases released over 1, 2, 4, and 6 h in presence (+ NHDF) and absence of NHDF (- NHDF)

cells. The DMEM supernatants of the infected NHDF cells were applied on the zymograms. Clear regions against blue background indicate gelatin in the gel has been cleaved **c**) The depletion in the cell lysate over time indicating loss of cells, equal amount of protein was loaded. **d**) The reduction in fibrillar collagen content of the infected NHDF cells over incubation time. **e**) The cytotoxicity induced by toxins and proteases released by *Bacillus cereus* increased over time. The yellow background in d and e highlighted that the infected cells with *B. cereus*. Bright-field images captured by 20x objective, scale bar: 50 μm . Statistical analysis was performed with one-way ANOVA and statistical significance was analyzed by Tukey test. Significance was calculated by comparing non-infected *vs* infected cells (mean \pm SD, **** $p < 0.0001$, *** $p < 0.001$, ns non-significant). M (kDa): molecular weight marker.

The activity of the diphosphonates compounds on NHDF infection model

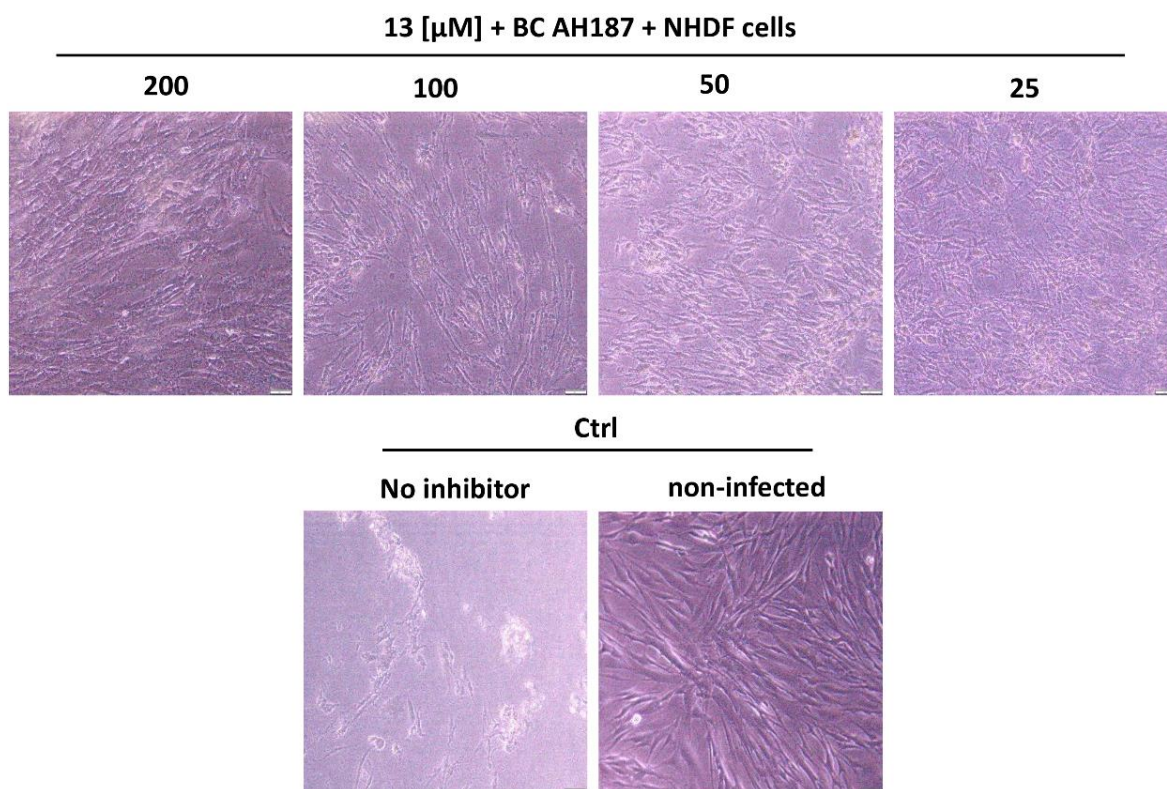


Figure S5. The bright-field images of infected fibroblast (NHDF) cells with *Bacillus cereus* AH187 and treated with various concentrations of 13. 20x objectives was used to take the images, scale bar: 50 μm , Ctrl: control.

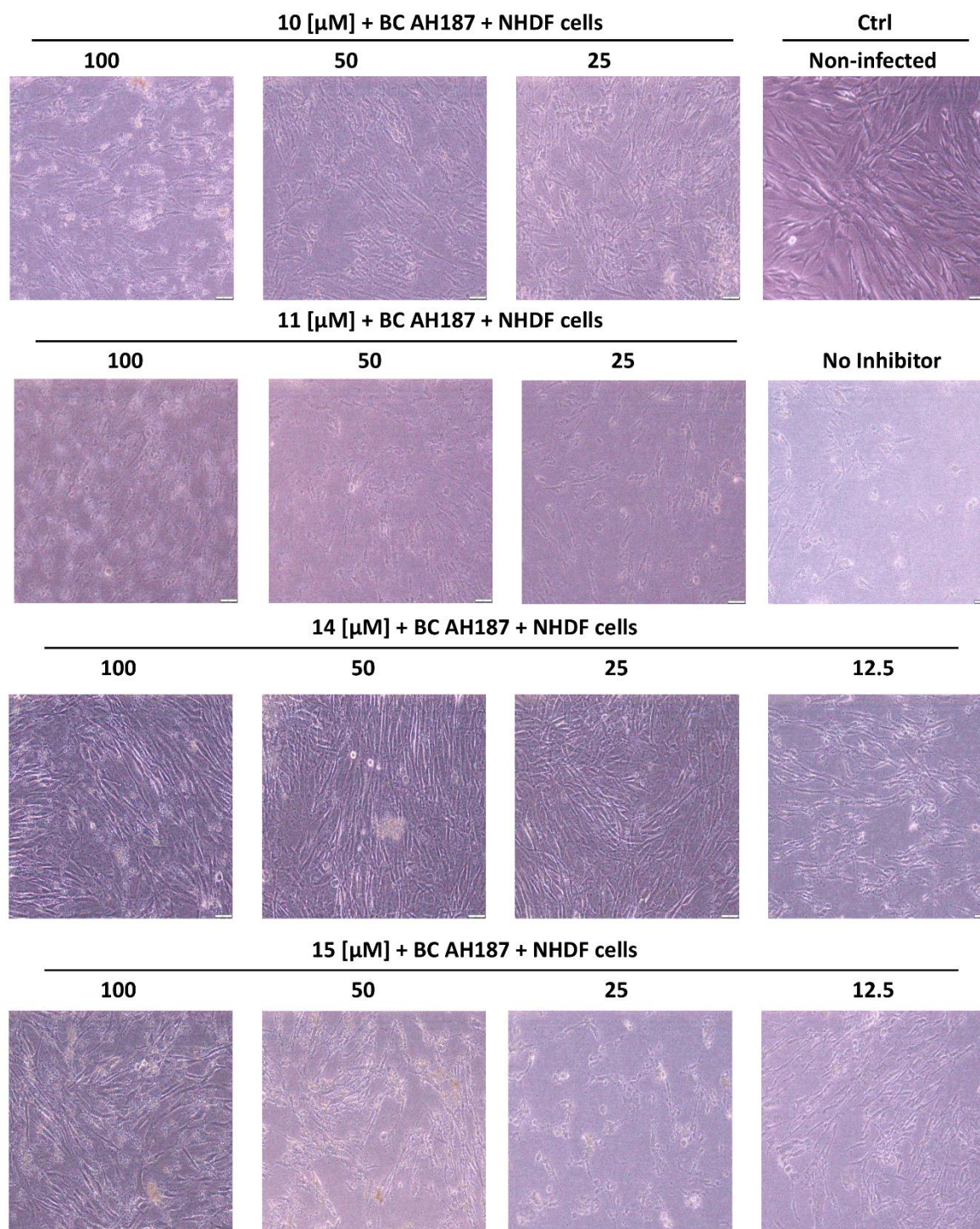


Figure S6. The bright-field images of infected fibroblast (NHDF) cells with *Bacillus cereus* AH187 and treated with various concentrations of 10, 11, 14, and 15. 20x objectives was used to take the images, scale bar: 50 μm .

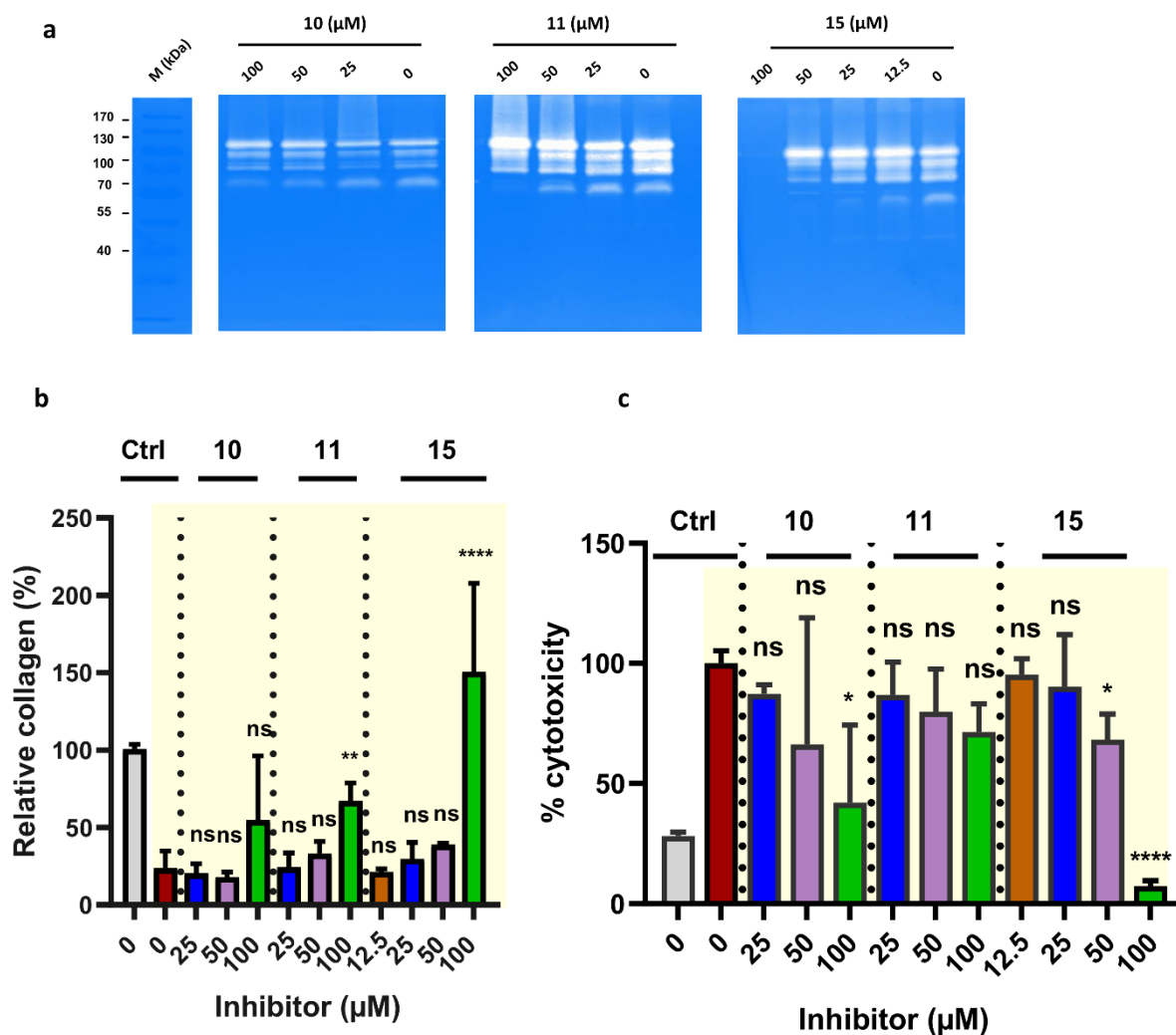


Figure S7. The activity of small molecule inhibitors on collagenases secreted by *Bacillus cereus* during infection of fibroblast (NHDF) cells. a) The anti-gelatinolytic activity of **10**, **11**, and **15**. The DMEM supernatants of the infected NHDF cells were applied on the zymograms. Clear regions against blue background indicate gelatin in the gel has been cleaved. **b)** The quantity of fibrillary collagens preserved in the infected NHDF cells treated with 6174, 6169, and 6180. **c)** The change in the cytotoxicity upon the treatment with ColQ1 inhibitors. The yellow background in d and e highlighted that the infected cells with *B. cereus*. One-way ANOVA was used for statistical analysis, and the Tukey test was used to determine statistical significance. The significance of the results was determined by comparing non-treated vs compound-treated cells (mean \pm SD, **** $p \leq 0.0001$, ** $p \leq 0.01$, * $p \leq 0.05$, ns non-significant). M (kDa): molecular weight marker, Ctrl: control.

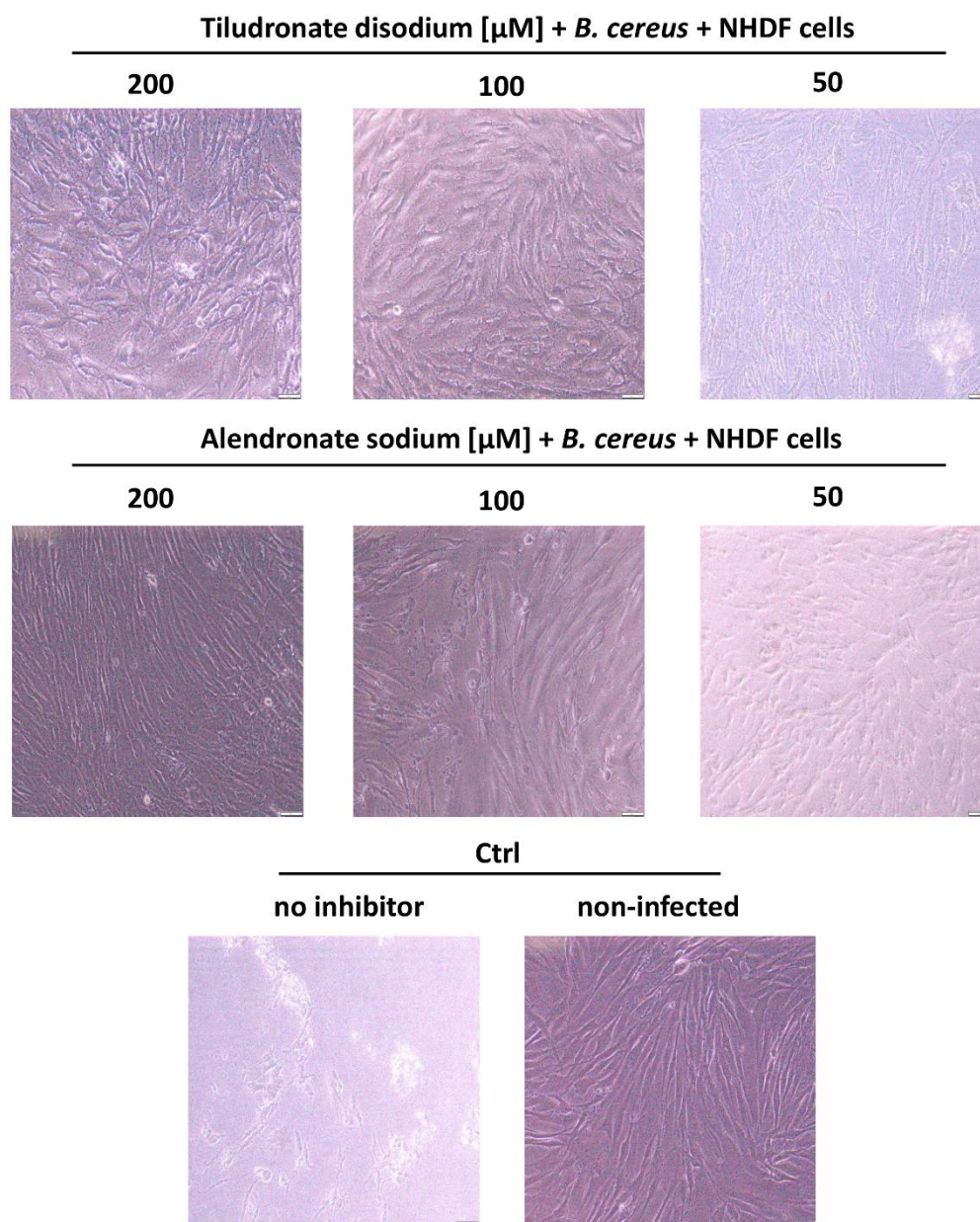
The activity of the FDA-approved diphosphonates drugs on NHDF infection model

Figure S8. The bright- field images of infected fibroblast (NHDF) cells with *Bacillus cereus* AH187 and treated with various concentrations of tiludronate disodium and alendronate sodium. 20x objectives used to take the images, scale bar: 50 μm . Ctrl: control.

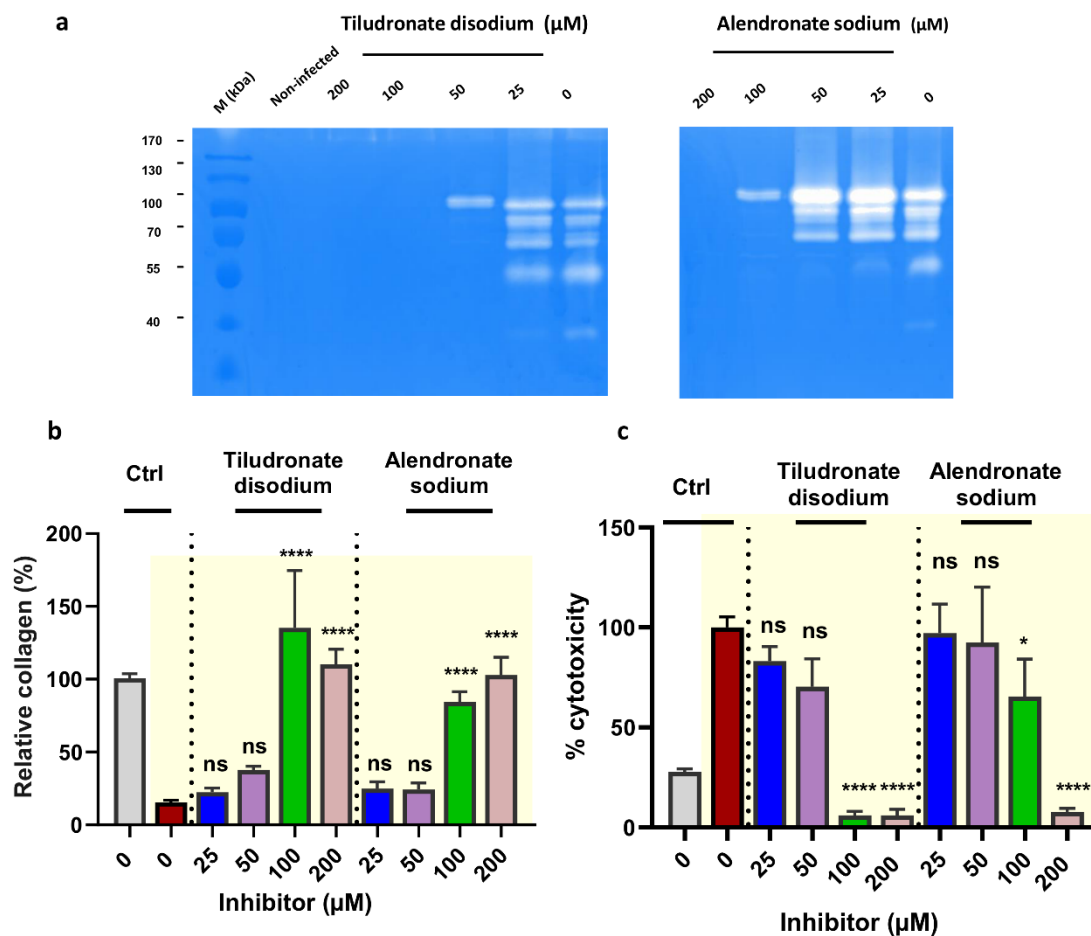


Figure S9. The activity of FDA-approved diphosphonate drugs on collagenases secreted by *Bacillus cereus* during infecting fibroblast (NHDF) cells. a) The anti-gelatinolytic activity of **tiludronate disodium** and **alendronate sodium**. The DMEM supernatants of the infected NHDF cells were applied to the zymograms. Clear regions against blue background indicate gelatin in the gel has been cleaved. **b)** The quantity of fibrillary collagens preserved in the infected NHDF cells treated with **tiludronate disodium** and **alendronate sodium**. **c)** The change in the cytotoxicity upon the treatment with ColQ1 inhibitors. The yellow background in d and e highlighted that the cells were infected with *B. cereus*. One-way ANOVA was used for statistical analysis, and the Tukey test was used to determine statistical significance. The significance of the results was determined by comparing non-treated vs compound-treated cells (mean \pm SD, **** $p \leq 0.0001$, ** $p \leq 0.01$, * $p \leq 0.05$, ns non-significant). M (kDa): molecular weight marker, Ctrl: control.

The activity of the hydromates on NHDF infection model

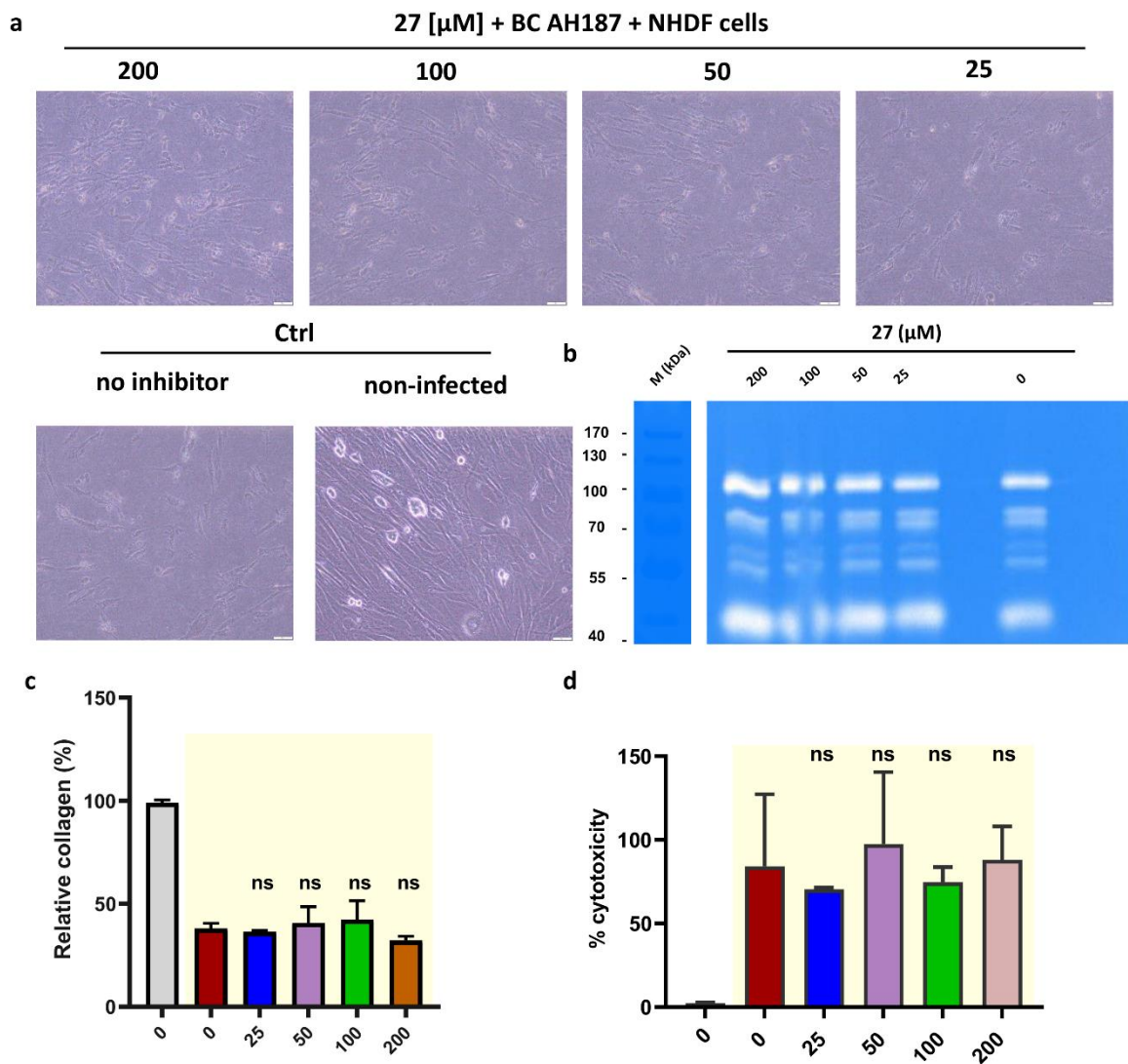


Figure S10. The effect of 27 on *Bacillus cereus*-infected fibroblast (NHDF) cells. **a**) Bright-field images of NHDF cells. **b**) Gelatin zymograms of collagenases produced by *Bacillus cereus* during the treatment with 27. The DMEM supernatants of the infected NHDF cells were applied on the zymograms. Clear regions against blue background indicate gelatin in the gel has been cleaved. **c**) Relative collagen amount left in the NHDF cells after the infection and the treatment with 27. **d**) The cytotoxicity of *Bacillus cereus* released toxins and collagenases in presence of 27. The yellow background in **d** and **e** highlighted that the cells were infected with *B. cereus*. One-way ANOVA was used for statistical analysis, and the Tukey test was used to determine statistical significance. The significance of the results was determined by comparing non-treated vs compound-treated cells (mean \pm SD, ns non-significant). M kDa): molecular weight marker, Ctrl: control.

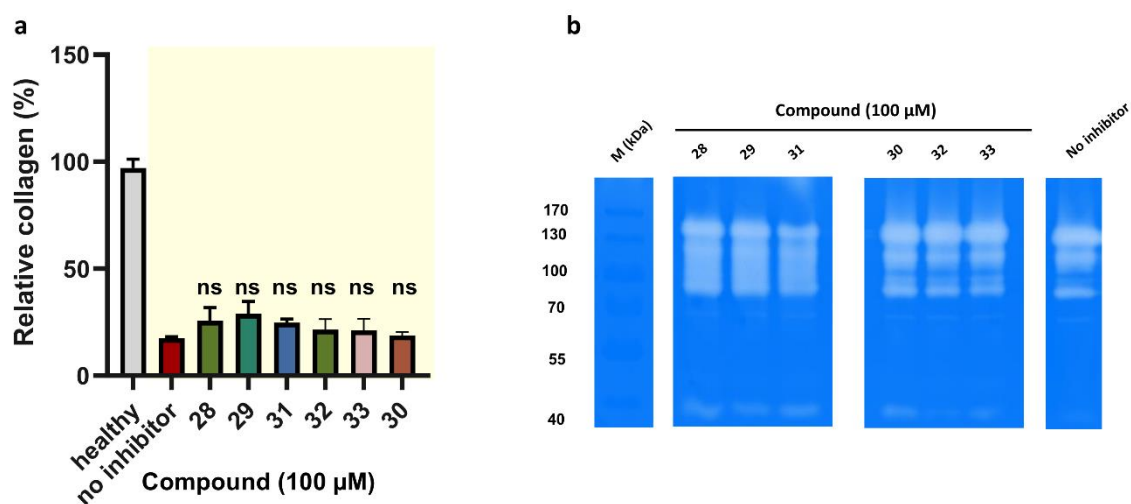


Figure S11. The effect of hydroxamic acid-based compounds on *Bacillus cereus*-infected fibroblast (NHDF) cells. a) Relative collagen amount left in the NHDF cells after the infection and the treatment with or without the hydroxamates. The yellow background in d and e highlighted that the cells were infected with *B. cereus*. **b)** Gelatin zymograms of collagenases produced by *Bacillus cereus* during the treatment with the hydroxamates. The DMEM supernatants of the infected NHDF cells were applied on the zymograms. Clear regions against blue background indicate gelatin in the gel has been cleaved. M (kDa): molecular weight standard.

Stability of 27 in DMEM buffer of NHDF infection model

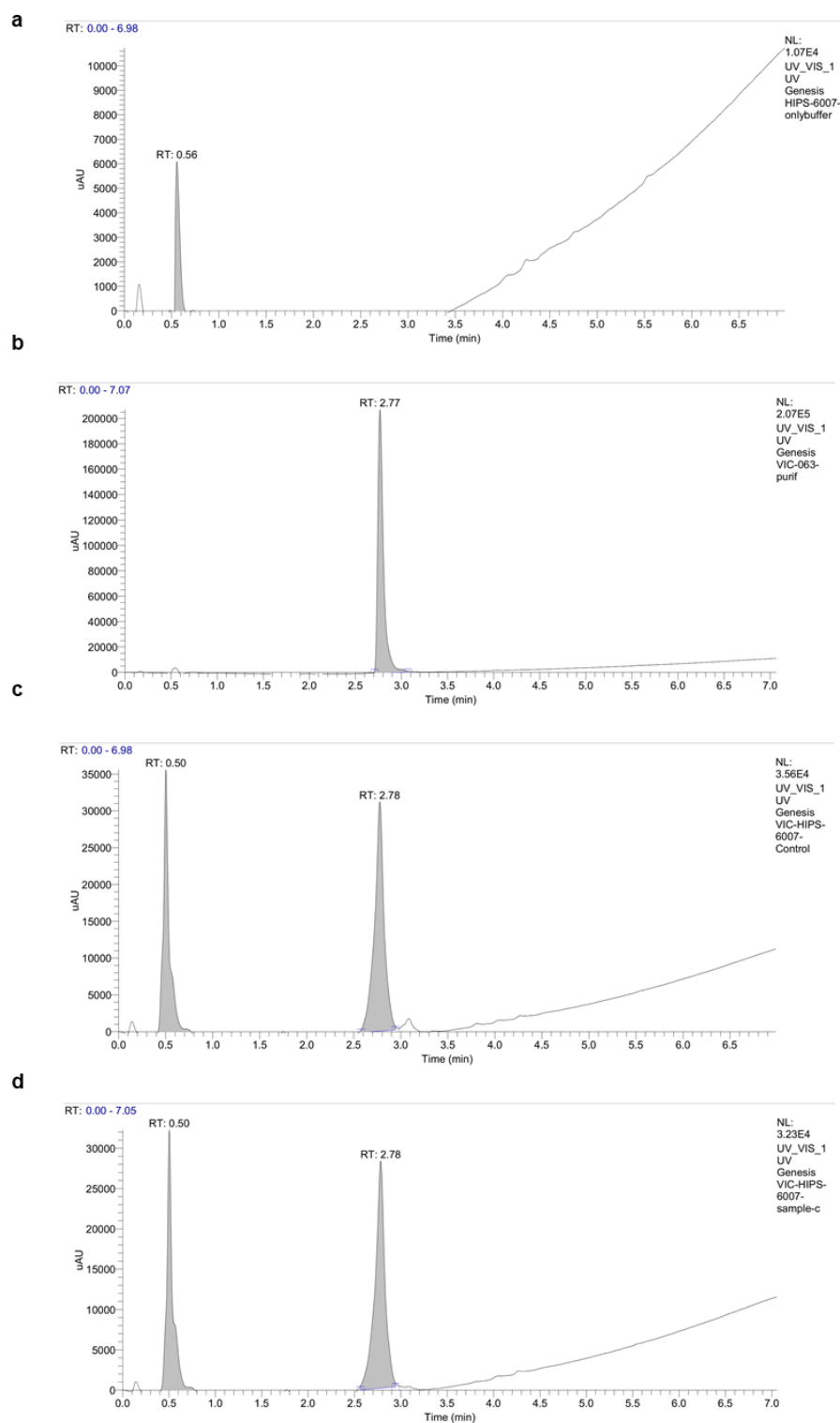


Figure S12. LC-MS UV spectra of a) DMEM medium b) compound 27 in DMSO and without incubation c) compound 27 in DMEM medium without incubation d) compound 27 in DMEM with incubation at 37 °C for 5 h.

Reversibility assay results

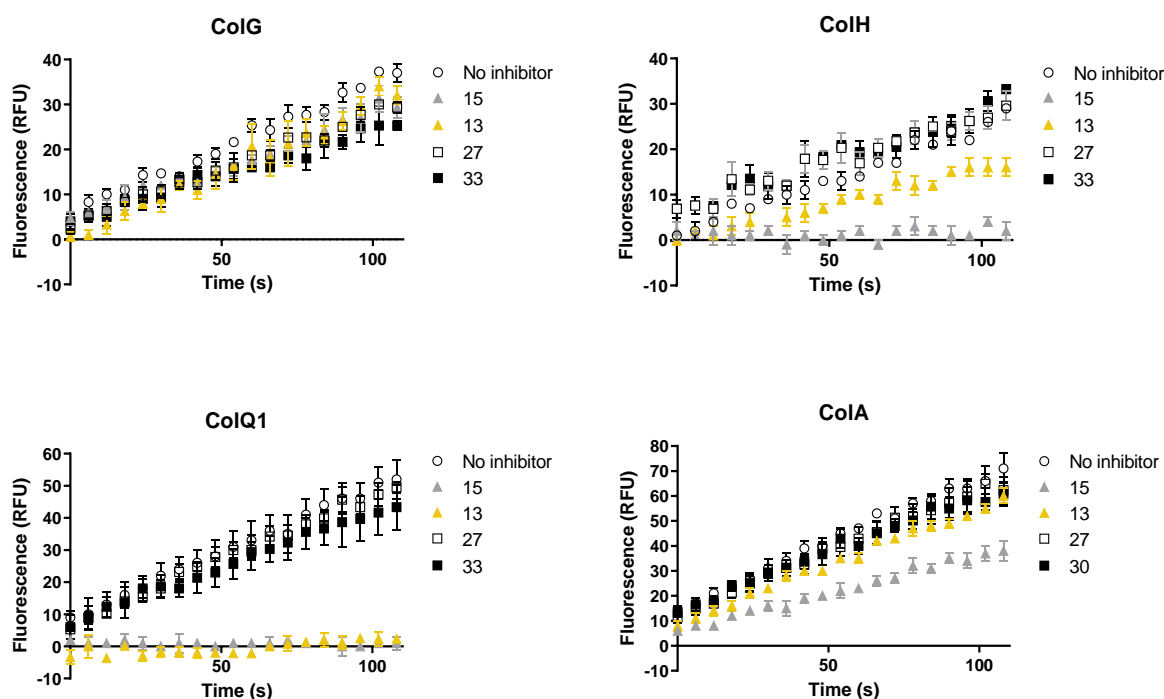


Figure S13. Reversibility of inhibition of ColG, ColH, ColQ1 and ColA by the hydroxamates 27 and 33 and the diphosphonates 13 and 15. Rapid dilution assay to test reversibility of peptidase interaction with compounds. Recovery of enzymatic activity was measured after incubation of each enzyme in the absence or presence of inhibitor. Progress curves were monitored for 2 min after 1:100 dilution of the enzyme-inhibitor complex and after addition of substrate to initiate the reaction.

Mass spectrometric analysis of protein-inhibitor reactions

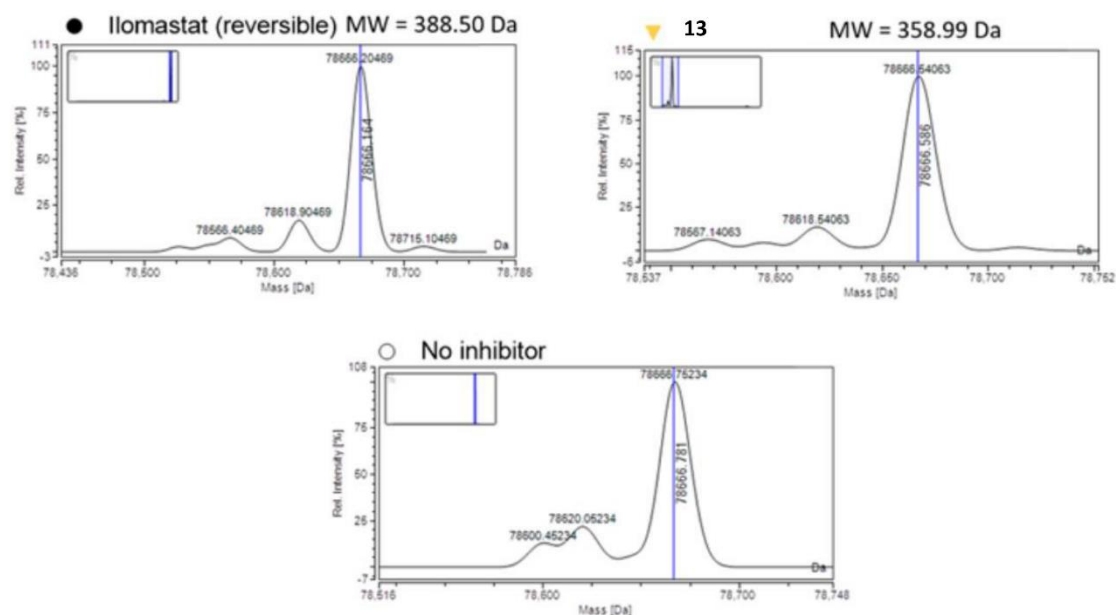


Figure S14. Mass spectrometric analysis of ColQ1-CU-ligand interactions. The mass spectrum of the collagenase unit of ColQ1 treated with ilomastat, a reversible inhibitor, 13, and no inhibitor. The average mass of the ColQ1 in all cases was 78566.5 ± 0.3 Da.

Effect of the diphosphonates on the TEER of epithelial cells

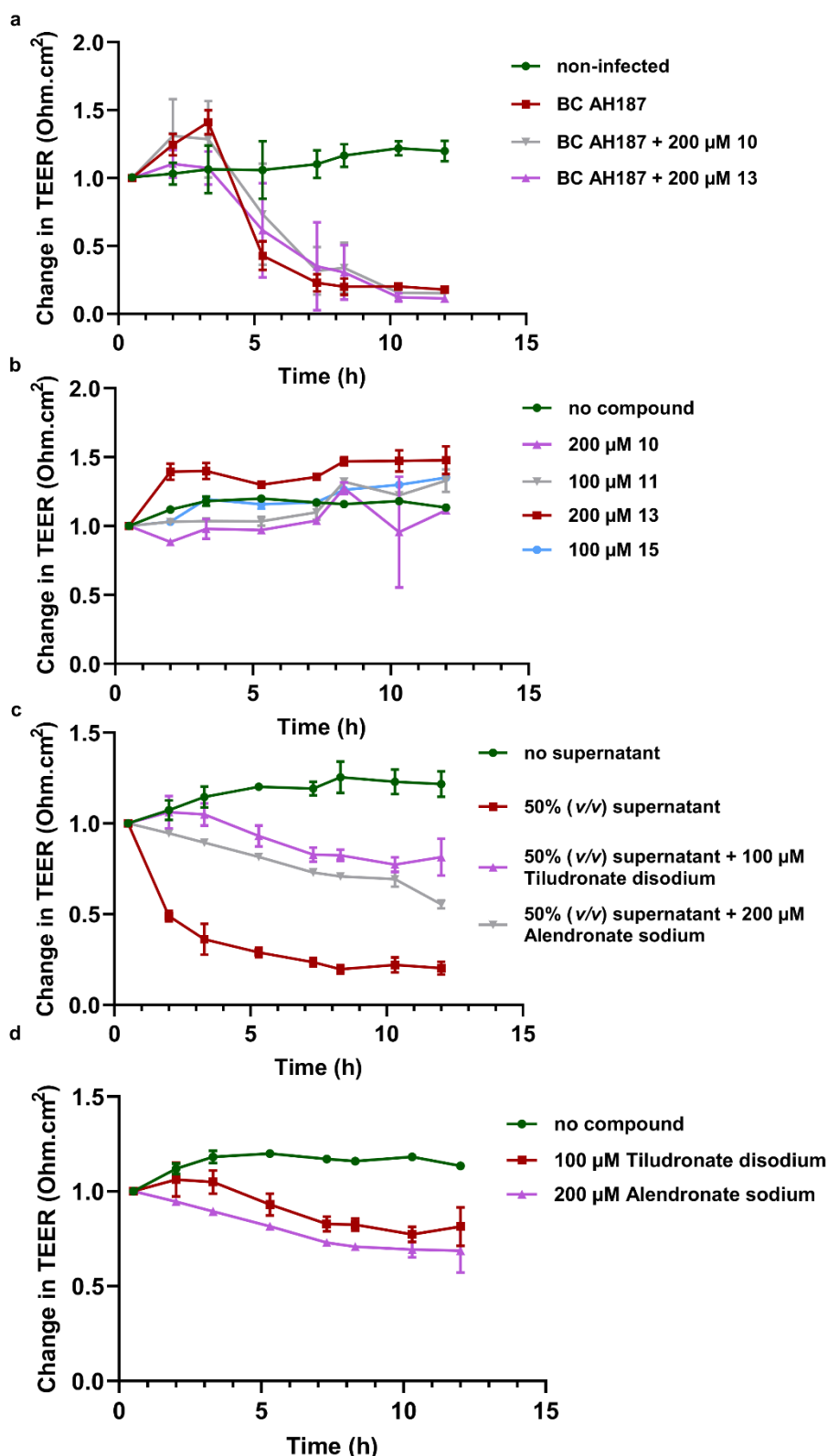


Figure S15. The effect of ColQ1 inhibitors on the transepithelial electrical resistance (TEER) of Madin–Darby Canine Kidney (MDCK) cells. **a**) Effect of 10 and 13 on the TEER of MDCK cells infected with *Bacillus cereus* AH187. **b**) The influence of ColQ1 inhibitor on the TEER of non-infected MDCK cells. **c**) Effect of FDA-approved drugs (tiludronate disodium and alendronate sodium) on the TEER of MDCKII cells treated with the BC AH187 supernatant. **d**) The influence of the FDA-approved drugs on the TEER of non-infected MDCK cells.

Each curve represents average \pm standard deviation of three independent experiments for **a** and **c** and two independent experiments for **b** and **d**.

Galleria mellonella infection model

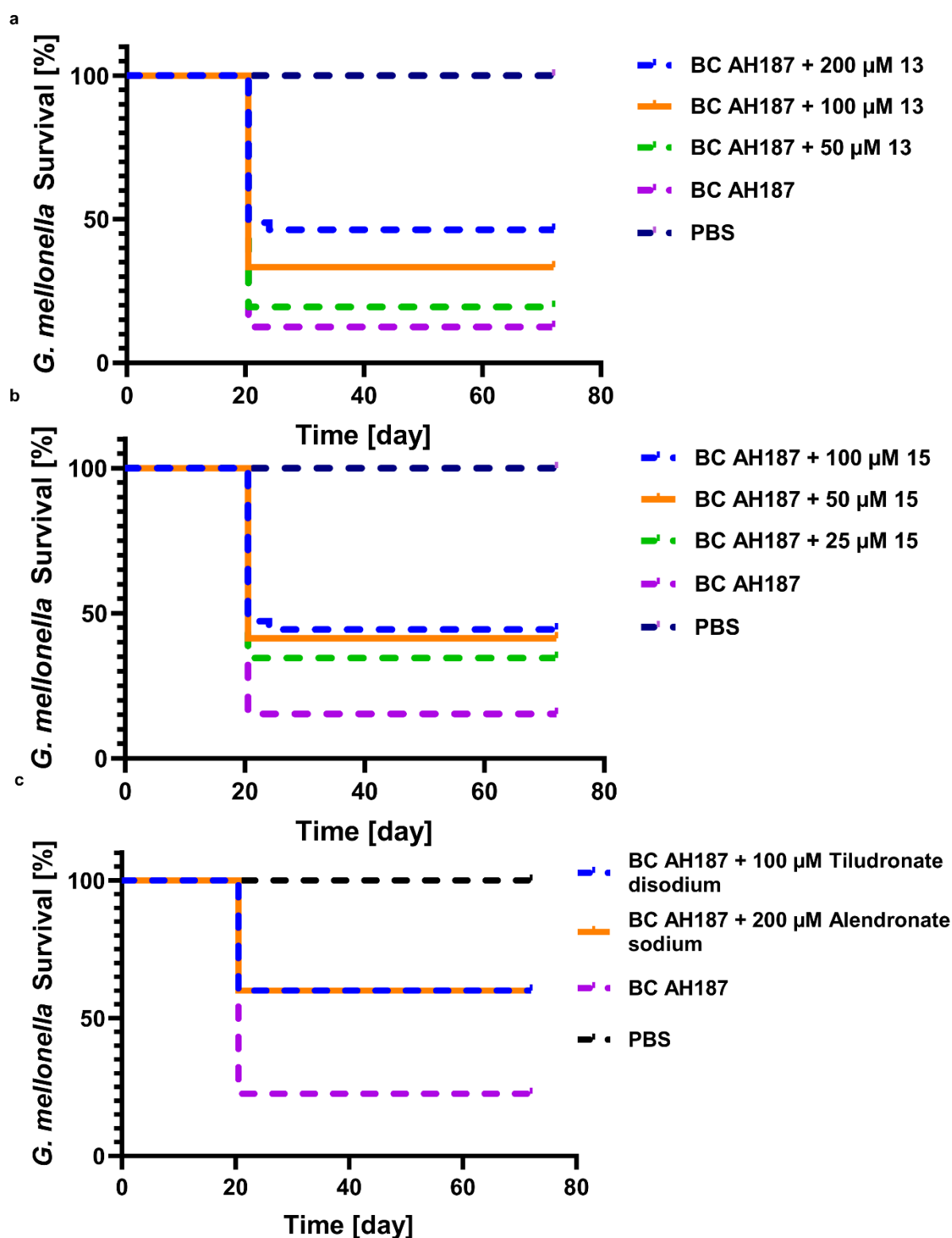


Figure S16. Probability of survival of the *Bacillus cereus*-infected *Galleria mellonella* larvae treated with and without compounds **13**, **15**, tiludronate disodium and alendronate sodium. **a**) The survival analysis of the infected larvae treated with compound **13** various concentrations (50–200 μ M) and **b**) compound **15** (25–100 μ M). **c**) FDA-approved diphosphonate drugs at 100 or 200 μ M. Each curve represents results of three independent

experiments, statistical difference between groups treated with 200, 100 and 50 μM of compound **13** and with *B. cereus* AH187 and treated with only *B. cereus* AH187 is $p = 0.0008$, $p = 0.0283$ and $p = 0.393$, respectively. While, between groups treated with 100, 50, and 25 μM of **15** and treated with only *Bacillus cereus* AH187 is $p = 0.0149$, $p = 0.0357$ and $p = 0.1128$, respectively. The statistical difference with 100 μM **tiludronate disodium** and 200 μM **alendronate sodium** and with *B. cereus* AH187 is $p = 0.0032$ (log-rank test). The survival rate for the larvae treated with both compounds in PBS was 100%.

Chemistry

The supplementary information of the chemistry part will be available online when the manuscript is submitted.

3 Final Discussion

Antivirulence agents are gaining attraction these days and becoming a potential approach to combat infections caused by multidrug-resistant bacteria. Bacterial collagenases are essential targets among several virulence factors produced by *P. aeruginosa*, *B. cereus*, and *C. histolyticum*. They play crucial roles in the infection process. Therefore, complete biological characterization of these virulence factors is important to fully comprehend their specific role during infection and to validate them as potential antivirulence targets. In this thesis, we verified the pathogenic activity of bacterial collagenases using pre-clinical models and small-molecule inhibitors. These models were first established with recombinant collagenase or bacterial csn and further developed into infection models. In all cases, we tested bacterial collagenases, which have been shown to be significant for the dissemination of bacteria and their other toxins. We also evaluated the activity of novel small-molecule inhibitors, which showed promising activity in such systems that mimic the pathogenic conditions generated by collagenases-producing bacteria. Furthermore, these inhibitors have demonstrated broad-spectrum inhibition against several bacterial collagenases, high selectivity over human off-targets, low *in vitro* or *in vivo* toxicity, and high chemical stability.

Our findings in this thesis will be discussed in more detail in the following subsections. Compounds referenced in the next subsections of the thesis are denoted with an uppercase letter (A, B, C, D, or E) referring to the relevant chapter, followed by an Arabic number according to the publication or manuscript numbering.

3.1 SAR, binding mode, and initial biological evaluation of *N*-aryl-3 mercaptosuccinimides, diphosphonates, and hydroxamates.

A. *N*-Aryl-3 mercaptosuccinimides. To broaden the SAR of our previously reported *N*-aryl mercaptoacetamide inhibitors such as **A5** on the aromatic moiety, we designed and synthesized derivatives of this class of inhibitors. The inhibitory data on LasB revealed that electronegative substituents such as chlorine or fluorine are beneficial for activity (**A7–A27**), especially di-substituted derivatives. In contrast, electron-donating group substituents (*e.g.*, dimethoxy) have a negative impact on the activity (**A22**). Furthermore, the activity was not improved by adding a carbon spacer adjacent to the thiol group (**A50** and **A51**). We previously demonstrated that LasB and ColH inhibitors have some structural similarities, thus the SAR was also explored on ColH. Our previous data highlighted that polar substituents in *para*-position of *N*-aryl mercaptoacetamides are beneficial for activity, and the same was observed for the new class

(A25). Since this class has a similar structure to our previous class of *N*-aryl mercaptoacetamides, we assumed the interaction with LasB and ColH to be comparable.

B. Diphosphonates. The thiol group, which we reported on in the previous classes is characterized by its oxidation to disulfide, resulting in a loss of activity. This makes it difficult to evaluate the biological activity of the compounds. To identify potent and chemically stable clostridial and bacillary collagenases inhibitors, we tested 38 LasB inhibitors for inhibition of ColQ1. This screening revealed two new classes of inhibitors (**D13** and **D27**) with high activity and chemically stable ZBGs, namely diphosphonates and hydroxamates. We also tested a number of FDA-approved diphosphonates for their effect on ColQ1-CU (diphosphonates are commonly used in the treatment of bone diseases). According to the initial screening of the diphosphonate **D13** and its synthesized derivatives against ColQ1-CU, the presence of both phosphonate groups is required for inhibition, indicating that the phosphonate group acts as a ZBG to the catalytic zinc ion (**D17** and **D16**). Compound **D13** loses its activity when the 3,4-dichloro residue is replaced by a 3-methoxy, 4-hydro (**D12c**), or 3,4-dihydro (**D7c**). The FDA-approved drugs **D tiludronate disodium** and **D alendronate sodium** resulted in moderate inhibition of ColQ1-CU (63 ± 3 and $76 \pm 1\%$, respectively) at 100 μM . In contrast, the other evaluated FDA-approved diphosphonate-based drugs showed no inhibition.

The crystal structure of ColG-PD (a close homologue of ColQ1) in complex with **D13** at 1.95 Å resolution confirmed its binding mode. The compound was found in the primed binding pocket next to a non-functional binding site at the back of the peptidase domain. With the use of a polder map, the inhibitor could be modeled into the active site. One of the phosphonate groups acts as ZBG, interacting with Glu555 and Tyr607, while the aromatic scaffold of **D13** and the chlorides form hydrophobic interactions with Phe515, His523, and Ile576 in the primed binding pockets.

C. Hydroxamates. Seven compounds that differ in the *alpha*-substituent of this class were subjected to a brief SAR analysis. Compounds with *o*-acetamide-substituted phenoxy groups were the preferred terminal group, and small modifications in the *alpha*-position were tolerated as in **D27** and **D33**.

The crystal structure of **D27** with ColG-PD solved at 1.80 Å resolution could justify the SAR data. The inhibitor occupies the active site from the S3 pocket to the S2' binding site. The *ortho*-acetamide group in the S3 binding pocket forms a hydrogen bond with the edge strand *via* the backbone amide of Glu498. The aromatic phenoxy ring is engaged in π - π stacking interactions with the side chain of Trp539. This explains the observed preference for the *ortho*-configuration of the acetamide group.

Activity on bacterial collagenases and selectivity over human off-targets

Having a common structural motif that inhibits different bacterial collagenases is extremely intriguing, especially if the inhibitor can be utilized to treat infections caused by multiple bacteria that produce collagenases.

The compounds in Chapters A and D were tested against several bacterial collagenases and human MMPs as representative off-targets. The most active compounds **A20**, **A25**, **D14**, **D15**, **D27**, and **D alendronate sodium**, showed high activity against clostridial (ColH and ColG and/or ColT) and *bacillus* (ColQ1 and/or ColA) collagenases, indicating their broad-spectrum inhibition. Besides the promising activities on target, the low activities against human off-targets are a critical parameter that has to be monitored to avoid undesirable side effects. To cover a broad range of these off-targets, several representative human MMPs with different depths of the S1' binding pocket were selected. These comprise MMP-1 or/and -7 (shallow), MMP-2 or/and -8 (intermediate) and MMP-3 or/and -14 (deep). This choice of three different pocket types allows us to evaluate the impact on other non-tested MMPs. In addition, other human off-targets were investigated, including TACE (ADAM-17), HDAC-3, and HDAC-8. MMP-1, -3, and -7 as well as HDAC-3 and -8 were not inhibited by **A13** and **A25**, although MMP-2, -8, -14, and TACE were inhibited to some extent at 100 μ M. To avoid off-target activity, these two *N*-aryl mercaptoacetamides should be further optimized. Compounds containing a diphosphonate or hydroxamate (**D14**, **D15**, **D27**, and **D alendronate sodium**) had negligible activity on the prior mentioned human off-targets at 100 μ M. Only compound **D tiludronate disodium** and **D13** showed some inhibition on MMP-1 or -2 or -3.

The compounds **A25** and **A15** exhibited no cytotoxicity on three human cell lines and an MTC of ≥ 30 μ M in an *in vivo* toxicity model based on zebrafish embryos, which is greater than the MTC observed for the corresponding *N*-aryl mercaptoacetamides **A5** (MTC = 10 μ M). Furthermore, **A15** and **A25** had no effect on the viability of *C. histolyticum* and *P. aeruginosa*. Similarly, several compounds (**D14**, **D15**, **D27**, and **D alendronate sodium**) displayed low *in vitro* cytotoxicity on four human cell lines and no anti-bacterial activity on *B. cereus*.

These data constitute a significant prerequisite for the promising application of these protease inhibitors for the treatment of the infections caused by collagenase-producing bacteria. They also indicate the need for additional biological evaluation to ensure their potency in more advanced models.

3.2 Establishment of pre-clinical models to investigate the effect of bacterial collagenase

To allow a new molecule to enter clinical trials, pre-clinical tests on living cells or organisms strongly influence the development of novel compounds. Pre-clinical models assist us to

understand and measure the interaction of the new compound with a biological system that mimics the conditions in humans. Therefore, simple and advanced *in vitro* cell-based, *ex vivo* pig-skin, and *in vivo* *G. mellonella* pre-clinical models were established. With the help of these models, we aimed to investigate the collagenolytic activity of bacterial collagenase against collagen and the impact of their inhibition. Collagen is a structural protein that makes up 90% of the ECM. It has a variety of functions, it provides skin flexibility and structure. In wound infections, it aids wound closure and healing by activating the clotting cascade and stimulates fibroblast cells to produce more collagen in the wound bed. Thus, collagen breakdown would provide entry sites into deep host tissue, allowing bacteria and their toxins to spread and reduplicate in the infection site. Here, we studied the collagenolytic activity of a recombinantly generated ColQ1, collagenases-containing csn of *B. cereus*, wild-type and *lasB* knockout *P. aeruginosa*. In a previous report, it has been shown that *B. cereus* collagenases have a collagenolytic activity that is greater than or similar to the well-studied clostridial collagenases. Therefore, the collagenases produced by *B. cereus* AH187 strain (produces two collagenases, ColQ1 and ColA) were selected as representative collagenases to further validate and study the effect of collagenase inhibition in infection sittings. Moreover, the lack of information on the recently discovered *B. cereus* ColQ1 and other *B. cereus* collagenases supported the focus of this thesis to be on *B. cereus* collagenases. The infection was evaluated on two of the previously mentioned models, *in vitro* cell-based and *in vivo* *G. mellonella* models. The data of this section will be addressed in more detail below:

***In vitro* cell-based models challenged with collagenase containing culture supernatants.**

Cell-based assays are effective for determining the effect of external stimuli on overall cell activity. In comparison to biochemical assays, they provide useful information in a biological and physiological context and can be used for early-stage proof of inhibitor efficacy.

Here, we aimed to investigate the role of bacterial collagenases during infection *in vitro* using skin (NHDF, HaCaT) and lung (A549) cells. The NHDF and HaCaT cells were chosen for their capacity to produce fibrillar collagens and their involvement in the wound-healing process after the wound infection, which is a common disease and is caused by multiple collagenase-producing bacteria. The A549 cells were chosen because of their high elastin and collagen content and given that the lung is one of the organs that is highly targeted by *P. aeruginosa*. To establish the models, the effect of the csn was first studied by applying different concentrations to the cells and investigating the cytotoxic effect (with MTT assay and live/dead fluorescence imaging) after 24 and 48 h of incubation. The viability of the three cells was decreased upon the treatment with the csn, as illustrated in Chapter B and Chapter E. A concentration of 0.07%

and 1.25% (v/v) of the *B. cereus* csn showed 50% drop in the cytotoxicity after 24 h incubation on HaCaT and NHDF cells, respectively. The same was detected with the wild-type *P. aeruginosa* csn, a concentration of 5% (v/v) wild-type csn reduced 50% of the viability of the A549 and NHDF cells. While *lasB* knockout *P. aeruginosa* csn demonstrated viability in a range of 80–100%, suggesting that LasB induces cytotoxicity. Additionally, the bright-field images revealed considerable cell rounding, detachment, and shrinkage in all investigated cell lines with the wild-type csn, indicating apoptosis.

***In vitro* cell-based infection models.** To establish a more complex model that mimics the damage caused by collagenase-producing bacteria and to examine the effect of collagenase inhibition, we developed two *in vitro* cell-based infection models. NHDF cells and MDCK II cells were chosen for this purpose. MDCK II cells are epithelial cells that protect the body's cavities against any toxic substances. They were used to investigate if collagenase plays a role in attacking the epithelial barrier during infection.

To establish the NHDF infection model, the release of collagenases by *B. cereus* over time was evaluated with a gelatin zymography. The zymograms showed that the release is increasing over time and the bacteria need at least 4 h to produce a considerable amount of collagenases. The infected cells showed 100% loss in cell viability (LDH assay) after 4 h of infection, whereas before this time, the viability was still high. This might be due to the high release of collagenases and other toxins. The fibrillar collagens of the infected NHDF cells were quantified (picosirius red assay), the amount of fibrillar collagens was significantly decreased by 50% after 4 h of the infection. Cell morphology and attachment were also affected, the spindle-shaped morphology of the NHDF cells changed to round-shaped morphology and cell detachment was induced, signifying cell death (Chapter D).

MDCK II cells were cultured on a cell insert to mimic the *in vivo* environment of the epithelial cells. *B. cereus* or csn was added to the epithelial cells, and the change in the TEER value was assessed over time. In both cases, namely cells treated with *B. cereus* or csn, the TEER value was reduced over time until it reached a very low value owing to epithelial cell detachment (Chapter D).

***Ex vivo* pig-skin model.** *Ex vivo* models allow for greater repeatability since they do not raise ethical concerns and provide a well-controlled artificial environment for experimentation. To elucidate the effect of collagenases and the inhibition efficacy of our inhibitors, we studied the effect of *B. cereus* csn and recombinantly produced ColQ1 in a living mammalian tissue. As previously stated in Chapters A and B, DMEM medium that lacks phenol red was used to maintain the tissue viability as it keeps the thermal stability of ColQ1 (determined by the

thermal-shift assay) and the presence of phenol red could interfere with the colorimetric Hyp assay. Furthermore, the concentrations of *B. cereus* csn and ColQ1 used for inhibitor testing were determined based on the effect detected by four concentrations (0, 35, 65, and 100% v/v) and (0, 100, 300, 500 nM), respectively. Collagen degradation was measured calorimetrically using a Hyp assay and microscopically using SHG confocal and immunofluorescence microscopes. Our data highlighted that 300 nM of ColQ1 showed a significant release of Hyp of 40 ± 5 $\mu\text{g}/\text{mL}$, and 65% (v/v) of the csn showed 50 ± 5 $\mu\text{g}/\text{mL}$ after 24 h incubation. To investigate the collagenase-specific effects, we focused on ColQ1 in the imaging methods and in the inhibition studies. SHG microscopy showed a lower SHG signal as well as wide gaps between collagen structures at 300 nM. The immunofluorescence images underlined the degradation effect of ColQ1 on the tested fibrillar collagens I, III, and IV. Based on these findings, we hypothesized that collagenolytic activities reduce skin tissue integrity, allowing bacteria to penetrate deeper into the tissue.

***In vivo Galleria mellonella* model.** To explore the pathogenicity of the bacterial collagenase and its inhibition in a simple *in vivo* model, *Galleria mellonella* larvae were used. This model is being used in microbial-infection research as a substitute for murine models due to its ease to obtain and use without the need for specialized equipment and ethical constraints. Furthermore, the innate immune system mechanisms are closely similar to those of mammals. The effect of recombinantly produced ColQ1 and *B. cereus* csn, as well as wild-type and *lasB* knockout *P. aeruginosa* csn were all tested. As illustrated in the Kaplan–Meier survival analysis in Chapter B, the survival of the larvae was reduced upon the treatment with the catalytically active ColQ1 (20% drop at 300 nM) and collagenase-containing csn (15% drop at 100% (v/v)). While the catalytically inactive mutant of ColQ1 (E502A) exhibited no change in the survival at any of the concentrations tested after eight days of treatment. The wild-type *P. aeruginosa* csn reduced the survival of the larvae to 35% at 50% (v/v), whereas the *lasB* knockout *P. aeruginosa* csn showed no change in the survival at 50% (v/v) after six days of incubation (Chapter E), highlighting the importance of LasB in triggering the mortality of the larvae. This model was further developed into an infection model using the *B. cereus* AH187 strain. Injecting 4×10^6 CFU/mL of *B. cereus* into larvae lowered the survival by 90% and caused melanization after 2 days of infection (Chapter D).

These findings indicate the detrimental effect exerted by collagenase and other toxins of the collagenase-producing bacteria. This damage could be linked to the triggering of melanization processes in the larvae since the dead larvae turned black in all cases, as proposed before for LasB. In addition, collagenases have been demonstrated to decompose hemolymph proteins of

the larvae into small peptides, provoking an immune response that eventually leads to their death.

These results prompted us to explore the importance of collagenase inhibition during infection; this will be discussed below in **subsection 3.3**.

3.3 Further biological evaluation of the collagenase inhibitors in infection-mimicking settings

***In vitro* collagen-cleavage assay.** As mentioned before, collagen is the most abundant supporting protein in the ECM, thus preserving its structure and function will prevent bacteria from spreading further into deep tissues. Collagenase inhibitors reported in Chapters B and D were tested for their ability to protect the COL I structure using a collagen-cleavage assay. We showed that the compounds (75 μM of **B1** and 6 μM of **B2**) maintained the integrity of the alpha-1,-2, and beta chains of COL I from the decomposition effect of ColQ. **D13** and its active derivatives (*i.e.*, **D11**, **D14**, **D15**, and others) inhibited the collagen cleavage at up to 3 or 1 μM . Similar findings were observed for the hydroxamate compounds (**D27** and **D33**). Some of the less active compounds were also tested and a clear degradation was detected at high concentrations as in the case of **D16**, **D21**, and others. These data emphasized the activity of the compounds as well as their ability to protect the structure of COL I. This calls for testing the compounds in more complex models and investigating their activity in an infection setting.

***In vitro* cell-based model.** The activity of the compounds was then assessed using the models described before in subsection 3.2. Compounds **B1** and **B2** were tested for their activity against 1.25% (v/v) of *B. cereus* csn, which was used to challenge the NHDF and HaCaT cells. Both compounds displayed dose-dependent efficacies and maintained the viability of both cells, 600 μM of **B1** showed $80 \pm 20\%$ viability and 100 μM of **B2** showed $70 \pm 25\%$ in comparison with no inhibitor conditions where the viability was $20 \pm 10\%$. The live/dead imaging data were consistent with the MTT data, demonstrating a high number of viable cells in contrast to dead cells.^[164] Similar to *B. cereus* and *C. histolyticum* collagenase inhibitors, LasB of *P. aeruginosa* inhibitors **E11**, **E12**, **E19**, **E20** showed a significant increase in the viability of NHDF and A549 cells challenged with the wild-type *P. aeruginosa* csn. While they did not affect the viability of the cells treated with *lasB* knockout *P. aeruginosa* csn. These data confirm that the compounds only target LasB and not other virulence targets in the csn.

The activity of the diphosphonates and hydroxamates was assessed in more complex settings using NHDF and MDCK II infection models. The gelatin zymography results showed that the

gelatinolytic activity of the released collagenases of the infected cells with the inhibitors was demolished. The diphosphonate **D13**, **D14**, and **D15** suppressed the cleavage of the gelatin that was co-polymerized with the polyacrylamide matrix of SDS-PAGE at 200 μM , 100 μM , and 100 μM , respectively. Other diphosphonate derivatives (**D10** and **D11**) had a lower effect on gelatin turnover at 100 μM . The diphosphonate FDA-approved drugs **D tiludronate disodium**, and **D alendronate sodium** inhibited collagenase completely at 100 μM . In contrast, the hydroxamates **D27** and **D33** did not show any inhibition of collagenase activity at 200 μM .

This promising activity of the diphosphonate compounds was further evaluated with other assays that detect cell attachment, fibrillar collagen content, and viability of NHDF cells. The synthesized **D13**, **D14**, and **D15** (>50 μM) and FDA-approved **D tiludronate disodium**, and **D alendronate sodium** (>100 μM) diphosphonate compounds showed a dose-dependent efficacy and sustained the attachment of the cells and their spindle-shaped morphology. The viability (LDH assay) and collagen quantification (picosirius red assay) revealed that in presence of these inhibitors, the cell viability and fibrillar collagens were significantly enhanced. The hydroxamate compounds **D27** and **D33**, on the other hand, showed no improvement, which is in line with the zymography data but contradicts the activity in the cleavage assays. This prompted us to investigate the binding of both classes; our findings revealed that diphosphonate compounds bind in a reversible quick, slow, or very slow dissociation mode depending on the bacterial collagenase. While the hydroxamates have a fast reversible dissociation mode. These data could explain the low activity of hydroxamates in the infection model.

Further analysis was performed to investigate the compound protection effect on the level of TEER of MDCK II cells. The TEER of the infected cells and challenged cells with *B. cereus* csn and treated with our inhibitors **D14**, **D15**, **D tiludronate disodium**, **D alendronate sodium**, and others was maintained over 12 h (Chapter D). These results support our theory that bacterial collagenases might be involved in attacking the epithelial barrier during infection, which could enhance the dissemination of bacteria and their toxins.

Ex vivo pig-skin model. To examine the effect of collagenase inhibition *ex vivo* in a model that mimics the degradation effect in a living tissue containing collagen, we tested our inhibitors described in Chapters A, B, and C. Concentrations of 100 μM of **A25**, 100 μM of **B1**, and 0.5 μM of **B2** reduced the Hyp release, indicating their efficacy in maintaining the collagen structure of the tissue from the collagenolytic effect of 300 nM ColQ1. Furthermore, SHG and immunofluorescence imaging data for **B1** and **B2** displayed a high density of collagen fibers, which matched the morphology of untreated tissue control. These data emphasized the implications of collagenase inhibition during infection as it assists in maintaining the integrity

of the tissue. These data inspired us to combine these two compounds with a collagen inducer protein called Hsp47. We hypothesized that in wound infections caused by bacteria that generate collagenases; our small inhibitors (**C1** and **C2**) would prevent the collagenolytic activity, maintaining the collagen scaffold of the ECM. Furthermore, Hsp47 will create new well-organized collagen molecules, which could accelerate wound healing. This was confirmed using the *ex vivo* pig-skin model challenged with ColQ1 and evaluated with microscopic methods such as SHG, PLM, and TEM as well as bio-analytical methods such as LC-MS/MS Hyp-based assay and EIA. Our data from these methods highlighted the activity of this combination and call for additional studies to evaluate this approach in more simple and advanced systems (Chapter C).

***In vivo* Galleria mellonella model.** Finally, to translate the *in vitro* activity of the compounds *in vivo*, we tested them on *G. mellonella* larvae. Compounds **B1** (at 150 μ M) and **B2** (at 5 μ M) diminished the virulence activity of ColQ1 and the collagenases in the *B. cereus* csn, enabling the larvae to survive for the duration of the experiments. The survival of the larvae challenged with the wild-type *P. aeruginosa* csn was also improved upon treatment with **D19** and **D11**. This model was further evolved into a *B. cereus* infection model and was used to examine the effect of the diphosphonates. As shown in Chapter D, compounds **D14**, **D15** enhanced the survival by 50% and 35%, respectively at 100 μ M. Both FDA-approved drugs **D tiludronate disodium** and **D alendronate sodium** boosted the survival by 40% at 100 and 200 μ M, respectively. Full survival improvement was not observed with the compounds, suggesting that the toxicity is caused not only by collagenases but also by other secreted toxins such as non-hemolytic and sphingomyelinase enterotoxins, all of which might operate together to kill the larvae.

To summarize, these biological findings indicate how the *in vitro* efficacy of our bacterial collagenase inhibitors could be translated into significant effects in systems that are more complex. Using the cellular assays, we were able to demonstrate reduced collagenase activity, improved viability, maintained cell attachment, cell morphology, and fibrillar collagens. As well as preserved TEER of epithelial cells. Furthermore, we showed this effect in collagen of the *ex vivo* pig-skin model. Finally, we verified the *in vivo* efficacy on *G. mellonella* larvae for several inhibitors mentioned in this thesis. These findings reflect the various contributions of bacterial collagenase in the pathogenicity of *C. histolyticum*, *B. cereus*, and *P. aeruginosa* clearly emphasizing the potential of these extracellular proteases as therapeutic targets toward the development of new, urgently needed anti-infectives.

4 Perspectives

As described in this thesis, bacterial collagenases have a significant role in the pathogenicity of bacteria. This role was elucidated using simple pre-clinical models and further studied with new classes of inhibitors, which are characterized by their high and broad-spectrum activity on bacterial collagenases, high selectivity over human off-targets, and low cytotoxicity. The data presented in this work highlighted bacterial collagenases as promising candidates for antivirulence development. Furthermore, they provide an opportunity for the development of new anti-infective agents with the ability to evaluate them in biological systems that are closer to the pathophysiological conditions.

These are some possible steps to take in these projects:

- I. To investigate the precise roles of bacterial collagenases, a collagenase knockout strain of *C. histolyticum* and *B. cereus* may be produced, the mutant strains will also offer targeted validation information for the collagenase inhibitors.
- II. Although collagen has been recognized as a natural substrate for bacterial collagenases, immunological substrates, and other structural proteins have not been explored as thoroughly as LasB substrates, thus additional natural collagenase substrates can be investigated further.
- III. Exploring the impact of combining collagenase inhibitors with collagen inducers such as Hsp47 or ascorbic acid *in vitro* and *in vivo* in infection environments.
- IV. Solving the three-dimensional structures of *B. cereus* collagenases (ColQ1 and ColA) to better understand the binding of the compounds with them.
- V. Pharmacokinetic assessment of the identified inhibitors *in vitro* and later *in vivo*.
- VI. Assessment of the compound's effectiveness in an *in vivo* mouse infection model.
- VII. Finding new collagenase inhibitors by screening new chemical and natural product libraries against bacterial collagenases in order to further explore inhibitors with novel binding modes and chemical entities.

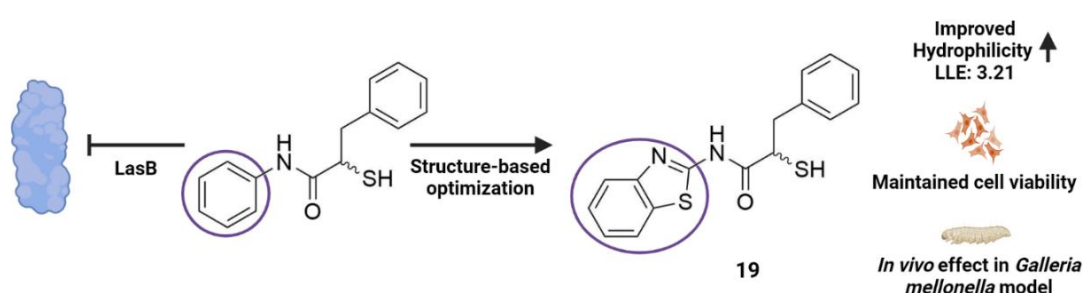
5 Appendix

Additional Results, Chapter E

Structure-based Design of α -Substituted Mercaptoacetamides as Inhibitors of the Virulence Factor LasB from *Pseudomonas aeruginosa*

Cansu Kaya, Isabell Walter, Alaa Alhayek, Roya Shafiei, Anastasia Andreas, Jelena Konstantinović, Esther Schönauer, Asfandyar Sikandar, Gwenaëlle Jézéquel, Jörg Haupenthal, Rolf Müller, Hans Brandstetter, Rolf W. Hartmann, Anna K.H. Hirsch

This part of the thesis has been submitted to *ACS Infect. Dis.*



Abstract

Antivirulence therapy has become a widely applicable method for fighting infections caused by multidrug-resistant bacteria. Among the many virulence factors produced by the Gram-negative bacterium *Pseudomonas aeruginosa*, elastase (LasB) stands out as an important target as it plays a pivotal role in the invasion of the host tissue and evasion of the immune response. In this work, we explored the recently reported LasB inhibitor class of α -benzyl-*N*-aryl mercaptoacetamides by exploiting the crystal structure of one of the compounds. Our exploration yielded inhibitors with maintained inhibitory activity, selectivity, and increased hydrophilicity. These inhibitors were found to reduce the pathogenicity of the bacteria and to maintain the integrity of lung and skin cells in the diseased state. Furthermore, the two most promising structures increased the survival rate of infected larvae by up to 60% *in vivo* in the *Galleria mellonella* model.

Introduction

The lack of efficient therapeutics on the market for targeting resistant bacteria calls for the development of novel pathoblockers.^[1,2] These pathoblockers can disarm the bacteria rather than killing by inhibiting its pathogenic properties and thereby combat notorious nosocomial infections. *P. aeruginosa* is a Gram-negative bacterium that causes around 10% of hospital-acquired infections and shows a high incidence in immunocompromised patients and in patients with cystic fibrosis (CF).^[3-6] This opportunistic bacterium features several important mechanisms contributing to resistance development. Its efflux pumps can efficiently transport undesired antimicrobials out of the cell, while the secretion of β -lactamases eliminates the effect of β -lactam antibiotics by hydrolyzing their β -lactam ring.^[7-10] Furthermore, its low outer-membrane permeability prevents antibiotics from entering the cell and represents a challenge for the development of effective antibiotics.^[11-13] This all underlines the urgent need to develop novel therapeutic options for the treatment of infections caused by these bacteria.

Rather than focusing on bacterial viability, combating resistant bacteria by targeting their virulence factors has recently gained more attention.^[14,15] These extracellular proteins are secreted by pathogenic bacteria and play an important role in various mechanisms, such as biofilm formation, invasion of host cells and evasion of the immune response, thus contributing to establishment and the progression of the disease.^[16] The development of inhibitors of such targets can facilitate the clearance of the pathogen either by the host immune system or by antibiotics.^[17,18] The main advantage of this method is the reduced selection pressure on the bacteria, which reduces the risk of resistance development by blocking the colonization and infiltration of the host, and the fact that the commensal bacteria remain unaffected.^[14] Although

only a few small-molecule inhibitors have approached clinical application, numerous *in vitro* and *in vivo* studies support the efficacy of this strategy.^[14,19] One recent successful example is the antibody drug bezlotoxumab, which is market approved and used as a toxin B neutralizer in the treatment of *C. difficile* infections.^[20]

LasB is considered as the key virulence factor secreted by *P. aeruginosa*.^[21] It is a zinc-metalloprotease responsible for pathogenic invasion of tissues and development of acute infections.^[16,22] It can degrade elastin, fibrin and collagen, which are vital components of lung tissue, blood vessels and skin.^[23] It is also involved in the inactivation of human immunoglobulins A and G as well as the cytokines gamma-interferon and tumor necrosis factor alpha.^[24–29] All these collective mechanisms of LasB make it an attractive target for an antivirulence based therapy.

Over the past few years, different inhibitor classes such as natural products^[29], phosphoramidon (Pam)^[31] and several non-peptidic inhibitors^[32] have been reported as inhibitors of LasB. Virtual screening campaigns also reported fragment-like inhibitors with sub-micromolar activity (**Figure 1**, compound 1).^[33] Small synthetic molecules such as thiols, hydroxamates or mercaptoacetamides^[34–39] are commonly reported because of their metal-chelating motifs (**Figure 1**, compound 2). A successful fragment-merging strategy has recently identified α -benzyl-*N*-aryl mercaptoacetamides as potent LasB inhibitors that are highly selective over a range of human metalloenzymes (**Figure 1**, Compound 3).^[40]

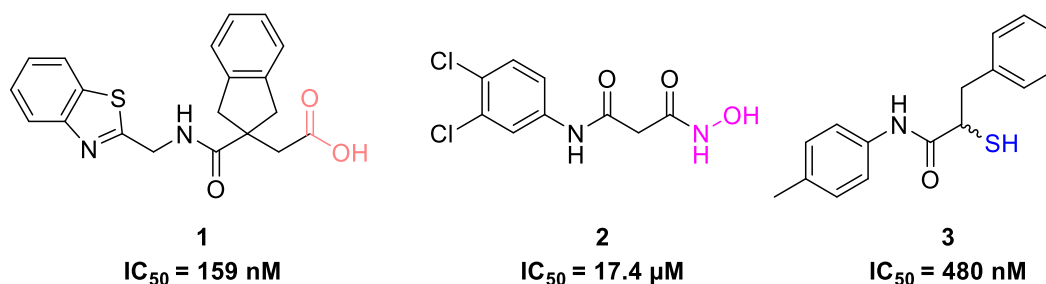


Figure 1. Structures of reported LasB inhibitors.^[33,38,40] Zinc-binding moieties are colored.

The major bottleneck in the development of potent LasB inhibitors is the problem of selectivity with respect to mammalian metalloenzymes, which play a prominent role in metabolism.^[41] Matrix metalloproteinases (MMPs) are a family of zinc-dependent endopeptidases with a catalytic domain containing Zn^{2+} ion.^[42] This poses a selectivity issue with respect to the inhibitors bearing zinc-chelating motifs. Based on the depth of their S1' binding pocket, MMPs are divided into three classes: deep, intermediate, and shallow. Considering these differences in structure, pre-assessment of selectivity for designed inhibitors is important to have effective inhibitors with an acceptable selectivity profile.

Results and Discussion. We recently reported a successful fragment-merging strategy leading to the discovery of a highly selective and potent class of α -benzyl-*N*-aryl mercaptoacetamides as LasB inhibitors.^[40] The binding mode of this class was rationalized by an X-ray crystal structure of compound **5** (**Figure 2**) with LasB. A 12-fold boost in potency ($IC_{50} = 0.48 \pm 0.04 \mu\text{M}$) observed for inhibitor **3** compared to compound **4** also resulted in an *in vivo* effect in a *Galleria mellonella* model, demonstrating the success of this class in reducing bacterial pathogenicity.

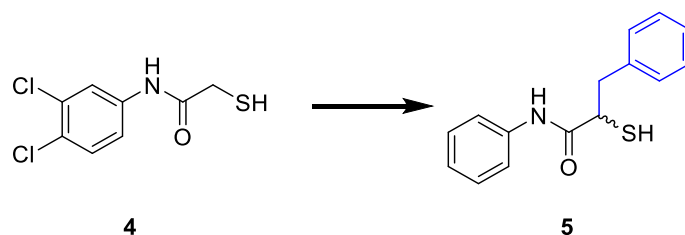


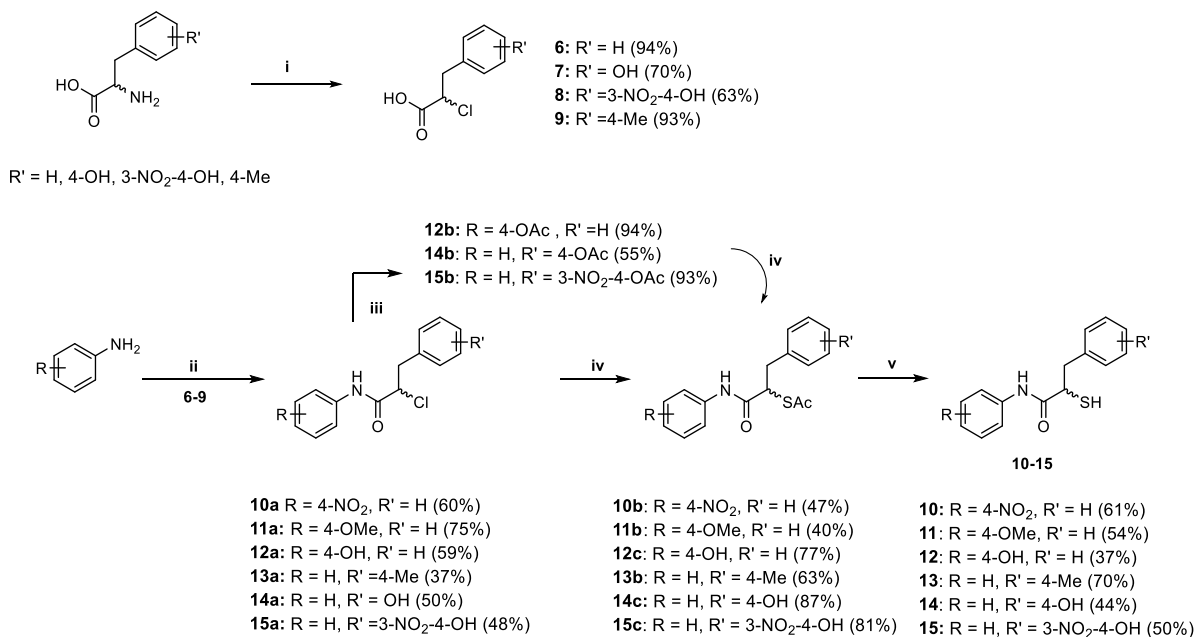
Figure 2. Structure of previously reported LasB inhibitor *N*-aryl mercaptoacetamide **4**^[42] and α -benzyl-*N*-aryl mercaptoacetamide derivative **5**.^[40]

In this work, we embarked on the multiparameter optimization of compound **5** aided by structure-based design. We synthesized a total of 13 derivatives by varying the substituents and evaluated them against LasB. We identified promising inhibitors with maintained efficacy and selectivity. These inhibitors also reduced the pathogenicity of *P. aeruginosa* during the diseased state in lung and skin cell lines. Demonstration of an *in vivo* efficacy in a *Galleria mellonella* model highlights the potential of this class of inhibitors as effective antivirulence agents.

Synthesis and evaluation of α -benzyl-*N*-alkyl mercaptopropionamide derivatives. As we observed a significant improvement in potency by introduction of a small-sized methyl substituent on the *N*-aryl ring, we analyzed whether other small-sized substituents would show the same effect on activity. Consequently, we synthesized six derivatives bearing mainly small substituents on both *N*-aryl and benzyl rings and evaluated their inhibitory activity against LasB. The synthetic route is represented in **Scheme 1**.

The synthesis started with diazotization and subsequent chlorination of the corresponding commercially available racemic amino acids.^[43] Coupling of the α -chloro carboxylic acid (**6–9**) with the respective aniline gave the desired amide function (**10a–15a**). Intermediates containing hydroxyl groups were protected by a reaction with acetic anhydride (**12b, 14b, and 15b**). The thioacetate function was introduced via an S_N2 reaction using potassium thioacetate. Final deprotection of the thioacetate under basic conditions yielded compounds **10–15** in 20–

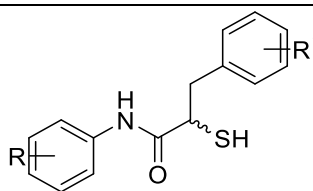
88% yield as free thiol. The inhibitory activity of the final compounds against LasB was determined as previously reported (Table 1).^[42]



Scheme 1. Synthetic scheme of the α -benzyl-*N*-aryl mercaptoacetamide class. (i) sodium nitrite, 6 N HCl, 0 °C – r.t., 16 h; (ii) thionyl chloride, DMF, 70 °C, 1 h, aniline derivative, DMF, 0 °C – r.t., 16 h; (iii) Et₃N, DMAP, DCM, acetic anhydride, 0 °C – r.t., 30 min; (iv) potassium thioacetate, acetone, r.t., 5 h; (v) 2 M aq. NaOH solution, MeOH, r.t., 1.5 h.

Table 1. Structures and inhibitory activities of α -benzyl *N*-aryl mercaptopropionamide derivatives 3, 5, and 10–15 against LasB.^a

Compound	R	R'	IC ₅₀ (μM)
3	4-Me	H	0.48 ± 0.04
5	H	H	1.2 ± 0.1
10	4-NO ₂	H	1.0 ± 0.1
11	4-OMe	H	0.7 ± 0.03
12	4-OH	H	0.6 ± 0.04
13	H	4-Me	2.8 ± 0.3
14	H	4-OH	7.4 ± 0.6



Compound	R	R'	IC ₅₀ (μM)
15	H	3-NO ₂ -4-OH	2.5 ± 0.2

^aMeans and SD of at least two independent experiments.

We previously showed the *para*-position to be the most favourable for a methyl group on the *N*-aryl ring. Based on this information, we introduced all three substituents in *para* position for compounds **10**, **11**, and **12** in this part of the molecule.

Compound **10** with an electron-withdrawing nitro group demonstrated a slight improvement in activity compared to the unsubstituted parent structure **5**. Compared to the most potent structure compound **3**, however, the IC₅₀ value was determined to be still two-fold higher. A slight improvement in potency was achieved through the methoxy group in compound **11** (IC₅₀ = 0.7 ± 0.03 μM). Following this observation, we also introduced a hydroxyl group (compound **12**), which maintained the activity in a similar range as compounds **10** and **11**.

Overall, electron-donating substituents on the *N*-aryl ring showed a stronger inhibitory effect, irrespective of their hydrophilicity (**11**, **12**), while electron-withdrawing, polar substituents such as in compound **10** did not significantly improve the activity compared to compound **5**.

Introduction of various substituents on the benzyl ring in *para*-position yielded mainly unfavorable interactions. Having a hydrophilic hydroxyl group in compound **14** led to a six-fold decrease in activity as compared to compound **5**. Even though addition of a strong electron-withdrawing nitro substituent in *meta*-position in compound **15** compensated for the loss in activity, it remained low in comparison to modifications on the phenyl ring. Surprisingly, introducing a methyl group in *para*-position in compound **13** did not create a significant change, as it showed a two-fold decrease in activity of compound **3**, only restoring the activity of compound **15**. These observations imply that nitro substituent seems to be beneficial for the activity, however, a deeper exploration with different substituent is necessary for fine tuning of the activity.

Replacement of the *N*-aryl ring with heterocycles. The crystal structure of compound **5** allowed us to examine different strategies for further optimization.^[40] We previously discovered that the *N*-arylamide group in the S1' pocket is stabilized by H-bonding and hydrophobic

interactions. Introduction of a methyl substituent on *para*-position has improved the lipophilic interactions in S1 pocket (**Figure 3**). To further improve these core interactions, we performed a molecular docking study to replace the *N*-aryl ring with various heterocycles.

Heterocycles are utilized in medicinal chemistry for tuning of various physicochemical properties such as polarity, hydrogen bonding capacity and solubility. Pyridines, thiazoles and benzimidazoles are commonly present in many natural products and in anti-infective drugs, providing diverse pharmaceutical applications.^[45,46]

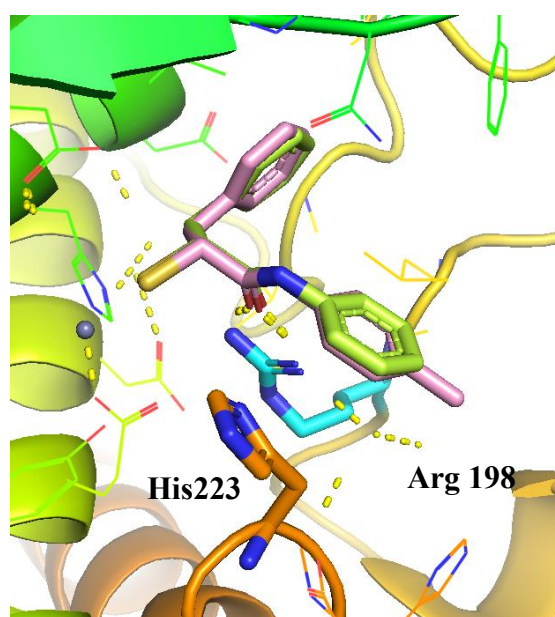


Figure 3. Superposition of LasB (cyan surface) in complex with compound 5 (lime green, major conformation shown, PDB code: 7OC7) and modeling of hit structure 3 (pink) with key interacting residues. The phenyl group occupies the S1' binding-site of the enzyme. The active-site Zn²⁺ cation is shown as a gray sphere. All figures are generated using PyMOL V.2.5 software.^[44]

We selected several heterocycles differing in size and substituents and generated docking poses in the binding pocket of LasB using SeeSAR 11.1 and visualized the interactions with PyMOL V.2.5 software (**Figure S1**).^[44,47] Figures showing docked compounds as stick representation were generated using PyMOL V.2.5 software. As we previously observed a preference for the *R*- confirmation of the ligands in the binding pocket of LasB, all compounds were docked in their *R*- configuration. Predicted interactions in the binding pocket for two selected derivatives pyridine and benzothiazole are shown in **Figure 4**.

Upon replacement of the *N*-aryl with a pyridyl ring, the docking study predicted similar interactions as compound 5 hydrophobic interactions of the benzyl ring with Val137 and Leu and cation- π interaction with Arg198 (**Figure 4A**). Additionally, a potential H-bonding of the N-atom in the ring with Asn112 could be predicted. Introducing a slightly larger benzothiazolyl

ring (**Figure 4B**) led to some additional π - π stacking interactions with His223 residues along with cation- π interactions with Arg198. In most of the docking poses, the orientation of the heterocyclic compounds did not differ significantly from the crystal structure of **5** in complex with LasB.

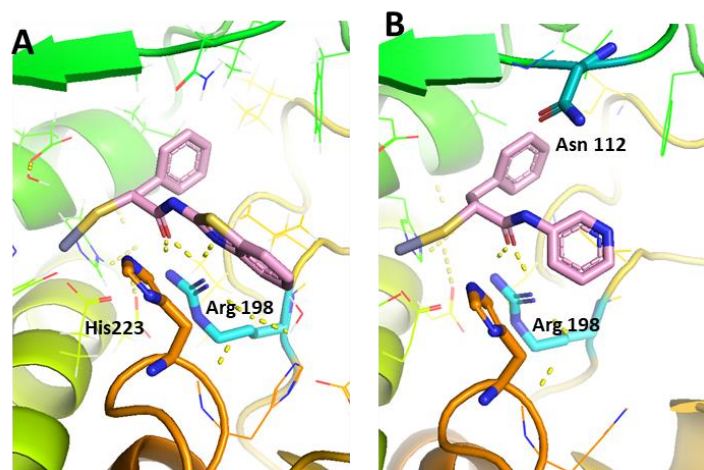
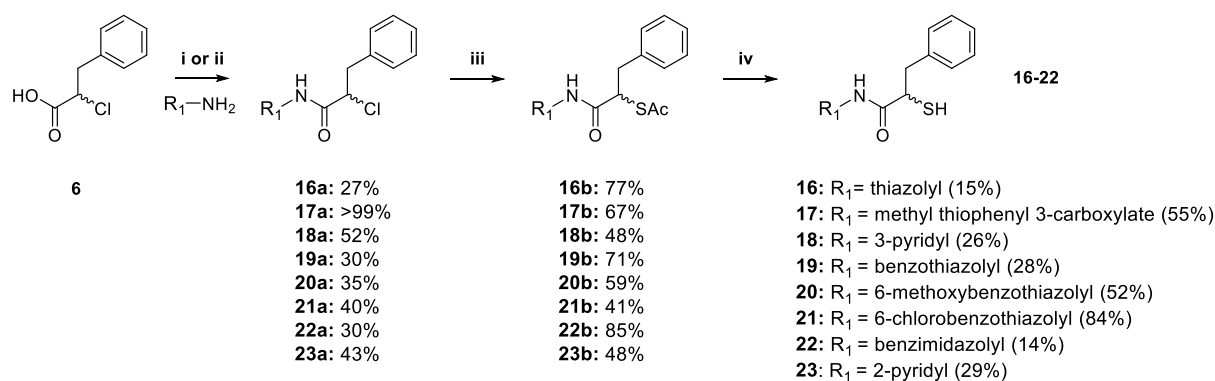


Figure 4. Selected docking poses for A) pyridyl B) benzothiazolyl replacement. The interactions in the binding pocket of LasB (PDB code: 7OC7) are predicted by SeeSAR 11.1 and visualized using PyMOL V.2.5 softwares. The dashed lines represent H-bonds of less than 2.15 Å.

Synthesis and evaluation of α -benzyl *N*-heteroaryl mercaptoacetamide derivatives. Based on the input from docking, we selected and synthesized seven heterocyclic compounds. The synthetic route is summarized in **Scheme 2**. The synthesis of heterocyclic derivatives **16–23** was achieved by coupling compound **6** with the corresponding heterocyclic anilines using either ethyl chloroformate or 1-[bis(dimethylamino)methylene]-1H-1,2,3-triazolo[4,5-b] pyridinium 3-oxide hexafluorophosphate (HATU) as the coupling reagent. Nucleophilic substitution of chlorine yielded the corresponding thioacetate intermediates **16b–23b**, which were hydrolyzed under basic conditions to afford free thiol derivatives **16–23** in moderate to good yield (14–84%). IC_{50} values for all seven derivatives against LasB were determined as reported previously (**Table 2**).⁴³

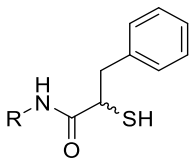
Replacement of the *N*-aryl with a thiazolyl in compound **16** ($IC_{50} = 1.6 \pm 0.1 \mu M$) maintained the potency in the range of compound **5**. Interestingly, with a relatively small substituent, methyl thiophenyl 3-carboxylate in compound **17**, we observed an almost five-fold drop in IC_{50} , presumably caused by unfavorable interactions due to the highly hydrophobic nature of the binding pocket. Introducing a pyridyl ring in compound **18** increased the activity back almost six-fold compared to compound **17**. Nevertheless, it did not improve the potency further compared to compounds **5** and **16**.

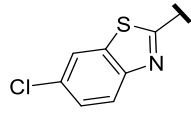
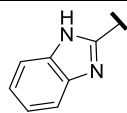


Scheme 2. Synthetic scheme of heterocyclic derivatives. (i) Et₃N, ethyl chloroformate, THF, r.t. overnight; or (ii) HATU, DIEA, DCM, overnight; (iii) potassium thioacetate, acetone, r.t., 5 h; (iv) 2 M aq. NaOH solution, MeOH, r.t., 1.5 h.

Table 2. Structures and inhibitory activities of α -benzyl *N*-heteroaryl mercaptopropionamides 5 and 16–22 against LasB.^a

Compound	R	IC ₅₀ (μ M)
5		1.2 \pm 0.1
16		1.6 \pm 0.1
17		8.0 \pm 1.1
18		1.2 \pm 0.04
19		0.7 \pm 0.1
20		1.0 \pm 0.1



Compound	R	IC ₅₀ (μM)
21		2.4 ± 0.2
22		7.6 ± 1.4

^aMeans and SD of at least two independent experiments.

Upon introduction of a larger benzothiazolyl ring in compound **19**, the activity increased two-fold (IC₅₀ = 0.7 ± 0.1 μM) compared to **16**. This improvement presumably stems from additional π-π stacking with the surrounding histidine residues for compound **19** as predicted by the docking poses. Although similar in size, the benzimidazolyl compound **22** led to a dramatic decrease in the inhibitory activity (IC₅₀ = 7.6 ± 1.4 μM). Comparison of interactions of two structures in the binding pocket of LasB (**Figure 5**) reveals a slightly different binding mode for compound **22** lacking some key interactions like H-bonding with surrounding Arg198 residue compared to compound **19**. These observations highlight the importance of the correct heterocycle-mediated interactions within the binding pocket for improving potency.

As much as the ring size, the nature of the substituents also plays a role on the fine-tuning of the activity, as depicted by the three-fold decrease in activity of compound **21** with a chloro-substituted benzothiazolyl ring compared to compound **20** bearing a methoxy group on the benzothiazolyl ring.

Although replacement of the *N*-aryl ring did not significantly improve the activity, compound **19** (IC₅₀ = 0.7 ± 0.1 μM) with a benzothiazolyl ring demonstrated an activity in the range similar to our previous hit **3** (IC₅₀ = 0.48 ± 0.04 μM), while adding a slightly more hydrophilic nature to this class of inhibitors. This observation could be valuable in future formulation studies of these inhibitors, to overcome potential solubility issues by lowering their logD values. Indeed, calculation of Ligand Efficiency (LE) and Lipophilic Ligand Efficiency (LLE) of compounds **3** (LE: 0.43, LLE: 2.37) and **19** (LE: 0.48, LLE: 3.21) revealed that we were able to improve

the hydrophilicity by maintaining LE and the inhibitory activity in the same range. To further demonstrate the potential of these inhibitors as pathoblockers against LasB, we selected compounds **11** and **12** along with the two heterocyclic derivatives, compounds **19** and **20** and evaluated them further in several *in vitro* and *in vivo* assays.

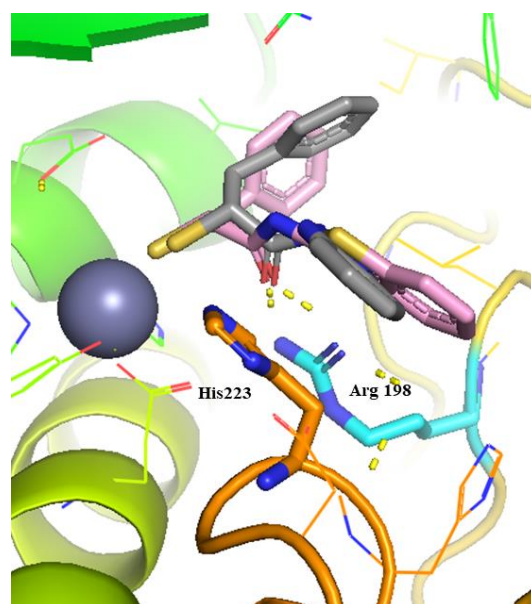


Figure 5. Superposition of compound 19 (pink) and compound 22 (light gray) in the binding pocket of LasB (PDB code: 7OC7). The active-site Zn²⁺ cation is shown as a gray sphere. The dashed lines represent H-bonds of less than 2.15 Å.

Targeting other virulence factors. We previously demonstrated that the inhibitors of LasB can also target bacterial collagenases.^[50] Collagenase H (ColH), secreted by the Gram-positive bacterium *Clostridium histolyticum*, is a zinc-containing enzyme that causes tissue destruction by degrading collagen and is involved for various diseases in humans.^[49] Similar to LasB, this extracellular metalloenzyme is capable of invading the host cell and acquiring nutrients to evade the immune defense. We previously demonstrated that the inhibitors of LasB can also target bacterial collagenases.^[50] Consequently, we determined the inhibitory activity of our LasB inhibitors against this virulence factor.

The IC₅₀ values were in the low nanomolar range (**Table S1**) for several selected α -benzyl-*N*-aryl derivatives, indicating the potential of this class for broad-spectrum inhibition of bacterial metalloproteases.

Among four selected heterocyclic derivatives, only compound **19** showed a significant inhibition of ColH (K_i : $0.1 \pm 0.01 \mu\text{M}$). This observation is noteworthy, as this compound is also a potent inhibitor of LasB.

Antibacterial Activity. To detect possible antibacterial activities, we assessed the inhibitory effect of compounds **12** and **19** against *P. aeruginosa* PA14. The minimum inhibitory concentration (MIC) assay showed no reduction of bacterial density up to 100 μ M for both inhibitors, as expected for antivirulence agents.

Selectivity against MMPs and TACE as human off-targets. Inhibition of other zinc-containing enzymes is described frequently for inhibitors of LasB, hindering the development of selective compounds. Matrix metalloproteases (MMPs) are calcium dependent zinc-metalloenzymes, playing crucial roles in the human body.^[49] To confirm the excellent selectivity we had previously reported for this class of inhibitors, we tested compounds **11**, and **12** and **19** for their activity against six representative MMPs, and the three human off-targets tumor necrosis factor- α -converting enzyme (TACE) or ADAM17, HDAC-3 and HDAC-8 (Table 3).^[50,51]

Table 3. Activities of four LasB inhibitors against selected MMPs and further human off-targets. (n.i. = <10% inhibition at 100 μ M)^a

Off-targets	3	11	12	19
MMP-1	n.i.	n.i.	n.i.	n.i.
MMP-2	n.i.	n.i.	n.i.	n.i.
MMP-3	n.i.	n.i.	n.i.	n.i.
MMP-7	n.i.	n.i.	n.i.	n.i.
MMP-8	n.i.	12 \pm 2	19 \pm 4	n.i.
Off-targets	3	11	12	19
MMP-14	n.i.	n.i.	n.i.	n.i.
IC ₅₀ (μ M)				
ADAM17	4.8 \pm 1.5	4.1 \pm 0.1	2.3 \pm 1.4	10.4 \pm 0.2
HDAC-3	>100	>100	>250	>100
HDAC-8	>100	>100	>250	>100

^aMeans and SD of at least two independent experiments.

All tested inhibitors demonstrate a high selectivity over MMPs, whereas they showed relatively low selectivity for TACE (ADAM17) with IC_{50} values between 2 and 10 μM . Therefore, optimization strategies to improve selectivity towards this target are still necessary to develop pathoblockers, which are closer to a potential therapeutic application.

Cytotoxicity. We next evaluated the cytotoxicity of compounds **12** and **19** against three human cell lines to further support the potential therapeutic use of our compounds. Both inhibitors did not show any toxicity against human hepatoma (HepG2), human embryonic kidney (HEK) 293 and adenocarcinomic human alveolar basal epithelial (A549) cells up to 100 μM .

In vivo zebrafish embryo toxicity. In view of their maintained potency, relatively high selectivity, and the lack of cytotoxicity, we next evaluated compounds **11** and **19** in an *in vivo* toxicity study using zebrafish embryos. These embryos possess a high degree of genetic similarity compared to the human genome, offering a feasible, medium-throughput *in vivo* toxicity screening.^[52,53] Additionally, the lethality and malformation during the development of embryonic zebrafish can also be assessed with this experiment. A maximum tolerated concentration (MTC) of $\leq 30 \mu\text{M}$ was obtained for compound **19** and $\leq 2 \mu\text{M}$ for compound **11** (**Table S2**).

Validation of the effect of LasB Inhibitors. Before validating the effect of selected inhibitors, we examined the cytotoxic effect of LasB-containing supernatant *in vitro*. The wild-type (wt) PA14 culture supernatant and LasB knockout ($\Delta lasB$) PA14 culture supernatant were investigated on A549 and human dermal fibroblasts (NHDF) cells. As shown in **Figures S2**, the wt PA14 supernatant reduced the viability (determined with MTT assay) and showed dose-dependent effects in both cell lines. A concentration of 15% (*v/v*) decreased the viability to $10 \pm 5\%$ and $40 \pm 5\%$ of A549 and NHDF after one day incubation, respectively. In contrast, the $\Delta lasB$ PA14 supernatant exhibited less effect on the viability after one day of incubation, 15% (*v/v*) showed $80 \pm 20\%$ viability and its effect was prominent in day two of incubation on both cells (**Figure S2**). The effect on cell morphology and attachment of both supernatants at 15% (*v/v*) was also examined with bright-field imaging, the wt PA14 induced cell detachment and rounding, indicating cell death (**Figures S3** and **S4**). While 15% (*v/v*) $\Delta lasB$ PA14 supernatant showed negligible effect in cell morphology and attachment of both cell lines. These data underline the role of LasB in inducing cell death.

In the next step, we selected compounds **11**, **12**, **19**, and **20** due to their high activity in enzyme assay, low cytotoxicity, and high selectivity over human off-targets to verify their effect against LasB in this cell-based assay. A mixture of various concentrations of compounds and 15% (*v/v*)

wt PA14 supernatant or $\Delta lasB$ PA14 supernatant was prepared and incubated with the cells for one day.

Cell viability was assessed by the MTT assay and live/dead cells visualization. The MTT results in **Figures 6** and **S6** revealed that the selected compounds improved the viability of the cells and reduced the cytotoxic effect of the wt PA14 supernatant in a dose-dependent manner (**Figures 6** and **S5**). For instance, compounds **19** and **20** showed $80 \pm 15\%$ increase in the viability of A549 cells at 50 μM , this effect was less with lower concentrations (**Figure 6a**). Whereas the compounds did not affect the activity of the $\Delta lasB$ PA14 supernatant and the viability was similar to the control (no inhibitor). (**Figure 6b**).

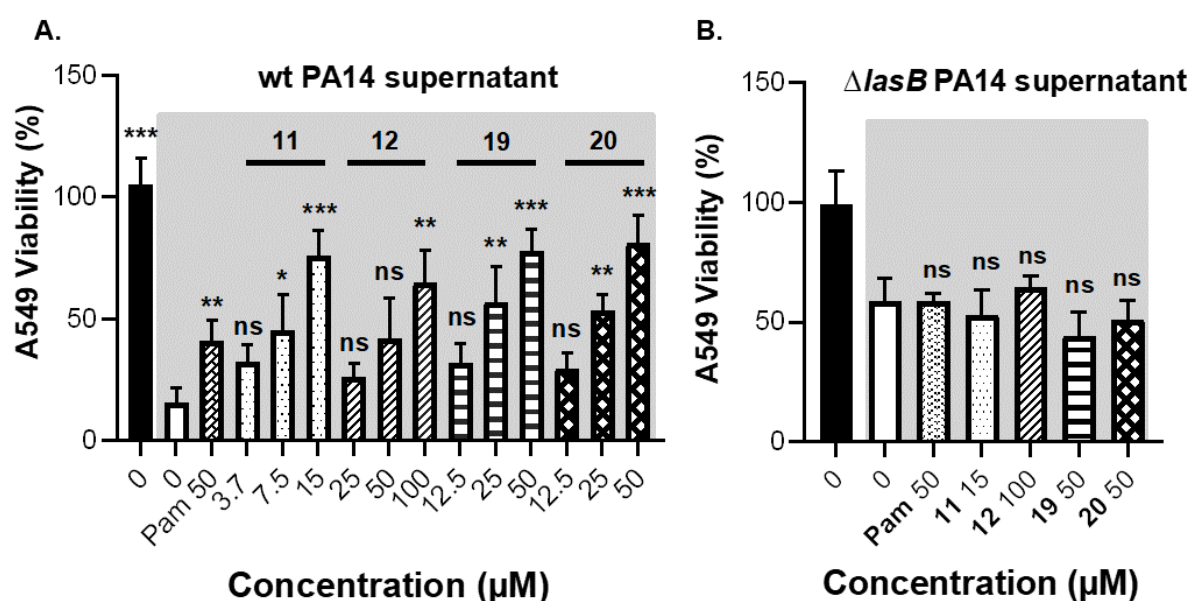


Figure 6. Viability of cells treated with 11, 12, 19, 20, and 15% (v/v) wt PA14 supernatant or $\Delta lasB$ PA14 supernatant (A) Dose-dependent effect of the compounds on A549 viability treated with wt PA14 supernatant; (B) no effect of the compounds on A549 cells treated with $\Delta lasB$ PA14 supernatant. Supernatant-treated groups are backgrounded in gray. Each graph is a representation of three independent experiments \pm SD. One-way ANOVA was performed for each experiment following Dunnett's multiple comparisons test. The mean of each column was compared with the mean of the negative control (ns: not significant, *: $p \leq 0.05$, **: $p \leq 0.01$, *: $p \leq 0.001$). wt PA14: wild-type *P. aeruginosa* PA14, $\Delta lasB$ PA14: LasB knockout *P. aeruginosa* PA14.**

Following this, live/dead staining showed an improved cell adhesion and live cell counts in both cell lines, when treated with LasB inhibitors and wt PA14 supernatant (**Figures S7** and **S9**) while no effect on the viability of the cells challenged with $\Delta lasB$ PA14 supernatant and treated with our inhibitors (**Figures S8** and **S10**). Our data confirmed that our compounds are selective and only active against LasB, but not against other virulence targets in the supernatant. Moreover, these findings imply that our inhibitors can maintain the integrity of lung and skin cells during the disease state induced by *P. aeruginosa*, and may reduce the bacterial propagation through the cells.

***Galleria mellonella* in vivo model.** To analyze the anti-virulence activity of LasB inhibitors *in vivo*, we used a simple model based on *Galleria mellonella* larvae. We have used this model previously to evaluate treatment options for *P. aeruginosa*.^[40] We injected the larvae with a mixture of the compounds and wt PA14 supernatant, incubated them for six days, and recorded survival once per day (Figure 7). Our results show that wt PA14 supernatant reduced the survival of larvae to 35% after six days of incubation, whereas the $\Delta lasB$ PA14 supernatant resulted in the survival of all larvae. Compound 4, used as a control, showed an improvement in survival from 35% to 79% (in presence of wt PA14 supernatant). Compared to larvae treated with wt PA14 supernatant only, 0.5 nmol of compound 11 increased the survival from 35% to 70% after six days. Interestingly, the performance of both compounds 11 and 19 was comparable with compound 4 with survival rates up to 75%. These results validate that our inhibitors are potential candidates to block the pathogenicity of *P. aeruginosa*.

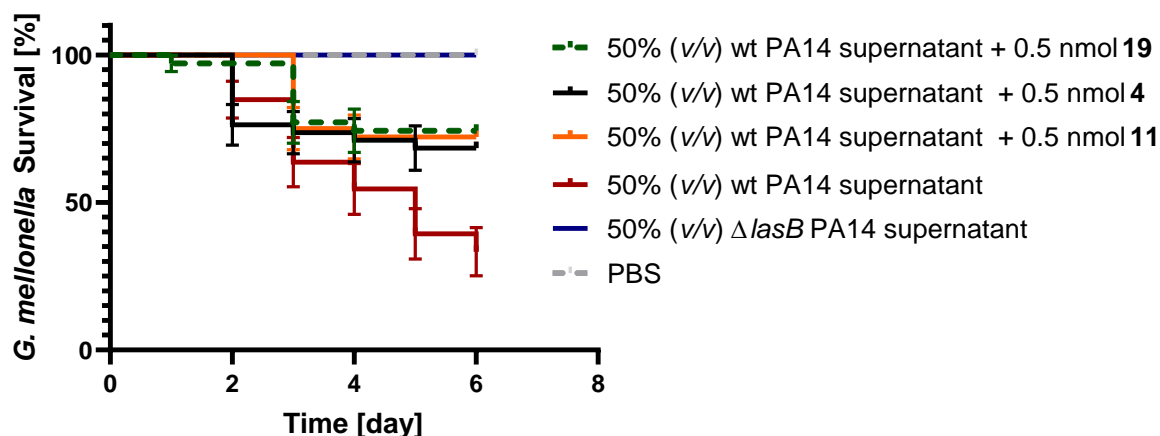


Figure 7. Kaplan–Meier survival analysis of larvae treated with 0.5 nmol of compounds 4, 11, and 19 and 50% (v/v) wt PA14 supernatant. The survival was improved when wt PA14 supernatant challenged larvae were treated with compounds. Each curve represents results of three independent experiments. The statistical difference between groups treated with wt PA14 supernatant and compound 19, 11, and 4 is $P = 0.0013$, 0.0016 , and 0.0116 (log-rank test), respectively. The survival of the group treated with $\Delta lasB$ PA14 supernatant did not change compared to the wt PA14 supernatant treated group ($P = 0.0001$). The survival of larvae treated with 0.5 nmol of the compounds (in sterile PBS) showed 100% viability. wt PA14: wild-type *P. aeruginosa*, $\Delta lasB$ PA14: LasB knockout *P. aeruginosa*.

Conclusions

In this work, we applied a structure-based optimization approach to extend the chemical space of the recently identified LasB inhibitor class of α -benzyl-*N*-aryl mercaptoacetamides. By exploiting the crystal structure of LasB with the previously reported inhibitor 5, we first explored the effect of different substituents on both sides of the mercaptoacetamide core and synthesized six derivatives. We then replaced the *N*-aryl ring with different heterocycles varying in size and substituents and synthesized seven derivatives. Although no notable improvement in potency was observed with these derivatives, we were able to identify three

compounds (**11**, **12**, and **19**) with a maintained selectivity against selected human off-targets and a restored low micromolar inhibitory activity against LasB. With no signs of toxicity against human cell lines as well as zebrafish embryos, these compounds also demonstrated a reduction in the pathogenicity of *P. aeruginosa* and maintained the integrity of lung and skin cells treated with the LasB-containing supernatant. Inspired by these results, the *in vivo* efficacy of compounds **11** and **20** was further explored using an *in vivo* model based on *Galleria mellonella* larvae. The survival rate of the larvae challenged with wt PA14 supernatant was slightly increased in the presence of both compounds. This achievement is noteworthy considering the gain in potency and increased hydrophilicity with this new class of compounds. In addition to this, the inhibitory effect of this class of inhibitors against the structurally similar target ColH from *Clostridium histolyticum* was also investigated, revealing several inhibitors with submicromolar K_i against this promising target, such as compound **19**. In view of the current antimicrobial resistance crisis, our results highlight the potential of this class of inhibitors as attractive candidates for becoming effective pathoblockers in reducing bacterial pathogenicity while diminishing potential resistance development. Further optimization strategies on both binding pockets should be explored to ensure an improved physicochemical and pharmacokinetic profile and to address the potential stability issues associated with the free thiol group in this class of inhibitors.

Methods General Chemistry. All reagents were used from commercial suppliers without further purification. Procedures were not optimized regarding yield. NMR spectra were recorded on a Bruker AV 500 (500 MHz) spectrometer at room temperature. Chemical shifts are given in parts per million (ppm) and referenced against the residual proton, ^1H , or carbon, ^{13}C , resonances of the >99% deuterated solvents as internal reference. Coupling constants (J) are given in Hertz (Hz). Data are reported as follows: chemical shift, multiplicity (s = singlet, d = doublet, t = triplet, dd = doublet of doublets, dt = doublet of triplets, m = multiplet, br = broad and combinations of these) coupling constants and integration. Liquid chromatography-mass spectrometry (LC-MS) was performed on a LC-MS system, consisting of a DionexUltiMate 3000 pump, autosampler, column compartment, and detector (Thermo Fisher Scientific, Dreieich, Germany) and ESI quadrupole MS (MSQ Plus or ISQ EC, Thermo Fisher Scientific, Dreieich, Germany). High-resolution mass was determined by LC-MS/MS using Thermo Scientific Q Exactive Focus Orbitrap LC-MS/MS system. Purity of the final compounds was determined by LC-MS using the area percentage method on the UV trace recorded at a wavelength of 254 nm and found to be >95%.

Synthesis of Intermediates and Final Compounds

General procedure A: Synthesis of chloro acid derivatives 6–9 from amino acid

Amino acid (1.0 eq) was dissolved in 6 N HCl (2 mL/mmol or until mostly dissolved) under nitrogen atmosphere and cooled to -5 °C. NaNO₂ (1.5–2.5 eq) was dissolved in water (0.3 mL/mmol amino acid) and added dropwise slowly. The mixture was stirred overnight while warming to r.t. The reaction mixture was extracted with EtOAc/THF (3:1). Combined organic extracts were washed with saturated aq. NaCl solution and dried over anh. Na₂SO₄. The solvent was removed under reduced pressure to obtain the product. The crude is used in the next steps without further purification.

General procedure B: Synthesis of derivatives 10a–15a using thionyl chloride

The acid (1.0 eq), SOCl₂ (2.0 eq) and a few drops of DMF were heated to 70 °C for 1 h. The cooled mixture was added dropwise to a solution of the corresponding aniline (1.1 eq) in DMF (1 mL/mmol) at 0 °C. The mixture was stirred overnight at r.t. The reaction was quenched with water and extracted with EtOAc (3×). Combined organic extracts were washed with saturated aq. NaCl solution and dried over anh. Na₂SO₄. The solvent was removed under reduced pressure to obtain the crude product. The purification was done by column chromatography or flash chromatography.

General Procedure B-1: Synthesis of coupling derivatives 16a, 19a–21a using ethylchloroformate as coupling reagent

The acid (1.2 eq) was dissolved in THF and cooled in an ice-bath. Et₃N (1.2 eq) was added, followed by addition of ClCO₂Et (1.3 eq). After 5 minutes, ice-bath was removed, and reaction was stirred at r.t. for 30 minutes. The corresponding amine (1.0 eq) was slowly added. The reaction was monitored using TLC or LC-MS. After the reaction was completed, volatiles were evaporated under reduced pressure and crude product was purified using column chromatography.

General Procedure B-2: Synthesis of coupling derivatives 17a, 18a, 22a using HATU as coupling reagent

The acid (1.5 eq) was dissolved in DCM (10 mL) at r.t. and to this DIEA (1.5 eq) and HATU (1.5 eq) were added. The corresponding aniline (1 eq) was then added to this mixture and the reaction was monitored by LC-MS. The reaction is extracted with saturated aq. NaCl solution (1×) then dried over anh. Na₂SO₄. The crude is purified using reverse phase flash chromatography (H₂O+0.1 %FA/ACN+0.1%FA 95:5 → 5:95).

General procedure C: Protection of hydroxyl group in derivatives 12b, 14b and 15b

The amide (1.0 eq), Et₃N (2.0 eq) and 4-dimethylaminopyridine (0.03 eq) were dissolved in DCM (5 mL/mmol) and cooled to 0 °C. Acetic anhydride (2.0 eq) was added dropwise. The solution was warmed to r.t. and stirred for 30 min. The reaction was washed with DCM, washed with saturated aq. NaCl solution, and dried over anh. Na₂SO₄. The solvent was removed under reduced pressure to obtain the crude product.

General procedure D: Synthesis of thioacetate derivatives 10b, 11b, 12c, 13b, 14c, 15c and 16b–22b

The corresponding chloro derivative (1.0 eq) was dissolved in acetone under argon atmosphere. To this solution, CH₃COSK (1.5–2.0 eq) was added and the reaction was stirred for 2–6 h at r.t. It was monitored by TLC or LC-MS. The reaction was quenched with water and extracted with EtOAc (3×). Combined organic extracts were washed with saturated aq. NaCl solution and dried over anh. Na₂SO₄. The solvent was removed under reduced pressure to obtain the crude product. The purification was done by flash chromatography.

General procedure E: Hydrolysis of thioacetate for derivatives 10–15 and 16–22

Thioacetate (1.0 eq) was dissolved in methanol (5 mL/mmol) under argon atmosphere and 2 M aqueous NaOH solution (2.0 eq) or solid NaOH (3.0 eq) was added. The reaction was stirred 1–3 h at r.t. before quenching with 1 M HCl. Reaction was extracted with EtOAc and washed with 0.5 M HCl. Combined organic extracts were washed with saturated aqueous NaCl solution and dried over anh. Na₂SO₄ and filtered. The solvent was removed under reduced pressure to obtain the crude product. The purification was done by column chromatography or preparative HPLC (H₂O+0.05%FA/ACN+0.05%FA, 95:5 → 5:95). For more polar compounds, instead of quenching the reaction with 1 M HCl, pH was adjusted to acidic using Amberlite IR-120. After filtration, Amberlite was washed with MeOH (3×), the solvent was evaporated, and the product was purified using preparative HPLC (H₂O+0.05%FA/ACN+0.05%FA, 95:5 → 5:95).

2-Chloro-3-phenylpropanoic acid (6).

Compound **6** was prepared according to general procedure **A**, using DL-phenylalanine (1 g, 6.0 mmol) and NaNO₂ (1.46 g, 21.2 mmol). The crude product was obtained as yellow oil and used without further purification (1.05 g, 94%). ¹H NMR (500 MHz, CDCl₃) δ ppm: 7.37–7.24 (m, 5H), 4.51 (dd, *J* = 7.8, 6.9 Hz, 1H), 3.42 (dd, *J* = 14.0, 6.7 Hz, 1H), 3.21 (dd, *J* = 14.1, 7.9 Hz, 1H). MS (ESI⁻) *m/z* 183.25 [M–H]⁻, 147.23 [M–H–HCl]⁻.

2-Chloro-*N*-(4-methoxyphenyl)-3-phenylpropanamide (11a).

Compound **11a** was prepared according to general procedure **B**, using compound **6** (200 mg, 1.08 mmol), SOCl₂ (157 μL, 2.17 mmol) and *p*-anisidine (147 mg, 1.19 mmol). Purification was done by flash chromatography (Hex/EtOAc, 100:0 to 0:100). The product was obtained as

green solid (234 mg, 75%). ¹H NMR (500 MHz, CDCl₃) δ ppm: 8.01 (br s, 1H), 7.38–7.24 (m, 7H), 6.90–6.86 (m, 2H), 4.71 (dd, *J* = 7.8, 4.4 Hz, 1H), 3.81 (s, 3H), 3.52 (dd, *J* = 14.3, 4.4 Hz, 1H), 3.32 (dd, *J* = 14.3, 7.6 Hz, 1H). MS (ESI⁺) *m/z* 290.04 [M+H]⁺.

***S*-(1-((4-Methoxyphenyl)amino)-1-oxo-3-phenylpropan-2-yl) ethanethioate (11b).**

Compound **11b** was prepared according to general procedure **D**, using compound **11a** (230mg, 0.95 mmol) and potassium thioacetate (162 mg, 1.42 mmol). Purification was done by flash chromatography (Hex/EtOAc, 100:0 to 0:100). The product was obtained as yellow solid (126 mg, 40%). ¹H NMR (500 MHz, CDCl₃) δ ppm: 7.81 (br s, 1H), 7.37–7.34 (m, 2H), 7.33–7.23 (m, 5H), 6.86–6.81 (m, 2H), 4.28 (dd, *J* = 8.4, 7.2 Hz, 1H), 3.79 (s, 3H), 3.44 (dd, *J* = 14.0, 8.4 Hz, 1H), 3.01 (dd, *J* = 14.1, 7.1 Hz, 1H), 2.38 (s, 3H). ¹³C NMR (126 MHz, CDCl₃) δ ppm: 197.4, 168.3, 156.7, 137.9, 130.9, 129.5, 128.8, 127.2, 114.3, 121.8, 55.7, 48.7, 36.1, 30.7. MS (ESI⁺) *m/z* 330.08 [M+H]⁺, 288.08 [M–Ac+2H]⁺.

2-Mercapto-*N*-(4-methoxyphenyl)-3-phenylpropanamide (11).

Compound **11** was prepared according to general procedure **E**, using compound **11b** (95 mg, 0.29mmol) and 2 M NaOH aq. solution (290 μL, 0.58 mmol) in MeOH (2 mL). Purification was done by flash chromatography (Hex/EtOAc, 100:0 to 0:100). The final product was obtained as white solid (45 mg, 54%). ¹H NMR (500 MHz, CDCl₃) δ ppm: 7.90 (br s, 1H), 7.37–7.33 (m, 2H), 7.31 (d, *J* = 7.5 Hz, 2H), 7.28–7.23 (m, 3H), 6.89–6.84 (m, 2H), 3.80 (s, 3H), 3.70 (dt, *J* = 8.9, 6.6 Hz, 1H), 3.36 (dd, *J* = 13.7, 6.7 Hz, 1H), 3.24 (dd, *J* = 14.0, 6.4 Hz, 1H), 2.10 (d, *J* = 8.9 Hz, 1H). ¹³C NMR (126 MHz, CDCl₃) δ ppm: 169.5, 156.9, 137.5, 130.4, 129.6, 128.7, 127.3, 122.1, 114.3, 55.6, 45.9, 41.7. HRMS (ESI⁺) *m/z* calcd. for C₁₆H₁₈NO₂S [M+H]⁺ 288.10527, found 288.10453.

***N*-(Benzo[d]thiazol-2-yl)-2-chloro-3-phenylpropanamide (19a).**

Compound **19a** was synthesized according to the general procedure **B-1**, using compound **6** (626 mg, 3.39 mmol), 2-aminobenzothiazole (422 mg, 2.81 mmol), Et₃N (476 μL, 3.39 mmol) and ClCO₂Et (355 μL, 3.72 mmol) in THF (33 mL). The final product was purified using flash chromatography (DCM/MeOH, 100:0 to 95:5). Final product was obtained as off-white oil (324 mg, 30%). ¹H NMR (500 MHz, CDCl₃) δ ppm: 7.86 (d, *J* = 7.9 Hz, 1H), 7.78 (m, 1H), 7.47 (t, *J* = 7.7 Hz, 1H), 7.36 (t, *J* = 7.6 Hz, 1H), 7.32–7.23 (m, 3H), 7.21–7.18 (m, 2H), 4.76–4.70 (m, 1H), 3.56–3.51 (m, 1H), 3.29 (dd, *J* = 14.4, 7.8 Hz, 1H). ¹³C NMR (126 MHz, CDCl₃) δ ppm: 167.1, 157.3, 148.2, 135.3, 132.3, 129.6, 128.8, 127.7, 127.72, 126.7, 124.6, 121.7, 121.3, 60.3, 41.2. MS (ESI⁺) *m/z* 316.98 [M+H]⁺.

***S*-(1-(Benzo[d]thiazol-2-ylamino)-1-oxo-3-phenylpropan-2-yl) ethanethioate (19b).**

Compound **19b** was prepared according to general procedure **D**, using compound **19a** (323 mg, 1.02 mmol) and potassium thioacetate (174 mg, 1.53 mmol) in acetone (10 mL). Purification was done by flash chromatography (Hex/DCM, 100:0 to 0:100). The final product was obtained as yellow solid (257, 71%). ¹H NMR (500 MHz, acetone-*d*₆) δ ppm: 11.24 (s, 1H), 8.02–7.88 (m, 1H), 7.69 (d, *J* = 8.1 Hz, 1H), 7.43 (m, 1H), 7.35–7.26 (m, 5H), 7.24–7.17 (m, 1H), 4.72 (dd, *J* = 8.7, 6.9 Hz, 1H), 3.41 (dd, *J* = 13.8, 8.7 Hz, 1H), 3.06 (dd, *J* = 13.8, 6.9 Hz, 1H), 2.36 (s, 3H). ¹³C NMR (126 MHz, CDCl₃) δ ppm: 196.2, 169.1, 157.6, 148.4, 136.9, 132.3, 129.3, 128.8, 127.4, 126.5, 124.3, 121.5, 121.2, 47.9, 35.9, 30.5. MS (ESI⁺) *m/z* 357.01 [M+H]⁺, 314.90 [M–Ac+H]⁺.

***N*-(Benzo[d]thiazol-2-yl)-2-mercapto-3-phenylpropanamide (19).**

Compound **19** was prepared according to general procedure **E**, using compound **19b** (128 mg, 0.36 mmol) and 2 M NaOH aq. solution (359 μL, 0.72 mmol) in MeOH (3 mL). Purification was done by flash chromatography (Hex/EtOAc, 7:3). The final product was obtained as white solid (30 mg, 28%). ¹H NMR (500 MHz, CDCl₃) δ ppm: 7.85 (d, *J* = 7.8 Hz 1H), 7.76 (d, *J* = 8.1, 1H), 7.49–7.44 (m, 1H), 7.39–7.36 (m, 1H), 7.29–7.27 (m, 1H), 7.25–7.15 (m, 4H), 3.87–3.80 (m, 1H), 3.40 (dd, *J* = 14.0, 7.0 Hz, 1H), 3.24 (dd, *J* = 14.0, 6.8 Hz, 1H), 2.26–2.17 (m, 1H). ¹³C NMR (126 MHz, CDCl₃) δ ppm: 170.7, 159.0, 145.5, 136.7, 131.0, 129.4, 128.9, 127.5, 127.2, 125.0, 121.9, 120.2, 44.7, 41.1. HRMS (ESI⁺) *m/z* calcd. for C₁₆H₁₅N₂OS₂ [M+H]⁺ 315.06203, found 315.06178.

References

- 1 Mesaros, N.; Nordmann, P.; Plésiat, P.; Roussel-Delvallez, M.; Eldere, J. Van; Glupczynski, Y.; Laethem, Y. Van; Jacobs, F.; Lebecque, P.; Malfroot, A.; Tulkens, P. M.; Bambeke, F. Van. *Pseudomonas Aeruginosa: Resistance and Therapeutic Options at the Turn of the New Millennium. Clin. Microbiol. Infect.* 2007, 13 (6), 560–578. <https://doi.org/http://dx.doi.org/10.1111/j.1469-0691.2007.01681.x>.
- 2 Gary Taubes. The Bacteria Fight Back. *Science* (80-.). 2008, 321 (5887), 356–361. <https://doi.org/10.1126/science.321.5887.356>.
- 3 Magill, S. S.; Edwards, J. R.; Bamberg, W.; Beldavs, Z. G.; Dumyati, G.; Kainer, M. A.; Lynfield, R.; Maloney, M.; McAllister-Hollod, L.; Nadle, J.; Ray, S. M.; Thompson, D. L.; Wilson, L. E.; Fridkin, S. K. Multistate Point-Prevalence Survey of Health Care–Associated Infections. *N. Engl. J. Med.* 2014, 370 (13), 1198–1208. <https://doi.org/10.1056/nejmoa1306801>.
- 4 Ma, Y. X.; Wang, C. Y.; Li, Y. Y.; Li, J.; Wan, Q. Q.; Chen, J. H.; Tay, F. R.; Niu, L. N. Considerations and Caveats in Combating ESKAPE Pathogens against Nosocomial Infections. *Adv. Sci.* 2020, 7 (1). <https://doi.org/10.1002/advs.201901872>.
- 5 Valenza, G.; Tappe, D.; Turnwald, D.; Frosch, M.; König, C.; Hebestreit, H.; Abele-Horn, M. Prevalence and Antimicrobial Susceptibility of Microorganisms Isolated from Sputa of Patients with Cystic Fibrosis. *J. Cyst. Fibros.* 2008, 7 (2), 123–127. <https://doi.org/10.1016/j.jcf.2007.06.006>.
- 6 Sordé, R.; Pahissa, A.; Rello, J. Management of Refractory *Pseudomonas Aeruginosa* Infection in Cystic Fibrosis. *Infect. Drug Resist.* 2011, 4 (1), 31–41. <https://doi.org/10.2147/IDR.S16263>.
- 7 Pos, K. M. Drug Transport Mechanism of the AcrB Efflux Pump. *Biochim. Biophys. Acta - Proteins Proteomics* 2009, 1794 (5), 782–793. <https://doi.org/10.1016/j.bbapap.2008.12.015>.
- 8 Li, X. Z.; Plésiat, P.; Nikaido, H. The Challenge of Efflux-Mediated Antibiotic Resistance in Gram-Negative Bacteria. *Clin. Microbiol. Rev.* 2015, 28 (2), 337–418. <https://doi.org/10.1128/CMR.00117-14>.
- 9 J. Wolter, D.; D. Lister, P. Mechanisms of β -Lactam Resistance Among *Pseudomonas Aeruginosa*. *Curr. Pharm. Des.* 2012, 19 (2), 209–222. <https://doi.org/10.2174/138161213804070311>.
- 10 Li, X. Z.; Livermore, D. M.; Nikaido, H. Role of Efflux Pump(s) in Intrinsic Resistance of *Pseudomonas Aeruginosa*: Resistance to Tetracycline, Chloramphenicol, and Norfloxacin. *Antimicrob. Agents Chemother.* 1994, 38 (8), 1732–1741. <https://doi.org/10.1128/AAC.38.8.1732>.
- 11 Pang, Z.; Raudonis, R.; Glick, B. R.; Lin, T. J.; Cheng, Z. Antibiotic Resistance in *Pseudomonas Aeruginosa*: Mechanisms and Alternative Therapeutic Strategies. *Biotechnol. Adv.* 2019, 37 (1), 177–192. <https://doi.org/10.1016/j.biotechadv.2018.11.013>.
- 12 Strateva, T.; Yordanov, D. *Pseudomonas Aeruginosa* - A Phenomenon of Bacterial Resistance. *J. Med. Microbiol.* 2009, 58 (9), 1133–1148. <https://doi.org/10.1099/jmm.0.009142-0>.
- 13 Nikaido, H.; Yoshimura, F. Permeability of *Pseudomonas Aeruginosa* Outer Membrane to Hydrophilic Solutes. *J. Bacteriol.* 1982, 152 (2), 636–642.
- 14 Dickey, S. W.; Cheung, G. Y. C.; Otto, M. Different Drugs for Bad Bugs: Antivirulence Strategies in the Age of Antibiotic Resistance. *Nat. Rev. Drug Discov.* 2017, 16 (7), 457–471. <https://doi.org/10.1038/nrd.2017.23>.
- 15 Rasko, D. A.; Sperandio, V. Anti-Virulence Strategies to Combat Bacteria-Mediated Disease. *Nat. Rev. Drug Discov.* 2010, 9 (2), 117–128. <https://doi.org/10.1038/nrd3013>.
- 16 Strateva, T.; Mitov, I. Contribution of an Arsenal of Virulence Factors to Pathogenesis of *Pseudomonas Aeruginosa* Infections. *Ann. Microbiol.* 2011, 61 (4), 717–732. <https://doi.org/10.1007/s13213-011-0273-y>.

- 17 Heras, B.; Scanlon, M. J.; Martin, J. L. Targeting Virulence Not Viability in the Search for Future Antibacterials. *Br. J. Clin. Pharmacol.* 2015, *79* (2), 208–215. <https://doi.org/10.1111/bcp.12356>.
- 18 Clatworthy, A. E.; Pierson, E.; Hung, D. T. Targeting Virulence: A New Paradigm for Antimicrobial Therapy. *Nat. Chem. Biol.* 2007, *3* (9), 541–548. <https://doi.org/10.1038/nchembio.2007.24>.
- 19 Wagner, S.; Sommer, R.; Hinsberger, S.; Lu, C.; Hartmann, R. W.; Empting, M.; Titz, A. Novel Strategies for the Treatment of Pseudomonas Aeruginosa Infections. *J. Med. Chem.* 2016, *59* (13), 5929–5969. <https://doi.org/10.1021/acs.jmedchem.5b01698>.
- 20 Rounds, J.; Strain, J. Bezlotoxumab for Preventing Recurrent Clostridium Difficile Infections. *S. D. Med.* 2017, *70* (9), 422–423. <https://doi.org/10.1056/nejmoa1602615>.
- 21 Bastaert, F.; Kheir, S.; Saint-Criq, V.; Villeret, B.; Dang, P. M. C.; El-Benna, J.; Sirard, J. C.; Voulhoux, R.; Sallenave, J. M. Pseudomonas Aeruginosa LasB Subverts Alveolar Macrophage Activity by Interfering with Bacterial Killing through Downregulation of Innate Immune Defense, Reactive Oxygen Species Generation, and Complement Activation. *Front. Immunol.* 2018, *9* (JUL), 1–18. <https://doi.org/10.3389/fimmu.2018.01675>.
- 22 Liu, P. V. Extracellular Toxins of Pseudomonas Aeruginosa. *J. Infect. Dis.* 1974, *130* (November), S94–S99. <https://doi.org/10.1093/infdis/130.Supplement.S94>.
- 23 Morihara, K.; Tsuzuki, H.; Oka, T.; Inoue, H.; Ebata, M. Pseudomonas Aeruginosa Elastase: Isolation, Crystallization and Preliminary Characterization. 1965, *240* (8), 3297–3304.
- 24 Heck, L. W.; Morihara, K.; McRae, W. B.; Miller, E. J. Specific Cleavage of Human Type III and IV Collagens by Pseudomonas Aeruginosa Elastase. *Infect. Immun.* 1986, *51* (1), 115–118.
- 25 Heck, L. W.; Alarcon, P. G.; Kulhavy, R. M.; Morihara, K.; Mestecky, M. W.; Russell, J. F. Degradation of IgA Proteins by Pseudomonas Aeruginosa Elastase. *J. Immunol.* 1990, *144*, 2253–2257.
- 26 Holder, I. A.; Wheeler, R. Experimental Studies of the Pathogenesis of Infections Owing to Pseudomonas Aeruginosa: Elastase, an IgG Protease. *Can. J. Microbiol.* 1984, *30* (9), 1118–1124.
- 27 Galloway, D. R. Pseudomonas Aeruginosa Elastase and Elastolysis Revisited: Recent Developments. *Mol. Microbiol.* 1991, *5* (10), 2315–2321. <https://doi.org/10.1111/j.1365-2958.1991.tb02076.x>.
- 28 Parmely, M.; Gale, A.; Clabaugh, M.; Horvat, R.; Zhou, W. Proteolytic Inactivation of Cytokines by Pseudomonas Aeruginosa. *Infect. Immun.* 1990, *58* (9), 3009–3014.
- 29 Mariencheck, W. I.; Alcorn, J. F.; Palmer, S. M.; Wright, J. R. Pseudomonas Aeruginosa Elastase Degrades Surfactant Proteins A and D. *Am. J. Respir. Cell Mol. Biol.* 2003, *28* (4), 528–537. <https://doi.org/10.1165/rcmb.2002-0141OC>.
- 30 Oda, K.; Koyama, T.; Murao, S. Purification and Properties of a Proteinaceous Metallo-Proteinase Inhibitor from Streptomyces Nigrescens TK-23. *Biochim. Biophys. Acta* 1979, *571*, 147–156.
- 31 Nishino, N.; Powers, J. C. Pseudomonas Aeruginosa Elastase - Development of a New Substrate, Inhibitors and an Affinity Ligand. *J. Biol. Chem.* 1979, *255* (8), 3482–19.
- 32 Fullagar, J. L.; Garner, A. L.; Struss, A. K.; Day, J. A.; Martin, D. P.; Yu, J.; Cai, X.; Janda, K. D.; Cohen, S. M. Antagonism of a Zinc Metalloprotease Using a Unique Metal-Chelating Scaffold: Tropolones as Inhibitors of P. Aeruginosa Elastase. *Chem. Commun.* 2013, *49* (31), 3197–3199. <https://doi.org/10.1039/c3cc41191e>.
- 33 Leiris, S.; Davies, D. T.; Sprynski, N.; Castandet, J.; Beyria, L.; Bodnarchuk, M. S.; Sutton, J. M.; Mullins, T. M. G.; Jones, M. W.; Forrest, A. K.; Pallin, T. D.; Karunakar, P.; Martha, S. K.; Parusharamulu, B.; Ramula, R.; Kotha, V.; Pottabathini, N.; Pothukanuri, S.; Lemonnier, M.; Everett, M. Virtual Screening Approach to Identifying a Novel and Tractable Series of Pseudomonas Aeruginosa Elastase Inhibitors. *ACS Med. Chem. Lett.* 2021, *12* (2), 217–227. <https://doi.org/10.1021/acsmchemlett.0c00554>.

- 34 Cathcart, G. R. A.; Quinn, D.; Greer, B.; Harriott, P.; Lynas, J. F.; Gilmore, B. F.; Walker, B. Novel Inhibitors of the *Pseudomonas Aeruginosa* Virulence Factor LasB: A Potential Therapeutic Approach for the Attenuation of Virulence Mechanisms in Pseudomonas Infection. *Antimicrob. Agents Chemother.* 2011, *55* (6), 2670–2678. <https://doi.org/10.1128/AAC.00776-10>.
- 35 Burns, F. R.; Paterson, C. A.; Gray, R. D.; Wells, J. T. Inhibition of *Pseudomonas Aeruginosa* Elastase and *Pseudomonas Keratitis* Using a Thiol-Based Peptide. *Antimicrob. Agents Chemother.* 1990, *34* (11), 2065–2069. <https://doi.org/10.1128/AAC.34.11.2065>.
- 36) Zhu, J.; Cai, X.; Harris, T. L.; Gooyit, M.; Wood, M.; Lardy, M.; Janda, K. D. Disarming *Pseudomonas Aeruginosa* Virulence Factor Lasb by Leveraging a *Caenorhabditis Elegans* Infection Model. *Chem. Biol.* 2015, *22* (4), 483–491. <https://doi.org/10.1016/j.chembiol.2015.03.012>.
- 37 Adekoya, O. A.; Sjøli, S.; Wuxiuer, Y.; Bilot, I.; Marques, S. M.; Santos, M. A.; Nuti, E.; Cercignani, G.; Rossello, A.; Winberg, J. O.; Sylte, I. Inhibition of Pseudolysin and Thermolysin by Hydroxamate-Based MMP Inhibitors. *Eur. J. Med. Chem.* 2015, *89*, 340–348. <https://doi.org/10.1016/j.ejmech.2014.10.009>.
- 38 Kany, A. M.; Sikandar, A.; Yahiaoui, S.; Hauptenthal, J.; Walter, I.; Empting, M.; Köhnke, J.; Hartmann, R. W. Tackling *Pseudomonas Aeruginosa* Virulence by a Hydroxamic Acid-Based LasB Inhibitor. *ACS Chem. Biol.* 2018, *13* (9), 2449–2455. <https://doi.org/10.1021/acscchembio.8b00257>.
- 39 Pfaff, A. R.; Beltz, J.; King, E.; Ercal, N. Medicinal Thiols: Current Status and New Perspectives. *Mini-Reviews Med. Chem.* 2019, *20* (6), 513–529. <https://doi.org/10.2174/1389557519666191119144100>.
- 40 Kaya, C.; Walter, I.; Yahiaoui, S.; Sikandar, A.; Alhayek, A.; Konstantinović, J.; Kany, A. M.; Hauptenthal, J.; Köhnke, J.; Hartmann, R. W.; Hirsch, A. K. H. Substrate-inspired Fragment Merging and Growing Affords Efficacious LasB Inhibitors. *Angew. Chemie Int. Ed.* 2021. <https://doi.org/10.1002/anie.202112295>.
- 41 Jobin, P. G.; Butler, G. S.; Overall, C. M. New Intracellular Activities of Matrix Metalloproteinases Shine in the Moonlight. *Biochim. Biophys. Acta - Mol. Cell Res.* 2017, *1864* (11), 2043–2055. <https://doi.org/10.1016/j.bbamcr.2017.05.013>.
- 42 Agrawal, A.; Romero-Perez, D.; Jacobsen, J. A.; Villarreal, F. J.; Cohen, S. M. Zinc-Binding Groups Modulate Selective Inhibition of MMPs. *ChemMedChem* 2008, *3* (5), 812–820. <https://doi.org/10.1002/cmdc.200700290>.
- 43 Kany, A. M.; Sikandar, A.; Hauptenthal, J.; Yahiaoui, S.; Maurer, C. K.; Proschak, E.; Köhnke, J.; Hartmann, R. W. Binding Mode Characterization and Early in Vivo Evaluation of Fragment-Like Thiols as Inhibitors of the Virulence Factor LasB from *Pseudomonas Aeruginosa*. *ACS Infect. Dis.* 2018, *4* (6), 988–997. <https://doi.org/10.1021/acsinfectdis.8b00010>.
- 44 Publication, A. (S)-2-Chloroalkanoic Acids of High Enantiomeric Purity From (S)-2-Amino Acids: (S)-2-Chloropropanoic Acid. *Org. Synth.* 1988, *66* (September), 151. <https://doi.org/10.15227/orgsyn.066.0151>.
- 45 Schrödinger, L., & DeLano, W. (2020). P. R. from <http://www.pymol.org/pymo>. The PyMOL Molecular Graphics System, Version 2.0 Schrödinger, LLC. 2021.
- 46 Prachayasittikul, S.; Pingaew, R.; Worachartcheewan, A.; Sinthupoom, N.; Prachayasittikul, V.; Ruchirawat, S.; Prachayasittikul, V. Roles of Pyridine and Pyrimidine Derivatives as Privileged Scaffolds in Anticancer Agents. *Mini-Reviews Med. Chem.* 2016, *17* (10), 869–901. <https://doi.org/10.2174/1389557516666160923125801>.
- 47 Boiani, M.; Gonzalez, M. Imidazole and Benzimidazole Derivatives as Chemotherapeutic Agents. *Mini-Reviews Med. Chem.* 2005, *5* (4), 409–424. <https://doi.org/10.2174/1389557053544047>.
- 48 SeeSAR v.11.1, BioSolveIT GmbH, Sankt Augustin, G. 2021. Available from: <Http://Www.Biosolveit.de/SeeSAR>.
- 49 Schönauer, E.; Kany, A. M.; Hauptenthal, J.; Hüsecken, K.; Hoppe, I. J.; Voos, K.; Yahiaoui, S.; Elsässer, B.; Ducho, C.; Brandstetter, H.; Hartmann, R. W. Discovery of a Potent Inhibitor Class with High

- Selectivity towards Clostridial Collagenases. *J. Am. Chem. Soc.* 2017, jacs.7b06935. <https://doi.org/10.1021/jacs.7b06935>.
- 50 Konstantinović, J.; Yahiaoui, S.; Alhayek, A.; Haupenthal, J.; Schönauer, E.; Andreas, A.; Kany, A. M.; Müller, R.; Koehnke, J.; Berger, F. K.; Bischoff, M.; Hartmann, R. W.; Brandstetter, H.; Hirsch, A. K. H. N-Aryl-3-Mercaptosuccinimides as Antivirulence Agents Targeting *Pseudomonas Aeruginosa* Elastase and *Clostridium* Collagenases. *J. Med. Chem.* 2020, 63 (15), 8359–8368. <https://doi.org/10.1021/acs.jmedchem.0c00584>.
- 51 Sternlicht, M. D.; Werb, Z. How Matrix Metalloproteinases Regulate Cell Behavior. *Annu. Rev. Cell Dev. Biol.* 2001, 17 (1), 463–516. <https://doi.org/10.1146/annurev.cellbio.17.1.463>.
- 52 Gooz, M. ADAM-17: The Enzyme That Does It All. *Crit. Rev. Biochem. Mol. Biol.* 2010, 45 (2), 146–169. <https://doi.org/10.3109/10409231003628015>.
- 53 Ropero, S.; Esteller, M. The Role of Histone Deacetylases (HDACs) in Human Cancer. *Mol. Oncol.* 2007, 1 (1), 19–25. <https://doi.org/10.1016/j.molonc.2007.01.001>.
- 54 MacRae, C. A.; Peterson, R. T. Zebrafish as Tools for Drug Discovery. *Nat. Rev. Drug Discov.* 2015, 14 (10), 721–731. <https://doi.org/10.1038/nrd4627>.
- 55 Chakraborty, C.; Sharma, A. R.; Sharma, G.; Lee, S. S. Zebrafish: A Complete Animal Model to Enumerate the Nanoparticle Toxicity. *J. Nanobiotechnology* 2016, 14 (1), 1–13. <https://doi.org/10.1186/s12951-016-0217-6>.

Supporting information

Supplementary Figures

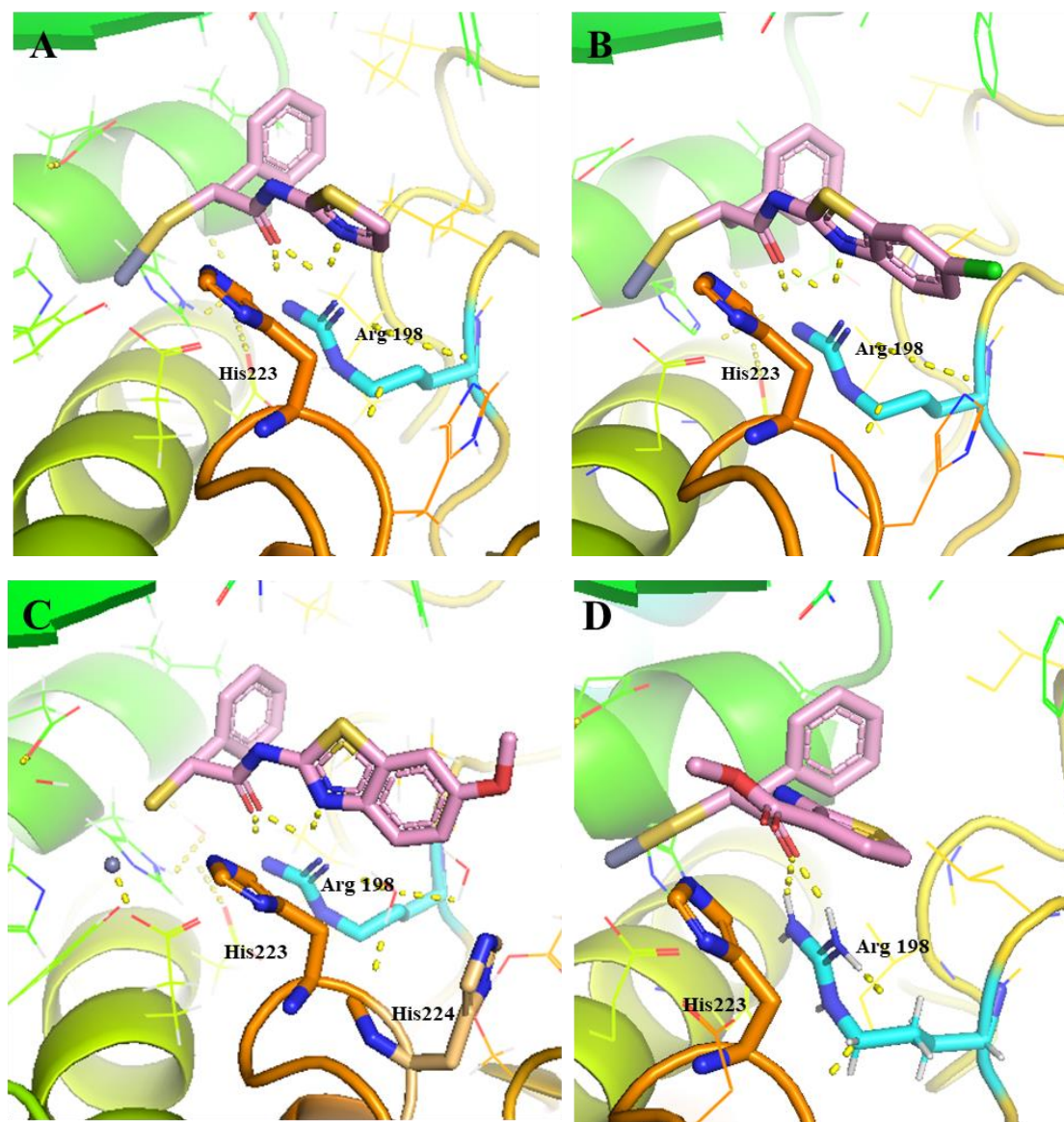


Figure S1. Docking poses for A) Thiazole, B) 6-chlorobenzothiazolyl, C) 6-methoxybenzothiazolyl and D) Methyl thiophenyl 3-carboxylate replacement in the LasB ligand binding pocket. Figures are generated using PyMOL V.2.5 software.¹¹

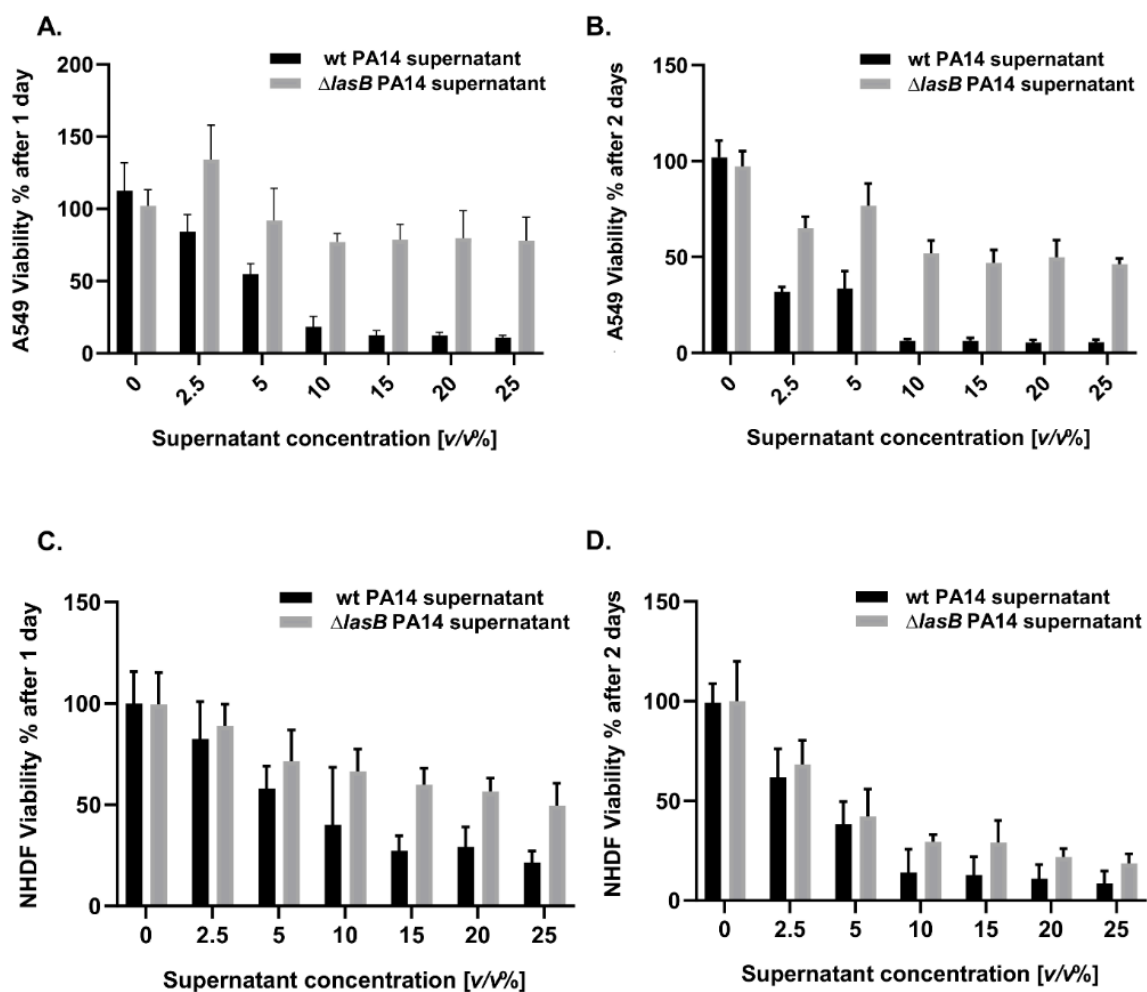


Figure S2. Illustration of the dose-dependent cytotoxic effect of wt) PA14 and $\Delta lasB$ PA14 supernatant on normal human dermal fibroblast (NHDF) and adenocarcinomic human alveolar basal epithelial (A549) cells. **A)** wt PA14 supernatant reduces the viability of A549 cells after 24 h incubation compared with $\Delta lasB$ PA14 supernatant. **B)** wt PA14 supernatant effect on the cell viability after 48 h incubation with A549 cells, the viability is further minimized. **C)** wt PA14 supernatant effect on NHDF cell after 24 h incubation, its cytotoxic effect on NHDF cells is less than on A549 cells **D)** The cytotoxic effect of wt supernatant after 48 h incubation with NHDF cells is improved. This confirms that LasB is one of the major virulence factors present in the supernatant. The low cytotoxic effect observed with the $\Delta lasB$ PA14 supernatant might be due to effect of other extracellular toxins than LasB such as phospholipase, LasA, phytotoxic factors and exotoxins.¹⁴ Each graph is a representation of three independent experiments \pm SD. The percentage shows the amount of supernatant in the whole volume of Dulbecco's Modified Eagle Medium (DMEM) and cells. PA14: wild-type *Pseudomonas aeruginosa*, $\Delta lasB$ PA14: LasB knockout *P. aeruginosa*.

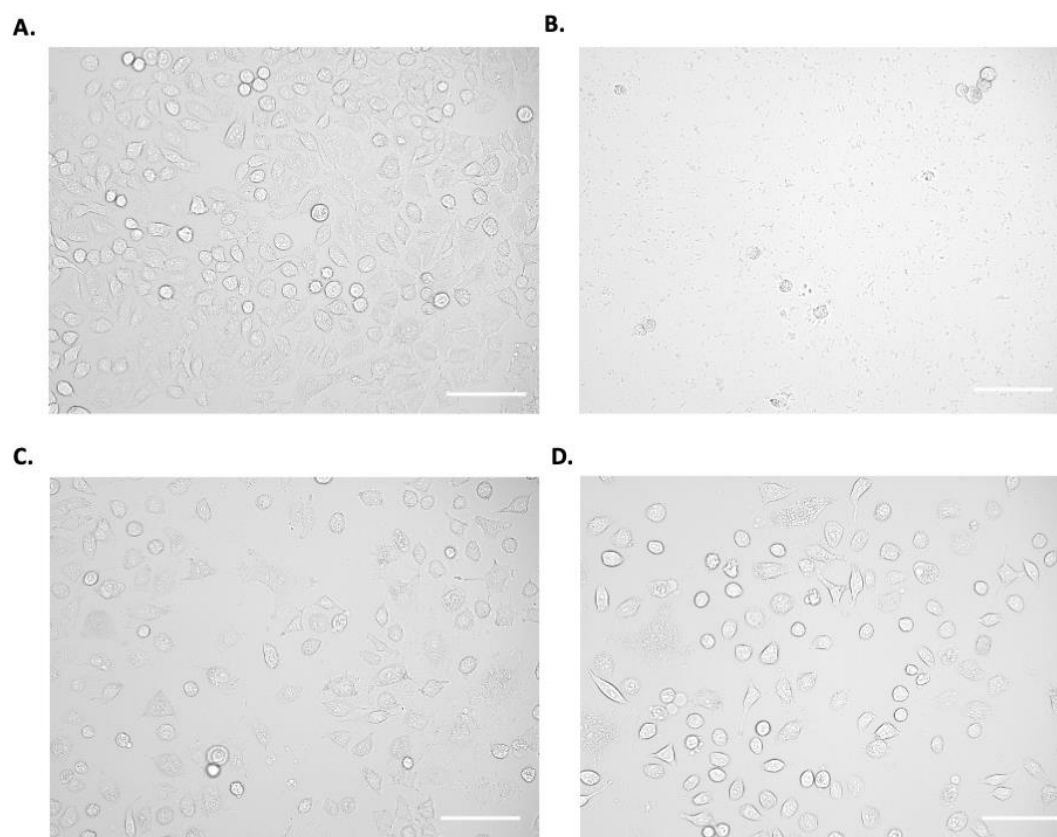


Figure S3. Visualization of differently treated adenocarcinomic human alveolar basal epithelial (A549) cells. **A)** Untreated cells; **B)** Cells treated with 15% (v/v) wt PA14 supernatant, cell density significantly reduced compared with untreated cells; **C)** A549 cells treated with 15% (v/v) $\Delta lasB$ PA14 supernatant; cell density is still high, and the morphology of the cells did not change; **D)** Cells challenged with wt PA14 supernatant and treated with Pam; their cell integrity and morphology were maintained. Images were generated with 20X objective by Leica Las X and modified with the software Fiji ImageJ (Scale bar: 100 μ m). wt PA14: wild-type *Pseudomonas aeruginosa*, $\Delta lasB$ PA14: LasB knockout *P. aeruginosa*.

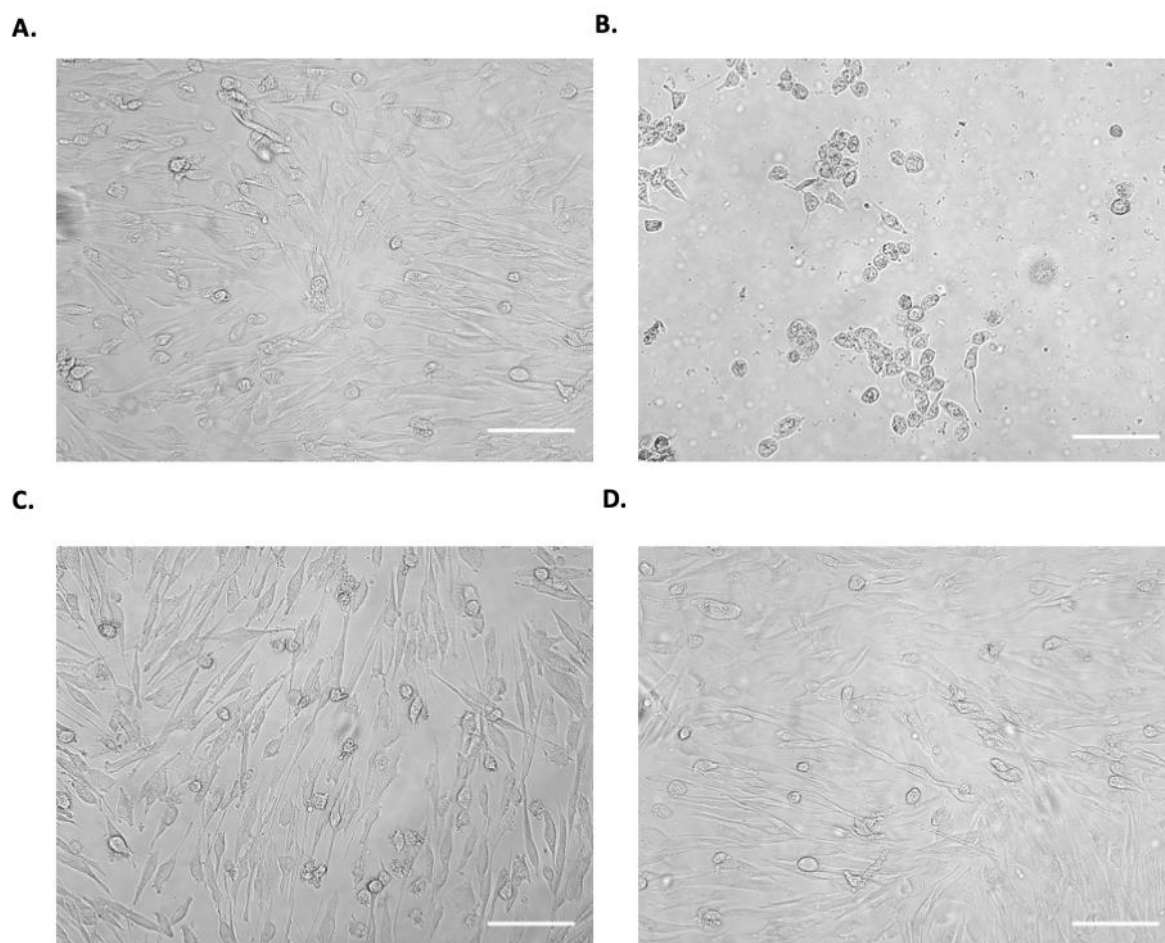


Figure S4. Visualization of differently treated normal human dermal fibroblast (NHDF) cells. **A)** Untreated cells; **B)** Cells treated with 15% (v/v) wt PA14 supernatant, cell density significantly reduced compared with untreated cells; **C)** Cells treated with 15% (v/v) $\Delta lasB$ PA14 supernatant; the cell density is still high, and the morphology of the cells did not change; **D)** Cells challenged with wt PA14 supernatant and treated with Pam; their cell integrity and morphology were maintained. Images were generated with 20X objective by Leica Las X and modified with the software Fiji ImageJ (Scale bar: 100 μm). wt PA14: wild-type *Pseudomonas aeruginosa*, $\Delta lasB$ PA14: LasB knockout *P. aeruginosa*.

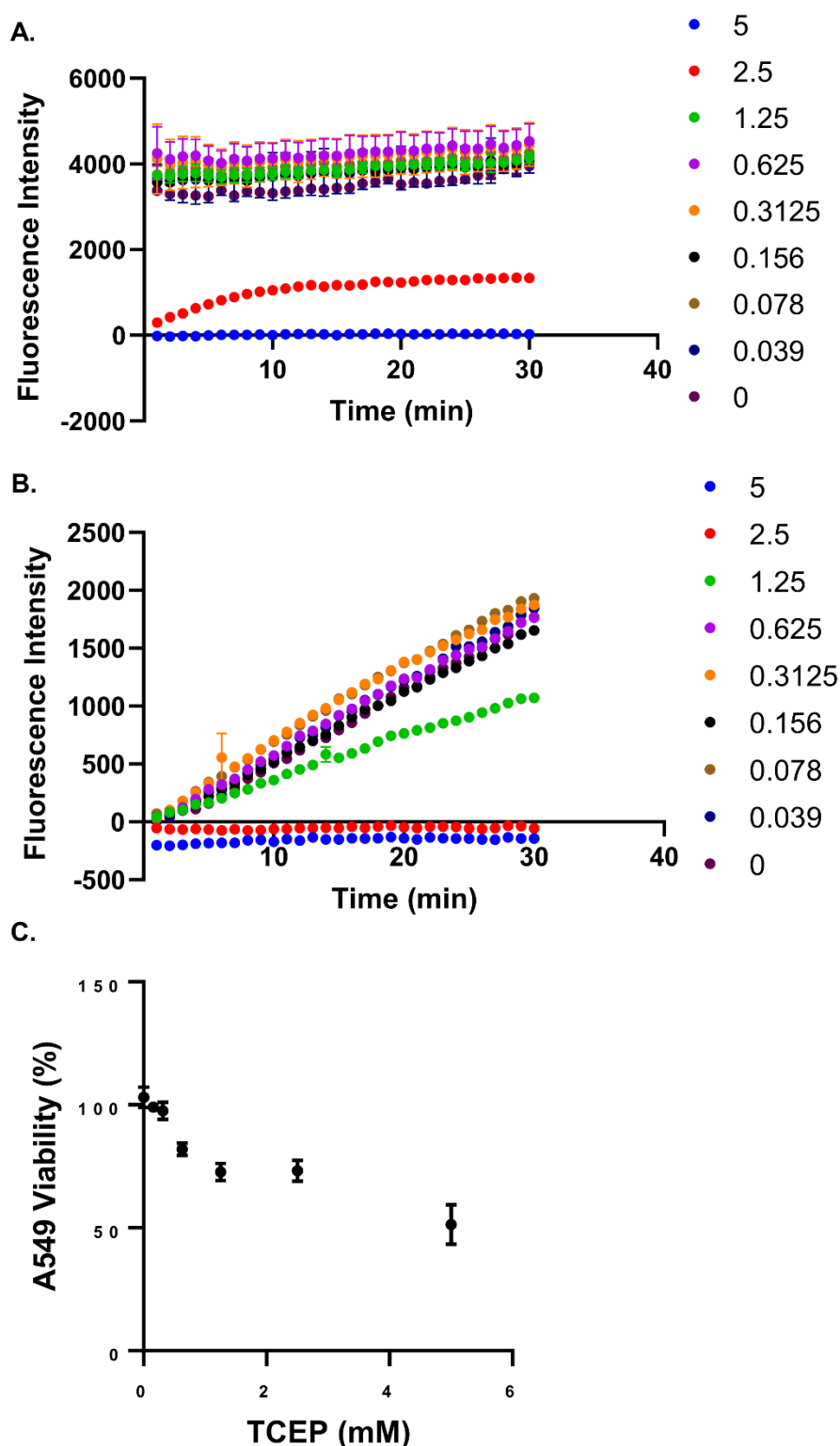


Figure S5. Effect of a reducing agent on LasB activity. **A)** Activity of LasB presented in 10% (v/v) wt PA14 supernatant incubated with different concentrations (mM) of TCEP, similar to pure LasB high concentration of TCEP (*i.e.*, 5 and 2.5 mM) inhibited the activity of LasB in the supernatant. **B)** Effect of various concentrations (mM) of TCEP on 0.3 nM pure LasB. The activity was completely lost with 5 mM and 2.5 mM while at 0.6 mM and lower concentrations, it is similar to no TCEP conditions. **C)** Effect of TCEP concentrations on viability of A549 cells. 0.3 mM TCEP showed no effect on cell viability while higher concentrations showed a reduction in the cell viability which was evaluated with MTT assay. Each curve represents a mean \pm SD of at least two independent experiments. wt PA14: wild-type *Pseudomonas aeruginosa*.

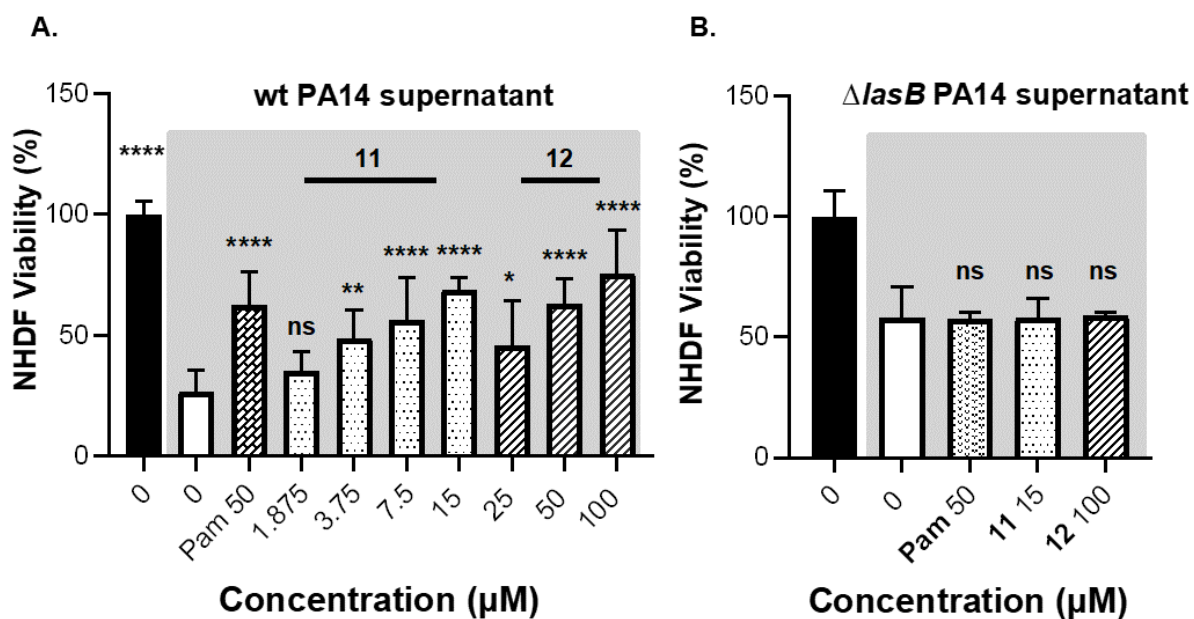


Figure S6. Viability of normal human dermal fibroblast (NHDF) cells treated with 11 and 12 and 15% (v/v) wt PA14 or $\Delta lasB$ PA14 supernatant. **A)** Concentrations-dependent effects of compounds on the viability of NHDF cells treated with wt PA14 supernatant; **B)** Viability of NHDF cells treated with $\Delta lasB$ PA14 supernatant and the highest tested concentration of compound that was used with PA14 supernatant. Each graph is a representation of three independent experiments \pm SD. One-way ANOVA was performed for each experiment following Dunnett's multiple comparisons test and moreover, the mean of each column was compared with the mean of the negative control (ns: not significant, *: $p \leq 0.05$, **: $p \leq 0.01$, ****: $p \leq 0.0001$). wt PA14: wild-type *Pseudomonas aeruginosa*, $\Delta lasB$ PA14: LasB knockout *P. aeruginosa*.

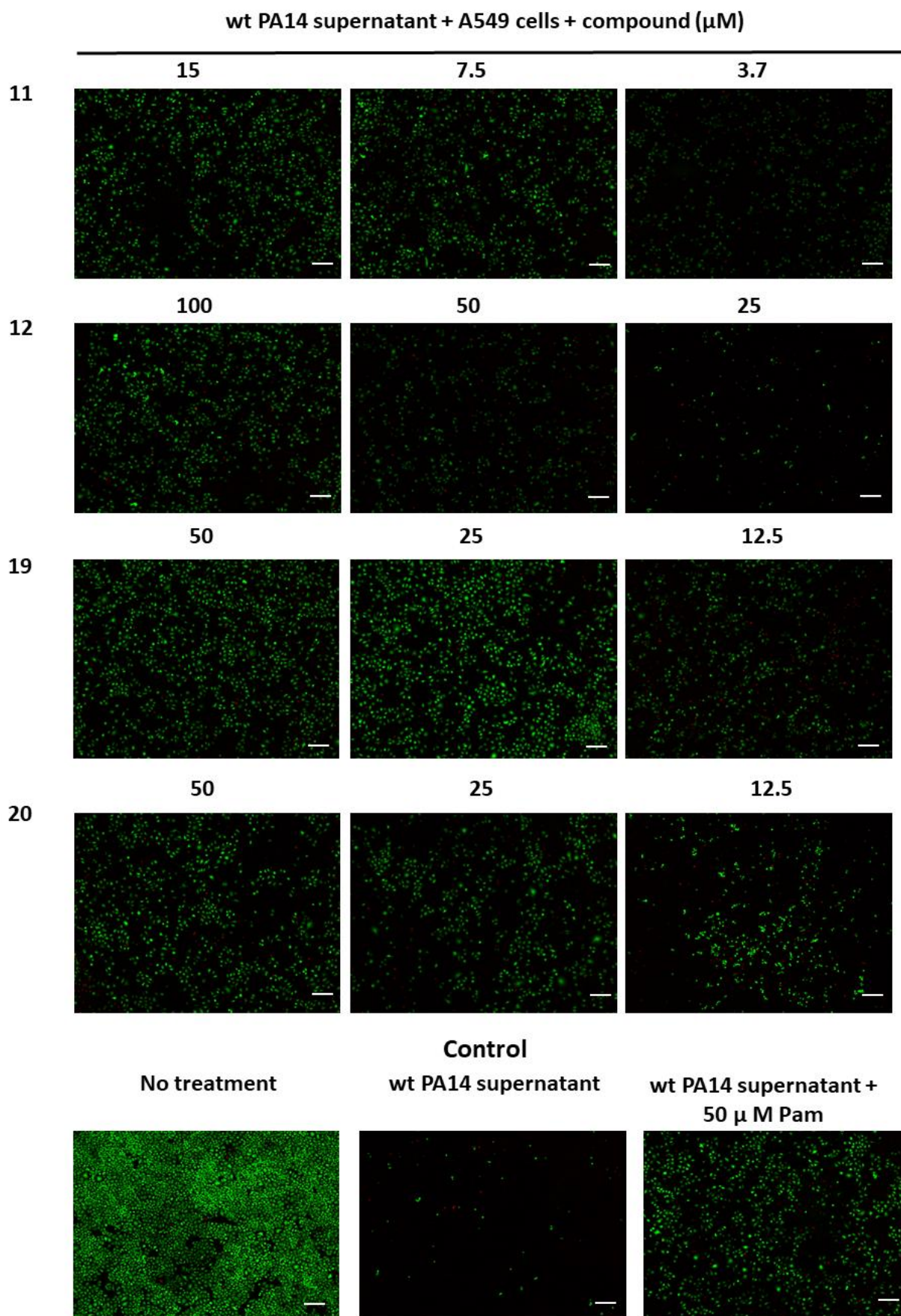


Figure S7. Visualization of the effects of compounds 11, 12, 19 and 20 on wt PA14 supernatant treated adenocarcinomic human alveolar basal epithelial (A549) cells. Live/dead staining was carried out with fluoresceine diacetate and propidium iodide. Living cells are shown in green and dead cells in red. Red signal in some cases was lost because the detached cells were washed away after the rinsing step with PBS (scale bar: 200 μm). wt PA14: wild-type *Pseudomonas aeruginosa*.

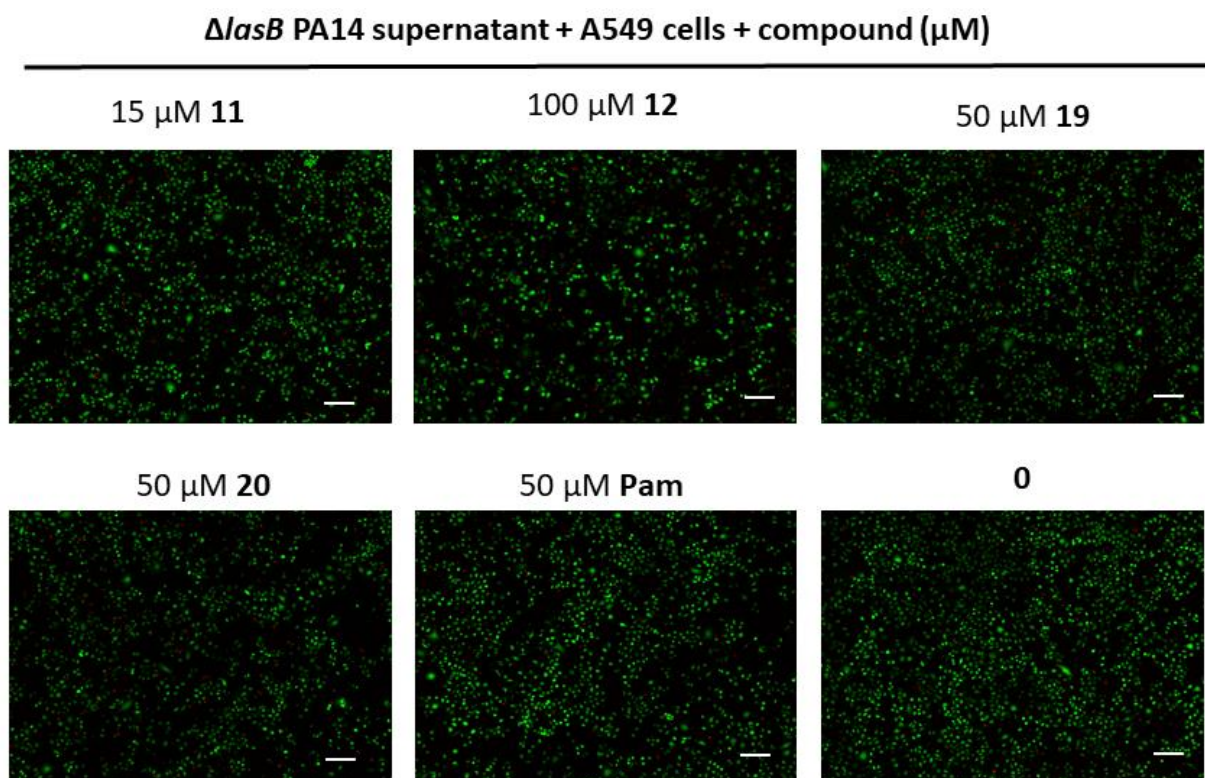


Figure S8. Visualization of effect of compounds 11, 12, 19 and 20 on ΔlasB PA14 supernatant applied adenocarcinomic human alveolar basal epithelial (A549) cells. Live/dead staining was carried out with fluoresceine diacetate and propidium iodide. Live cells are showed in a green and dead cells in red. Scale bar: 200 μm . Red signal in some cases was lost because the detached cells were washed away after the rinsing step with PBS. ΔlasB PA14: LasB knockout *Pseudomonas aeruginosa*.

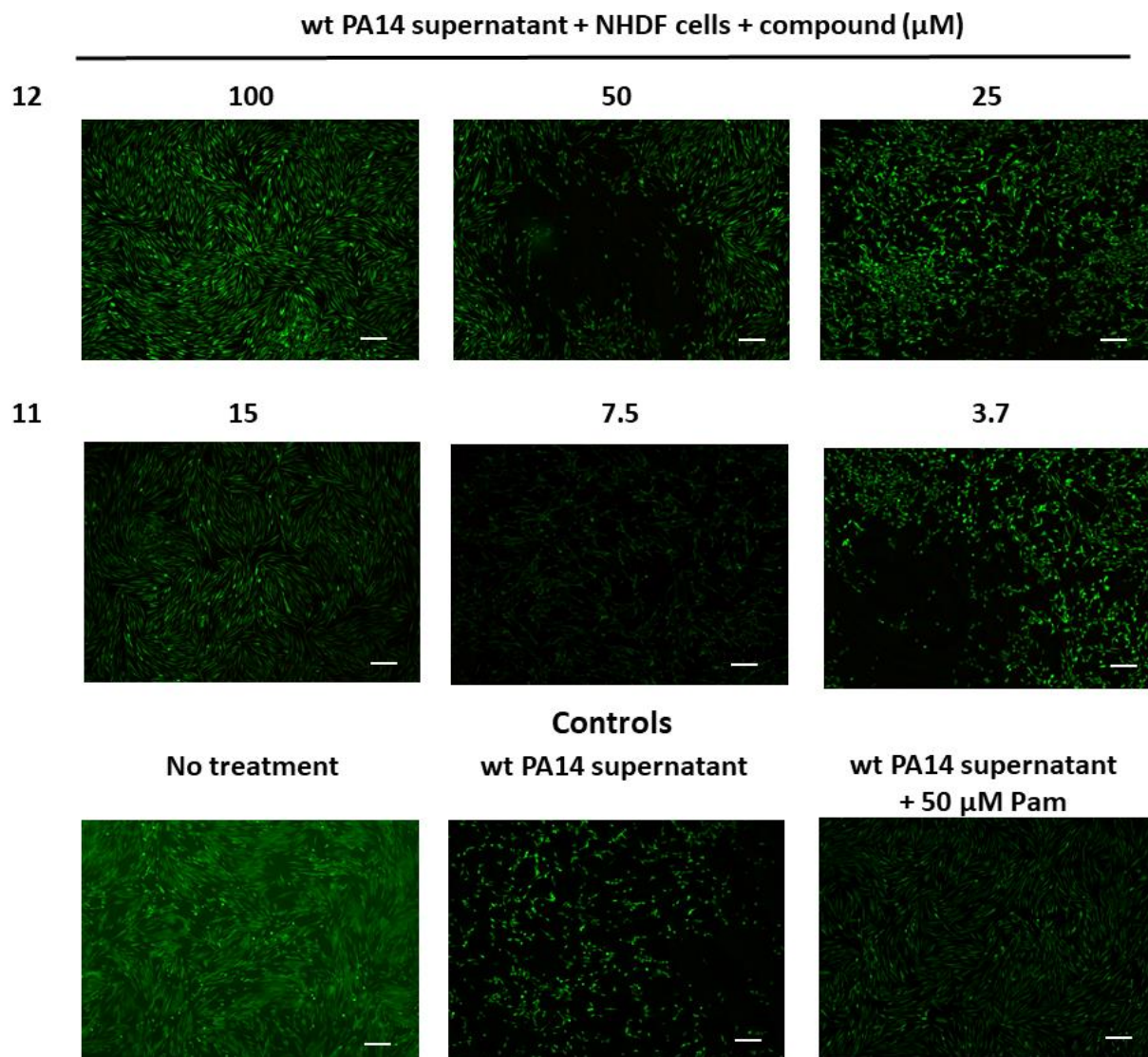


Figure S9. Visualization of the effects of compounds 11 and 12 on wt PA14 supernatant treated human dermal fibroblasts (NHDF) cells. Live/dead staining was carried out with fluoresceine diacetate and propidium iodine. Living cells are shown in green and dead cells in red (Scale bar: 200 μm). Red signal in some cases was lost because the detached cells were washed away after the rinsing step with PBS. wt PA14: wild-type *Pseudomonas aeruginosa*.

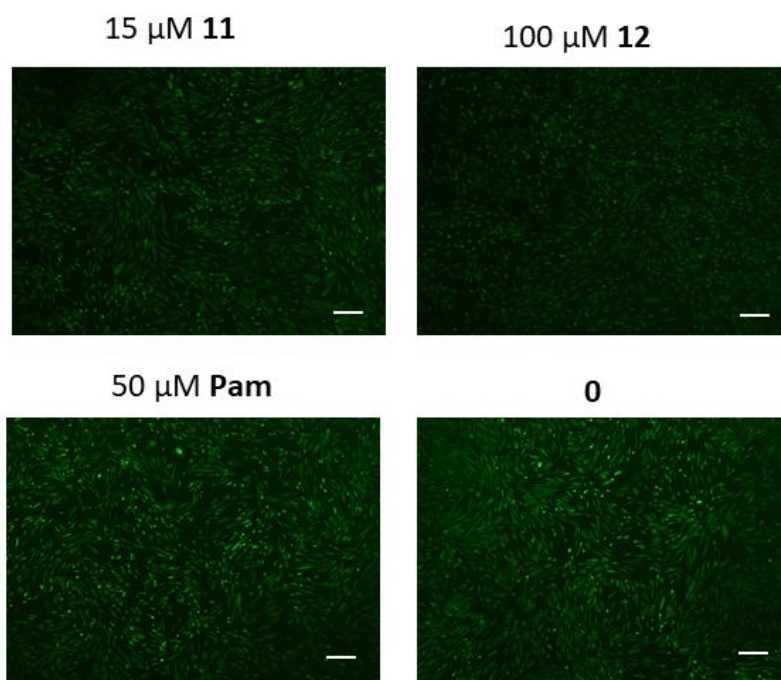
$\Delta lasB$ PA14 supernatant + NHDF cells + Compound

Figure S10. Visualization of effect of compounds 11 and 12 on $\Delta lasB$ PA14 supernatant applied human dermal fibroblasts (NHDF) cells. Live/dead staining was carried out with fluoresceine diacetate and propidium iodine. Live cells are shown in green and dead cells in red. Scale bar: 200 μ m. Red signal in some cases was lost because the detached cells were washed away after the rinsing step with PBS. $\Delta lasB$ PA14: LasB knockout *Pseudomonas aeruginosa*.

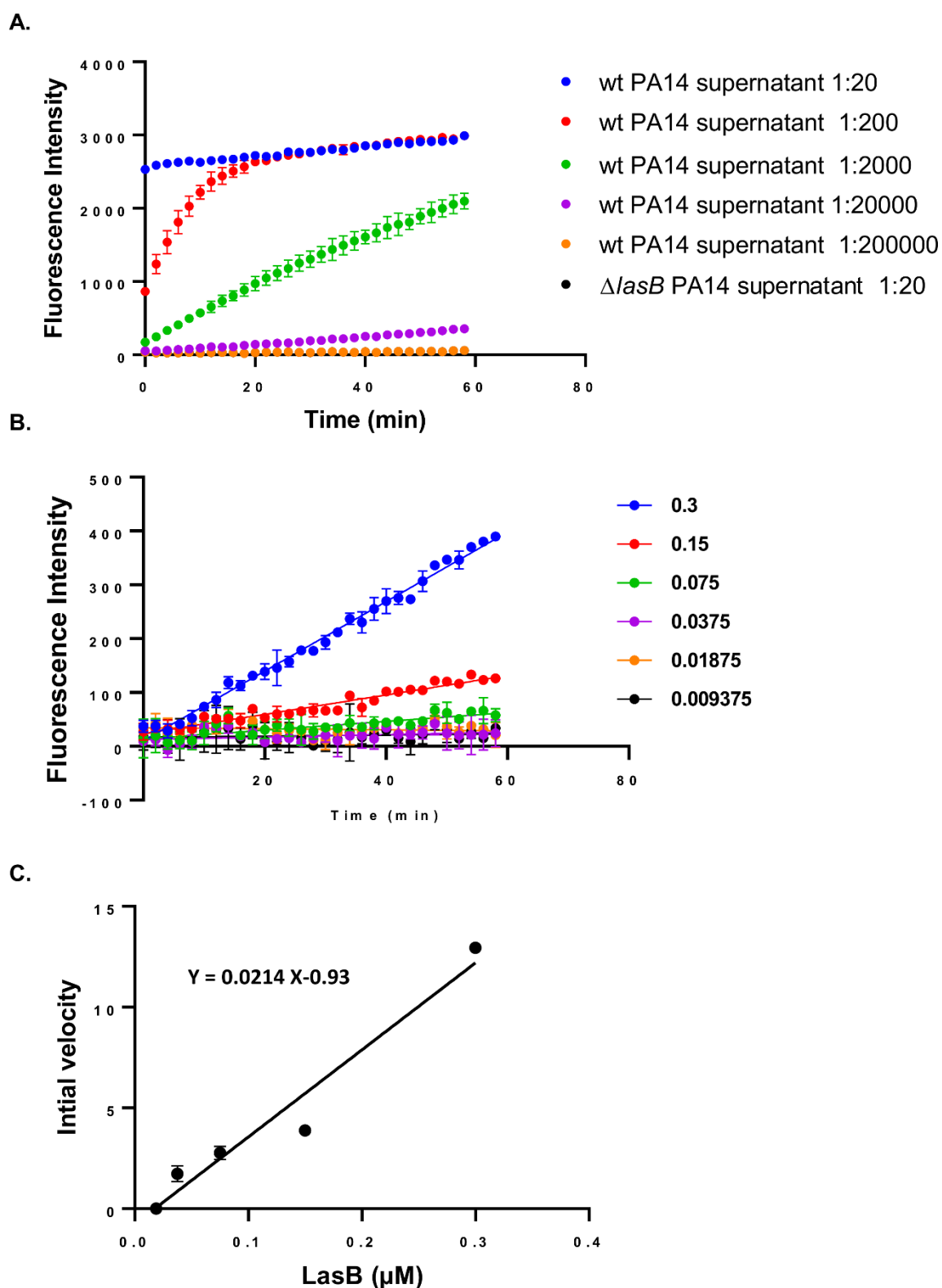


Figure S11. Supernatant evaluation of LasB activity assay. A) The activity of serially diluted wt PA14 and $\Delta lasB$ PA14 supernatants B) The activity of various concentrations of pure LasB. C) The calibration curve that was created from the initial velocity that we calculated from graph B. The calibration curve estimates that 100% supernatant has 0.88 μM of LasB.

Supplementary Tables

Table S1. K_i values for six selected compounds against ColH-PD and % inhibition of ColH-PD at 1 μ M concentration of six selected compounds.^a K_i values and residual activities are determined as described previously.⁷

Compound	R ₁	R ₂	K_i (μ M)
3	Ph	4-Me	0.05 \pm 0.01
5	Ph	H	0.4 \pm 0.04
11	4-OMe-Ph	H	0.04 \pm 0.01
12	4-OH-Ph	H	0.1 \pm 0.02
19	benzothiazolyl	H	0.1 \pm 0.01
20	6-methoxybenzothiazolyl	H	28 \pm 1

Compound	R ₁	R ₂	% inh. of ColH-PD @ 1 μ M
10	4-NO ₂ -Ph	H	88 \pm 2
13	Ph	4-Me-Ph	69 \pm 3
14	Ph	4-OH	63 \pm 2
15	Ph	3-NO ₂ -4-OH	74 \pm 5
16	thiazolyl	H	34 \pm 3
20	6-chlorobenzothiazolyl	H	73 \pm 2

^aMeans and SD of at least two independent experiments.

Table S2. Zebrafish embryotoxicity results for compounds **11** and **19**.

Compound	Concentration (μM)	2 dpf	3 dpf	4 dpf	5 dpf	Survival rate %
11	100	all dead	-	-	-	0
	50	imp. dev., turbid body	all dead	-	-	0
	30	imp. dev.	all dead	-	-	0
	2	OK	OK	OK	OK	100
19	100	imp. dev.	5 imp. dev.	5 imp. dev.	5 imp. dev.	0
	50	imp. dev.	5 imp. dev.	5 imp. dev.	5 imp. dev.	50
	30	OK	OK, 3 imp. dev.	OK, 3 imp. dev.	OK, 3 imp. dev.	70
	2	OK	OK	OK	OK	100
Danieau's ctrl	-	OK	OK, 1 malf., 1 dead	OK	OK	80
DMSO ctrl	1%	OK	OK, 1 malf.	OK	OK	100

malf. = body curvature

impaired dev. = impaired development, pericardial edema

No toxicity signs were observed for compound **11** at a concentration of 2 μM . However, all concentrations above (30 μM , 50 μM , and 100 μM) have led to a toxicity of 100%.

30% of larvae showed toxicity signs, such as impaired body development and pericardial edema, when incubated with compound **19** at a concentration of 30 μM . The two highest concentrations (50 μM and 100 μM) were lethal for all larvae resulting in a survival rate of 0%. A comparable ratio of malformation was also found in the control groups (with only Danieau's medium or 1% DMSO). Therefore, observed body malformation in larvae incubated in compound can be considered as not related to compound treatment.

Experimental Methods

LasB Inhibition Assay. The purification of LasB from *P. aeruginosa* P14 supernatant as well as the subsequent performance of the FRET-based *in vitro* inhibition assay was performed as described previously.¹

***In vitro* ColH Inhibition Assay.** The purification of ColH-PD and determination of the inhibitory activities of the selected compounds were performed as described previously.^{2,3} In short, enzyme and inhibitor or buffer control were preincubated for 1 h at RT, before the reactions were initiated by the addition of the quenched fluorescent substrate Mca-Ala-Gly-Pro-Pro-Gly-Pro-Dpa-Gly-Arg-NH₂ (Mca = (7-Methoxycoumarin-4-yl)acetyl; Dpa = N-3-(2,4-dinitrophenyl)-L-2,3-diaminopropionyl) (FS1-1). The increase in fluorescence was monitored for 2 min 24 s (Excitation: 328 nm, Emission: 392 nm) at 25°C. The final concentrations were 2 nM ColH-PD, 10 μM compound, 250 mM Hepes pH 7.5, 400 mM NaCl, 10 mM CaCl₂, 10 μM ZnCl₂, 2% DMSO, and 2 μM FS1-1. The percentage of enzyme inhibition was calculated in relation to a reference without a compound added, only plus buffer control. The concentrations of the compound were optimized according to Murphy.⁴ The apparent inhibition constant (K_i^{app}) value was determined by non-linear fitting to the Morrison equation⁵ following a two-stage regression analysis strategy for tight-binding inhibitors.⁶ Regression analysis was performed using GraphPad Prism 9.0.0 (Graph Pad Software, San Diego, CA, USA). The experiments were performed under first order conditions ($[S_0] \ll K_M$), which resulted in an approximation of the K_i^{app} to the true inhibition constant (K_i), and, therefore, the results are reported as K_i values.

Antibacterial Activity assay. Minimum inhibitory concentration (MIC) assays were performed as described previously.¹ The MIC value was higher than 100 μM for compounds **12** and **19**. At 100 μM, the bacterial growth was reduced by less than 10% for both compounds.

Inhibition Assays with human off-targets. Assays focusing on the inhibition of human MMPs and ADAM17 were performed as described previously.^{7,8}

Cytotoxicity Assay. The toxicity of selected compounds toward HepG2, A549 and HEK293 cells was determined as described previously.^{1,9} Compounds **12** and **19** showed no relevant cytotoxic behaviour against the human hepatoma cell line (HepG2), human embryonic kidney (HEK) 293 cells and adenocarcinomic human alveolar basal epithelial cells (A549) with IC₅₀ values higher than 100 μM.

Docking Studies. Modelling of derivatives of compound **5** in the LasB ligand binding pocket (PDB:7OC7) were performed using SeeSAR 11.1 (BioSolveIT GmbH, Sankt Augustin,

Germany)¹⁰ software and the interactions are visualized using PyMOL Molecular Graphics System, Version 2.5 Schrödinger, LLC.¹¹ All interaction figures are created with PyMOL v.2.5

Zebrafish Experiments. Maximum Tolerated Concentration (MTC) assay was performed with minor modifications according to the procedure described in literature.¹² After successful mating of parent fish from the AB wild-type line, embryos were collected, sorted and kept until the next day at 28 °C in 0.3× Danieau's medium [17 mM NaCl, 2 mM KCl, 1.8 mM Ca(NO₃)₂, 1.5 mM HEPES (pH 7.1 – 7.3), 0.12 mM MgSO₄ and 1.2 μM methylene blue]. The assay was performed in 96-well plates using zebrafish embryos at 1 day post fertilization (dpf). Compound solutions in 0.3× Danieau's medium were prepared freshly on the day of experiment with a final DMSO concentration of 1% (v/v). Single zebrafish embryos were placed in a 96-well microtiter plate - one embryo per well and ten embryos per condition - and directly incubated in the corresponding compound solutions. The embryos were monitored daily via microscopy until 120 hours post fertilization (hpf) (Table SI). All described experiments were performed with zebrafish embryos younger than 120 hpf and are therefore not classified as animal experiments according to EU Directive 2010/63/EU. Protocols for husbandry and care of adult animals are in accordance with the German Animal Welfare Act (§11 Abs. 1 TierSchG).

Preparation of *P. aeruginosa* culture supernatants and LasB activity evaluation.

The LasB knockout *P. aeruginosa* $\Delta lasB$ PA14 was kindly provided by the Häussler group (Twincore, Hannover, Germany). *P. aeruginosa* $\Delta lasB$ PA14 (parental strain: "*P. aeruginosa* PA14 (DSM 19882)") is a knockout mutant with markerless in-frame deletion (in frame deletion with pEX18Ap (no antibiotic resistance introduction)), as described in Casilag et al.¹³ Overnight cultures of a single colony of wild-type (wt) and $\Delta lasB$ PA14 strains were grown in lysogeny broth medium at 37 °C with constant shaking at 200 rpm. The next day, the culture was centrifuged at 4 °C, 5,000 rpm for 30 min. Then, the supernatant was passed through a membrane filter of 0.2 μm to sterilize it. The supernatant was aliquoted and stored at –80 °C until use. LasB activity of both supernatants was evaluated using the FRET-based assay which was described previously (**Figure S11**).

Cell-based *in vitro* experiments. A549 cells were purchased from Sigma Aldrich and NHDF cells were provided from Leibniz Institute for New Materials (INM) (Saarbrücken, Germany). Both cell lines were cultured in cell culture plates with a 150 X 20 mm diameter. The cells were incubated with Dulbecco's modified Eagle's medium (DMEM) (Gibco) supplemented with 10% (v/v) fetal bovine serum (FBS, Gibco) and 1% (v/v) Penicillin-Streptomycin (Pen-Strep) at 37 °C under 5% CO₂ in a humidified incubator. 50,000 NHDF cells/well and 100,000 A549 cells/well were seeded in 96-well plates (Greiner) and incubated for 24 h at 37 °C and 5% CO₂

so that the cells reached a confluency of 90%. For imaging purposes, the cells were plated on 96 well glass bottom plates (Cellvis). Next, the cells were treated with (0–25%) PA14 or $\Delta lasB$ PA14 supernatant. to compare between their cytotoxic effects. 15% of each s.n. was used in the next experiments with compounds. To prevent disulfide formation of our compounds, we added tris(2-carboxyethyl) phosphine (TCEP) as a reducing agent and optimized its concentration in the assay before the evaluation of the compounds. A mixture of PA14 supernatant (*i.e.*, wild-type or mutant), various concentrations of LasB inhibitors, 40 μM ZnCl_2 and CaCl_2 and 300 μM TCEP was preincubated for 30 min and directly added to the cells. The optimized concentration of TCEP did not show any toxic effect on cells and did not affect LasB activity. Phosphoramidon was included in the experiments as LasB reference inhibitor. A mixture of DMEM with TCEP, 40 μM ZnCl_2 , CaCl_2 and 1% DMSO was used as a control. In order to determine the cell viability, we conducted two different assays: an MTT assay and a live/dead staining followed by imaging using a Leica epifluorescence microscope (DMI8, Leica microsystem CMS GmbH). The MTT assay is a method that can be used to determine the metabolic activity of cells, since active cells are able to reduce the MTT dye (3-(4,5-Dimethylthiazol-2-yl)-2,5-Diphenyltetrazolium Bromide) to the purple formazan precipitate which can be dissolved, and its absorbance can be measured. In the MTT assay, the cells were washed twice with 200 μL of sterile PBS, followed by addition of DMEM containing 5 mg/mL of MTT solution. The cells were incubated at 37 °C, 5% CO_2 for 2 h. In a next step, the MTT solution was carefully removed and 200 μL of 100% DMSO was added to dissolve the purple formazan crystals. After this, we measured the absorbance at 550 nm using a PHERastar plate reader (BMG Labtech, Ortenberg, Germany). The viability of the cells was related to untreated control wells/cells. Live/dead staining was performed using fluorescein diacetate (FDA) to stain living cells and propidium iodide (PI) to stain the dead ones. The cells were seeded and incubated with the s.n. as described before. After 1 day of incubation, the cells were washed 3 times with sterile PBS and then 0.03 mg/mL FDA and 0.02 mg/mL PI were added into each well and incubated for 5 min at 37 °C and 5% CO_2 . Imaging was performed using 5x magnification to have a general overview about the cell behavior. 20x magnification was used as well to visualize the change in the morphology of the cells in the bright field channel.

Results of duplicate of three independent experiments were plotted and illustrated using GraphPad Prism v.8 and presented as mean values \pm standard deviation. The statistical analysis of variance was performed with ANOVA followed by Dunnett's multiple comparisons test. Statistical significance was calculated by comparing non-treated cell *vs* treated cells and a *P* value less than 0.05 was significant. For image illustration purposes, the brightness and contrast

were optimized for all images based on the values of control (no treatment) images for each channel.

In vivo Galleria mellonella virulence assay. *G. mellonella* larvae were purchased from BioSystems Technology (Exeter, United Kingdom), stored at 8 °C in the dark and used within 2 weeks. Prior to injection, larvae were immobilized by incubation for 10–15 min on ice. Then, the injection was performed using an LA120 syringe pump (Landgraf Laborsysteme, Langenhagen, Germany) supplied with a 1 mL syringe (B. Braun, Melsungen, Germany) and Sterican 0.30 × 12 mm, 30G × 1.5 sterile needles (B. Braun). The larvae were injected with 10 μ L of sample into the right proleg. The larvae were classified into various groups based on the applied treatment. Two negative control groups supplemented with no injection to control the quality of the larvae and a buffer control group injected with sterile PBS were included. A positive control group was also included, and the larvae were administered with 50% wt PA14 supernatant. To test the anti-virulence effect of LasB inhibitors, a mixture of 50% wt PA14 csn, LasB inhibitor and 300 μ M TCEP were incubated for 30 min at 37 °C and injected into the larvae. A group of larvae injected with 50% Δ *lasB* PA14 supernatant was also involved. All groups were incubated at 37 °C and inspected once per day for 4 days post-treatment and to record mortality. The larvae were considered dead if they are black and do not move when stimulated by contact with the forceps. The survival analysis was performed using GraphPad Prism v 8, data were plotted using the Kaplan–Meier method and statistical significance between groups was calculated with log-rank test. The data of three independent experiments were combined and plotted in the survival curve, 30 larvae in total were included for each conditions.

Chemistry

The supplementary information of the chemistry part will be available online when the manuscript is accepted.

References

- 1 Kany, A. M.; Sikandar, A.; Hauptenthal, J.; Yahiaoui, S.; Maurer, C. K.; Proschak, E.; Köhnke, J.; Hartmann, R. W. Binding Mode Characterization and Early in Vivo Evaluation of Fragment-Like Thiols as Inhibitors of the Virulence Factor LasB from *Pseudomonas Aeruginosa*. *ACS Infect. Dis.* 2018, 4 (6), 988–997. <https://doi.org/10.1021/acsinfecdis.8b00010>.
- 2 Eckhard, U.; Schönauer, E.; Brandstetter, H. Structural Basis for Activity Regulation and Substrate Preference of Clostridial Collagenases G, H, and T. *J. Biol. Chem.* 2013, 288 (28), 20184–20194. <https://doi.org/10.1074/jbc.M112.448548>.
- 3 Schönauer, E.; Kany, A. M.; Hauptenthal, J.; Hüsecken, K.; Hoppe, I. J.; Voos, K.; Yahiaoui, S.; Elsässer, B.; Ducho, C.; Brandstetter, H.; Hartmann, R. W. Discovery of a Potent Inhibitor Class with High Selectivity toward Clostridial Collagenases. *J. Am. Chem. Soc.* 2017, 139 (36), 12696–12703. <https://doi.org/10.1021/jacs.7b06935>.
- 4 Murphy, D. J. Determination of Accurate KI Values for Tight-Binding Enzyme Inhibitors: An in Silico Study of Experimental Error and Assay Design. *Anal. Biochem.* 2004, 327 (1), 61–67. <https://doi.org/10.1016/j.ab.2003.12.018>.
- 5 Morrison, J. F. Kinetics of the Reversible Inhibition of Enzyme-Catalysed Reactions by Tight-Binding Inhibitors. *Biochim. Biophys. Acta - Enzymol.* 1969, 185 (2), 269–286. [https://doi.org/10.1016/0005-2744\(69\)90420-3](https://doi.org/10.1016/0005-2744(69)90420-3).
- 6 Kuzmič, P.; Elrod, K. C.; Cregar, L. M.; Sideris, S.; Rai, R.; Janc, J. W. High-Throughput Screening of Enzyme Inhibitors: Simultaneous Determination of Tight-Binding Inhibition Constants and Enzyme Concentration. *Anal. Biochem.* 2000, 286 (1), 45–50. <https://doi.org/10.1006/abio.2000.4685>.
- 7 Schönauer, E.; Kany, A. M.; Hauptenthal, J.; Hüsecken, K.; Hoppe, I. J.; Voos, K.; Yahiaoui, S.; Elsässer, B.; Ducho, C.; Brandstetter, H.; Hartmann, R. W. Discovery of a Potent Inhibitor Class with High Selectivity towards Clostridial Collagenases. *J. Am. Chem. Soc.* 2017, jacs.7b06935. <https://doi.org/10.1021/jacs.7b06935>.
- 8 Kany, A. M.; Sikandar, A.; Yahiaoui, S.; Hauptenthal, J.; Walter, I.; Empting, M.; Köhnke, J.; Hartmann, R. W. Tackling *Pseudomonas Aeruginosa* Virulence by a Hydroxamic Acid-Based LasB Inhibitor. *ACS Chem. Biol.* 2018, 13 (9), 2449–2455. <https://doi.org/10.1021/acscchembio.8b00257>.
- 9 Hauptenthal, J.; Baehr, C.; Zeuzem, S.; Piiper, A. RNase A-like Enzymes in Serum Inhibit the Anti-Neoplastic Activity of siRNA Targeting Polo-like Kinase 1. *Int. J. Cancer* 2007, 121 (1), 206–210. <https://doi.org/10.1002/ijc.22665>.
- 10 SeeSAR v.11.1, BioSolveIT GmbH, Sankt Augustin, G. 2021. Available from: <Http://Www.Biosolveit.de/SeeSAR>.
- 11 Schrödinger, L., & DeLano, W. (2020). P. R. from <http://www.pymol.org/pymo>. The PyMOL Molecular Graphics System, Version 2.0 Schrödinger, LLC. 2021.
- 12 Chakraborty, C.; Sharma, A. R.; Sharma, G.; Lee, S. S. Zebrafish: A Complete Animal Model to Enumerate the Nanoparticle Toxicity. *J. Nanobiotechnology* 2016, 14 (1), 1–13. <https://doi.org/10.1186/s12951-016-0217-6>.
- 13 Casilag, F.; Lorenz, A.; Krueger, J.; Klawonn, F.; Weiss, S.; Häussler, S. The LasB Elastase of *Pseudomonas Aeruginosa* Acts in Concert with Alkaline Protease AprA To Prevent Flagellin-Mediated Immune Recognition. *Infect. Immun.* 2016, 84 (1), 162–171. <https://doi.org/10.1128/IAI.00939-15>.
- 14 Liu, P. V. Extracellular Toxins of *Pseudomonas Aeruginosa*. *J. Infect. Dis.* 1974, 130 (November), S94–S99. <https://doi.org/10.1093/infdis/130.Supplement.S94>.

Abbreviations

DNA	Deoxyribonucleic acid
RNA	Ribonucleic acid
QS	Quorum sensing
MMPs	Matrix metalloproteases
LasB	<i>Pseudomonas aeruginosa</i> elastase B
LasA	<i>Pseudomonas aeruginosa</i> elastase A
WHO	World Health Organization
CF	Cystic fibrosis
ECM	Extracellular matrix
ZBG	Zn ²⁺ -binding group
ColH	<i>Clostridium histolyticum</i> (<i>Hathewayia histolytica</i>) collagenase H
ColG	<i>Clostridium histolyticum</i> (<i>Hathewayia histolytica</i>) collagenase G
ColB	<i>Bacillus thuringiensis</i> collagenase B
ColQ1	<i>Bacillus cereus</i> collagenase Q1
ColA	<i>Bacillus cereus</i> collagenase A
CU	Collagenase unit
PD	Peptidase unit
PlcR	Pleiotropic regulon phospholipase C regulator
SAR	Structure–activity relationships
DMAP	4-Dimethylaminopyridine
Pyr	Pyridine
DCM	Dichloromethane
DME	Dimethoxyethane
THF	Tetrahydrofuran
IC ₅₀	The half maximal inhibitory concentration
TCEP	Tris(2-carboxyethyl)phosphine hydrochloride
HepG2	Hepatocellular carcinoma cell line
HEK293	Embryonal kidney cell line
A549	Lung carcinoma cell line
HDAC	Histone deacetylase
TACE	Tumor necrosis factor- α -converting enzyme
MTC	Maximum tolerated concentration

MIC	Minimum inhibitory concentration
DMEM	Dulbecco's Modified Eagle's Medium
csn	Culture supernatant
FRET	Fluorescence resonance energy transfer;
NHDF	Normal human dermal fibroblast cells
HaCaT	Human epidermal keratinocyte cells
MTT	Microculture tetrazolium assay
Hyp	Hydroxyproline
COL	Collagen
SHG	Second harmonic generation
RPMI	Roswell Park Memorial Institute
Pen-Strep	Penicillin-streptomycin
FBS	Fetal bovine serum
FCS	Fetal calf serum
DMSO	Dimethyl sulfoxide
FDA	Fluorescein diacetate
PI	Propidium iodide
PBS	Phosphate buffered saline
DAPI	4',6-Diamidino-2-phenylindole
Hsp47	Heat shock protein 47
ER	Endoplasmic reticulum
EIA	Enzyme-immunosorbent assay
TEM	Transmission electron microscope
PLM	Polarization light microscope
ONBY	O-nitro benzyl tyrosine
H47	Wild-type Hsp47
H47 _{Y>ONBY}	In active variant of Hsp47
H47 _{Y>ONBYhv}	Photoactivatable variant of Hsp47
LDH	Lactate dehydrogenase
TEER	Transepithelial electrical resistance
MDCK II	Madin-Darby Canine Kidney II
M (kDa)	Molecular weight standards in kilo Dalton
BHI	Brain heart infusion medium

Publications of the Author Included in This Thesis and Contribution Declaration

Publication A: Konstantinović, J. [⊥], Yahiaoui, S. [⊥], Alhayek, A. [⊥], Hauptenthal, J., Schönauer, E., Andreas, A., Kany, A.M., Müller, R., Koehnke, J., Berger, F.K., Bischoff, M., Hartmann, R.W., Brandstetter, and H., Hirsch, A.K.H., (2020). *N*-Aryl-3-mercaptosuccinimides as Antivirulence Agents Targeting *Pseudomonas aeruginosa* Elastase and *Clostridium* Collagenases. *J. Med. Chem.* 63, 8359–8368. <https://doi.org/10.1021/acs.jmedchem.0c00584>

[⊥] these authors contributed equally

Contribution: The author established the *ex vivo* pig-skin model and tested the most active compound discovered in this work. She conceived, prepared the figures, and wrote the manuscript together with Konstantinovic, J. and Yahiaoui, S., who contributed equally. The author designed the cover art, which was selected for the front page of the journal.

Publication B: Alhayek, A., Khan, E.S., Schönauer, E., Däinghaus, T., Shafiei, R., Voos, K., Han, M.K.L., Ducho, C., Posselt, G., Wessler, S., Brandstetter, H., Hauptenthal, J., del Campo, A., and Hirsch, A.K.H., (2022). Inhibition of Collagenase Q1 of *Bacillus cereus* as a Novel Antivirulence Strategy for the Treatment of Skin-Wound Infections. *Adv. Ther.* 2100222. <https://doi.org/10.1002/adtp.202100222>

Contribution: The author established and performed the *in vitro* cell-based assays, *ex vivo* pig skin model, and the *in vivo* survival study with *Galleria mellonella* model. She further conducted *in vitro* collagen-cleavage assay, the MTT assay, fluorescence imaging of the cells. She also prepared the tissue for imaging and assisted in acquiring the imaging of the tissue. The author analyzed the data and images and conceived and wrote the paper.

Publications of the Author not Included in This Thesis and Contribution Declaration

Publication C: Kaya, C., Walter, I., Yahiaoui, S., Sikandar, A., Alhayek, A., Konstantinović, J., Kany, A.M., Hauptenthal, J., Köhnke, J., Hartmann, R.W., Hirsch, A.K.H., (2022). Substrate-Inspired Fragment Merging and Growing Affords Efficacious LasB Inhibitors. *Angew. Chemie Int.* <https://doi.org/10.1002/anie.202112295>

Contribution: The author performed the *in vivo* *G. mellonella* experiment, described the methods and results, prepared the figures, and reviewed the manuscript.

Publication D: Jumde, R.P., Guardigni, M., Gierse, R.M., Alhayek, A., Zhu, D., Hamid, Z., Johannsen, S., Elgaher, W.A.M., Neusens, P.J., Nehls, C., Hauptenthal, J., Reiling, N., Hirsch, A.K.H., (2021). Hit-optimization using target-directed dynamic combinatorial chemistry: development of inhibitors of the anti-infective target 1-deoxy-d-xylulose-5-phosphate synthase. *Chem. Sci.* 12, 7775–7785. <https://doi.org/10.1039/d1sc00330e>.

Contribution: The author expressed and purified the drDXS protein used in DCC experiment, performed the stability study of the protein, and tested the compounds *in vitro* with the enzyme-based assay. She also described the methods and results, prepared the figures, and reviewed the manuscript.

Publication E: Voos, K., Schönauer, E., Alhayek, A., Hauptenthal, J., Andreas, A., Müller, R., Hartmann, R.W., Brandstetter, H., Hirsch, A.K.H., Ducho, C., (2021). Phosphonate as a Stable Zinc-Binding Group for “Pathoblocker” Inhibitors of Clostridial Collagenase H (ColH). *ChemMedChem* <https://doi.org/10.1002/cmdc.202000994>

Contribution: The author tested the most active compound on the *ex vivo* pig-skin model. She also described the methods and results, prepared the figures, and reviewed the manuscript. The author designed the cover art, which was selected for the front page of the journal together with Voos, K.

Publication F: Gierse, R.M., Reddem, E.R., Alhayek, A., Baitinger, D., Hamid, Z., Jakobi, H., Laber, B., Lange, G., Hirsch, A.K.H., and Groves, M.R., (2021). Identification of a 1-deoxy-D-xylulose-5-phosphate synthase (DXS) mutant with improved crystallographic properties. *Biochem. Biophys. Res. Commun.* <https://doi.org/10.1016/j.bbrc.2020.12.069>

Contribution: The author expressed and purified drDXS and its truncated variant and conducted the kinetic and stability comparisons between the wild-type and truncated drDXS with an enzyme-coupled assay. She also described the methods and results, prepared the figures, and reviewed the manuscript.

Publication G: Mancini, F., Unver, M.Y., Elgaher, W.A.M., Jumde, V.R., Alhayek, A., Lukat, P., Herrmann, J., Witte, M.D., Köck, M., Blankenfeldt, W., Müller, R., and Hirsch, A.K.H., (2020). Protein-Templated Hit Identification through an Ugi Four-Component Reaction. *Chem. – A Eur. J.* <https://doi.org/10.1002/chem.202002250>

Contribution: The author tested the protein stability with a thermal-shift assay and selected the conditions to keep the protein stable for the time of the KTGS experiment. She also described the methods and results, prepared the figures, and reviewed the manuscript.

Manuscripts of the Author Submitted or in Preparation and Contribution Declaration

Manuscript A: Kaya, C., Walter, I., Alhayek, A., Shafiei, R., Andreas, A., Konstantinović, J., Schönauer, E., Sikandar, A., Jézéquel, G., Hauptenthal, J., Müller, R., Brandstetter, H., Hartmann, R.W., and Hirsch, A.K.H., Structure-based Design of α -Substituted Mercaptoacetamides as Inhibitors of the Virulence Factor LasB from *Pseudomonas aeruginosa* (manuscript submitted)

Contribution: The author designed and performed the *in vitro* cell-based assay, the MTT assay, and live/dead imaging with a fluorescence microscope with the most active compounds. She also performed the *in vivo* *G. mellonella* model. The author described the methods and results, prepared the figures, and reviewed the manuscript.

Manuscript B: Gierse, R.M., Oerlemans, R., Gawriljuk, V.O., Reddem, E., Alhayek, A., Baitinger, D., Jakobi, H., Laber, B., Lange, G, Hirsch, A.K.H., and Groves, M.R., Crystal structure of 1-deoxy-D-xylulose-5-phosphate synthase (DXPS) from *Mycobacterium tuberculosis* (manuscript submitted)

Contribution: The author expressed and purified the wild-type and truncated variant of DXS from *Mycobacterium tuberculosis*. She also conducted the kinetic and stability comparisons between the wild-type and truncated DXS with an enzyme-coupled assay. She also described the methods and results, prepared the figures, and reviewed the manuscript.

Manuscript C: Alhayek, A.¹, Khan, E.S.¹ *et al.* Cocktail therapy approach to treat wound infections induced by collagenase-producing bacteria (manuscript in preparation)

Contribution: The author designed and performed the *ex vivo* pig-skin model, also contributed to the skin sample preparation, imaging with microscopes and images analysis. She developed and performed the LC-MS/MS-based assay and performed the EIA assay. The author analyzed the data and wrote the manuscript together with Essak Khan, who contributed equally.

Manuscript D: Alhayek A. *et al.* Discovery and Characterization of Novel, Potent Inhibitors of Clostridial and Bacillary Collagenases (manuscript in preparation)

Contribution: The author established the *in vitro* and *in vivo* infection models. She also performed the *in vitro* cell-based assays, picosirius red assay, LDH release assay, zymography,

TEER assay, *in vivo* *G. mellonella* infection model. The author tested the compounds in the *in vitro* collagen-cleavage assay and in the aforementioned assays. She analyzed the data, conceived, and wrote the manuscript.

Manuscript E: Konstantinović *et al.* Inhibitors with Improved Stability, Solubility and Potency towards *Pseudomonas aeruginosa* Elastase LasB. (manuscript in preparation)

Contribution: The author performed the *in vitro* cell-based assay, the MTT and picrosirius red assays, and live/dead imaging with a fluorescence microscope. She also performed the *in vivo* *G. mellonella* infection model and selected and tested the compounds with and without antibiotics. The author described the methods and results, prepared the figures, and reviewed the manuscript.

Manuscript F: Voos *et al.* The Discovery of Highly Potent and Selective Inhibitors of *P. aeruginosa* Virulence Factor LasB and *C. histolyticum* Virulence Factor ColH. (manuscript in preparation)

Contribution: The author performed the *in vitro* cell-based assay, the MTT assay, and the live/dead imaging with a fluorescence microscope. She also performed the *in vivo* *G. mellonella* model and selected and tested the compounds against the PA14 and *lasB* knockout PA14 supernatant. The author described the methods and results, prepared the figures, and reviewed the manuscript.

Manuscript G: Alhayek, A., Gawriljuk, V.O., Josten, E., Gierse, R., Herrmann J., Stadler, M., Reiling, N., Müller, R., Groves, R.M., Hirsch, A.K.H., Identification and characterization of Natural-product inhibitors of the *Mycobacterium tuberculosis* 1-Deoxy-D-Xylulose 5-Phosphate Synthase (DXPS) (manuscript in preparation)

Contribution: The author performed the kinetic study of the *Mycobacterium tuberculosis* DXS, screened the natural product and crude extract libraries, and the selectivity study on pyruvate dehydrogenase off-target. She also performed competitive and binding studies. The author analyzed the data, conceived, and wrote the manuscript.

Conference Contributions

Alhayek A.; Abdelsamie S. A.; Schönauer E.; Camberlein V.; Hutterer E.; Posselt G.; Hauptenthal J.; Brandstetter H.; Wessler S.; and Hirsch A. K. H.: Discovery and Characterization of Novel, Potent Inhibitors of Clostridial and Bacillary Collagenases, Proceedings of 39th Winter School on Proteinases and Their Inhibitors, Virtually, February, 2022

Alhayek A.; Abdelsamie A. S.; Camberlein V.; Hutterer E.; Posselt G.; Schönauer E.; Hauptenthal J.; Brandstetter H.; Wessler S.; and Hirsch A. K. H.: Targeting collagenase activity in *Bacillus cereus* associated pathologies, DphG, Virtually, October, 2021

Alhayek, A.; Hauptenthal, J.; Khan S. E.; Schönauer E.; Däinghaus T.; Shafiei R.; Voos K.; Ducho C.; Brandstetter H.; Campo del A.; and Hirsch A. K. H. : Targeting collagenase activity in *Bacillus cereus* associated pathologies. ECCMID, Virtually, July, 2021

Kiefer A. F.; Konstantinović, J; Abdelsamie A. S; Shütz C.; Jumde R.; Kiefer A. F.; Kaya C.; Voos K.; Walter I.; Yahiaoui S.; Kany A.; **Alhayek A.**; Klein A.; Sikandar A.; Köunke J.; Hauptenthal J.; Ducho C.; Harmann R. W.; Hirsch A. K. H. :Discovery of sub-micromolar Inhibitors of the Virulence Factor LasB from *Pseudomonas aeruginosa* using Rational Design, ECCMID, Virtually, July, 2021

Alhayek, A.; Hauptenthal, J.; Khan S. E.; Schönauer E.; Däinghaus T.; Shafiei R.; Voos K.; Ducho C.; Brandstetter H.; Campo del A.; and Hirsch A. K. H. : Targeting collagenase activity in *Bacillus cereus* associated pathologies. HIPS Symposium, Virtually, May, 2021

Konstantinović, J; Abdelsamie A. S; Shütz C.; Kaya C.; Voos K.; Walter I.; Yahiaoui S.; Kany A.; **Alhayek A.**; Klein A.; Sikandar A.; Köunke J.; Hauptenthal J.; Ducho C.; Harmann R. W.; Hirsch A. K. H. :Discovery of Nanomolar Inhibitors of the Virulence Factor LasB from *Pseudomonas aeruginosa* using Rational Design, HIPS symposium, Virtually, May, 2021

Alhayek, A.; Hauptenthal, J.; Khan S. E.; Schönauer E.; Däinghaus T.; Shafiei R.; Voos K.; Ducho C.; Brandstetter H.; Campo del A.; and Hirsch A. K. H. : Targeting collagenase activity in *Bacillus cereus* associated pathologies. Proceedings of 38th Winter School on Proteinases and Their Inhibitors, Virtually, February, 2021

Alhayek, A.; Khan S. E.; Däinghaus, T; Schönau, E.; Schafiei, R.; Voos, K.; Docho, C.; Haupenthal, J.; Brandstetter, H.; del Campo, A.; and A. K. H. : Establishment of an *ex vivo* pig skin model to evaluate activity of pathoblocker agents. Proceeding 11th Helmholtz Centre for Infection Research (HZI) Retreat, Virtually, Saarbrücken, October, 2020

Alhayek, A.; Konstantinović, J.; Yahiaoui, S.; Haupenthal, J.; Schönauer, E.; Sikandar, A.; Kany, A.; Andreas, A.; Müller, R.; Köhnke, J.; Nimmegern, A.; Bischoff, M.; Hartmann, R. W.; Brandstetter, H.; Hirsch, A. K. H. (2020): Succinimides as novel pathoblocker agents targeting extracellular bacterial metalloproteases LasB and ColH. Proceedings of 37th Winter School on Proteinases and Their Inhibitors, March, Tiers am Rosengarten, Italy, 2020

Alhayek, A.; Haupenthal, J.; Konstantinović, J.; Yahiaoui, S.; Schönauer, E.; Kaya C; Brandstetter, H.; Hartmann, R. W.; Hirsch, A. K. H. : Biological evaluation of novel pathoblockers targeting extracellular bacterial metalloproteases LasB and ColH. PhD day for Natural Sciences Department, Saarbrücken, Germany, 2019

Alhayek, A.; Haupenthal, J.; Konstantinović, J.; Yahiaoui, S.; Schönauer, E.; Kaya C; Brandstetter, H.; Hartmann, R. W.; Hirsch, A. K. H. : Biological evaluation of novel pathoblockers targeting extracellular bacterial metalloproteases LasB and ColH. Vienna summer school, Vienna, Austria, 2019

Jumde. R.; **Alhayek, A.;** Gierse, R.; Hirsch, A. K. H. : Identification of Inhibitors of the Anti-infective Target DXS Using Dynamic Combinatorial Chemistry. Proceedings of the 2nd Molecules Medicinal Chemistry Symposium facing novel challenges in drug discovery, August, Barcelona, Spain, 2019

Johannsen, S.; Jumde, R.; **Alhayek, A.;** Gierse, R.; Masini, T.; Zhu, Di; Haupenthal, J.; Hirsch, A. K. H. : Identification of inhibitors of the anti-infective targets DXS. HIPS symposium, Saarbrücken, Germany, 2019

Curriculum Vita

Alaa Alhayek

Date of birth: 05.02.1992
Place of birth: Gaza/Palestine

CONTACT

🏠 Distelfeld 3, 66121, SB, Germany

☎ + 4915736963318

✉ alaahayek12@hotmail.com

🌐 Alaa Alhayek

PERSONAL SKILLS

- Comprehensive knowledge in pharmaceutical science, biology, and molecular biology
- Multiyear experience in drug discovery
- Able to work in a highly interdisciplinary environment (team-oriented, organized, flexible, quick acting, with excellent communication skills)
- Proven experience in teaching, supervising Master's students, working in international teams

SOFTWARE SKILLS

MS Office, Chromeleon, ChemDraw, Origin, GraphPad Prism, LeadIT, SeeSAR, Fiji image J, Image lab, Chimera, snapGene

LANGUAGES

Arabic: native
English: B2
German: B1

EDUCATION

10/2017 – 09/2018: Master of Science in Pharmacy.

University of Saarland, Helmholtz Institute for Pharmaceutical Research Saarland, Saarbrücken, Germany, GPA 1.2, Supervisor: Prof. Dr. Anna Hirsch, Research Topic: "Characterization of the 1-Deoxy-D-Xylolose 5-Phosphate Synthase (DXS) Protein and Its Inhibitors"

08/2010 – 06/2015: Bachelor of Science in Pharmacy

Alazhar University, Gaza, Palestine, GPA 90.3%

PROFESSIONAL EXPERIENCE

10/2018 – present: Dr. rer. nat. (Ph.D.), Helmholtz Institute for Pharmaceutical Research Saarland (HIPS), Saarbrücken, Germany (Prof. Dr. Anna Hirsch)

01/2021 – 06/2021: exchange PhD student, University of Salzburg, Salzburg, Austria.

05/2017 – 07/2017: Researcher trainee, University of Jordan, Amman, Jordan.

11/2016 – 05/2017: DAAD scholarship, Clinical pharmacist trainee, Hospital of University of Jordan, Amman, Jordan.

07/2016 – 10/2016: Responsible pharmacist, Al-Baraa Pharmacy, Gaza, Palestine

06/2015 – 06/2016: Teaching Assistant of several courses at Alazhar University, Faculty of Pharmacy

09/2013 – 07/2014: Researcher trainee at Drug Analysis Center, Alazhar University, Gaza, Palestine

In the period 06/2015-06/2016 I worked as a Teaching Assistant at the Alazhar University, Faculty of Pharmacy: Pharmacology, Therapeutics, and General chemistry

HONOURS AND AWARDS

2022: Best speaker award at the 39th winter school on proteases and inhibitors, online

2021: EMBO short-term fellowship for mobility

2021: Erasmus fellowship for mobility

2021: Best poster presentation award at the 38th winter school on proteases and inhibitors, online

2020: The Henner Graeff Foundation – young investigator award in the 37th winter school on proteases and inhibitors, Tiers, Italy

2016: DAAD fellowship to study clinical pharmacy at the University of Jordan, Amman, Jordan

2015: Best student that graduated from the Bachelor of Science in Pharmacy Programme in the 2015 academic year (shared with another student), Faculty of Pharmacy, Alazhar University, Gaza

Acknowledgment

This PhD has been a life-changing experience for me, and it would not have been possible without the help and advice of many people. I would like to express my gratitude to the following people for easing the passage through my PhD journey.

I would like to express my special appreciation and warmest thanks to my advisor Prof. Dr. Anna K. H. Hirsch, who made this work possible. Her friendly guidance and expert advice have been invaluable throughout my study. Thank you for encouraging my research and for allowing me to grow as a research scientist. Your advice on both research as well as on my career have been invaluable.

I would also like to thank my committee members, Prof. Dr. Jesko Köhnke, Prof. Dr. Silja Wessler, Dr. Jennifer Hermann, and Dr. Jörg Hauptenthal. Thanks for your valuable recommendations and suggestions during my PhD which have contributed greatly to the improvement of my work and inspired me to think outside the box.

I am grateful to all of those with whom I have had the pleasure to work during this and other related projects in particular my Bachelor, Master's students, and our collaborators from Salzburg University, Saarland University, and Leibniz Institute for Materials.

I would like to express my gratitude to Prof. Dr. Silja Wessler and Prof. Dr. Hans Brandstetter and their groups for their nice hospitality during my six months stay in Salzburg University. Evelyn, Sabine, Sebastian, Isabella, Mirosław, Marina, Mieria, Esther, Iris, Alex, and Gernot thanks for your support during my time and thanks for the scientific discussion which have been of great benefit to my work. I am also grateful for the funding sources EMBO short-term fellowship which covered my stay in Salzburg University. I am indebted to all my friends in Austria who opened their homes to me during my stay and who were always so helpful in numerous ways. Special thanks to Evelyn, Dani, Johanna and her kids, Cyrus, Max, and Marina. I am forever thankful to the coworkers at the Department of Drug Design and Optimization at HIPS for their friendship and support, and for creating a cordial working environment.

I would like to thank all my PhD and postdoc colleagues, with whom I have shared moments of stress but also of big excitement. Their presence was very important in a process that is often felt as tremendously solitaire. A warm word for my colleagues and great friends Mostafa, Jelena, Cansu, Federica, Yingwen, and Christine, who always managed to make me feel special and with whom I had the best lunch and tea breaks.

I would also like to say a heartfelt thank you to my friends in Palestine, USA, UK, Australia, and Germany for believing in me and encouraging me to follow my dreams. Special thanks go to Ghamdan, Huda, and Sara for helping in whatever way they could during this challenging

period. Thanks to my family in Palestine for their support which has been unconditional all these years. Dad, Mom, my siblings: Nedaa, Esraa, Ramze, Ahmed, and Saja, despite the six years and 2,943 km between us, without your support I would have not been reached this stage. The last words go to my husband Mohammed and my little baby Sophia, who have given me the extra strength and motivation to get things done and keep going especially in the last couple of months of this journey. Thanks to my love Mohammed for standing always by my side throughout this PhD, living every single moment of it, and without whom, I would not have had the courage to embark on this journey in the first place. Darling Sophia, this thesis was written during my pregnancy with you, despite all the hard pregnancy symptoms, all it took me was one little kick from you to make everything feel alright. This thesis is dedicated to my beloved Mohammed and to my daughter Sophia.